Efficiently starting and preferentially filling a potato

Leveraging models to investigate the multiple roles of SP6A in source-sink dynamics

Bas van den Herik

Efficiently starting and preferentially filling a potato

Leveraging models to investigate the multiple roles of SP6A in source-sink dynamics

Het efficiënt starten en bij voorkeur vullen van een aardappelknol het gebruik van modellen om de verschillende rollen van SP6A in source-sink dynamica te onderzoeken

met een samenvatting in het Nederlands

Proefschrift

ter verkrijging van de graad van doctor aan de
Universiteit Utrecht
op gezag van de
rector magnificus, prof. dr. H.R.B.M. Kummeling,
ingevolge het besluit van het college voor promoties
in het openbaar te verdedigen op

woensdag 17 januari 2024 des middags te 4.15 uur

door

Bastiaan Mees van den Herik

geboren op 4 juni 1994
te Gorinchem

Promotor

Prof. dr. K.H.W.J. ten Tusscher

Copromotor

Dr. C.W.B. Bachem

Beoordelingscommissie

Prof. dr. J. Evers
Prof. dr. T. Hölttä
Prof. dr. S. Prat
Prof. dr. R. Sasidharan
Dr. S. Sonnewald

Table of contents

Chapter 1
General introduction

Plants are essential for most life on Earth as their ability to photosynthesize allows them to convert and store the energy of the sun into sugars as well as produce oxygen. In doing so they provide the two essential ingredients for aerobic respiration fueling most heterotrophic life forms. Plant growth and production is therefore a major determinant of ecosystem functioning as well as agronomic productivity. However, not all parts of a plant take part in photosynthesis, as such the distribution of sugars from source leaves across various sink organs plays a major role in determining overall plant growth. A carbon source is any part of the plant that produces sugars, while a sink is a part of the plant that consumes or stores sugars. In general, mature leaves are the main sources of sugars in the plant, while the growing leaves, roots, developing flowers, and fruits are the main carbon sinks. The balance between the production of sugars in source tissues and their utilization in sink tissues is critical for the efficient growth of plants (Fernie et al., 2020; Smith et al., 2018). If there are too many sinks relative to sources, there may not be enough sugars available to support their growth and development. On the other hand, if there are too few sinks relative to sources, there may be an excess of sugars that accumulate in the leaves, leading to reduced photosynthesis and ultimately reduced growth.

Major changes in source-sink relations during a plant's lifecycle

Plants, like any organism, evolved to efficiently reproduce. To generate as many offspring as possible, they have to make investment choices. Producing new leaves is initially a smart investment as of the great sugar returns from photosynthesis, yet without sufficient water and nutrients provided by the roots the efficiency of photosynthesis is quickly reduced. Correctly balancing sink organs is thus of utmost importance to optimize plant growth and reproduction. On a similar note, if reproductive organs are produced late in the season, the plant has time to increase its size before reproduction, enabling it to create more offspring, yet this benefit comes at the risk of an early terminating warm season, and prolonged exposure to chances of e.g. flooding, herbivory or pests that may prohibit ever reaching the reproductive stage. Therefore, these investment decisions must be regulated on the whole plant level, as such the source-sink balance is tightly controlled through a complex network of biochemical pathways, hormonal signaling, and biophysics (Chang & Zhu, 2017; Fernie et al., 2020).

Due to the evolutionary selection on the regulation of source-sink dynamics, plants exhibit remarkable flexibility in regulating their source-sink balance to optimize their growth, development, and reproduction. They show this flexibility across a diverse range of environmental conditions and during developmental transitions introducing major changes in

numbers and activities of sources and sinks (Bäurle & Dean, 2006). Initially, in seedlings, the embryonic leaves, i.e. cotyledons, serve as a sucrose source to establish the first plant growth. During the following vegetative stage, roots and young leaves serve as major sinks. As plant development progresses, a transition from vegetative to floral stage occurs in most plants, leading to flowers, fruits, and seeds becoming the primary recipients of sugars. Lastly, in the case of annual plants, a controlled process of senescence takes place, redirecting sugars from all organs towards the reproductive organs through sucrose remobilization (Gregersen et al., 2013; Rankenberg et al., 2021). In perennial species, such as trees and shrubs, leaf senescence occurs in favor of sucrose storage in the woody trunks and roots (Furze et al., 2018).

Various abiotic and biotic stresses also exert a profound influence on the dynamics between sinks and sources. For instance, water stress can accelerate developmental transitions independently of their natural order, thereby altering the plant's overall source-sink status (Yang et al., 2001). Water stress can also lead to nutrient imbalances and impaired sugar transport, which in turn can lead to reduced photosynthesis (Bezrutczyk et al., 2018; Shao et al., 2020) and can thus disrupt the source-sink balance. Similarly, high temperatures and drought can lead to reduced sugar production in the source and increased sugar usage in the sinks (Moore et al., 2021). Biotic stresses, such as pathogenic infections, can create new sinks by creation of an additional strong sucrose sink or causing organ death, removing sinks. In short, source-sink balance is of great importance for maintaining proper growth, development, and overall physiological functioning.

Long-distance transport connects sources and sinks

Plants must continually maintain an equilibrium between their sources and sinks. This balancing act operates at both the level of individual organs and the whole plant. As an example of local organ control there is a tight feedback of leaf starch levels on photosynthesic activity, while on the whole plant level signaling molecules such as trehalose-6-phosphate (T6P) allow for upregulation of sink strength in response to source strength increase (Chang & Zhu, 2017; Fernie et al., 2020). A whole-plant level process that has been often overlooked in source-sink literature but that has recently gained more attention is the long-distance transport of sucrose through the vasculature (Lemoine et al., 2013; White et al., 2016). While developmental transitions of individual organs impact source or sink status on a local level, these changes also affect phloem sugar levels and consequently osmotic pressure and sap viscosity. These altered dynamics influence long-distance transport (Box 1), and consequently co-determines

the actually realized allocation of sucrose. Additionally, the stems connecting sources and sinks and carrying the long distance transport pathways act as often overlooked lateral sinks to support their own growth and maintenance. Sucrose loss along the long distance phloem constitutes an additional factor impacting effective sucrose allocation in distal sinks.

Source-sink relations as determinant of crop yield

Crop species such as wheat, rice, maize, and potato have been subjected to domestication and selective breeding processes, primarily focused on enhancing specific traits related to yield and pest resistance. As a result, the source-sink balance in these cultivated crops is generally less flexible compared to their wild counterparts (Chang & Zhu et al., 2018). Considerable breeding and research efforts have been dedicated to optimizing the source efficiency, specifically the efficiency of photosynthesis, resulting in significant yield improvements (Driever et al., 2017; Rosado-Souza et al., 2023). Recently, also sink-optimization showed promising results. Overexpression of TaTPP-7A, a T6P phosphorylation enzyme, that couples T6P to the energy and stress metabolism related SnRK1 pathway showed large redirection of sucrose towards wheat grains by increasing its sink-strength, significantly enhancing grain yield (Liu et al., 2023). Despite these advances in affecting source and sink efficiency, understanding of source-sink interactions at the whole plant level remains limited. It is self-evident that it is the amount of sucrose delivered to, and processed by, sink organs per unit of time that ultimately determines organ growth and yield. However, the above indicates that while simply enhancing sink strength may enhance yield under certain conditions, the timing of this enhanced sink strength relative to canopy area, plant architecture, development and season, as well as the highly complex interactions between source, sink and transport all affect final outcomes. Rationalized breeding for increasing, yet robust, yield through affecting sink dynamics will therefore benefit from an improved mechanistic understanding of whole plant source-sink dynamics, in which modeling studies are expected to be of major importance.
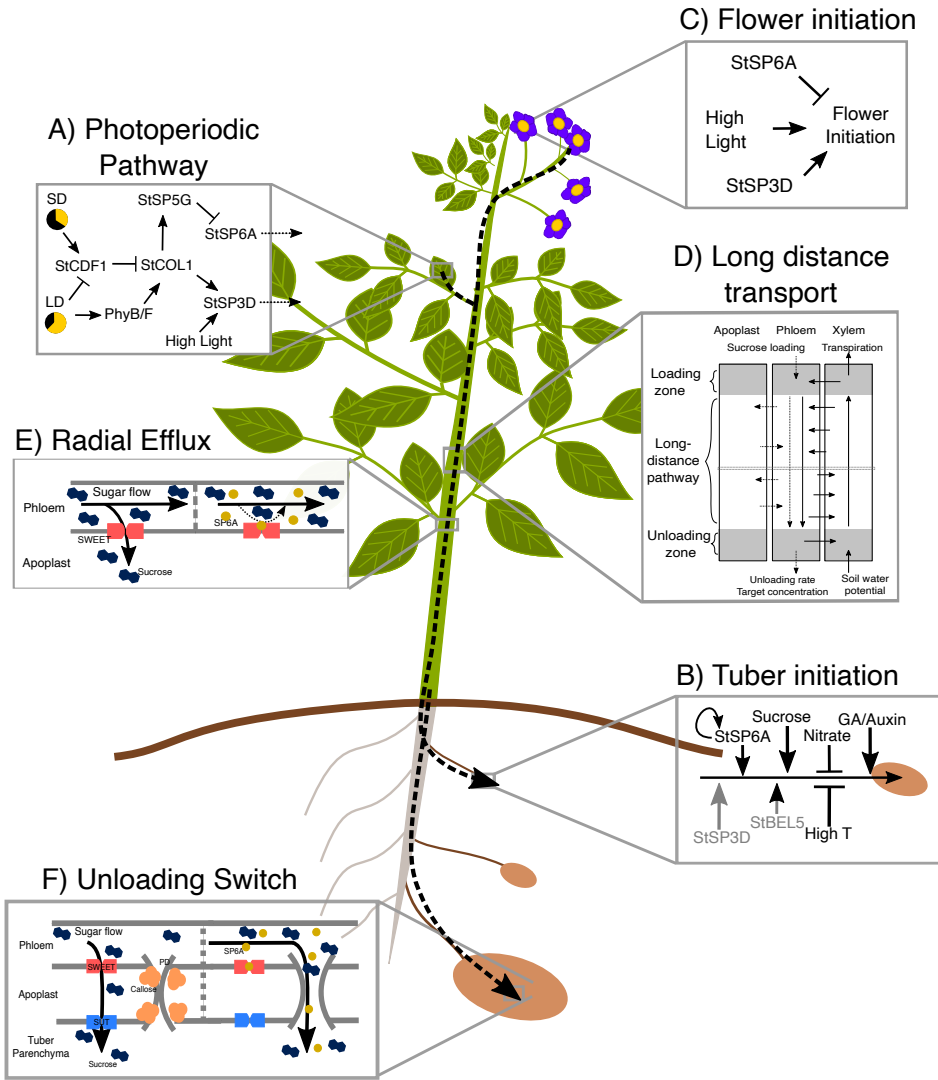
Figure 1.1 − Potato morphology with sinks highlighted and the molecular networks and impingement on transport and vice versa. Dotted arrows depict phloem flow, transporting sucrose, *StSP6A*, etc. **A)** The photoperiodic pathway controlling *StSP6A* and *StSP3D* expression. **B)** Tuber initiation is controlled by *StSP6A* and a wide array of other molecular and environmental signals. Grey signals are signals that are less certain to affect tuber initiation. **C)** Flower initiation is under the control of *StSP3D*, *StSP6A* and light conditions **D)** Schematic overview of long-distance transport in the phloem and xylem. **E)** Radial efflux and efflux-mitigation in the long-distance phloem. **F)** The unloading switch from stolon tuber.

Box 1: Phloem and xylem transport (Fig 1.1D)

Water and solutes are transported in two different conduit systems in plants: the xylem and phloem. In the xylem water and nutrients (e.g. nitrate, phosphate, iron, boron) are transported upwards from the roots towards the shoot, while in the phloem photosynthates (sucrose) are transported from source leaves towards sinks throughout the plant. Additionally, both conduit systems transport various signaling molecules to coordinate root and shoot physiology and growth. Water flow in both the phloem and xylem result from hydrostatic pressure gradients, however the mechanisms in which the gradient is formed differ for both systems (Jensen et al., 2016). Xylem flow is described by the cohesion-tension theory. Negative pressure (tension) generated by transpiration in the leaves creates a pressure gradient between the root to the leaves, pulling water upwards via cohesive forces. Nutrients travel along with the water from the roots towards the shoot. In the phloem, water flow is generally described as an osmotically generated pressure flow (Thompson & Holbrook, 2003), described by the Munch hypothesis (Munch, 1930). In the source-leaves osmotic potential increases due to the loading of solutes which does subsequently draw water towards the phloem, increasing the hydrostatic pressure. The opposite occurs in the sink region. Here solutes are unloaded from the phloem, decreasing osmotic pressure, and as a result water is flowing towards the surrounding tissues, lowering local hydrostatic pressure. This process creates a pressure gradient, transporting water from sources to sinks while carrying solutes. The xylem and phloem are hydraulically connected, allowing radial water flow between the two. The movement of sucrose within the phloem involves both efflux (leakage) and influx (retrieval) processes. Recent studies have identified bidirectional and passive SWEET transporters as the main mediators of sucrose efflux (L.-Q. Chen et al., 2012). Sucrose retrieval from the apoplast back into the phloem is facilitated by SUC transporters, which employ a sucrose-proton symporter mechanism (Hafke et al., 2005).

Potato – an interesting crop from the source-sink perspective

In this thesis, potato (*Solanum tuberosum*), a tuberous crop, is used as model system to investigate source-sink dynamics. Potato, besides its versatility in the kitchen, is important for global food security as the fourth largest crop, and the largest non-cereal crop (FAO, 2021).

1

From a source-sink perspective it is an interesting species due to its competing reproductive sinks and their closely related developmental molecular dynamics. Potato plants can reproduce sexually through the formation of flowers and the production of seeds, but most potato plants propagate clonally via their tubers, which is also where the agricultural value of potato lies. Potato tubers are formed by radial extension of underground stems, called stolons. Tubers are strong sugar sinks, using sugar partly for growth, but mainly for storing large amounts of starch and proteins. Upon tuber formation, a new strong sink is thus formed coinciding with large local and systemic physiological changes. Systemically, the occurrence of a set of strong new tuber sinks leads to the abortion of flowering (Plantenga, Bergonzi, Bachem, et al., 2019) and post-tuberization senescence, in which leaves start to senesce during the exponential tuber growth phase (Kloosterman et al., 2013). Also, changes in vasculature structure and abundance occur, further changing the connection between sources and sinks, thereby affecting their dynamics (Lehretz et al., 2021). Locally, tuber onset at the stolon coincides with a switch from apoplastic (transporter-mediated) to symplastic (plasmodesmata-mediated) unloading (Viola et al., 2001) and large metabolic changes during tuber onset. Metabolism in tubers switches from energy to storage metabolism, involving a transition from growth associated apoplastic cell-wall invertase (cwInv) to starch synthesis associated cytoplasmic sucrose-synthase (SuSy) mediated sucrose cleavage (Nazarian-Firouzabadi & Visser, 2017; Viola et al., 2001). Overall, these local and systemic changes over its lifecycle make potato an interesting model crop to investigate in terms of source-sink dynamics.

Competing reproductive sinks with intertwined developmental regulation

The developmental regulation of both sexual and asexual reproduction in potato is intertwined. The generally accepted molecular model of flower and tuber onset regulation revolves around the tuberigen *StSP6A*, and the florigen *StSP3D*, two FLOWERING LOCUS T (FT)-like proteins of the potato PHOSPHATIDYLETHANOLAMINE BINDING PROTEINS (PEBP) family (Navarro et al., 2011). *StSP6A*, and to a lesser extent *StSP3D*, are under the control of the photoperiodic pathway in potato leaves. Under long days this pathway blocks *StSP6A* production, and thus tuber onset, via *StSP5G*, *StCO* and *StCDF1* (Fig 1.1A, Abelenda et al., 2014; Kloosterman et al., 2013). Under tuber inductive short days, *StSP6A* is produced in the leaves and transported to stolons via the phloem where it initiates tuber onset (Fig 1.1B, Navarro et al., 2011) via the tuberigen activation complex (TAC), comprised of *StSP6A*, *St14-3-3s* and *StFDL1*. Interestingly, modern cultivars lost the dependency on day light through *StCDF1*, but kept *StSP6A* dependency, which made potato cultivation possible at higher latitudes (Kloosterman et al., 2013). *StSP3D* was identified

as the florigen in potato (Fig 1.1C, Navarro et al., 2011). *SP3D* is suggested to not be regulated by StCOL1 and is responsive to other environmental signals, such as high light (Plantenga, Bergonzi, Bachem, et al., 2019). More recent work has identified an additional role for *StSP3D* as a player in tuber onset in the absence of *StSP6A* by alternatively binding the TAC (Jing et al., 2023). Additionally, *StSP6A* was found to repress flower bud development (Plantenga, Bergonzi, Abelenda, et al., 2019), revealing a tight functional interplay between *StSP6A* and *StSP3D*. Besides these two important regulatory peptides, flowering and tuberization are also under control of environmental conditions (light intensity, temperature, drought), hormone levels and sucrose availability. For example, flowering is accelerated under high light conditions independent of *StSP3D* (Plantenga, Bergonzi, Bachem, et al., 2019), and increased sucrose export from leaves leads to earlier flowering as well as increased tuber size (Chincinska et al., 2008). Furthermore, tuberization also occurs in *StSP6A* knockdown plants (Navarro et al., 2011), suggesting that other known tuberization signals such as *StBEL5*, *StSP3D*, giberellin and sucrose play partly redundant roles (Fig 1.1B, Kondhare et al., 2020). Moreover, environmental conditions such as high temperature or nitrate inhibit tuber onset (Krauss, 1985). The general model proposed ~10 years ago discussed above thus seems somewhat oversimplified based on the most recent additions, nonetheless, it captures the basal dynamics around flower and tuber initiation under the control of the photoperiodic pathway.

A dual role for StSP6A via tuber onset initiation and radial efflux mitigation

Besides *StSP6A* initiating tuberization by activating tuber identity genes and thereby having a strong effect on whole plant sucrose allocation, it also binds to *StSWEET11*, a sucrose exporter located in the phloem. By doing this, an approximately 40% reduction of its sucrose transport capacity occurs (Abelenda et al., 2019). *In planta*, this interaction was shown to mitigate sucrose efflux from the phloem (Abelenda et al., 2019, Fig 1.1E). Consequently, *StSP6A* has a second role in modulating plant sugar status and allocation, thus impacting two instead of one key physiological process that influence source-sink dynamics (Fig 1.2), and as a result tuber growth 1) formation of strong sucrose sinks in the form of tubers (Fig. 1.1F) and 2) Long-Distance phloem transport (Fig. 1.1D,E).

Regulation of phloem sucrose in- and efflux is key to keeping the sucrose concentration gradient between source and sink tissues that is needed to drive water and sucrose flow (Minchin & Lacointe, 2017; Patrick et al., 2001). This is especially relevant during growth stages characterized by high sugar demand from strong sinks, such as the exponential tuber growth

phase. The leakage mitigation in the long-distance phloem facilitated by the *StSP6A-StSWEET11* interaction is hypothesized to increase sucrose delivery, and as a result tuber yield, by reducing sucrose efflux from the long-distance transport phloem (Abelenda et al., 2019). Concurrently with the induction of tuberization, a shift from apoplastic to symplastic unloading occurs, which is believed to enhance sugar delivery to the tubers (Viola et al., 2001). The *StSP6A-StSWEET11* interaction likely plays a role in reducing apoplastic unloading in tubers by decreasing the rate of active, *StSWEET11* mediated, apoplastic transport. By modulating these two physiological processes, *StSP6A* contributes to large changes in source-sink dynamics, via both the regulation of sugar transport and sink-dynamics.
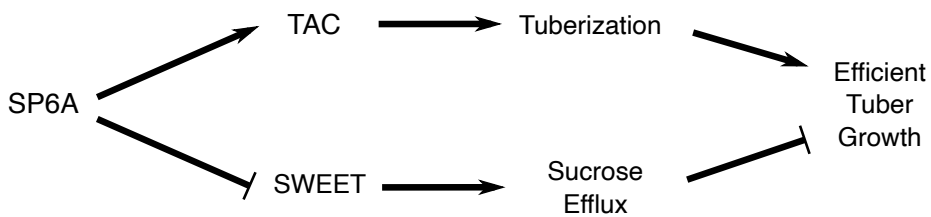
Figure 1.2. The dual role of SP6A and its hypothesized effect on tuber growth

Using models to study source-sink dynamics and the SP6A dual role

There is a long tradition in mechanistic modeling of plant physiology and sucrose transport, this history has been extensively reviewed by Prusinkiewicz (2004), Stirbet et al. (2020), Thompson & Holbrook (2003). Put simply, mathematical and computational models are invaluable in providing mechanistic understanding and predictive capacity when outcomes of biological processes depend on complex non-linear relationships and feedbacks between sub-processes playing out at various spatial and temporal scales (Prusinkiewicz, 2004).

Quantifying the precise contribution of *StSP6A*-driven processes to tuber yield is challenging experimentally. For example, measuring exact sucrose export rates and *StSP6A*-mediated reductions therein is currently impossible *in planta*. Furthermore, long-distance sucrose transport and sucrose unloading in the tuber are highly complex, multi-feedback biophysical processes. Long-distance phloem transport, as well as source- and sink-strengths all affect phloem sucrose concentration gradients, which in turn, affect phloem sap viscosity and pressure gradients, with these also determining phloem flow velocity, and providing feedback

into the sucrose concentration gradients. As a consequence, even if sucrose concentrations could be measured in a spatially resolved manner, this would not always answer whether this is a cause for or effect of changes in source, sink or long distance transport. On top of this, there is a hydraulic connection to surrounding tissues such as the xylem, further complicating matters. Unloading dynamics in sinks are boundary conditions for sucrose flow in the phloem, therefore the role of SP6A in the unloading switch in turn also influences the long-distance flow, and vice versa. Due to these complexities, mathematical modeling of water and sucrose transport in plants is an invaluable tool to unravel the effects of various aspects of sucrose transport on plant yield (Box 2, De Schepper & Steppe, 2010; Hölttä et al., 2006; Lacointe & Minchin, 2008; Mammeri & Sellier, 2017; Sevanto et al., 2011).

Unfortunately, there are currently no potato-specific models available to address these questions. There are large-scale agronomic models specific to potatoes that can predict field-level yields based on experimentally derived partitioning coefficients to determine sucrose distribution among sinks (ten Den et al., 2022). These models are applied to forecast crop yield in in real-time, and are used for precision farming applications. Comparing model simulations with the current state of the crop in the field could potentially identify yield gaps and inform crop management decisions (de Wit et al., 2019). However, these models do not provide insights into the mechanistic basis of sucrose partitioning between plant organs or incorporate the influence of signaling pathways, such as SP6A. Furthermore, they strongly rely on large scale datasets, which poses a large bottleneck (Corcoran et al., 2023). More detailed models, though not specific to potatoes, exist for describing individual plant performance based on plant physiology and architecture. Functional-Structural Plant Models (FSPMs) are computational models that aim to simulate the interactions between a plant's structure and its physiological functions. In FSPMs, structural representation is combined with mathematical equations that describe the physiological processes occurring within the plant, such as photosynthesis, respiration, nutrient uptake, and water and sucrose transport. Using these models, studies on the effect of architecture on water uptake (Schnepf et al., 2023), light intensity and competitive shading on photosynthesis (Sarlikioti et al., 2011) have been done. In theory, these models can be expanded to incorporate biophysically realistic growth, sugar transport and allocation, however, technically, this is still very difficult to achieve due to computational complications and the complexity of both architectural and biophysically realistic models in isolation alone (Seleznyova & Hanan, 2018). As a consequence, most current FSPMs typically assume that relative sink strength determines sucrose partitioning (Da Silva et al., 2011; de Vries et al.,

1

2021; Lescourret et al., 2011). These models implicitly assume that source and sink properties dominate over transport properties, which has been shown to be incorrect under some conditions (Pallas et al., 2010). Less structurally detailed, but biophysically detailed transport models depict sucrose and water transport as convective flows driven by osmotic pressure gradients. These models have predominantly focused on single-source, single-sink systems, such as isolated leaves and sinks (Hölttä et al., 2006; Minchin & Lacointe, 2017; Thompson & Holbrook, 2003), yet have demonstrated the importance of transport pathway properties. Consequently, there is a need for models that account for the biophysical details of both long distance phloem transport, its coupling to xylem dynamics and sink dynamics while being tailored to the specific characteristics of potato, and considering relevant aspects at both the whole plant and individual tuber level.

In this thesis

The general aim of this thesis is to better understand the effect of the dual role of *SP6A* on source-sink dynamics, especially on the efficiency of sucrose transport towards and unloading in tubers and its effect on tuber development, growth, and yield. We aim to achieve this by developing models to connect the changes in sink-dynamics caused by the development of tubers to changes in long-distance transport and source and sink dynamics in the whole plant perspective.

We first need an appropriate, potato-specific, model to investigate how *SP6A* affects transport efficiency. In **chapter 2** we set out to develop a single-sink mechanistic model for biophysical water and sucrose transport. As a starting point we used models for larger species, such as trees, that are typically applied to answer fundamental questions on the theoretical boundaries of long distance water and sucrose flow in plants. To parametrize the model for potato we used experimental observations on plant architecture, phloem geometry and general (bio) physical constants. The model further incorporates SWEET-mediated sucrose export and the SP6A-SWEET11 interaction. With this model we set out to substantiate the impact of efflux reduction in the highly complex biophysical background of the phloem and xylem. In **chapter 3** we extended the developed model to a two-sink model with the possibility to vary plant architecture (pathway length, xylem flow) and sink-properties (strength, affinity). The non-linear interplay between sink and transport pathway characteristics makes it difficult to assess the effect on sink resource allocation. Therefore, we set out to first mechanistically describe the relevance of plant architecture and physiology on sucrose allocation. With the model, we

then set out to understand how it is possible that SP6A seems to specifically benefit tuber growth. Mechanistically, a biased insertion of the signal only into phloem conduits directed towards tubers is hard to imagine as this would require upfront knowledge on the direction of these conduits, suggesting the specific enhancement of tuber yield must arise differently. We investigated this in a leaf-tuber-developing leaf case study to see if emergent properties in the transport pathway could lead to a preferential effect of SP6A to benefit tubers over other sink organs.

An often-made claim, taken as an assumption in the models developed in Chapters 2 and 3, is that upon tuber formation, the sink-strength of the organ greatly increases (Fernie et al., 2020). Additionally, it is generally assumed that passive, symplastic unloading is one or a few orders of magnitude more efficient than apoplastic unloading. The transition from apoplastic to symplastic unloading upon tuber formation is thus assumed to drive the increase in sink strength. In **chapter 4** we investigate how the increased sink-strength of a tuber is realized. We do this via a combined bioinformatics and modeling approach, focusing on the interplay between metabolic changes and unloading mode. Finally, the lack of a comprehensive, quantitative dataset on potato growth and sucrose dynamics over the course of development complicated extending the above modeling efforts to the entire potato lifecycle. In **chapter 5** we therefore generated such a dataset, and used the obtained data to put our previous results into perspective. We made a shift from the isolated, and theoretical, effects of long-distance transport and local unloading to the plant-level effect of SP6A and SP3D on sucrose competition between shoot and tubers. The data obtained showed a correlation in timing of tuber onset and leaf senescence. We used simple models to enhance our understanding of the experimentally observed role for SP6A in tuber synchronization and post-tuberization senescence. We investigated the putative presence of shared regulation in senescence and tuber onset, or the possibility of emergent behavior due to resource competition. **Chapter 6** then concludes the thesis by discussing and combining the main findings and highlighting promising directions for future research.

1

Box 2: Modeling water and sucrose transport in plants

In general, coupled xylem-phloem models explicitly describe water and solute flow in the phloem and water flow in the xylem via the Hagen-Poiseuille equations, or the functionally very similar Darcy-Weisbach equation. It is thus assumed that the phloem flow is fully developed (constant velocity profile), there is no radial flow and the flow is axisymmetric. The Hagen-Poiseuille equation decribes water flow (Q) as a function of the phloem/xylem radius (r), length (L), sap viscosity (η) and pressure gradient (ΔP), or ,in case of the Darcy-Weisbach equation, phloem/xylem area (A), hydraulic conductivity (k), length, and pressure gradient:

In the xylem typically the presence of solutes is ignored and the boundary conditions (transpiration rate/air water potential and soil water potential), together with the radial water exchange with the phloem determine the pressure gradient. In the phloem the pressure difference is the result of non-linear feedback between osmotic potential (van 't Hoff equation), sap viscosity (linear or non-linear function), conduit architecture and the boundary conditions (sucrose loading and unloading rate).

$$Q = \frac{\pi r^4 \Delta P}{8 \eta L} = \frac{Ak}{\eta} \cdot \frac{\Delta P}{L}$$

Water exchange between the xylem and phloem is typically modeled in a simplified manner as a water potential driven water flux over a semi-permeable membrane without describing the details of symplastic and apoplastic transport components. Generally, transport of sucrose from the phloem and apoplast into the xylem is ignored as limited data are available on the active sucrose uptake by tissues neighboring and symplastically connected to the xylem. Radial sucrose exchange between the phloem and the apoplast is included as SWEET and SUT-mediated sucrose transport described by Michaelis-Menten kinetics.

Chapter 2

Modeling the physiological relevance of sucrose export repression by an FT-homolog in the long-distance phloem of potato

Bas van den Herik, Sara Bergonzi, Christian W.B. Bachem, Kirsten ten Tusscher

Abstract

Yield of harvestable plant organs depends on photosynthetic assimilate production in source leaves, long-distance sucrose transport and sink-strength. While photosynthesis optimization has received considerable interest for optimizing plant yield, the potential for improving long-distance sucrose transport has received far less attention. Interestingly, a recent potato study demonstrates that the tuberigen StSP6A binds to and reduces activity of the StSWEET11 sucrose exporter. While the study suggested that reducing phloem sucrose efflux may enhance tuber yield, the precise mechanism and physiological relevance of this effect remained an open question. Here we develop the first mechanistic model for sucrose transport, parameterized for potato plants. The model incorporates SWEET-mediated sucrose export, SUT-mediated sucrose retrieval from the apoplast and StSP6A-StSWEET11 interactions. Using this model, we were able to substantiate the physiological relevance of the StSP6A-StSWEET11 interaction in the long-distance phloem for potato tuber yield, as well as to show the non-linear nature of this effect.

Introduction

Sucrose availability is a major determinant of plant organ growth and hence yield of harvestable crop organs, such as fruits, seeds, roots and tubers. Therefore, considerable research effort has been and is directed towards optimizing photosynthesis efficiency, and this has led to spectacular yield improvements in some crop species (Driever et al., 2017; Nölke et al., 2014). However, plant growth and yield ultimately depend on the amount of sucrose delivered to sink organs per unit of time. Photosynthate availability in source-leaves is thus not the only factor influencing yield, and long-distance transport, sink unloading mechanism and sink-strength also impact the final crop yield (Fernie et al., 2020). Indeed, it has been previously shown that coordinated regulation of source and sink strengths has a major impact on plant yield (Jonik et al., 2012).

Predicting the effect of photosynthate availability, sink-strength and long-distance phloem transport characteristics on plant yield is far from trivial. Similar sized improvements in photosynthesis efficiency may have variable effects on yield in different species due to different feedback regulations or differences in limiting factors (Fernie et al., 2020). Furthermore, sucrose transport is a highly complex, multi-feedback biophysical process, with source- and sink-strengths affecting phloem sucrose concentration gradients, which in turn, affect phloem sap viscosity and pressure gradients, with these also determining phloem flow velocity, and providing feedback into the sucrose concentration gradients. Although the xylem-mediated upward transport of water and mineral nutrients occurs through a distinct, transpiration induced pressure gradient, phloem and xylem water flows are hydraulically coupled, giving rise to additional feedbacks on phloem transport. Due to these complexities, mathematical modeling is an invaluable tool to unravel the effects of various aspects of sucrose transport on plant yield (De Schepper & Steppe, 2010; Hölttä et al., 2006; Lacointe & Minchin, 2008; Sellier & Mammeri, 2019; Sevanto et al., 2011). So far mathematical models have primarily been restricted to large plants and trees (>5m stem, Table S1). A first major goal of this study is therefore to develop a quantitative model for sucrose transport for an agronomically relevant crop species, potato, with source-sink distances of maximum 1.5m.

In addition to the long-distance convective transport of sucrose through the phloem from source to sink tissues, an exchange of sucrose between the phloem and the surrounding tissues also takes place. Export of phloem sucrose into the apoplast is mediated by so-called

SWEET transporters, which facilitate gradient-dependent bidirectional transport (Chen et al., 2012). Therefore, SWEET mediated sucrose transport depends on phloem and apoplast sucrose levels. Besides SWEETs, the SUT/SUC sucrose importers are expressed in the phloem (Hafke et al., 2005). These importers enable sucrose retrieval from the apoplast, thereby reducing net phloem sucrose loss (Minchin & Lacointe, 2017). Interestingly, in a recent study we showed that in heterologous expression experiments StSWEET11, an important potato phloem sucrose exporter, is bound by StSP6A, resulting in an approximately 40% reduction of its sucrose transport capacity (Abelenda et al., 2019). StSP6A is the tuberigen known to induce the developmental transition to tuber formation and enhancement of potato yield in greenhouse pot experiments (Navarro et al., 2011). These results suggest that, in addition to their potential role in the switch from apoplastic to symplastic unloading in the stolon (Abelenda et al., 2019), the StSP6A-StSWEET11 interaction increases yield by reducing sucrose efflux from the long-distance transport phloem. Although representing a plausible scenario, data from a transcriptomics analysis indicates that StSP6A also has a substantial effect on the expression of many other genes (Navarro et al., 2011). Thus, the observed StSP6A mediated enhancement of potato yield may not necessarily or solely arise from StSP6A induced reduction of StSWEET11 sucrose transport. Experimentally, these different contributions of StSP6A to yield improvement are not easy to tease apart. Moreover, quantifying SWEET sucrose export and StSP6A mediated reductions therein is difficult *in planta*. Therefore, a second major goal of this study is to use our model to study the potential physiological relevance of StSP6A mediated reduction of StSWEET11 sucrose export on potato yield.

To this end, we here develop the first quantitative, mechanistic model for sucrose transport in the stem of potato plants. The model is based on the well-established phloem and xylem transport models by Hölttä et al. (2006), Lacointe & Minchin (2008) and Thompson & Holbrook (2003), that we have fully re-parameterized to potato specific conditions. Using our model, we find that in potato, sucrose transport is dictated by viscous forces rather than sieve tube geometry. Next, we incorporated SWEET-mediated sucrose efflux, enabling us to estimate *in planta* SWEET transport rates necessary to reproduce physiologically relevant sucrose efflux, a value that cannot be easily extrapolated from available heterologous expression experimental data. Subsequently we extended the model with SUT-mediated sucrose retrieval. To arrive at realistic temporal dynamics for phloem and apoplast sucrose levels, we improved upon existing models incorporating efflux and retrieval dynamics (Cabrita et al., 2013; Minchin & Lacointe, 2017), incorporating realistic apoplast volumes as well as apoplast sucrose export

to neighboring tissues. As a final step we incorporated the StSP6A mediated 40% reduction of StSWEET11 mediated sucrose export. Our model confirms the physiological significance of StSP6A mediated StSWEET11 blockage when physiologically relevant StSWEET11 transport rates are assumed. Furthermore, we find that, as a result of the non-linearities and feedbacks present in sucrose transport a 40% reduction in StSWEET11 mediated-efflux results in a greater increase in sucrose retention, i.e. a larger than 40% reduction of yield loss.

Methods

We here provide a concise description of the model structure, assumptions, equations, and implementation. A more detailed version of the methods is provided in the supplementary materials.

Model structure and main assumptions

We used the well-established model for phloem transport by Thompson & Holbrook (2003) and coupled phloem-xylem transport (Hölttä et al., 2006; Lacointe & Minchin, 2008) as a starting point (Table S2.1). Our model includes phloem (Ph), xylem (X) and apoplast (A) longitudinal compartments. Within these compartments, three variables were defined, water mass (W) in g, pressure (P) in MPa, and sucrose (S) in mol. Compartment volume (V) and sucrose concentration (C) were derived from the water mass and sucrose amount (Table 2.1). The stem was divided into three zones; loading zone, unloading zone and long-distance pathway (Van Bel, 2003), and discretized into N, cylindrical, elements (Figure 2.1A). The location (along the stem) and compartment type (phloem, xylem, apoplast) of the variables are notated using subscripts: $Var_{comp,j}$ in which comp represents the compartment and j the element position.

The model explicitly describes water and solute flow in the phloem, water flow in the xylem, SWEET and SUT mediated sucrose exchange between the phloem and the apoplast, and water exchange between the xylem and phloem. Water flow in the xylem is driven by water transpiration in the topmost element as described by the cohesion-tension theory, while phloem water flow is driven by a hydrostatic pressure gradient induced by sucrose loading and unloading as described by the Münch-hypothesis. Water exchange between phloem and xylem is modeled in a simplified manner as a water potential driven water flux over a semi-permeable membrane (Eq. 3), without describing the details of symplastic and apoplastic transport components. Inherent to this simplified description in which water dynamics in the

apoplast are ignored is the assumption that apoplastic water volume stays constant (implying non-growth conditions), and that no axial flow occurs in the apoplastic space. Importantly, this axial apoplastic water flow is considered far less efficient than phloem bulk flow, making this an acceptable approximation. Radial transport of sucrose from the phloem and apoplast to the xylem is also ignored as limited data is available on the active sucrose uptake by tissues neighboring and symplastically connected to the xylem. Available data suggest that imported sucrose serves to fuel secondary cell wall thickening and other local processes rather than long-distance xylem transport (Aubry et al., 2019). This results in relatively minor xylem sucrose levels that can be ignored for the purposes of this study, as has been done in previous modeling work (Holtta et al. 2006; de Schepper & Steppe, 2010). These assumptions are further supported by the low concentrations of sucrose in xylem fluid measurements (Pagliarani et al., 2019; Secchi & Zwieniecki, 2016). Further, we did not include the potential presence of a radial sucrose gradient in the apoplastic compartment as assuming a gradient would enhance sucrose levels next to the phloem while decreasing from sucrose levels away from the phloem. Consequently, sucrose retrieval efficiency from the apoplast to the phloem would be enhanced due to a gradient, and our simulations represent a worst-case scenario.

2

Table 2.1. *Symbols and units for the used variables in the model*

Variable	*Symbol*	*Units*
Water mass	W	g
Sucrose	S	mol
Pressure	P	MPa
Volume	V	m^3
Sucrose concentration	C	mol/m^3
Axial water flow	$J_{W,ax,in/out,Ph/X,j}$	g/s
Axial sucrose flow	$J_{S,ax,in/out,Ph/X,j}$	mol/s
Radial water flow	$J_{W,rad,in/out,Ph/X,j}$	g/s
Radial sucrose flow	$J_{S,rad,in/out,Ph/X,j}$	mol/s
Water potential	$\Phi_{Ph/X,j}$	MPa
Axial area	$A_{Ph/X,j}$	m^2
Radial area	$A_{rad,j}$	m^2
Osmotic potential	$\Pi_{X,j}$	MPa
Dynamic viscosity	$\mu_{Ph,j}$	MPa/s
Sucrose loading	$L_{Ph,j}$	mol/s
Sucrose unloading	$U_{Ph,j}$	mol/s
Sucrose efflux/retrieval	$E_{Ph,j}$	mol/s
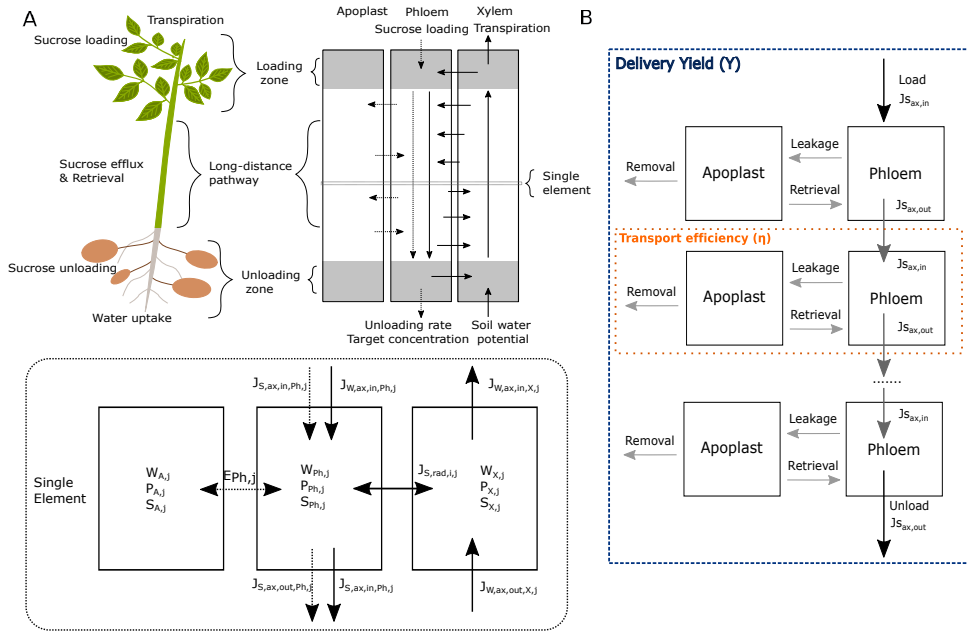
Figure 2.1. Overview of the model architecture, processes and yield/efficiency. A) Modeled processes and localization in the plant are depicted left, A schematic, longitudinal model overview with the loading and unloading zones indicated in grey is shown on the right, water flow is depicted with solid arrows and sucrose flow with dotted arrows. The xylem and phloem boundary conditions at the top and bottom are shown. On the bottom, a zoom-in on a single element, consisting of neighboring phloem, xylem and apoplast compartments. Depicted are the in- and outflow of water and sucrose as well as the variables included in a single element (j). B) Transport efficiency and delivery yield (Eq. 14 & 15). Delivery yield is calculated over the complete system (dashed line), whereas the transport efficiency is calculated per element (dotted line).

Model equations

Water & Pressure

Water transport in the stem is described using the following system of equations:

$$\frac{\partial W_{\frac{Ph}{X},j}}{\partial t} = \left(J_{W,ax,in,\frac{Ph}{X},j} - J_{W,ax,out,\frac{Ph}{X},j} + J_{W,rad,in,\frac{Ph}{X},j} - J_{W,rad,out,\frac{Ph}{X},j} \right) \rho \qquad \text{(eq. 1)}$$

$$J_{W,\frac{Ph}{X},j,ax} = A_{i,j} \frac{k_{i,j}}{\mu_{i,j}} \frac{\partial P_{\frac{Ph}{X},j}}{\partial x} = A_{\frac{Ph}{X},j} \frac{k_{\frac{Ph}{X},j}}{\mu_{\frac{Ph}{X},j}} \frac{P_{\frac{Ph}{X},j-1} - P_{\frac{Ph}{X},j}}{x} \qquad \text{(eq. 2)}$$

$$J_{W,rad,in,Ph,j} = L_r A_{rad,j} \left(\Psi_{X,j} - \Psi_{Ph,j} \right) \qquad \text{(eq. 3)}$$

$$\Pi_{Ph,j} = - \rho RT \left(0.998 m_{Ph,j} + 0.089 m_{Ph,j}^2 \right) \text{ with } m_{Ph,j} = \frac{C_{Ph,j}}{\rho \left(1 - C_{Ph,j} V_{suc} \right)} \qquad \text{(eq. 4, Michel, 1972)}$$

$$\mu_{Ph,j} = \mu_X exp \left(\frac{4.68 * 0.956 \phi_{Ph,j}}{1 - 0.956 \phi_{Ph,j}} \right) \text{ with } \phi_{Ph,j} = \frac{V_{suc} S_{Ph,i}}{V_{suc} S_{Ph,i} + V_{Ph,i}} \qquad \text{(eq. 5, Morison, 2002)}$$

$$\frac{\partial P_{\frac{Ph}{X},j}}{\partial t} = \epsilon_{\frac{Ph}{X},j} \frac{1}{W_{\frac{Ph}{X},j}} \frac{\partial W_{\frac{Ph}{X},j}}{\partial t} \qquad \text{(eq. 6)}$$

$$A_{Ph,j} = A_0 e^{\frac{\left(P_{Ph,j} - P_0 \right)}{\epsilon_{Ph,j}}} \qquad \text{(eq. 7, Thompson & Holbrook, 2003)}$$

with $J_{W,ax,in,Ph/X,j}$ axial water inflow and $J_{W,rad,in,Ph/X,j}$ radial water inflow, $\psi_{Ph/X,j}$ water potential, $\Pi_{Ph,j}$ phloem osmotic potential, $\mu_{Ph,j}$ phloem sap viscosity and $A_{Ph/X,j}$ axial area. All variables are defined in table 2.1, while parameters are described in table 2.2. The axial outflow rate is set equal to the inflow rate of the element below, similarly the radial inflow rate in the phloem is set equal to the outflow rate of the xylem. As boundary conditions in the phloem we set the respective inflow and outflow equal to zero. For the boundaries in the xylem we applied measured water transpiration and soil water potential.

Sucrose

Sucrose transport is described using the following set of equations:

$$\frac{\partial S_{Ph,j}}{\partial t} = J_{S,ax,in,Ph,j} - J_{S,ax,out,Ph,j} - J_{S,Rad,Ph,j} \qquad \text{(eq. 8)}$$

$$J_{S,ax,in,Ph,j} = J_{W,ax,in,Ph,j} * C_{Ph,j-1} \qquad \text{(eq. 9)}$$

$$J_{S,rad,Ph,j} = L_{Ph,j} - U_{Ph,j} - E_{Ph,j} \qquad \text{(eq. 10)}$$

$$U_{Ph,j} = v_{unload} * \left(C_{Ph,j} - C_{target} \right) \qquad \text{(eq. 11)}$$

$$E_{Ph,j} = v_{MaxSWEET} V_{Ph,j} \frac{C_{Ph,j}}{C_{Ph,j}+K_{mIn}} - v_{MaxSWEET} V_{Ph,j} \frac{C_{A,j}}{C_{A,j}+K_{mEx}} - v_{MaxSUC} V_{Ph,j} \frac{C_{A,j}}{C_{A,j}+K_{mSUC}} \qquad \text{(eq. 12)}$$

$$\frac{dS_{A,j}}{dt} = E_{Ph,j} - v_{resp} \frac{C_{A,j}}{C_{A,j}+K_{mR}} \qquad \text{(eq. 13)}$$

With $J_{S,ax,in,Ph,j}$ axial sucrose inflow, sucrose outflow is set equal to sucrose inflow of the element below, equal to the approach taken for water flow. $J_{S,rad,Ph,j}$ radial sucrose transport, consisting of a constant uptake at the loading zone ($L_{Ph,j}$), concentration dependent loss at the unloading zone ($U_{Ph,j}$) and SWEET-mediated bi-directional exchange with- and SUC-mediated retrieval from the apoplast along the long-distance pathway ($E_{Ph,j}$). We observed that increasing loading rate, i.e. increasing photosynthetic efficiency, enhances sucrose delivery (Figure S2.1). For loading rates beyond a factor 2.5x the standard loading rate, a viscosity induced increase in resistance resulted in non-physiologically realistic high sucrose concentrations, pressure and flow velocities. *In planta*, this regime is likely prevented by feedback regulation on sucrose import, photosynthesis and sink strength, absent in our current model. Further note that through maintaining a constant target tuber concentration (C_{target}) and employing a high unloading rate (v_{unload}), our model system is in a non sink-limited regime (Figure S2.1). This enables us to focus on the impact of changes in long-distance phloem transport on tuber sucrose delivery.

Defining transport efficiency and delivery yield

Since we are interested in the effects of efflux and retrieval on potato tuber formation, we define two quantification measures (Figure 2.1B). To quantify the effect of sucrose efflux and retrieval along the stem we introduce the measure of transport efficiency (η). We define it as the ratio of sucrose output over sucrose input per element, which for steady-state simplifies to the ratio of axial outflow over inflow:

$$\eta = \frac{outflow}{inflow} = \frac{J_{S,ax,out,Ph,j}}{J_{S,ax,in,Ph,j}}$$
(eq. 14)

A 100% transport efficiency implies that all sucrose received from a shootward oriented phloem element is passed on by the current element to its rootward element, lower transport efficiencies indicate sucrose loss. To measure the effective supply of sucrose to the tubers and compare between different simulations we introduce the measure of delivery yield (Y), which we define as the ratio of the amount of sucrose unloaded over the amount loaded in a given time interval (ranging from t_0 to t_{end}, by default over a 24h period starting after steady-state was reached):

$$Y = \frac{\sum\limits_{j=1}^{N} \int\limits_{t_0}^{t_{end}} \left(U_{Ph,j}\right)}{\sum\limits_{j=1}^{N} \int\limits_{t_0}^{t_{end}} \left(L_{Ph,j}\right)}$$
(eq. 15)

Model parameters, implementation and simulations

An extensive description of how parameter values were derived can be found in the supplemental methods. The system of differential equations was implemented in MatlabR2019b and was solved using the build-in solver ode15s, using an integration time step of Δt=1s. All simulations were started from zero initial pressure and sucrose. The initial element water mass was calculated from the model dimensions, resulting in an initial water mass per element of 5.9e-4g in the phloem loading/unloading zones, 1.1e-4g in the phloem long-distance zone, 2.1e-3g in the xylem loading/unloading zones and 1.1e-2g in the xylem long distance zone. The modeled plant stem was spatially discretized using a non-homogeneous mesh with 20 elements with a fine-grained spatial resolution of x=0.005m in the loading and unloading zone and 30 elements with a coarse-grained spatial resolution of x=0.0267m in the long-distance pathway. The non-homogeneous discretization mesh allowed for a reduction in the number of elements used in the long-distance zone without sacrificing resolution in the loading and unloading zones where high precision is needed due to steep gradients in sucrose as a result of sucrose loading and

unloading and resulting enhanced lateral water fluxes. This approach reduced simulation time without significantly affecting model outcomes (Figure S2.2). The source code used for model simulations is available on: http://www-binf.bio.uu.nl/khwjtuss/PotatoSucroseTransport.

Results

A baseline potato-specific transport model

To test the validity of the developed model we benchmarked it against the main results from Thompson & Holbrook (2003) using identical parameter settings (Table 2.2). Model outcomes are quantitatively highly similar (Figure S2.3, Table S2.2), the observed small differences may arise from differences in model implementation details (e.g. used numerical solver) as earlier discussed by Mammeri and Sellier (2017). Adding a non-zero xylem potential resulted in decreased phloem volume (2.1%) and water flow (6.4%), increased sucrose concentration

Table 2.2. Parameters for the Thompson & Holbrook (2003) and the potato-specific model

| Parameters	Symbol	Thompson and Holbrook	Potato	Units	References potato parameters
Density of water	ρ	0.998e6		g/m^3	-
Partial molal volume sucrose	V_{suc}	0.2155e-3		m^3/mol	-
Gas constant	R	8.314e-6		MPa m^3 / K/mol	-
Temperature	T	293		K	-
Radial hydraulic membrane permeability	L_r	5e-8		m/Mpa/s	-
Dynamic viscosity water/xylem	μ_x	1.0019e-9		MPa/s	-
Stem length	I	5	1	m	Vos & van der Putten (1998)
Phloem sieve element radius	r_p	7.5e-6 at t=0	8.4e-6 (10.7e-6 before tuning) at t=0	m	Aliche et al. (2020) Mullendore et al. (2010)

Table 2.2. Parameters for the Thompson & Holbrook (2003) and the potato-specific model (continued)

Parameters	Symbol	Thompson and Holbrook	Potato	Units	References potato parameters
Xylem conduit radius	r_x	-	30e-6	m	Aliche et al. (2020)
Axial permeability phloem	K_p	0.928e-12	3.82e-12	m^2	Mullendore et al. (2010)
Elastic modulus phloem	ε_p	17	30	MPa	Nobel (2005)
Elastic modulus xylem	ε_p	-	750	MPa	Irvine & Grace (1997)
Transpiration rate	J_{trans}	-	0.02	g/s	Schans & Arntzen (1991)
Water potential soil	Ψ_{soil}	-	0	MPa	Perämäki et al. (2001)
Sucrose loading rate	v_{load}	7.95e-11 (mol/m/s)	1e-8 (mol/s)	-	Derived from: Pourazari et al. (2018) Zeeman et al. (2010) Zheng et al. (2016)
Unloading rate	v_{unload}	v_load (mol/m/s)	0.5e-10 (m3/s)	-	-
Boundary concentration unloading zone	C_{target}	500	50	mol/m^3	Derived from: Bethke et al. (2009) Duarte-Delgado et al. (2016) Leggewie et al. (2003) Ross & Davies, (1992)
Number of phloem sieve elements	E_{phloem}	-	100	-	Derived from: Aliche et al. (2020) Hölttä et al. (2009) Sibout et al. (2008)
Number of xylem conduits	E_{xylem}	-	150	-	Aliche et al. (2020)
Max. apoplast removal rate	R_{max}	-	0.4e-8	mol/s	Estimated
Affinity constant removal	$K_{m,R}$	-	5	mol/m^3	Estimated

(6.9%) and a small decrease in pressure gradient (-0.5%) (Figure S2.3, Table S2.2), consistent with earlier work (De Schepper & Steppe, 2010; Hölttä et al., 2006; Sevanto et al., 2011). Further, when simulating nighttime (switching off transpiration), Münch-counterflow equal to phloem flow was observed in the xylem, as observed earlier (De Schepper & Steppe, 2010; Hölttä et al., 2006).

After this validation we transformed the model to potato specific parameters, assuming a stem-length of 1m, with loading and unloading zones of 0.1m. We incorporated plant architectural and mechanical data on stem length, phloem and xylem characteristics (conduit radius, abundance and resistance, elastic modulus). Parameter values are provided in Table 2 and their detailed derivation in the supplementary methods section. Changing the stem length within the expected variation, e.g. 0.5-1.5m, did not qualitatively alter the outcomes and only had a minor impact on the transport characteristics (supplemental figure 2.4). An important difference between potato and previously modeled plants was the higher axial permeability in the phloem, which results from differences in sieve-element and sieve-plate architecture (Mullendore et al., 2010). We derived a potato-specific lower limit for the phloem sucrose loading rate of 1e-8 mol/s, which is of the same order of magnitude as values used in previous studies when scaling these to the dimensions of our potato model (0.59e-8 mol/s for Thompson & Holbrook (2003) and 6.24e-8 mol/s for Hölttä et al. (2006). Our initial parameter settings resulted in a steady-state flow velocity in the base of the stem of 0.23 mm/s, which is in the same order of magnitude as the 0.34 mm/s measured in potato (Aliche et al., 2020; Prusova, 2016). Given that sieve tube radius data were taken from tomato rather than potato, we decreased sieve tube radius by 21.5.% to 8.4e-6m to reproduce the measured potato sap flow velocity of 0.34 mm/s, equal to a transit time of 49 minutes. In Figure 2.2 we show, starting from all zero initial conditions, the temporal dynamics (insets) and resulting steady-state gradients for the potato-specific model. Xylem pressure reached its steady-state almost instantly, much faster than the phloem, that reached steady-state in 3.9h. In steady-state, the model generated sucrose concentrations of 1.69M at the loading zone, 1.23M at the middle of the stem, and 1.17M at the start of the unloading zone, resulting in a sucrose gradient of 0.46M/m$_{length}$ between the end of the loading zone and the beginning of the unloading zone. While no experimental data on potato sucrose gradients in the phloem was available, sucrose concentrations range from 1.35M (Kehr et al., 1998) to 1.8M (Pescod et al., 2007) in leaf phloem, indicating that our model lies well within the range of physiologically realistic values. As a further support of our model, a theoretical study by Jensen et al. (2013) demonstrated that the optimal concentration of sucrose for

efficient transport is 1.01M, close to our observed values. Additionally, they reported potato as the species with the highest phloem sucrose concentration in their review of 41 different species. Simulated steady-state turgor pressure in the middle of the stem was 3.8MPa (closely matching the osmotic pressure of 4.1MPa). Again, no data on potato phloem pressure was available, however pressure measurements in other plants range from 0.6-2.4MPa (D. B. Fisher
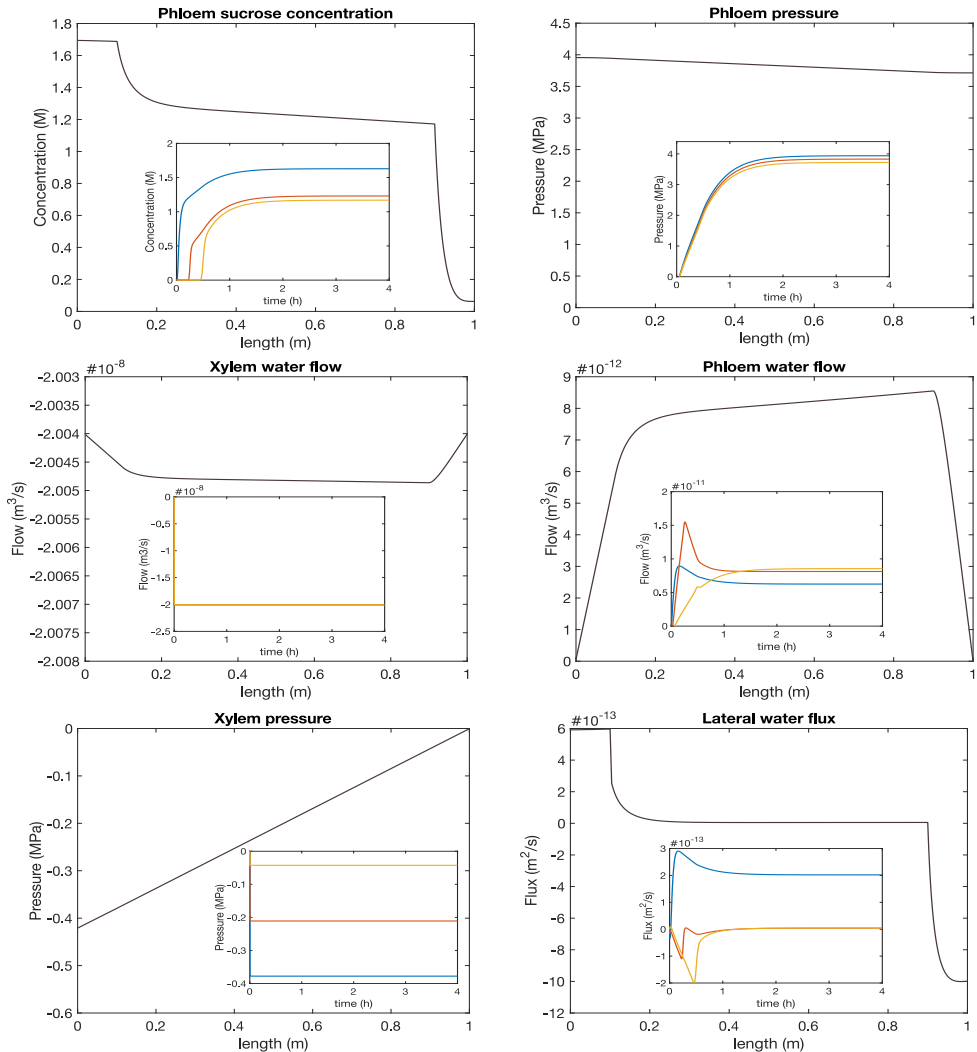
Figure 2.2. Gradients and dynamics of the baseline potato-specific model. The figures show the steady-state gradient over the length of the stem. The insets show the dynamics towards the steady-state, where the blue line is the top element of the long distance pathway, red the middle element and yellow the bottom element.

& Cash-Clark, 2000; Turgeon, 2010). In wheat (*Triticum aestivum*), in which the highest phloem pressure was measured, sucrose concentrations ranged from 0.25M (Hayashi & Chino, 1986) to 0.51M (D. Fisher & Gifford, 1987). The steady-state pressure gradient generated by the model is 0.2Mpa/m, in the upper end of the range of experimentally observed pressure gradients (0.03-0.2Mpa/m; Hammel, 1968). Overall, the high hydrostatic pressure is in line with reports of steeper pressure gradients in herbaceous species and active loaders (Comtet et al., 2017), and the higher sucrose concentration in crop species (Jensen et al., 2013).

Despite the high axial permeability in potato and the here observed high hydrostatic pressure, sap flow velocity did not exceed previously reported values (Hölttä et al., 2006; Thompson & Holbrook, 2003; Windt et al., 2006), as one may naively expected from combining these two factors. Instead, the high sucrose concentration resulted in high viscosity and hence a high transport resistance.

Effect of SWEET-mediated efflux on transport characteristics

Variation in SWEET v_{max}

We next set out to study the potential effects of StSWEET11-mediated sucrose efflux from the phloem on transport characteristics. We started with a worst-case scenario, in which we ignored SUT-mediated retrieval from the apoplast, enabling us to explore the maximum effect on sucrose transport. SWEET-mediated sucrose transport has been experimentally quantified, but available data was restricted to non-potato SWEETs of different types (AtSWEET12, and VvSWEET7, Table S2.3). Experimental characterizations of SWEET transport are performed in heterologous expression systems, with expression levels and presence of co-factors likely different from the *in planta* conditions, suggesting that particularly measured v_{max} values should be treated with caution when extrapolating them to *in planta* transport. Indeed, reported values ranged from 0.0012 (Chen et al., 2012) to 0.148 mol/m³/s (Breia et al., 2020). Therefore, we first explored a broad range of v_{max} values (such that over the entire stem length it equals 0 to 100% of the total loading rate with a K_m of 10mM) and quantified the effect and physiological significance on sucrose delivery. Simulated steady-state gradients for different export rates (Figures 2.3A-B, S2.5) were qualitatively similar to the results of Minchin & Lacointe (2017). Below efflux rates of 5% of the baseline loading rate the effect of efflux along the stem was very small, and concentration and pressure gradients, as well as axial and lateral water flow decreased by less than 2%. At efflux rates of 10% the difference became more pronounced

(Figure 2.3A-B, orange line) with concentration and pressure gradients decreasing 5%, this decrease increased linearly with increasing export rate. In this efflux-only scenario, delivery yield (Figure 2.1B) linearly decreased with efflux rate (Figure 2.3C). In line with the decreased sucrose concentrations resulting from efflux, we observed a substantial decrease in hydrostatic pressure levels, whereas the pressure gradient itself was much less affected. Finally, for efflux rates beyond 0.25x the baseline loading rate, the water flow velocity profile inverted, with higher flow rates at the top of the stem and decreasing along the stem, similarly to the results of Minchin & Lacointe (2017) (Figure 2.3B). Our broad exploration of efflux rates thus indicates that these rates must amount to a minimum of 5-10% of the solute loading rate to result in significant differences in transport characteristics and efficiency.

We then implemented the range of experimentally reported v_{max} values in our model (Figure 2.3A-B green, light blue, red lines; Figure 2.3C, orange dots). The lower bound AtSWEET12 transport rate resulted in a decrease in sucrose delivery of 0.2% compared to the baseline, no-efflux model, whereas the reported upper rate resulted in a 2.4% decrease. Implementation of the VvSWEET7 transport rate resulted in a 28.9% decrease in sucrose delivery and strongly changed transport dynamics (Figure 2.3A-B, red line). Thus, only the transport rate reported for VvSWEET7 significantly affected sucrose transport. Transport rates of VvSWEET7 and AtSWEET12 may differ due to structural differences at protein level, but differences in experimental conditions in the heterologous expression system are likely to also have contributed significantly. Based on the observation that stem apoplastic sucrose concentration is 61% lowered for knockout of StSWEET11 and 278% increased for up-regulation of StSWEET11 (Abelenda et al., 2019), and StSWEET11 transport thus significantly affects stem sucrose transport, we stipulate that *in planta* StSWEET11 transport rates must lie in the range of or above the rate reported for the VvSWEET7 rather than those for AtSWEET12. Importantly, our estimates for SWEET transport rate values that significantly affect sucrose transport efficiency were done in efflux-only simulations, and hence represent a lower bound for the *in planta* situation in which also retrieval mechanisms operate.

Variation in SWEET K_m

K_m values for VvSWEET7 and AtSWEET12 were found to lie between 10mM and 73mM (Table S2.3). It is noteworthy that typical potato phloem sap sucrose concentration exceeds 1M (Kehr et al., 1998; Pescod et al., 2007), indicating that SWEET transporters typically operate at or near their maximum transport potential. Similar to the StSWEET11 v_{max}, we investigated the

impact of different K_m values on sucrose transport characteristics, varying K_m values from 1 to 1000mM, while using the VvSWEET7 efflux rate. As expected, an increase in K_m decreased the effective efflux rate. A K_m increased from 10 mM to 75mM decreased total efflux with 5.2%, whereas an increase to 500mM decreased efflux with 39.1%. In contrast, a decrease to 1mM, increased efflux by only 0.7%, due to the near saturation of SWEET transport already occurring at the default K_m of 10mM (Figure 2.3D, orange line). For higher K_m values we observed a large increase in the variance of element specific transport efficiency along the stem (Figure 2.3D, blue dots). At high K_m, as the concentration decreased along the stem, transport efficiency increased due to reduced saturation of the transporter, effectively decreasing efflux rate. However, even for a total efflux rate equal to the loading rate and low K_m values, not all sucrose was lost prior to arrival at the unloading zone. Counterintuitively, despite the K_m of 10mM being up to 17 times lower than phloem sucrose concentrations, the decrease in sucrose concentration along the stem, still resulted in a small decrease in effective efflux-rate even for low K_m. In this simple efflux-only system, the saturating dynamics of the SWEET transporter already affects sucrose transport in a non-linear manner.

Efflux-retrieval dynamics and SWEET-efflux mitigation

SUT-mediated sucrose retrieval from the apoplast is expected to significantly mitigate sucrose loss. As discussed above, the SWEET v_{max} values estimated to have a physiologically relevant effect in absence of retrieval represent a lower bound. To ensure physiological relevance upon incorporation of a retrieval mechanism SWEET v_{max} values were doubled. Earlier theoretical work on the efflux-retrieval mechanism generated apoplast sucrose dynamics that were much slower than phloem transport (Minchin & Lacointe, 2017). Because of the slow apoplast timescale, this resulted in excessively long, physiologically unrealistic times to equilibrate (up to 10^4 h), making them only suitable for studying steady-state dynamics. Here, we aim for our model to also be suitable to investigate transient sucrose transport dynamics.

The effect of the apoplast volume

Minchin & Lacointe (2017) assumed that apoplast volume was 1000 times larger than that of the phloem. This implies that for sucrose exchange between phloem and apoplast, a change in phloem concentration is accompanied by a 1000-fold smaller change in apoplast concentration, and thus likely plays an important role in slow apoplast dynamics. Indeed, similar to their observations, we did find a linear relation between equilibration time and apoplast volume (Figure 2.4A, Blue line), decreasing from 3031h for apoplast volumes of 1000 times

phloem volume to 30h for apoplast volumes of 10 times the phloem volume. For small apoplast volumes (<2x phloem volume) the equilibration time was not solely determined by apoplast volume and the linear relation no longer applied. Next, we estimated what would be a realistic phloem-apoplast ratio from available volume measurements. Measurements on potato leaves reported that 5% of leaf volume is composed of vasculature and 3% of apoplast (Leidreiter et al., 1995). In absence of further data, we assume that, given the highly vascularized nature of plant leaves, this data represents and upper limit of the vascular volume fraction in the entire plant. Additionally, we assume that the apoplastic fraction is approximately constant in different potato plant organs. Further, we have a phloem volume of 0.0252mL and a xylem volume of 0.42mL in the model. From this, we derived that the total volume share of the phloem is 0.28%. From a 3% volume share for the total apoplastic compartment in the stem, we then arrive at the apoplastic volume being 3/0.28=10.7 times larger than the phloem volume. While this calculation was based on a series of assumptions, we expect this estimate to be in the correct order of magnitude. Thus, from hereon we continue the simulations with an apoplast volume of 10 times that of the phloem volume.

The effect of apoplastic sucrose removal

Above we show that for an apoplast volume of 10 times the phloem volume equilibration time was 30.0h, as compared to the 3.9h for the model without apoplast retrieval and otherwise similar settings. Based on this, we expect that other factors may contribute to shortening equilibrium time as well. Apoplastic sucrose is taken up by neighboring cells for their growth and maintenance as well as consumed by resident pathogens (Chen, 2014; Lemoine et al., 2013). These processes, which all contribute to irreversible loss of sucrose from the apoplast we here named apoplastic sucrose removal. We hypothesized that incorporating these processes would reduce equilibration time and investigated this by varying the maximum rate of sucrose removal (R_{max}) between 0 and 1e-8 mol/s, using Michaelis-Menten kinetics with a constant $K_{m,R}$ of 5mM. Without apoplastic sucrose removal, the apoplast sucrose concentration at the middle of the stem was 105.2 mM, which was significantly higher than the measured concentration in the potato stem apoplast of approximately 10mM (Abelenda et al., 2019). Implementation of sucrose removal in the apoplast strongly decreased the sucrose concentration in the apoplast to 56.8mM for an apoplast removal rate of 0.1e-8 mol/s and 11.8mM for a removal rate of 0.4e-8 mol/s, the latter closely fitting the experimental data. In parallel with a decrease mostly in apoplast, but also phloem sucrose concentrations, higher sucrose removal rates indeed resulted in a strong decrease in equilibration times (Figure 2.4B, orange line). For the highest

the delivery yield (Y) for ERRS increased relative to ERR simulations, as less efflux occurred due to decreased SWEET v_{max}. Y increased from 71.9% (ERR) to 84.3% (ERRS) of loaded sucrose. Reduction of StSWEET11-mediated efflux by StSP6A results in an increased sucrose retention in the phloem and thus a decrease in yield loss (100-Y) from 28.1 % to 15.7% of loaded sucrose. Interestingly, a 40% decreased v_{max} thus resulted in a 44.1% decrease in yield loss. The StSP6A-mediated reduced efflux leads to lower apoplast sucrose levels, which due to the saturated dependence of sucrose removal on sucrose levels causes a more than linear decrease in apoplast sucrose removal. As a consequence, decrease in yield loss is larger than

2
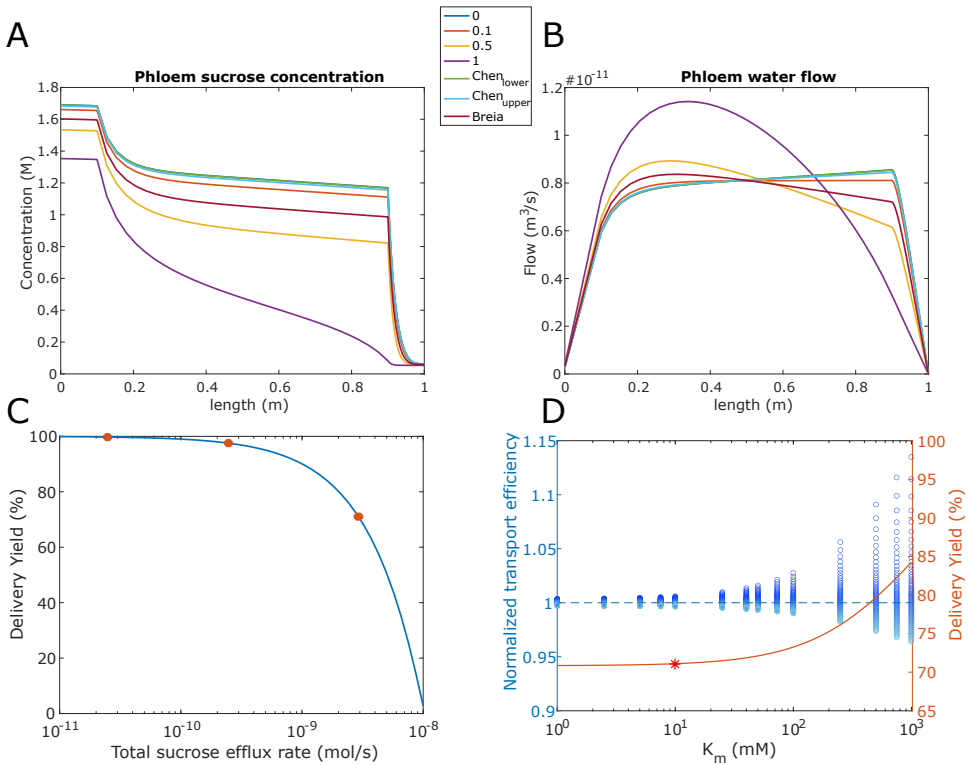
Figure 2.3. The effect of sucrose efflux. A) Sucrose concentration gradient for different efflux rates (0, 0.1, 0.5 & 1 times baseline loading) and the SWEET rates from literature. B) Water flow gradient for equal efflux rates. C) Delivery yield along a range of efflux rates (v_{max}). The orange dots represent experimentally measured vmax values (Chen et al., 2012; Breia et al., 2020). D) Effect of the affinity constant (K_m) on efflux. Dots represent transport efficiency along the stem normalized for mean efficiency per element, the color gradient represents the location in the long-distance zone, with dark indication shootward and light more rootward position. The orange line represents the delivery yield and the red star represents the transport efficiency at the K_m (10mM) used in all other simulations.

modeled sucrose removal rate, equilibration time was only slightly higher than for simulations without apoplast (4.7h to 3.9h). A similar linear dependence between equilibration time and apoplastic volume for absence and presence of sucrose removal (Figure 2.4A, orange line), yet this linear dependence occurred considerably above the apoplastic volume threshold. As a consequence, for a sufficiently high removal rate and 10 times higher apoplast than phloem volume, we stay outside the regime where apoplast volume determined equilibration times. Overall, inclusion of apoplastic sucrose removal representing sucrose consumption elsewhere, further improved the fit between simulated and measured apoplastic sucrose concentrations as well as decreased the time for simulations to equilibrate.

Including sucrose retrieval and removal also strongly improved delivery yield compared to the worst-case efflux-only (EO) case, with efflux-retrieval-removal (ERR) asymptotically approaching EO yield levels as removal rates increase (Figure 2.4B). This asymptotic decline of yield arises from the saturating Michaelis-Menten kinetics for apoplastic sucrose removal combined with the decrease in apoplast concentration sucrose concentration for high removal rates, causing the same increase in removal rates to have less and less effect on sucrose levels.

The effect of the StSWEET11-StSP6A interaction

Fixing the v_{max} of the apoplastic sucrose removal rate at 0.4e-8 mol/s, we next set out to study the effect of StSP6A on equilibration times and transport characteristics. We started simulations from a steady-state with fully operational SWEET sucrose-efflux and then decreased the SWEET v_{max} with 40% to simulate maximum StSP6A production. It took 2.8h to reach the new steady-state (Figure 2.4C). Instead of the instantaneous onset of maximum StSP6A production as modeled here, *in planta* it takes 2-4 days in leaves and 4-8 days in tubers to reach maximum StSP6A (Navarro et al., 2011). This implies that the timing of physiological StSP6A effects are dominated by StSP6A production dynamics rather than long-distance transport equilibration dynamics.

We compared transport efficiency and variation therein, along the stem for the different scenarios considered (Figure 2.4D). We see that compared to the scenario of efflux retrieval and apoplast removal (ERR), StSP6A introduction (ERRS) caused enhanced average transport efficiency, as well as a reduced decrease in efficiency along the stem due to a smaller sucrose gradient in the phloem (Figure 2.4D). A similar increase in average efficiency and decrease in efficiency variation can be seen for the transition from EO to ERR. Like transport efficiency,

efflux reduction. Depending on the parameter values, especially removal K_m, the decrease in yield loss increases further after StSP6A introduction. Increasing the sucrose removal K_m to 10mM, a yield loss decreases of 47.9% was obtained.

Transgenic StSWEET11 phenotypes

Transgenic StSWEET11 plants had large deviations in apoplast sucrose concentrations (Table S2.4, Abelenda et al. 2019). We recreated the StSWEET11 knockdown (StSWEET11 RNAi), StSWEET11 over-expression (35S:StSWEET11) and StSWEET11/StSP6A over-expression (35S:StSWEET11/SUC2:StSP6A) genotypes to test whether changed SWEET-activity in our model could reproduce the measured apoplastic sucrose differences.

Transgenics were simulated by changing the SWEET v_{max} equally to the reported fold-change reported by Abelenda et al. (2019), being approximately doubled for over-expression and decreased 20-fold for knockdown. The combined over-expression was simulated by first increasing the v_{max} 5-fold (mimicking the StSWEET11 over-expression) and subsequently decreasing this v_{max} by 95% (mimicking 100-fold StSP6A over-expression), as we expect that the StSP6A increase would strongly increase the binding of StSP6A to StSWEET11, blocking almost all transport activity. Simulated apoplast sucrose concentration changes compared to the measured concentration changes were lower in the knockdown (-99% to -61%) and higher in the over-expression line (+438% to +278%) whereas the simulated concentration change in the combined StSWEET11/StSP6A line was close to the measured concentration (-92% to -89%) (Table S2.4). Our model is a simplification by necessity and does not incorporate regulatory processes allowing for compensatory increases or decreases in other transporters, or efficiency of the SWEET transporter itself. In case of StSWEET11 over-expression the 35S promotor was used that leads to ubiquitous expression, leaving open the possibility that not all of the 20-fold increase in StSWEET11 levels in leaves occurs in the phloem. We therefore investigated the fold-changes in expression levels required in our simulated mutants to reproduce experimental observations. In case of StSWEET11 knockout, applying a 2.5-fold rather than 20-fold reduction in SWEET v_{max} resulted in an apoplast concentration of 2.2mM, close to the experimental observations, suggesting a substantial, but not complete, replacement by StSWEET11mediated efflux by other transporters in the case of StSWEET11 knockdown. Similarly, in case of StSWEET11 overexpression, a 1.5-fold rather than 2-fold increase in v_{max} resulted in a concentration of 34.9mM, suggesting that indeed substantial overexpression is outside the phloem or that retrieval was increased in case of increased SWEET-activity.
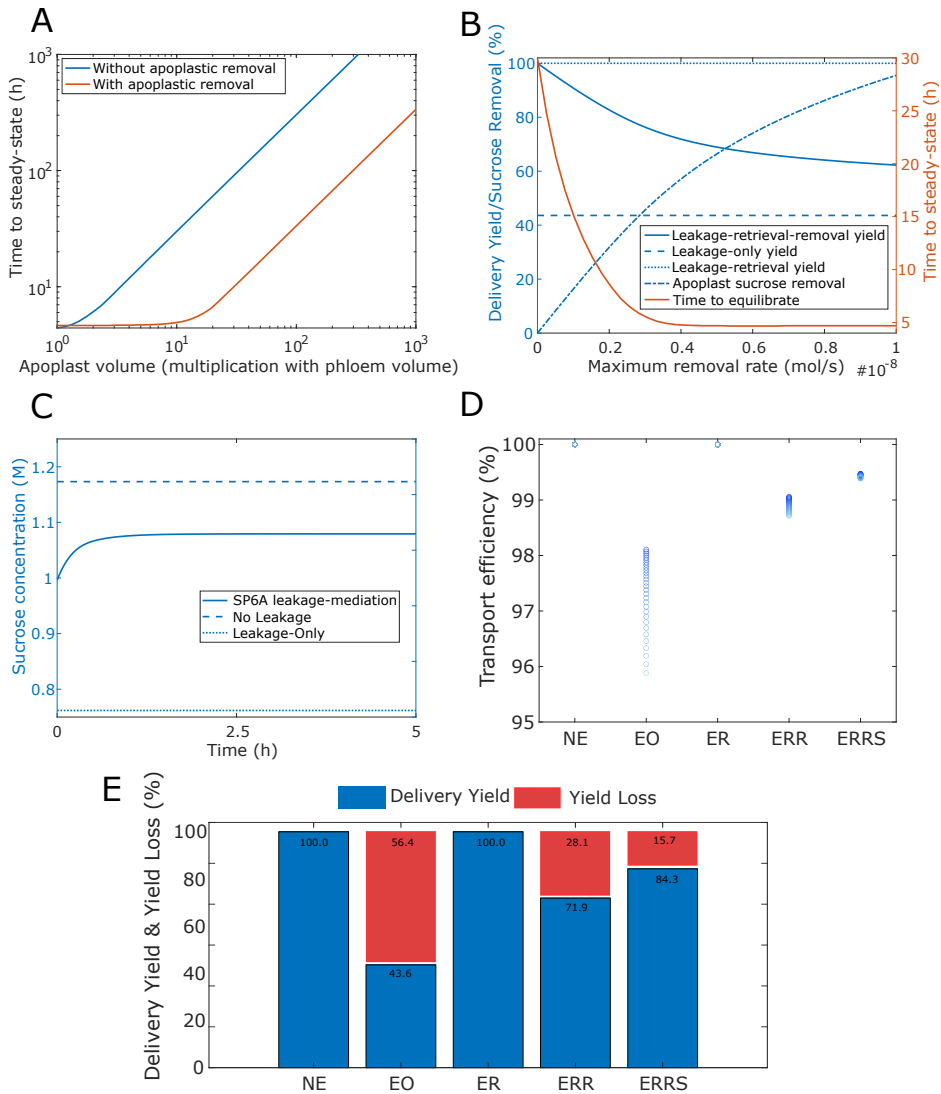
Figure 2.4. Efflux-retrieval dynamics and SWEET-efflux mitigation. A) Time to reach steady-state for varying apoplast volumes in a system with (0.4e-8 mol/s) and without apoplastic respiration and with a bidirectional SWEET and SUC transporters. B) Delivery yield (% of maximum in absence of efflux), apoplast sucrose removal (% of sucrose influx) and time to steady-state for varying removal rates in the apoplast. Apoplast sucrose removal is given as a percentage of sucrose influx in that specific compartment. C) Sucrose concentration after the introduction of StSP6A-mediated efflux-decrease and no-efflux and efflux-only scenarios as comparison. D) Transport efficiency per element for different efflux scenarios. The color gradient represents the location in the long-distance zone, with dark indication shootward and light more rootward position. NE: No-Efflux, EO: Efflux-only, ER: Efflux-Retrieval, ERR: Efflux-Retrieval-Removal, ERRS: Efflux-Retrieval-Removal-StSP6A. E) Delivery yield in the 24h after reaching steady-state for the same scenarios as in D.

Discussion

Tuber yield is not only dependent on assimilate production in source-leaves but also on long-distance transport and sink-strength. Recently, it was shown in heterologous expression experiments that the potato tuberigen StSP6A mediated a 40% reduction of StSWEET11 sucrose-export activity (Abelenda et al., 2019). Unfortunately, the complex multi-feedback nature of plant sucrose transport combined with the likely presence of additional StSP6A mediated changes make it hard to assess the physiological relevance of the StSP6A-SWEET interaction on tuber yield. To resolve this, we here developed a mechanistic mathematical model of long-distance phloem transport in potato incorporating SWEET/SUT-mediated sucrose transport to study the effect of the StWEET11-StSP6A interaction.

Mathematical models on water and sucrose transport have so far largely been restricted to large plants and trees. Therefore, as a first step we here developed the first quantitative, mechanistic model for sucrose transport in agronomically highly relevant potato plants. The model reproduced experimentally measured sap sucrose concentrations and velocities well. Interestingly, our model indicated that high viscosity in the phloem was the major resistance factor in potato, in contrast to sieve-tube geometry reported in earlier work on larger plants (Stanfield et al., 2019; Thompson & Holbrook, 2003). This result is consistent with the higher sucrose concentration (Jensen et al., 2013), shorter stem-length and higher flow velocity (Comtet et al., 2017; Windt et al., 2006) reported for herbaceous species, suggesting it might be a general property of small herbaceous crop species.

As a next step, we extended our model with SWEET sucrose transporters. Importantly, Abelenda and co-workers reported significant effects of StSWEET11 RNAi knockdown and overexpression on stem apoplast sucrose levels, supporting the physiological relevance of unblocked StSWEET11 mediated sucrose export in the stem (Abelenda et al., 2019). Importantly, SWEET transport rates were characterized in heterologous expression systems, resulting in highly variable reported maximum transport rates (Breia et al., 2020; Chen et al., 2012), with no data available for *in planta* transport rates. Using our model, we find that for SWEET mediated export to significantly affects sucrose transport characteristics, transport rates should lie in the upper range of the experimentally reported values. Importantly, these results were obtained in absence of simulated SUT-mediated sucrose retrieval, rendering this a lower boundary estimate and suggesting that *in planta* values should in fact lie at least a factor 1.5-2 higher. Our results

thus underline that caution should be taken when interpreting transport rates obtained in heterologous expression experiments.

Surprisingly, we found that earlier studies which used explicit apoplastic volume and SUC mediated sucrose retrieval, assumed very large apoplastic to phloem volume ratios (1000:1) (Minchin & Lacointe, 2017). However, simple geometric considerations on potato stem diameter and the percentage of stem area occupied by phloem and xylem tissue indicate that this ratio cannot exceed 10.7:1. Importantly, we demonstrated that application of realistic apoplast to phloem volume ratios significantly reduces the long equilibration times these earlier models were suffering from. In addition, in earlier models, sucrose could only leave the apoplast through SUC mediated re-uptake in the phloem. Therefore, after equilibration, SWEET mediated sucrose loss equals SUC mediated sucrose gain. Biologically, it seems logical to assume that sucrose efflux to the apoplast serves to supply surrounding stem tissue with energy, and hence that part of the sucrose efflux into the apoplast will be taken up and metabolized and thus no longer be available for re-uptake. Incorporating an apoplastic removal term to simulate this further decreased model equilibration time. Combined, these two adjustments ensure that the timescale of model dynamics are largely independent of whether an apoplast is explicitly simulated. We thus propose that our model is the first efflux-retrieval sucrose transport model resulting in biologically meaningful equilibration times.

Using the improved, potato-specific efflux-retrieval model, we studied the physiological significance of the StSP6A-mediated 40% efflux reduction. We found that after onset of StSP6A production, delivery yield increased over a physiologically relevant time-course of 3.5h. Furthermore, we demonstrate that for the deduced StSWEET11 transport rates used here, a reduction in StSWEET11-mediated efflux resulted in a significantly larger (10-20%) decrease in yield loss. This result not only supports the idea that StSP6A mediated StSWEET11 blockage is physiologically relevant for potato yield but once more demonstrates how the feedback and non-linearities in plant sucrose transport necessitate mechanistic modeling to understand and predict the effects of imposed changes. We hope and aim for the model developed in this study to serve as a valuable open-source tool for investigating yield improvement in agronomically relevant crop species. As our study illustrates, mathematical modeling is essential to highlight how, e.g. plant type differences determine which factors dictate phloem sap flow. Thus, modeling can play an important role in determining the type of optimization, photosynthesis, sink strength or long-distance transport, that for a particular crop species and condition is

likely to result in the largest yield increase. Our model is also intended as a starting point for the development of more sophisticated models. A first logical extension for future work would be to incorporate the distinct modes of symplastic and apoplastic unloading, necessary to investigate the tuberization switch and its potential dependence on the StSP6A-StSWEET11 interaction. Another important extension would be to explicitly include tuber growth and couple this to the transport model. While organ growth has been extensively modeled for swelling fruits such as tomato, kiwi, peach and grapes (Cieslak et al., 2016; Fishman & Génard, 1998; Hall et al., 2013; Zhu et al., 2019), tuber expansion arises through a combination of cell division and swelling, requiring more sophisticated organ growth modeling (Vreugdenhil et al., 1999). To enable the investigation of resource competition between organs, as well as source-sink distance on sink resource uptake it will be necessary to replace the single, unbranched, source-sink architecture applied here with a more realistic plant architecture. The feasibility of this approach was recently demonstrated (X.-R. Zhou et al., 2020). Finally, extension of the model with the regulatory networks controlling photosynthesis, plant architecture and the expression levels, patterns and activities of key factors such as StSP6A, SWEET and SUT would enable the incorporation of environmental factors impinging on these networks. Future model developments would greatly benefit from additional experimental data. As an example, detailed potato phloem morphology data and apoplast volume ratios could be obtained by a combined confocal and electron microscopy approach.

Acknowledgments

Author contributions

Conflict of interest

The authors declare there is no conflict of interest.

Supplementary methods

Model structure and assumptions

As described in the main manuscript methods section we used the well-established model for phloem transport by Thompson & Holbrook (2003) and coupled phloem-xylem transport in a discrete architecture (Hölttä et al., 2006; Lacointe & Minchin, 2008) as a starting point (Table S1).

The model explicitly describes water and solute flow in the phloem, water flow in the xylem, SWEET and SUT mediated sucrose exchange between the phloem and the apoplast, and water exchange between the xylem and phloem. Water flow in the xylem is driven by water transpiration in the topmost element as described by the cohesion-tension theory, while phloem water flow is driven by a hydrostatic pressure gradient induced by sucrose loading and unloading as described by the Münch-hypothesis. Boundary conditions in the xylem are set by the transpiration rate (top) and soil water tension (bottom). Phloem boundary conditions are set by loading rate (top) and unloading rate and target sucrose concentration (bottom). Furthermore, the phloem and xylem compartment volumes only change due to water inflow and outflow, no structural growth is included in the model. As a consequence of water content changes the compartment radii may elastically increase due to an increase in hydrostatic pressure. Compartments are assumed to be cylindrical, enabling calculation of axial and radial areas from compartment radius and the number of parallel conduits. For the calculation of the radial area ($A_{rad,j}$) shared between phloem and xylem we use the minimum of both. The phloem was divided into three zones: loading zone, unloading zone and long-distance pathway (Van Bel, 2003). Similar to earlier studies we assumed that the loading and unloading zone each span 10% of the total stem length. The stem is non-homogeneously discretized into N elements to simulate transport over a spatial and temporal scale, with x representing the element length (Figure 1A). The location (along the stem) and compartment type (phloem, xylem, apoplast) of the variables are notated using subscripts: $Var_{comp,j}$ in which comp depicts the compartment and j the element position.

Supplementary methods

Model equations

Here we provide a more extensive description of the origin and rationale of the used model equations.

Water & Pressure

Water transport in the stem is described using the mass-balance equation for each xylem and phloem element in the stem:

$$\frac{\partial W_{\frac{Ph}{X},j}}{\partial t} = \left(J_{W,ax,in,\frac{Ph}{X},j} - J_{W,ax,out,\frac{Ph}{X},j} + J_{W,rad,in,\frac{Ph}{X},j} - J_{W,rad,out,\frac{Ph}{X},j} \right)\rho \qquad \text{(eq. 1)}$$

with $J_{W,ax,in,i,j}$ the axial water inflow and $J_{W,ax,out,i,j}$ outflow between neighboring elements (axial outflow of element i is equal to the inflow of compartment i+1, Figure 1A), $J_{W,rad,in,i,j}$ describes the radial water flux between the phloem and xylem compartments and ρ is the density of water. Radial water flow is driven by the difference in water potential (ψ) between the xylem and phloem:

$$J_{W,rad,in,Ph,j} = L_r A_{rad,j} \left(\Psi_{X,j} - \Psi_{Ph,j} \right) \qquad \text{(eq. 2)}$$

with Lr the radial hydraulic membrane permeability and $A_{rad,j}$ the radial area between phloem and xylem. The water potential in the xylem is equal to the hydrostatic pressure as no solutes are assumed to be present. The water potential of the phloem is calculated from the hydrostatic pressure (P) and the osmotic potential (Π). Phloem sap Π was calculated using a non-linear relation for osmotic potential as function of sucrose concentration and the molal volume of sucrose (Michel, 1972):

$$\Pi_{Ph,j} = -\rho RT \left(0.998 m_{Ph,j} + 0.089 m_{Ph,j}^2 \right) \text{ with } m_{Ph,j} = \frac{C_{Ph,j}}{\rho \left(1 - C_{Ph,j} V_{suc} \right)} \qquad \text{(eq. 3)}$$

Axial water influx in both phloem and xylem elements is calculated using the Hagen-Poiseuille equation:

$$J_{W,\frac{Ph}{X},j,ax} = A_{i,j} \frac{k_{i,j}}{\mu_{i,j}} \frac{\partial P_{\frac{Ph}{X},j}}{\partial x} = A_{\frac{Ph}{X},j} \frac{k_{\frac{Ph}{X},j}}{\mu_{\frac{Ph}{X},j}} \frac{P_{\frac{Ph}{X},j-1} - P_{\frac{Ph}{X},j}}{x} \qquad \text{(eq. 4)}$$

with $k_{Ph/x,j}$ the axial permeability, $\mu_{Ph/x,j}$ dynamic viscosity and $A_{Ph/x,j}$ the axial area. The axial permeability in the xylem was not based on measured data but calculated from the xylem radius. In the xylem viscosity is assumed to be constant and equal to that of pure water, viscosity in the phloem is dependent on local sucrose concentration

Supplementary methods

and calculated using an empirically derived function based on the reference viscosity of pure water (μ_x), the volume fraction of sucrose (Φ) and molal volume of sucrose (Morison, 2002):

$$\mu_{Ph,j} = \mu_X exp\left(\frac{4.68*0.956\phi_{Ph,j,}}{1-0.956\phi_{Ph,j}}\right) \text{ with } \phi_{Ph,j} = \frac{V_{suc}S_{Ph,i}}{V_{suc}S_{Ph,i}+V_{Ph,i}}$$

(eq. 5, Morison, 2002)

For the top and bottom elements of the phloem, the respective inflow and outflow are set equal to zero as these boundaries are assumed to be impermeable for water. For the top and bottom elements of the xylem, respective outflow and influx depend on water transpiration and soil water potential.

Similar to Hölttä et al. (2006), the pressure differential was calculated homologous to Hooke's law:

$$\frac{\partial P_{\frac{Ph}{X},j}}{\partial t} = \epsilon_{\frac{Ph}{X},j}\frac{1}{W_{\frac{Ph}{X},j}}\frac{\partial W_{\frac{Ph}{X},j}}{\partial t}$$

(eq. 6)

with $\epsilon_{Ph/X,j}$ the elastic modulus. The elastic modulus is assumed constant over the length. As reversible expansion occurs in the phloem, the axial area of the conduits does change, this expansion was calculated using:

$$A_{Ph,j} = A_0 e^{\frac{(P_{Ph,j}-P_0)}{\epsilon_{Ph,j}}}$$

(eq. 7, Thompson & Holbrook, 2003)

Sucrose

Axial solute transport occurs through the phloem at a speed equal to the convective water flow. Here, as only sucrose is present as a solute, the axial solute flow can be written as:

$$J_{S,ax,in,Ph,j} = J_{W,ax,in,Ph,j} * C_{Ph,j-1}$$

(eq. 8)

Radial sucrose transport arises from sucrose uptake into the phloem at the loading zone ($L_{Ph,j}$), sucrose loss from the phloem at the unloading zone ($U_{ph,j}$) and exchange of sucrose towards and retrieval from the apoplast along the long-distance pathway ($E_{Ph,j}$), resulting in the following:

$$J_{S,rad,Ph,j} = L_{Ph,j} - U_{Ph,j} - E_{Ph,j}$$

(eq. 9)

Supplementary methods

where $L_{Ph,j}$ is only non-zero at the loading zone, $U_{Ph,j}$ is only non-zero at the unloading zone, and $E_{Ph,j}$ is only non-zero along he long distance transport zone.

Loading is incorporated as a constant inflow of sucrose along the loading zone. The loading rate per element is normalized to the number of elements in the loading zone, ensuring a constant overall loading independent of numerical resolution or plant size:

$$L_{Ph,j} = \frac{v_{load}}{N_{load}}$$

(eq. 10)

The passive, symplastic unloading of sucrose occurring during tuber formation and filling is concentration gradient dependent. We use a target concentration (C_{target}), representing the sucrose concentration in the tuber, as boundary condition for the system:

$$U_{Ph,j} = v_{unload} * \left(C_{Ph,j} - C_{target} \right)$$

(eq. 11)

To model sucrose efflux and retrieval along the long-distance pathway, we explicitly modeled SWEET and SUC/SUT mediated sucrose transport using Michaelis-Menten kinetics. The bidirectionality of SWEET transporters is incorporated through the use of separate import and export term with equal maximum transport rates but different affinities (Chen et al., 2012). Combined this results in the following equation:

$$E_{Ph,j} = v_{MaxSWEET} V_{Ph,j} \frac{C_{Ph,j}}{C_{Ph,j}+K_{mIn}} - v_{MaxSWEET} V_{Ph,j} \frac{C_{A,j}}{C_{A,j}+K_{mEx}} - v_{MaxSUC} V_{Ph,j} \frac{C_{A,j}}{C_{A,j}+K_{mSUC}}$$

(eq. 12)

The solute change in the phloem is given by:

$$\frac{\partial S_{Ph,j}}{\partial t} = J_{S,ax,in,Ph,j} - J_{S,ax,out,Ph,j} - J_{S,Rad,Ph,j}$$

(eq. 13)

The change in solute for xylem is equal to zero as no solute was assumed to be present in xylem. The solute change in the apoplast is equal to the inflow and outflow from the phloem. Additionally, we consider loss due to removal in the surrounding tissue:

$$\frac{dS_{A,j}}{dt} = E_{Ph,j} - v_{resp} \frac{C_{A,j}}{C_{A,j}+K_{mR}}$$

(eq. 14)

51

Supplementary methods

Transport efficiency and transport yield

In the main manuscript methods section, we defined two measures for the quantification of sucrose transport and delivery, Transport Efficiency (η) and Delivery Yield (Y) (Figure 1B). Transport efficiency, assuming steady state, was defines as the ratio of axial outflow over the axial inflow:

$$\eta = \frac{outflow}{inflow} = \frac{J_{S,ax,out,Ph,j}}{J_{S,ax,in,Ph,j}} \qquad \text{(eq. 15)}$$

Importantly, the same transport efficiency values can arise for different sucrose flux rates that will result in different sucrose supply to the tubers. To measure the effective supply of sucrose to the tubers we defined delivery yield, as the ratio of the amount of sucrose unloaded over the amount loaded in a given time interval (ranging from t_0 to t_{end}):

$$Y = \frac{\sum_{j=1}^{N} \int_{t_0}^{t_{end}} \left(U_{Ph,j} \right)}{\sum_{j=1}^{N} \int_{t_0}^{t_{end}} \left(L_{Ph,j} \right)} \qquad \text{(eq. 16)}$$

In steady-state, without efflux and retrieval, transport efficiency and delivery yield are 100% by definition. Given the closed nature of the system, loading rate/inflow necessarily is equal to the unloading rate/outflow (Figure 1B). When efflux is introduced in absence of retrieval, the system is no longer closed and by necessity; Unload = Load-efflux and thus both transport efficiency and delivery yield decrease. If instead, a combined efflux-retrieval mechanism is incorporated in the absence of apoplastic sucrose removal, we close the system again. As a consequence, in steady state, efflux equals retrieval and loading equals unloading resulting in 100% transport efficiency. In contrast, during the initial time transient preceding the steady state the apoplast is loaded and transport efficiency is reduced. This reduced sucrose delivery can also be observed when, instead of calculating steady state delivery, calculating delivery during this initial time period. If we combine a efflux-retrieval mechanism with apoplastic sucrose removal the system becomes open again, and outflow=inflow-removal, with the sucrose loss due to removal being equal to the difference between efflux and retrieval.

Supplementary methods

Baseline potato-specific parameterization

In the following section we describe how potato-specific parameter values were obtained from available data. Based on experimental data reporting a potato stem length of 0.5-1m in tuberizing plants (Vos & van der Putten, 1998), we set our potato model stem length to 1m. The number of xylem conduits in potato varies between 100 and 200, with a mean radius of 30μm (Aliche et al., 2020). No measurements for the number of potato phloem conduits is available. Instead we estimated these to be less abundant than xylem conduits based on measurements by Sibout et al. (2008) and theoretical considerations by Hölttä et al. (2009). We set the number of xylem conduits to 150 and the number of phloem conduits to 100. In absence of data on phloem axial permeability (k_p) and radius (r_p) in potato we used experimental measurements from its close relative, tomato (*Solanum lycopersicum*) (Mullendore et al., 2010). We estimate 10.7e-6m for r_p and 3.82e-12m^2 for k_p. The radial hydraulic conductivity was assumed to be equal to Thompson & Holbrook (2003) and the elastic modulus of phloem and xylem are set as 30MPa (Nobel, 2005) and 750Mpa (Irvine & Grace, 1997) respectively.

Water transport

The transpiration rate was set to 0.02g/s based on measurements of the transpiration rate of mature potato plants under standard conditions (Schans & Arntzen, 1991). As the soil water potential is generally reported as approximately zero (Perämäki et al., 2001), we here assumed a value of 0MPa.

Sucrose transport

The model tuber sucrose concentration was set at 50 mol/m^3, which is at the upper range of concentrations reported for potato tubers (2.92 − 5.84 mol/m^3 (Bethke et al., 2009), 2.92 − 43.8 mol/m^3 (Ross & Davies, 1992), 2.66 − 12.27 mol/m^3 (Duarte-Delgado et al., 2016), 17.2 mol/m^3 (Leggewie et al., 2003). Note that original data were in per gram fresh weight (FW) or dry weight (DW) and were converted to mol/m^3 using a FW/DW ratio of 7g/g (Jaarsma & de Boer, 2018) and a volume to mass ratio of 1mL/gFW. To estimate the baseline loading rate for the model we estimated the amount of sucrose unloading to tuber sinks, reasoning that sucrose input into the phloem should at least equal sucrose output from the phloem. In three months 500-800g tuber mass (Pourazari et al., 2018; Zheng et al., 2016), with a 20% dry matter content (Zeeman et al., 2010), is produced per plant, amounting to an overall efflux of sucrose to tuber sinks of about 1e-8 mol/s. To avoid sink limitation unloading rate was set at 0.1e-10 m^3/s.

Supplementary methods

SWEET and SUT characteristics

SWEET-mediated sucrose efflux from the long-distance phloem is thought to mainly occur via StSWEET11. While SWEET-mediated sucrose transport has been experimentally characterized, available data are restricted to non-potato SWEETs of different types. Chen et al. (2012) characterized AtSWEET12 using heterologous expression in Xenopus oocytes. They reported values for the affinity constant (K_m) for export of >10mM and import of 73mM, as well as a maximum uptake rate (v_{max}) of 1.2e-3 mol/m^3/s (after rewriting using their protocol). Export rates were not exactly quantified, but were up to 10 fold higher than import rates. The lower K_m and higher v_{max} values for export are consistent with SWEETs predominantly functioning as sucrose exporters. More recently, Breia et al. (2020) characterized VvSWEET7 using heterologous expression in *Saccharomyces cerevisiae*. They reported a Km for sucrose export of 40.08mM, and a v_{max} of 15.12 nmol sucrose/mgDW/min. Assuming an intracellular volume of yeast of 1.7 mL/gDW (Guijarro & Lagunas, 1984), this latter value can be rewritten as 0.148 mol/m^3/s. SUT-mediated sucrose retrieval into the phloem is mediated through StSUT1. While Riesmeier et al. (1993) characterized the K_m for sucrose at 1mM, they reported no value for the v_{max} of StSUT1. Schulze et al., (2000) characterized the StSUT1 K_m for sucrose at 1.7mM, and a v_{max} value of 210.2 nmol/10^{8}cells/min. Using a cellular volume of 30µm^3 (Bryan et al., 2010), this was rewritten as 0.117 mol/m^3/s. No other v_{max} values for StSUT1 were reported. As a comparison we used data from BvSUT1, a v_{max} of 0.12 nmol/mgFW/min was reported by Nieberl et al. (2017), which was rewritten to 0.0238 mol/m^3/s. Based on the above values, we set parameters for StSWEET11 to Km for export to 10mM, K_m for import to 70mM, v_{max} to 0.148 mol/m^3/s and the parameters for StSUT1 to a K_m of 1mM and v_{max} to 0.117 mol/m^3/s in our potato model, unless explicitly stated otherwise.

Supplementary tables

Table S1. Comparison of this work and previously published dynamic models.

	This work	**(Thompson & Holbrook, 2003)**	**(Hölttä et al., 2006)**	**(De Schepper & Steppe, 2010)**	**(Lacointe & Minchin, 2008)**
Target plant-type	Small crop-plant (potato, <1m)	Medium-sized plant (5m)	Large tree (>10m)	Small-Large tree (1-12m)	Variable architecture
Xylem inclusion	Dynamically included	Not included	Dynamically included	Dynamically included	Statically included
Resistance factor (sieve plates & viscosity)	-Experimentally derived axial conductivity (Mullendore et al., 2010) -Non-linear solute viscosity	- Sieve plates included via Sampson factor - Non-linear solute viscosity	- Sieve plates included via Sampson factor - Non-linear solute viscosity	Based on (Hölttä et al., 2006; Lacointe & Minchin, 2008; Steppe et al., 2006)	- Sieve plates included via Sampson factor - Non-linear solute viscosity
Axial flow	Pressure gradient (Hagen-Poiseuille)	Pressure gradient (Hagen-Poiseuille)	Pressure gradient (Darcy's law)	Pressure gradient (Resistance)	Pressure gradient (Resistance)
Radial flow	Water potential gradient	Water potential gradient	Water potential gradient	Water potential gradient	Water potential gradient
Pressure diffential calculation	Hooke's law	Hooke's law	Hooke's law	Hooke's law and Lockhart-equation	Volume conservation
Solute potential	Non-linear (empirical equation)	Non-linear (empirical equation)	Linar (van 't Hoff equation)	Linar (van 't Hoff equation)	Linar (van 't Hoff equation)
Dynamic radius?	Yes, wall elasticity	Yes, wall elasticity	Yes, wall elasticity and tapered initial coniditons	Yes, wall elasticity and irreversible growth	Static radius, a unique radius per element can be assigned initially

2

Supplementary tables

Table S1. Comparison of this work and previously published dynamic models. (continued)

	This work	**(Thompson & Holbrook, 2003)**	**(Hölttä et al., 2006)**	**(De Schepper & Steppe, 2010)**	**(Lacointe & Minchin, 2008)**
Loading/ unloading mechanism	Constant loading, target concentration unloading	Constant loading, target concentration unloading	Constant loading, target concentration unloading	Dependent on leaf and root concentrations	Constant loading, saturated unloading
Lateral solute loss	Yes, as a function of axial concentration	No	No	Yes, diffusion like kinetics included	Yes, diffusion and Michaelis-Ment en like kinetics
Sucrose respiration or storage	Sucrose removal in the apoplastic compartment	No	No	Storage incorporated in 'storage phloem'	Respiration and storage in 'phloem parenchyma'
Model architecture and compartments	Phloem, xylem, apoplast in the stem	Single isolated sieve element	Phloem, Xylem, Apoplast in complete stem	Phloem, Xylem, Cambium, Parenchyma in stem and leaf and root compartment	Phloem, Xylem, Cambium, Parenchyma in stem

Supplementary tables

Table S2. Model validation tests compared to results from Thompson & Holbrook (2003).

|	Thompson & Holbrook (2003)	Test 1, reproduction results Thompson & Holbrook (2003)	Test 2, inclusion variable xylem potential
Mean concentration (M)	0.892	0.843	0.899
Concentration gradient (M/m$_{length}$)	0.136	0.109	0.126
Mean pressure (MPa)	3.05	2.54	2.50
Pressure gradient (MPa/m)	0.68	0.389	0.386
Mean sap speed (mm/s)	0.20	0.22	0.21
Water flow in the middle of the stem (m3/s)	N.A.	4.58e-14	4.27e-14
Mean sucrose flow (mol/s)	N.A.	3.97e-14	3.96e-14
Lateral water flux in the middle of the stem (m2/s)	N.A.	6.25e-15	6.33e-15
Phloem volume (mm3)	1.056	1.027	1.016

2

Supplementary tables

Table S3. Functional characteristics of SWEET and SUC/SUT transporters.

Transporter	V_{max} (mol/m³/s)	K_m (mol/m³)	Experimental method	Reference
AtSWEET12	<0.012 (export) 0.0012 (import)	>10 (export) 73 (import)	Heterologous expression in *Xenopus* oocytes	Chen et al. (2012)
VvSWEET7	0.148	40	Heterologous expression in *Saccharomyces cerevisiae*	Breia et al. (2020)
StSUT1	-	1	Heterologous expression in *Saccharomyces cerevisiae*	Riesmeier et al, (1993)
	0.117	1.7	Heterologous expression in *Saccharomyces cerevisiae*	Schulze et al. (2000)
BvSUT1	0.0238	1.7	Heterologous expression in *Saccharomyces cerevisiae*	Nieberl et al. (2017)

Table S4. Measured and simulated apoplast concentrations for different genotypes. Percentage changed compared to wildtype is given in brackets for the upper two rows, in the bottom row the tuned parameter fold-change is given compared to the earlier used parameters.

	Wildtype	StSWEET11 RNAi	35S:StSWEET11	35S:StSWEET11 SUC2:StSP6A
Measured apoplast concentration (mM) (Abelenda et al., 2019)	9.6	2.8 (-61%)	36.2 (+278%)	1.0 (-89%)
Simulated apoplast concentrations (mM)	11.8	0.1 (-99%)	63.5 (+438%)	0.9 (-92%)
Tuned apoplast concentration (mM)	11.8	2.2 (↓8-fold)	34.9 (↓3.33-fold)	-

Supplementary figures
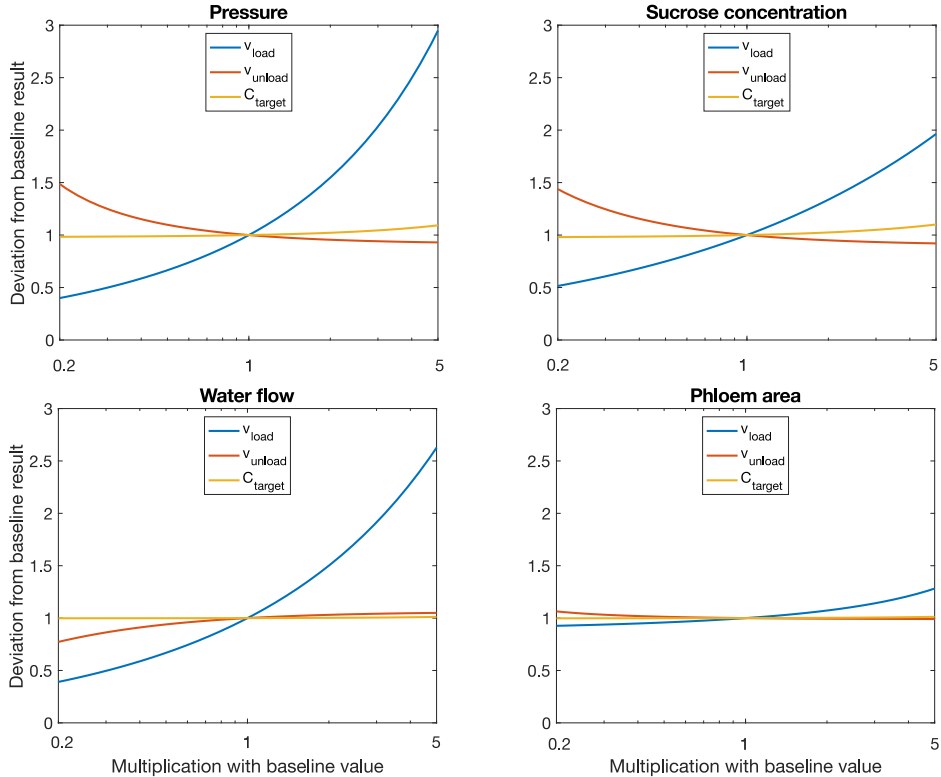
Supplemental figure 2.1. Effect of loading and unloading rates and target concentration on model outcomes. For loading rate, a 0.2 to 5 fold range corresponding to 0.2 to 5e-8 mol/s, for unloading rate a 0.2 to 5 fold range corresponding to 0.2e-11 to 0.5e-10 and for target concentration a 0.2 to 5 fold range corresponding to 10 to 250mM was used. Model outcomes are represented by mean pressure, mean sucrose concentration, mean water flow, and mean phloem area along the long-distance zone. Outcomes were normalized against model outcomes for default parameter settings. Simulations were performed in a model without sucrose efflux and retrieval.
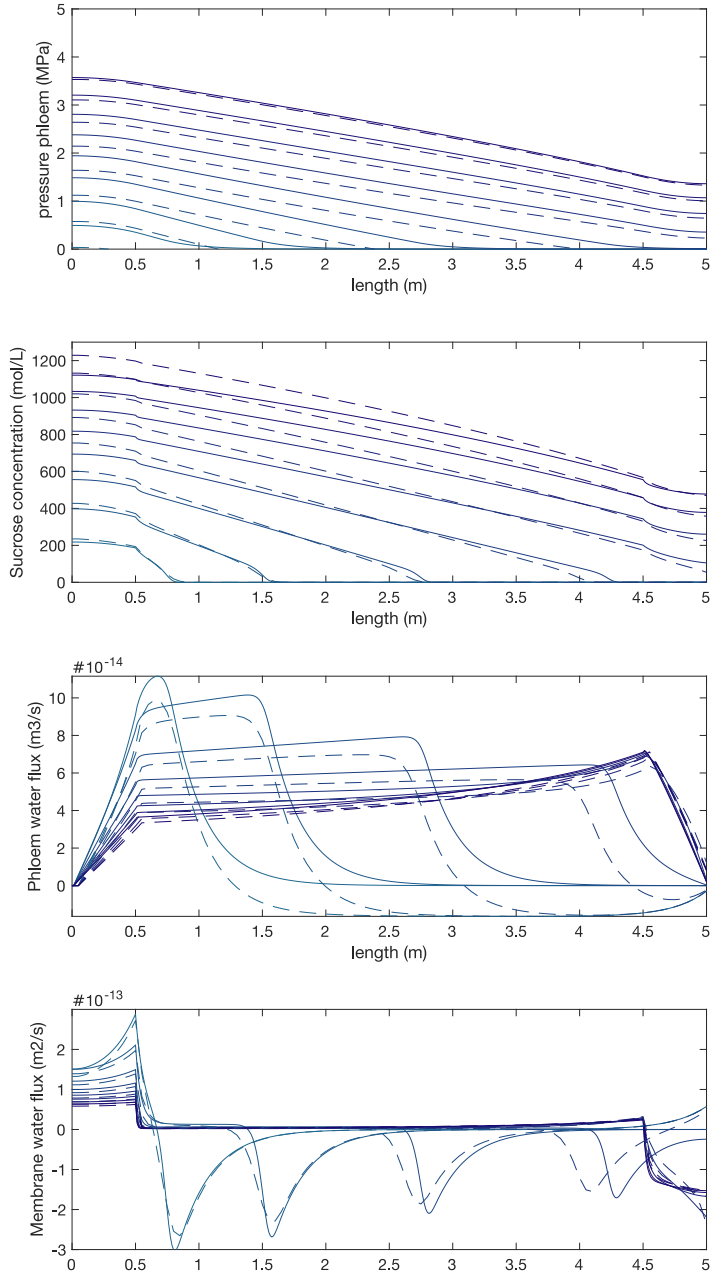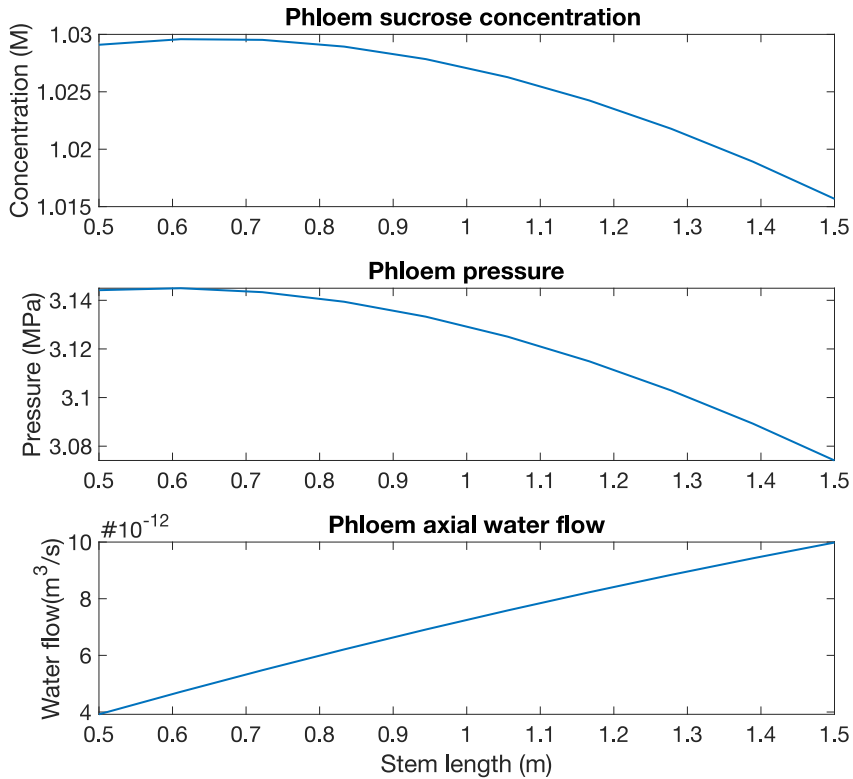
Supplementary figures
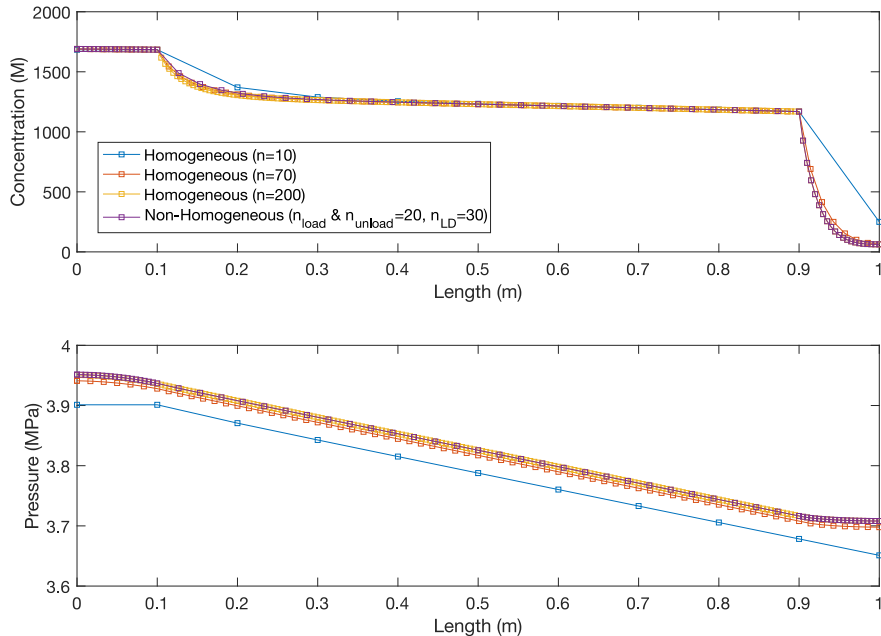
Supplemental figure 2.2. Effect of spatial discretization on model outcomes (sucrose and pressure gradient) and simulation times. The non-homogeneous discretization is used as a default in all simulations shown in other figures. The homogeneous discretization using n=200 elements corresponds to a space step of 0.005m, the space step used in default simulations for the loading/unloading zones. The homogeneous discretization using n=70 elements corresponds to a space step of 0.014m, corresponding to the same number of discretization elements as in the default simulations but now spread out evenly along the stem rather than using enhanced precision in the loading and unloading zones. The homogeneous discretization using n=10 elements corresponds to a space step of 0.1m, applied evenly along the stem. Simulations were performed in a model without sucrose efflux and retrieval.

(p. 62) Supplemental figure 2.3. Validation simulations of the model with parameters equal to Thompson & Holbrook (2003). Solid lines represent the simulations with a constant xylem potential of zero, dashed lines are the simulations with a variable xylem water potential. Different colors represent timepoints, from 10min (light) to 24h (dark).
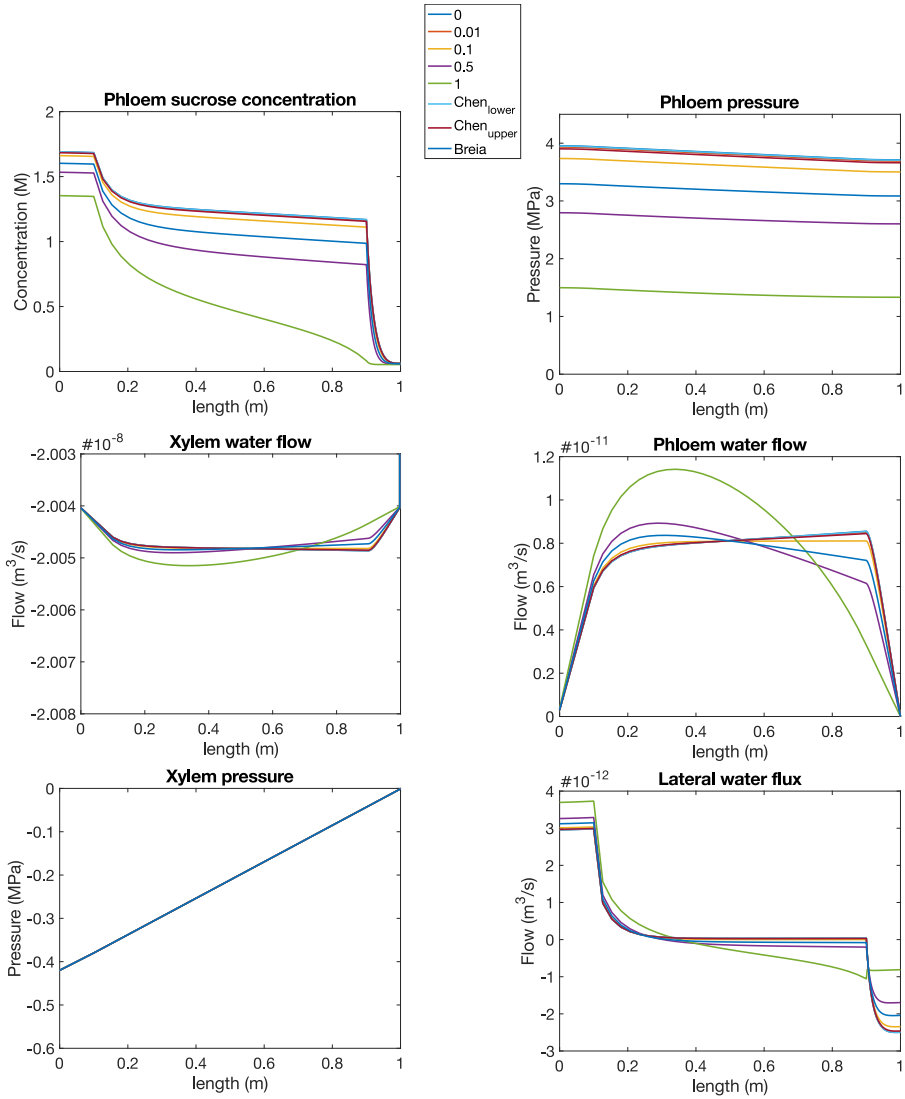
Supplementary figures

Supplementary figures

Supplemental figure 2.4. The effect of stem length variation on transport and phloem characteristics in the middle of the stem (L=0.5m). We assumed a plant height of 1m, whereas between individual plants, and over the course of plant growth both shorter and longer stem lengths may occur. To investigate the impact of differences in plant length we varied stem length between 0.5m and 1.5m, scaling the loading and unloading zones to 10% of stem length, while keeping loading/unloading rates and target concentration constant. Stem length did not qualitatively alter simulated gradients, in both smaller and larger plants an initial steep drop in sucrose concentration occurs, after which sucrose levels decrease more gradually. As expected, stem length has small quantitative effects, with concentration and pressure gradients increasing for shorter and decreasing for longer stems. For longer stems, lateral flow occurs along a longer distance, amounting to more water influx, increased sucrose dilution (resulting in the sucrose gradient along the stem) and increasing total water flow as more water has entered the phloem. Further, the time for the model to reach steady state conditions changes non-linearly from 3.0h to 3.9h to 6.1h when changing from 0.5 to 1 to 1.5m stem length. While in reality plants do not start from all zero initial conditions, these transient times do provide a measure for the time it takes for the sink-end of the plant to be able to fully respond to source-end changes.

Supplementary figures

Supplemental figure 2.5. Gradients at steady-state for different SWEET v_{max} values.

Chapter 3

Undirected sucrose efflux-mitigation by the FT-like SP6A preferentially enhances tuber resource partitioning

Bas van den Herik, Kirsten ten Tusscher

Abstract

Yield of harvestable plant organs depends on overall photosynthetic output and the subsequent distribution of the produced assimilates from source leaves across different sink organs. In this work we aim to obtain, using a two-sink transport model, mechanistic understanding of how the interplay between sink and pathway properties together determine sink resource partitioning. As a working example, we analyzed the partitioning of resources within potato plants, investigating the determinants of tuber sink yield. Our results indicated that, contrary to earlier work, with a spatially explicit biophysically detailed model, transport pathway properties significantly affect sink resource partitioning within the physiologically relevant domain. Additionally, we uncovered that xylem flow, through its hydraulic coupling to the phloem, and sucrose efflux along the phloem, also significantly affected resource partitioning. For tubers, it is the cumulative disadvantage compared to sink leaves (distance, xylem flow and sucrose efflux) that enables an undirected SP6A-mediated reduction of sucrose-efflux to preferentially benefit tuber resource partitioning. Combined with the SP6A-mediated sink strength increase, undirected SP6A introduction significantly enhances tuber resource partitioning.

Introduction

Photosynthesis and the subsequent distribution of produced assimilates across different sink organs together determine the yield of harvestable plant organs. Most research efforts have focused on optimization of photosynthesis (Driever et al., 2017; Nölke et al., 2014). However, competition for sucrose between sink organs also has a major impact on final crop yield. An important question is thus which factors affect sucrose partitioning between sinks, how the impact of these factors depends on sucrose availability and environmental conditions and how these different factors interact. As an example, in potato, upon tuber formation, sucrose delivery to tubers is substantially increased at the cost of other plant organs (Fernie et al., 2020). It is generally accepted that this enhanced tuber sucrose partitioning is achieved through a switch from symplastic to apoplastic unloading, increasing the sucrose unloading rate at tubers (Viola et al., 2001). However, this enhanced unloading operates against a background in which tuber organs may have a different affinity for sucrose than e.g., plant roots, reside at a larger distance from source leaves than young developing sink leaves, and differ physiologically from sink leaves which evaporate rather than take up water. To fully understand how much tuber unloading must increase for efficient tuber filling to occur and how this may be enhanced through targeted breeding, the importance of, and interplay with, other sink and transport pathway properties must be investigated.

Mathematical models have developed as an invaluable tool in investigating plant yield. However, to gain insight into factors determining resource partitioning, appropriate models considering all relevant aspects are needed. Currently, in large-scale agronomic models aimed at predicting field level yields as a function of plant type and environmental conditions, sucrose partitioning between sinks is based on experimentally measured, developmental stage specific, partitioning tables (de Wit et al., 2019). As such, these models provide no insight in the mechanistic basis of sucrose partitioning between plant organs. More detailed models describing individual plant performance as a function of plant physiology and architecture, such as the frequently used Functional Structural Plant (FSP) models, typically assume that relative sink strength determines sucrose partitioning (Da Silva et al., 2014; de Vries et al., 2021; Lescourret et al., 2011). These latter models thus implicitly assume that properties of the transport pathway such as resistance, length or relative nearness of different sinks to the source organs do not significantly impact sink resource allocation, which at least under certain conditions has been shown to be incorrect (Pallas et al., 2010).

In contrast, based on the generally accepted Münch-hypothesis, biophysically detailed transport models describe sucrose and water transport as a convective flow resulting from an osmotically driven pressure gradient (Hölttä et al., 2006; Lacointe & Minchin, 2008; Thompson & Holbrook, 2003). Besides automatically integrating pathway resistance and length, more detailed biophysical models can also include the effects of xylem water flow (Hölttä et al., 2006, 2009) and radial sucrose efflux (Minchin & Lacointe, 2017; van den Herik et al., 2021). In a single-sink context these biophysical transport models have highlighted the importance of pathway properties on transport dynamics, efficiency and thus eventually sucrose delivery to sinks. However, currently available two-sink models have produced conflicting outcomes on the relevance of pathway properties for sucrose partitioning. Minchin et al. (1993) demonstrated that, due to pathway resistance effects, for two sinks differing in sink-strength (v_{max}), the sink with the lowest v_{max} obtained a larger fraction of available sucrose than expected based on the v_{max} ratios alone. In other words, the weaker sink receives more sugar relative to its v_{max} than the stronger sink, while in absolute numbers the stronger sink is still dominant. This suggested that sink characteristics are not the sole determinants of resource competition. Paradoxically, results of a later study slightly extending the model of Minchin et al. (1993) by Bancal & Soltani (2002) suggested that for physiologically relevant source concentrations this phenomenon is negligible. This would imply that within the relevant range, sink characteristics fully dictate resource partitioning. Importantly, both models used a simplified phenomenological description of pathway resistance and its effect on transport, rather than explicitly modeling the osmotically driven pressure gradient driving transport. Recent work, integrating biophysically detailed transport dynamics in a multi-sink FSP-model, instead indicated that both distance and sink strength determine sugar partitioning in grape (Zhu et al., 2021). Thus, it remains unclear what the exact relevance of pathway properties is on resource partitioning and how this may depend on sink properties. A first goal of this study is therefore to investigate the impact of modeling choices for the relevance of pathway properties on resource partitioning.

While most often only the length and/or resistance of the pathway between source and sinks is considered relevant for resource partitioning, *in planta* extensive radial water and sucrose transport occurs along this pathway as well, also potentially affecting resource distribution. In addition to their roles in source and sink loading and unloading (Braun et al., 2014), SWEET transporters also facilitate bidirectional, gradient-dependent sucrose transport between the phloem and the apoplast in the long-distance phloem, with sucrose export from the phloem dominating (Chen et al., 2012), SUC/SUTs localized in the source region facilitate active, proton

coupled, sucrose loading into the phloem, while along the long-distance phloem these SUC/SUTs facilitate retrieval of sucrose from the apoplastic space (Hafke et al., 2005). Apart from these transporters' dependence on local sucrose levels, additional regulation of transport capacity takes place. As an example, in potato it was recently shown that the phloem mobile peptide StSP6A, or so-called tuberigen, inducing the transition from stolon to tuber under short day conditions (Navarro et al., 2011), binds to and thereby reduces StSWEET11 transport capacity by approximately 40% (Abelenda et al., 2019). The relevance of sucrose efflux from the long-distance transport phloem on resource partitioning has thus far not been investigated. Additionally, while sink strength and affinity have been generally considered as important properties for resource partitioning, so far physiological sink properties, particularly the direction and rate of water exchange with the environment and hence xylem flow, have not been considered. A second goal of this study is thus to obtain a mechanistic understanding of how the interplay between sink and pathway properties (length, xylem flow, sucrose efflux) together determine sink resource partitioning. As a working example, we will analyze the partitioning of resources within potato plants, investigating the determinants of tuber sink yield. The differences in sink strengths, locations, and physiological properties between developing leaves, roots and tubers provides an interesting context for studying sink resource partitioning. To this end, we used our previously developed biophysical transport model parameterized for potato (van den Herik et al., 2021) which we here extended from a single sink to a two-sink model.

Methods

According to the Münch-hypothesis, plant sucrose transport in the phloem occurs through convective flow generated by an osmotically driven pressure gradient that needs to overcome pathway resistance. Depending on the study, researchers have made different assumptions on the relevance of pathway resistance, the significance of feedback effects of sucrose concentration (via sap viscosity) thereon and the importance of explicitly modeling water transport, and the associated radial and xylem water transport. Below we briefly introduce three models for sucrose transport differing in these assumptions. To resolve whether the previously obtained paradoxical result that pathway resistance does not significantly impacts sink resource competition depends on modeling details these models were compared with regards to their results on sucrose partitioning between two sinks:

$$PC_1 = \frac{v_1}{v_1+v_2}$$

Where PC1 is the partitioning coefficient for sink 1, v_1 and v_2 are the respective unloading rates in the two sinks. For a system without radial solute flux, $v_1 + v_2$ is equal to the loading rate (v_0). (eq. 1)

2.1 Model overview and underlying assumptions

Model 1. No Resistance (VK model; Fig. 3.1A)

The no resistance or VK model (sink strength, v_{max}; sink affinity, k_m) is the simplest model we introduce. It assumes that there is no resistance in the phloem and thus no pressure gradient is required. Source concentration (c_0) is equal to sink concentration (c_1/c_2) as a result. Sink unloading rates are modeled using the Michaelis-Menten equation, implying an active unloading mode. Differences in partitioning between the two sinks thus solely depend on differences in sink v_{max} and K_m, enabling a simple analytical solution:

$$v1 = v_{max,1}\frac{c_1}{c_1+k_1} \quad \text{(eq. 2a)} \qquad v2 = v_{max,2}\frac{c_2}{c_2+k_2} \quad \text{(eq. 2b)} \qquad v_0 = v_1 + v_2 \quad \text{(eq. 2c)}$$

Model 2. Sucrose-dependent resistance (VKR model; Bancal & Soltani, (2002); Minchin et al., (1993); Fig 3.1B)

In the resistance or VKR model, transport resistance is included by introducing a total pathway resistance term (r_i) (Minchin et al., 1993). Consequently, source and sink concentrations are different ($c_0 \neq c_1 \neq c_2$) and resistance can impact resource partitioning. Bancal & Soltani (2002) further extended this model by including the influence of sucrose concentration on pathway resistance via sap viscosity. Specifically, sucrose concentrations halfway the pathway ($S_{1/2}$) are taken to compute overall pathway resistance. The equation used to calculate sucrose dependent resistance used by Bancal & Soltani (2002), valid for sucrose concentration between 0 and 1.5M, is:

$$R_S = R_3\left(0.685S_{\frac{1}{2}}^4 - 1.0411S_{\frac{1}{2}}^3 + 0.9512S_{\frac{1}{2}}^2 + 0.1364S_{\frac{1}{2}} + 0.3396\right)$$

(eq. 3)

Where R_3 is the reference viscosity at a sucrose concentration of 1M. The equation above directly gives a relation between sucrose concentration and pathway resistance. The equation is based on the viscosity effects on resistance, thus by replacing the reference resistance (R_3) for a reference viscosity, the effect of sucrose concentration on viscosity is obtained. For steady-state conditions the unloading rates in the sinks can be found by numerically solving the

system of equations below (i=1,2 for a 2-sink system):

$$v_0 - v_i = \frac{c0(c0-c_i)}{r_i} - \frac{v_{max,i}c_i}{k_i+c_i} = 0 \qquad \text{(eq. 4)}$$

In the comparison here we use this extended model of Bancal & Soltani (2002), including the sucrose dependent pathway resistance.

Model 3. Spatially explicit sucrose and water flows (Biophysically detailed model; van den Herik et al., 2021; Fig 3.1C)

The biophysically detailed model explicitly describes water and solute flow in the phloem resulting from osmotically driven pressure gradient as described by the Münch-hypothesis. Local pathway resistance depends on local phloem characteristics and sap viscosity (and hence sucrose concentrations), rather than a global pathway resistance being superimposed from calculated average pathway characteristics and sucrose concentrations. We initially only incorporated water ($J_{W, ax, Ph/X}$) and sucrose phloem flow ($J_{S, ax, Ph}$) as well as radial water flow ($J_{W, rad, Ph/X}$), to ensure conservation of water mass (W) and sucrose (S). These radial fluxes were modeled using the following equation:

$$J_{W,rad,Ph,j} = L_r A_{rad,j}\left(0 - \Psi_{Ph,j}\right), with \Psi_{Ph,j} = P_{Ph,j} + \Pi_{Ph,j} \qquad \text{(eq. 5a)}$$

Where L_r is the radial hydraulic membrane permeability, $A_{rad,j}$ the radial area between phloem and xylem, Ψ_{Ph} the phloem water potential, P_{Ph} the phloem turgor pressure and Π_{Ph} the phloem osmotic potential. For later simulations we also incorporated water flow in the xylem, which we described following the cohesion-tension theory. In these simulations radial water exchange occurs between phloem and xylem, following similar approaches by (Hölttä et al., 2006) and applied earlier by us in (van den Herik et al., 2021):

$$J_{W,rad,Ph,j} = L_r A_{rad,j}\left(\Psi_{X,j} - \Psi_{Ph,j}\right), with \Psi_{Ph,j} = P_{Ph,j} + \Pi_{Ph,j} \qquad \text{(eq. 5b)}$$

Because of the complexity the biophysically detailed model is solved numerically in an explicit geometry consisting of interconnected elements. For the current study we extended our previously developed model (van den Herik et al., 2021) to multiple sinks by endowing individual elements with the possibility for multiple inflow- and outflow-terms. Radial inflow and outflow can still be described by a single term within an element.

A) VK-model

C) Biophysically detailed model

B) VKR-model

O Single element (j)
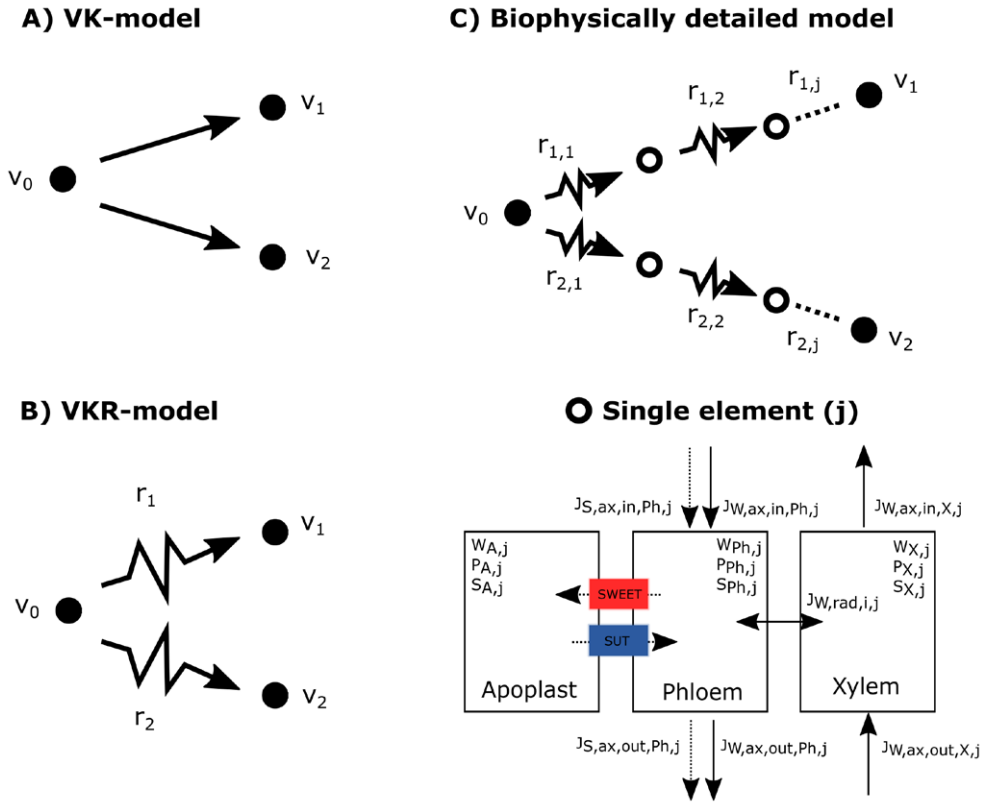
Figure 3.1. Model overview of the three compared models. A) Resource partitioning in the VK-model solely depends on the sink properties, as visualized by the straight lines leading from source (v_0) to sinks. **B)** Partitioning in the VKR-model does not only depend on sink properties, but also on pathway resistance (r). **C)** In the biophysically detailed model, pathway resistance depends on local conditions (open circles representing a single element). In a single element, water and sucrose flows are calculated based on local resistance, pressure and sucrose concentration. Furthermore, a single element consists not only of a phloem compartment, but also contains a xylem and apoplastic compartment with which water, respectively sucrose exchange occur.

Combined, this results in the reformulated water and sucrose mass-balances below:

$$\frac{\partial W_{\frac{Ph}{X},j}}{\partial t} = \left(\sum_{i=1}^{n} J_{W,ax,in,\frac{Ph}{X},j,i} - \sum_{i=1}^{m} J_{W,ax,out,\frac{Ph}{X},j,i} + J_{W,rad,\frac{Ph}{X},j} \right) \rho \qquad \text{(eq. 6a)}$$

$$\frac{\partial S_{Ph,j}}{\partial t} = \sum_{i=1}^{n} J_{S,ax,in,Ph,j,i} - \sum_{i=1}^{m} J_{S,ax,out,Ph,j,i} + J_{S,Rad,Ph,j} \qquad \text{(eq. 6b)}$$

where n is the amount of upward oriented elements connected to element j, and m the amount of downwards oriented elements connected to element j. Descriptions of the variables and parameters are given in tables 3.1 and 3.2. A more detailed description of the model, its underlying assumptions, and potato specific parametrization can be found in van den Herik et al., (2021). While the original single-sink model incorporated a passive unloading mechanism, in this work we included active unloading through incorporating a Michaelis-Menten equation to enable a one-to-one comparison with the VK and VKR model. Importantly, when comparing different types of sink organs -roots, leaves and tubers-, we maintain for all sinks an active unloading mode. We do this despite stolon ends upon tuberization switching from an active to passive unloading mode (Viola et al., 2001). The reason for not incorporating a passive unloading specific equation for tuber sinks is that this would introduce an additional dependence on the sucrose concentration assumed for tubers, complicating a comparison of how differences in sink properties such as xylem water transport and distance from source leaves affects resource partitioning.

In this more detailed model, there is no single parameter (r) for total pathway resistance. Instead, local pathway resistance depends on local viscosity and pressure differences. To see this more clearly, we rewrote the phloem specific water flowrate:

$$J_{w,ax,in,Ph} = A_{Ph}\frac{k_{Ph}}{\mu_{Ph}}\frac{\Delta P_{Ph}}{L} = N_{Ph}\pi a_{Ph}^2\frac{k_{Ph}}{\mu_{Ph}}\frac{\Delta P_{Ph}}{L} \qquad \text{(eq. 7a)}$$

in terms of pressure differential and resistance (r):

$$J_{w,ax,in,Ph} = \frac{\Delta P_{Ph}}{r_{Ph}}, \; where \; r_{Ph} = \frac{\mu_{Ph}L}{k_{Ph}N_{Ph}\pi a_{Ph}^2} \qquad \text{(eq. 7b)}$$

This yielded an expression for pathway resistance which is proportional to viscosity (μ) and pathway length (L), and inversely proportional to phloem axial permeability (k), number of phloem conduits (N) and individual phloem conduit radius (a). To study the effect of resistance on sucrose transport in this model and compare its effects to that in other models we varied pathway length as this parameter is directly proportional to resistance. While for the between model comparison we could have varied other resistance parameters from eq. 7b instead, we decided to vary length as this also enabled us to investigate the effect of different source-sink distances on resource partitioning, assuming all other pathway properties are equal. Importantly, *in planta*, hydraulic architecture/axial permeability of phloem may vary over the

length of the plant and/or between plant organs (Clerx et al., 2020), making the linear scaling of pathway length with resistance a simplifying assumption.

In the biophysical model, we used the equation for sucrose dependent viscosity as described by Morison (2002), i.e. using the volume fraction of sucrose (Φ) to calculate the viscosity:

$$\mu_{Ph,j} = \mu_\chi exp\left(\frac{4.68*0.956\phi_{Ph,j}}{1-0.956\phi_{Ph,j}}\right)$$ (eq. 8)

Given that the VKR and biophysical model use different equations to calculate viscosity we checked to what extent this results in a different sucrose concentration to viscosity mapping as this could potentially underlie differences in outcomes between the two models. Fig. S3.1 illustrates that despite the different applied equations a highly similar mapping occurs, indicating this cannot be the cause of differences in model results.

2.2 Simulation details and model implementation

Standard sink-strength was set at v_{max}=12.5nmol/s, sink-affinity was set at K_m=75mM and pathway resistance at r=7.5e12 Tmol s/m^6 (for the VKR model) or pathway length at l=0.25m (for the biophysically detailed model). The pathway length of 0.25m corresponds to an equal resistance as the VKR model for a sugar concentration of 0mM. That is, the resistances are equal for conditions in which viscosity effects of solutes are ignored. To investigate differences in resource partitioning between the three models we considered three different scenarios in a single-source, two-sink system, with the two sinks differing in either sink strength (v_{max}), sink affinity (K_m) or pathway resistance (r). For the v_{max} scenario we used 22.5nmol/s for sink 1 and 2.5 nmol/s for sink 2, for the K_m scenario we used 75mM for sink 1 and 750mM for sink 2, and for the resistance scenario we used 7.5 Tmol s m-6 and 150 Tmol s m^{-6} for the VKR model and 0.25m and 5m for the biophysical detailed model. To compare the three models, steady-state solutions for a range of loading rates (0.025 - 25 nmol/s) were computed and phloem-only conditions were used (eq. 5a). Above mentioned values were taken from Bancal & Soltani (2002), to enable comparison between their earlier results and our model outcomes. To validate the robustness of the analysis, we compared our results for a default zero-resistance shared pathway to a non-zero resistance shared pathway from source to sinks. This did not significantly affect the results (Fig S3.2).

Table 3.1. Symbols and units for the used variables/equations in the biophysically detailed model.

Variable	Symbol	Units
Water mass	$W_{Ph/X,j}$	g
Sucrose	$S_{Ph,j}$	mol
Pressure	$P_{Ph/X,j}$	MPa
Sucrose concentration	$C_{Ph,j}$	mol/m^3
Axial water flow	$J_{W,ax,in/out,Ph/X,j}$	g/s
Axial sucrose flow	$J_{S,ax,in/out,Ph/X,j}$	mol/s
Radial water flow	$J_{W,rad,Ph/X,j}$	g
Radial sucrose flow	$J_{S,rad,Ph,j}$	mol/s
Water potential	$\Phi_{Ph/X,j}$	MPa
Axial area	$A_{Ph/X,j}$	m^2
Radial area	$A_{rad,j}$	m^2
Osmotic potential phloem	$\psi_{Ph,j}$	MPa
Dynamic viscosity phloem	$\mu_{Ph,j}$	MPa s

The impact of xylem flow on resource partitioning was investigated using a constant water uptake of sink 2 (2e-8 m3/s, equal to total uptake in van den Herik et al., 2021) representing a root organ, while varying water flow in sink 1 between -1e-8 m^3/s (water evaporation equal to source) and 2e-8 m^3/s (water uptake equal to sink 2), representing organs on the continuum from leaf to tuber to root. Evaporation in the source region was set equal to the net sum of the water flows in both sinks, and simulations were performed for 3 different source loading rates. We also investigated 3 biologically realistic 2 sink scenarios (root-root, tuber-root, young sink leaf-root), where we imposed a soil water potential of 0MPa (Perämäki et al., 2001), simulating tubers by decreasing water uptake permeability by 90% relative to roots, and young leaves through an evaporation rate of 10% of that of mature leaves.

Radial sucrose transport between phloem and apoplast, and sucrose removal from the apoplast were modeled as done in van den Herik et al. (2021). In summary, bidirectional SWEET-transport facilitates efflux from the phloem (v_{max} = 0.148 mol/m^3/s, K_m = 70mM, Chen et al., 2012) and retrieval from the apoplast (v_{max} = 0.148 mol/m^3/s, K_m= 10mM, Chen et al., 2012), while SUT-transporters (v_{max} = 0.117 mol/m3/s, K_m = 1mM, Schulze et al., 2000) also facilitate retrieval

Table 3.2. Relevant parameters for the biophysically detailed model used in this work, for a full description of the model, parameters and parameter estimation see van den Herik et al. (2021).

Parameter	Symbol	Value	Units
Density of water	ρ	0.998e6	g/m^3
Radial hydraulic membrane permeability	L_r	5e-8	m/MPa/s
Dynamic viscosity water/xylem	μ_x	1.0019e-9	MPa/s
Phloem sieve element radius	a_{Ph}	8.4e-6 at t=0	m
Xylem conduit radius	a_x	30e-6	m
Axial permeability phloem	k_p	3.82e-12	m^2
Elastic modulus phloem	ε_p	30	MPa
Elastic modulus xylem	ε_x	750	MPa
Transpiration rate	J_{trans}	0.02	g/s
Water potential soil	ψ_{soil}	0	MPa

from the apoplast to the phloem. Efflux and retrieval rates were implemented as mol per m^3 per s and were therefore constant on a per length basis during the steady-state conditions at which we evaluate model outcomes. SP6A-mediated efflux-mitigation was modeled by decreasing the v_{max} of SWEETs by 40% as was reported by Abelenda et al. (2019).

The VK model was analytically solved. The system of equations describing the VKR model was solved in Matlab R2020b using the build in function 'fsolve' with a function threshold of 1e-13. Residual function values were checked to ensure the correctness of the solution and various initial values were used to search for alternative solutions of the system. We only considered biologically valid solutions, i.e. positive solute concentrations. The system of differential equations describing the biophysically detailed model was implemented in MatlabR2020b and was solved using the build-in solver 'ode15s', using an integration time step of $\Delta t = 1s$ using a non-homogeneous mesh for loading (20 elements, 0.005m/element), long-distance pathway (30 elements, 0.0083m/element) and unloading zones (20 elements, 0.005m/element) as described in detail by van den Herik et al. (2021). The source code for the biophysically detailed model, and implementation of the VKR and VK models is available on https://tbb.bio.uu.nl/khwjtuss/TwoSinkSucroseTransport/

Results

To investigate whether the previously found limited importance of pathway resistance on sink resource partitioning depends on modeling details we compared the previously used, simpler VKR model with the more detailed biophysical model, with the VK model serving as a baseline. First, we started with investigating model differences in a single sink setting.

Structural underestimation of sucrose concentration and resistance in the VKR model

A major difference between the VKR and biophysical model is the manner in which sucrose phloem concentrations are used to compute resistance. In the biophysical model sucrose gradients are computed in a spatially resolved manner with explicit source loading zones, sink unloading zones and lateral water transport resulting in non-linear gradients (Fig. 3.2A-C, blue lines). In contrast, the VKR model assumes a linear source-sink concentration gradient (Fig 3.2A-C, green lines indicate the linear gradient for the biophysical model). In the biophysical model local pathway resistance is subsequently computed from local sucrose concentration while in the VKR model an average, overall pathway resistance is computed from mean pathway sucrose concentration. This results in an underestimation of pathway sucrose concentration (Fig.3.2D,F) and resistance (Fig. 3.2E,G) when using a linear VKR-type gradient. The level of underestimation increases with concentration gradient steepness, i.e. increasing loading (Fig 3.2A versus B, Fig 3.2D,E) and unloading rates (Fig 3.2B versus C, Fig. 3.2F,G).

Instead of extracting a VKR-type gradient from the biophysical model we next explicitly simulate the VKR model using equal parametrization as for the biophysical model. Due to the dynamic feedback between resistance and concentration, the general tendency for lower resistances in the VKR model results in significantly less steep source-sink concentration gradients, and lower source concentrations (Fig 3.2A-C, orange lines). Importantly, these lower source concentrations in the VKR model result in an overestimation of the minimum loading rates necessary to obtain physiologically relevant source concentrations (0.1-2M).

Effects of resistance and biophysical detail on resource allocation

Next, we investigated the impact of using either a baseline VK, simple VKR or biophysical model on resource partitioning between two sinks. We hypothesized that the structural underestimation of pathway resistance in the VKR compared to the biophysically detailed model impacts resource partitioning.

Sink Strength (V$_{max}$)

At the onset of tuberization, a switch from symplastic to apoplastic unloading mode increases tuber sucrose unloading rate. As a logical first scenario we thus investigated the effect of differences in sink strength on resource partitioning. For $v_{max,1}$=22.5nmol/s and $v_{max,2}$=2.5nmol/s the simple VK model predicts the partitioning coefficient to equal the v_{max} ratio ($v_{max,1}$/$v_{max,2}$ = 90%) (Fig. 3.3A, dotted line). In absence of resistance, source concentration equals sink concentration, resulting in equal sink concentrations. This causes the sinks to be equally saturated, resulting in v_{max} values being the sole source of differences in sink uptake. In
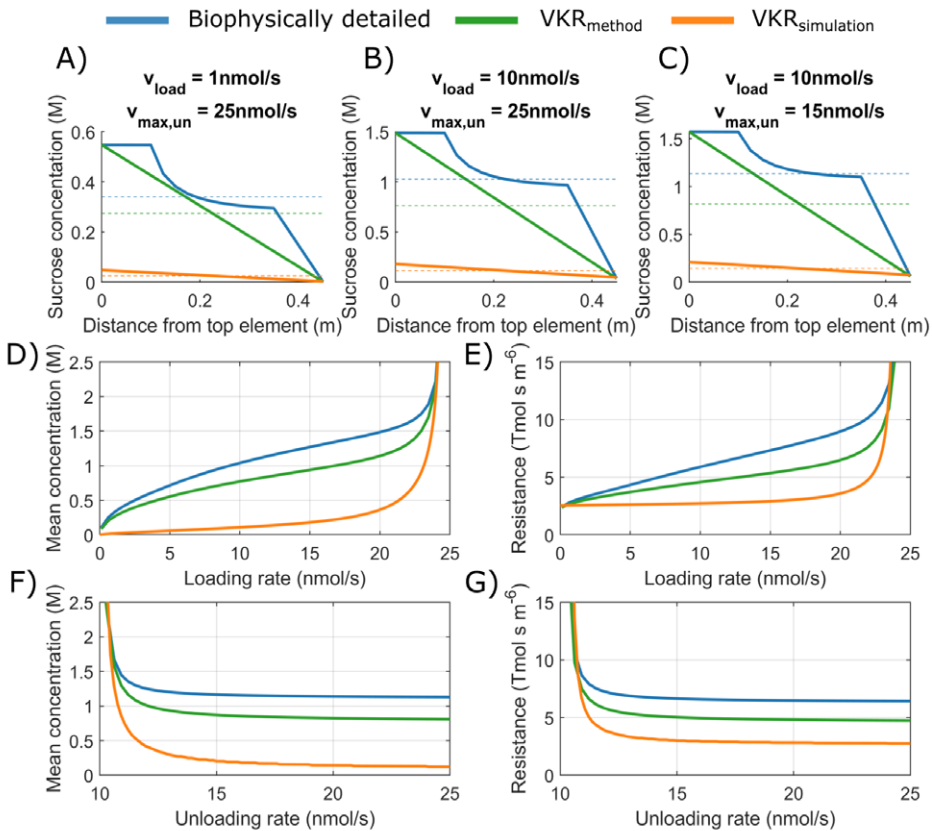

Figure 3.2. Sucrose concentration and resistance are underestimated when not including a spatial sucrose gradient. Concentration gradients for (A) v_{load} = 1 nmol/s, $v_{max,un}$=25nmol/s,(B) v_{load} = 10 nmol/s, $v_{max,un}$=25nmol/s (C), v_{load} = 10 nmol/s, $v_{max,un}$=15nmol/s. Dotted lines indicate mean pathway sucrose concentration. (D) Mean concentration as a function of source loading rate for a constant unloading rate of 25 nmol/s and (E) mean pathway resistance as a function of source loading rate. (F) Mean concentration as a function of sink unloading rate for constant loading rate of 10 nmol/s and (G) mean pathway resistance as a function of sink unloading rate.

contrast, the VKR model predicts the partitioning coefficient to start at 50% and increase in a saturating manner towards the v_{max} ratio defined 90% (Fig. 3.3A, dashed line). In the presence of resistance, differences between source and sink concentrations arise, allowing for between sink concentration differences. The higher unloading rate at sink 1 results in a lower local sink concentration (Fig. 3.3B, dashed blue vs. dashed orange line) and reduced saturation (Fig. 3.3C, compare position of blue versus orange squares on the saturation curves). This causes sink 1 resource partitioning to be lower than expected based on v_{max} ratio alone. Partitioning reaches the expected v_{max} defined value when both sinks approach saturation at high loading rates (approx. 20 nmol/s).

The biophysically detailed model predicts a slower, sigmoidal increase to 90% partitioning (Fig. 3.3A, solid line). In both the VKR and biophysical model, the higher $v_{max,1}$ resulted in a lower $c1$, lower mean pathway concentration and resistance, causing $r_1/r_2<1$ (Fig 3.3D). However, a lower c_1 also results in a steeper concentration gradient $c0-c1$, that is more underestimated in the VKR model than the c_0-c_2 gradient. As a consequence, the VKR model overestimates r_1-r_2 differences, resulting in a r_1/r_2 ratio closer to 1 in the biophysical model (Fig 3.3D). Thus, while absolute resistance levels are higher in both pathways, relative resistance differences between the two pathways are smaller in the biophysical model. Since the resistance difference acts against the v_{max} driven concentration gradient difference (lower resistance causes higher sink concentrations), the reduced relative resistance difference in the biophysical model allows for larger between sink concentration (Fig 3.3B) and saturation differences (Fig. 3.3C, compare location of the dots representing the biophysical model with the squares representing the VKR-model). This further diminishes the advantage of sink 1 from its higher v_{max}. Summarizing, over a large range of loading rates, an increased unloading at the tubers (with higher v_{max}) has less effect than expected based on unloading rates only.

Sink Affinity (k_m)

In addition to sink strength, plant sink organs may also differ in sucrose affinity. For higher sink 1 affinity (k_1=75mM, k_2=750mM), at equal sink concentrations, the effective uptake rate of sink 1 (v_1), is significantly higher than that of sink 2 (v_2). In the VK model, with its equal sink concentrations, this causes the partitioning coefficient to heavily favor sink 1 at low loading rates and hence sink concentrations (Fig. 3.4A, dotted line). At higher loading rates both sinks saturate, causing the partitioning to converge to the 50% defined by the equal v_{max} values. In the VKR model, the higher affinity of sink 1, and hence higher uptake at low loading rates,
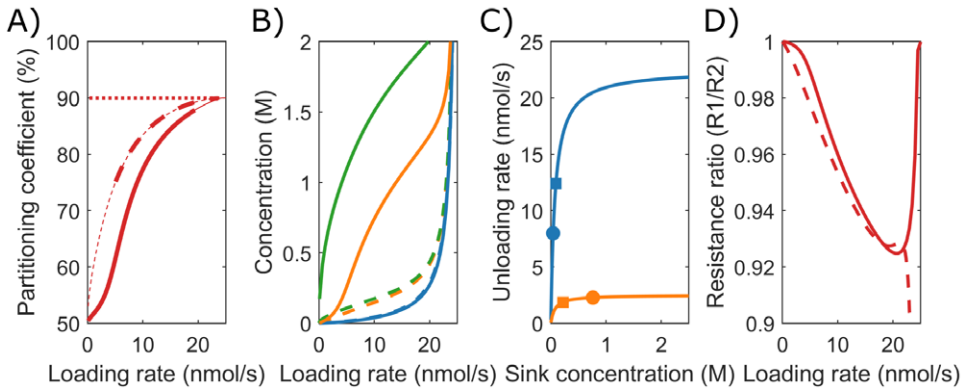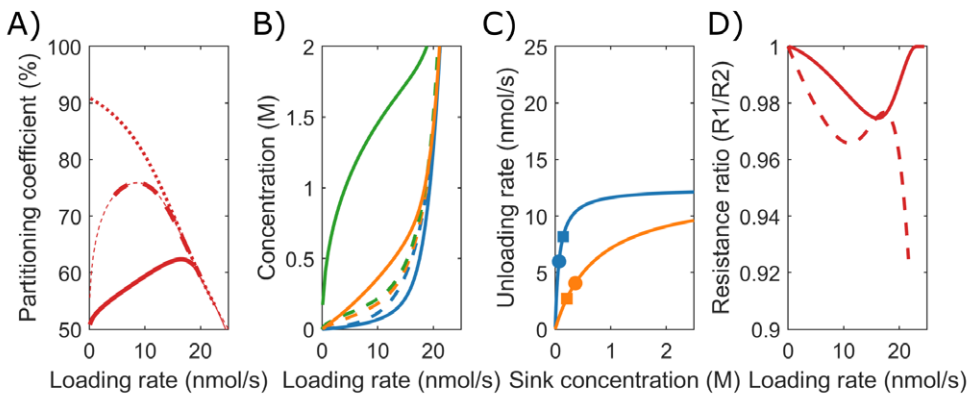
Figure 3.3. Impact of model choice on partitioning coefficients and the underlying mechanisms for different sink strengths (v_{max}). A) Partitioning coefficient for the VK (dotted), VKR (dashed) and biophysical (solid) models. The bold lines in (A) represent physiologically relevant conditions (0.1M<c0<2M), showing that the biophysical model has a much broader physiologically relevant range. B) Sink 1 (Blue), Sink 2 (Orange) and source (Green) sucrose concentrations. C) Michaelis-Menten curves for unloading rates, with dots representing the biophysical model and squares the VKR-model. D) Resistance ratios for the VKR (Dashed) and biophysical (Solid) models.

results in lower local concentration at sink 1 (Fig. 3.4B). Consequently, even though $k_2>>k_1$, sink 2 is more saturated than sink 1 (Fig. 3.4C). As a result, partitioning to sink 1 is lower than expected based on K_m differences for low loading rates. As loading rate increases first sink 1 approaches saturation, enabling it to profit from its higher affinity. As loading rates increase further (beyond 10nmol/s), sink 2 also approaches saturation, removing sink 1's higher affinity benefit and causing partitioning to approach the 50% defined by the equal v_{max} values (Fig. 3.4A, Dashed line). As above for the different unloading rates, source concentrations, source-sink concentration gradients, resistance ratio (Fig. 3.4D) and between sink concentration differences are larger in the biophysical model, explaining again the decreased advantage of sink 1 in the biophysical model (Fig. 3.4A, solid line).

Pathway resistance

Sink organs are formed at different positions in the plant, with different transport pathway lengths from source to sink resulting in different pathway resistances, e.g., tubers form at a larger distance from the sucrose providing source leaves than young developing sink leaves. Importantly, resistance both affects and is dependent on concentration differences. For comparison purposes we use equal baseline resistance values at zero sucrose concentrations

for the two models, while allowing net, sucrose dependent resistance values to differ. In the VK model partitioning equals the v_{max} defined value of 50% (Fig. 3.5A, dotted line) as all sink parameters are equal and resistance is not incorporated. For the VKR model, $r_1 << r_2$ ($r_1 = 7.5e12$ Tmol s/m^6 and $r_2 = 150$ Tmol s/m^6) implies that $c_1 >> c_2$ (Eq. 3), causing a reversal in the sink 1 and 2 concentration differences compared to the earlier two scenarios (Fig 5B, dashed lines). Additionally, between sink concentration differences are significantly larger. The higher r_2 now

Figure 3.4. Impact of model choice on partitioning coefficients and the underlying mechanisms for different sink affinities (K_m). A) Partitioning coefficient for the VK (dotted), VKR (dashed) and biophysical (solid) models. The bold lines in (A) represent physiologically relevant conditions ($0.1M < c_0 < 2M$), showing that the biophysical model has a much broader physiologically relevant range. **B)** Sink 1 (Blue), Sink 2 (Orange) and source (Green) sucrose concentrations. **C)** Michaelis-Menten curves for unloading rates, with dots representing the biophysical model and squares the VKR-model. **D)** Resistance ratios for the VKR (Dashed) and biophysical (solid) models.

leads to lower sink 2 concentrations and thus a lower unloading rate in sink 2 when sinks are not yet saturated (Fig. 3.5C, compare position of blue versus orange squares on the saturation curves), resulting in a higher partitioning towards sink 1 (Fig. 3.5A, dashed line). When sink 1 becomes saturated (~10nmol/s), a further increase in loading rate increases unloading at sink 2, increasing c_2, and decreasing sink 1 favored partitioning. As loading rate further increases, sink 2 also saturates and the v_{max} defined ratio of 50% partitioning is reached.

Again, in the biophysical model source concentrations are higher, source-sink gradients are steeper (Fig 3.5B) and relative resistance differences are smaller (Fig. 3.5D, r1/r2 slightly closer to 1 for unsaturated sinks). In the v_{max} and K_m scenarios, resistance differences oppose the v_{max}

and K_m driven sink concentration differences, which in turn limit v_{max} and K_m driven resource partitioning advantages. Here, it is solely the resistance difference that drives concentration differences instead, with these concentration differences causing rather than reducing resource partitioning advantages. Reduced relative resistance differences in the biophysical model now reduce rather than enhance between sink concentration (Fig 3.5B) and saturation differences (Fig. 3.5C, compare location of the dots representing the biophysical model with the squares representing the VKR-model) and thereby limit the advantage of a lower resistance for sink 1 relative to the VKR model. Thus, for a broad range of loading rates, the disadvantage that a tuber experiences from its larger transport pathway length and resistance is significantly less than expected based on resistance differences alone.

Xylem water flow differences affect sucrose partitioning

As phloem and xylem are hydraulically connected, changes in xylem water potential affect phloem water and solute transport (Konrad et al., 2019; Savage et al., 2016; Sevanto et al., 2011). An interesting question thus is whether, in addition to differences in sink characteristics and pathway resistance/length, differences between sink organs in terms of xylem water flow affects resource partitioning. Note that to investigate this only the biophysically detailed model is suitable. To investigate the impact of xylem flow on resource partitioning we used constant, equal VKR-characteristics, a constant water uptake of sink 2 representing a root organ, while varying water flow in sink 1. When sink 1 xylem water uptake rate equals that of sink 2 (2e-8 m^3/s), sucrose partitioning equals 50% (Fig. 3.6A). A linear increase in sink 1 resource allocation occurred when moving from gradually decreasing water uptake to gradually increasing water evaporation in sink 1. This increased allocation to sink 1 is stronger for lower loading rates, when sinks are less saturated (Fig. 3.6A). These results indicate that a smaller xylem counterflow, and even more so a xylem co-flow increased partitioning towards a sink.

Increased turgor gradient and sucrose concentration causes increased sucrose partitioning

To understand this phenomenon, we investigated scenarios in which sink 1 takes up water at a lower rate than sink 2 (Fig. 3.6B) or evaporates water (Fig. 3.6C). Both the lower water uptake and evaporation resulted in a more negative xylem potential in the pathway. Additionally, for an evaporating sink 1 a reversal in the xylem potential gradient occurs. As radial water flow is directed from high (least negative) to low (most negative) water potentials (Eq. 5b), differences in xylem potential impact lateral water flow and thereby phloem water potential. For phloem to deliver solutes to the sinks, water potentials in phloem and xylem must fulfill the constraint that
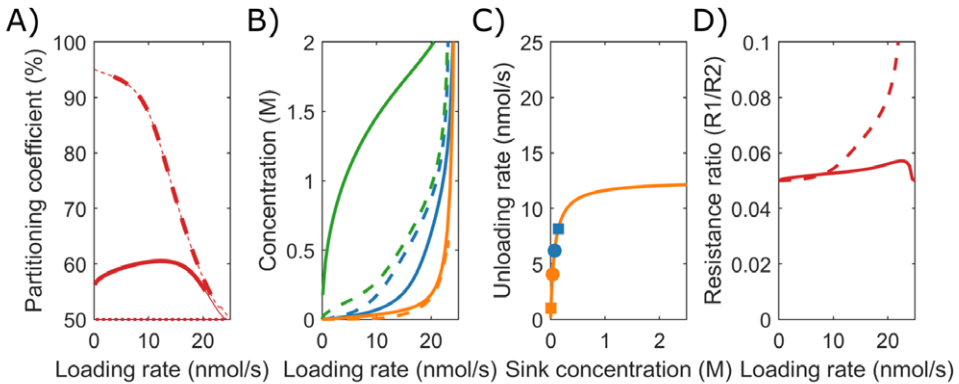
Figure 3.5. Impact of model choice on partitioning coefficients and the underlying mechanisms for different pathway resistance/length (r). A) Partitioning coefficient for the VK (dotted), VKR (dashed) and biophysical (solid) models. The bold lines in (A) represent physiologically relevant conditions ($0.1M<c_0<2M$), showing that the biophysical model has a much broader physiologically relevant range. B) Sink 1 (Blue), Sink 2 (Orange) and source (Green) sucrose concentrations. C) Michaelis-Menten curves for unloading rates, with dots representing the biophysical model and squares the VKR-model. D) Resistance ratios for the VKR (Dashed) and biophysical (solid) models.

lateral waterflow is directed towards the phloem in the source and long-distance pathway and towards the xylem in the sinks (Hölttä et al., 2006, 2009; Windt et al., 2006). The decreased (more negative) xylem water potential in the pathway towards sink 1 thus dictate an accompanying decrease in phloem water potential that is largest in the scenario where sink 1 evaporates water. Phloem water potential consists of a turgor pressure (P) and osmotic potential (Π) component. Our simulations show that the decreased (more negative) phloem potential in the pathway towards sink 1 arises from a combination of lower turgor pressure and more negative osmotic potential in both scenarios. A lower turgor pressure towards sink 1, combined with an equal turgor pressure at the branching point results in a larger turgor-pressure gradient and hence water flow towards sink 1 relative to sink 2. Additionally, the decreased osmotic potential arises from increased sucrose concentration in the pathway towards sink 1. The combined larger flow and higher sucrose concentration explain the increased sucrose partitioning towards sink 1, with a larger effect in the evaporation scenario where xylem and phloem potential become more negative.

Resource allocation differences between roots, tubers, and developing leaves
In the simulations above, we imposed water flow boundaries (influx or efflux rate) to

systematically investigate the influence of xylem water flow rate and direction on resource partitioning. However, in most model applications, xylem water flow rate and direction are not a control parameter but rather an emergent property from soil and atmosphere water potential or organ evaporation rates. We therefore also investigated 3 biologically realistic 2 sink scenarios (root-root, tuber-root, young sink leaf-root), where we imposed a soil water potential of 0MPa, simulating tubers by decreasing water uptake permeability by 90%, and young leaves through an evaporation rate of 10% of that of mature leaves. While this results in different, biologically more realistic, xylem water potentials (Fig. 3.7A)(Bland & Tanner, 1986), we again observe enhanced resource allocation to sinks with a reduced xylem counter flow (tuber versus root) and even more so for xylem co-flow (leaf versus root) (Fig. 3.7B). Summarizing, we demonstrate that not only sink VK or pathway resistance properties affect resource partitioning, but that also differences in xylem water flow influence partitioning via the hydraulic connection with the phloem. Differences in xylem water flow causes tubers to have a resource partitioning advantage relative to the roots yet a disadvantage relative to sink leaves.

Sucrose efflux further aggravates disadvantage of roots and tubers

Besides simulating the effect of xylem flow and radial water exchange between phloem and xylem, the biophysically detailed model is also capable of simulating the effects of radial sucrose exchange between phloem and the apoplast. This exchange is mediated by bidirectional SWEET-transporters (Chen et al., 2012) and active SUC/SUT-importers (Hafke et al., 2005). It was previously shown that sucrose efflux, retrieval and efflux mitigation can strongly affect phloem transport characteristics and sucrose delivery to sinks (Minchin & Lacointe, 2017; van den Herik et al., 2021). To investigate the impact of long-distance sucrose efflux, we simulate a young leaf and root/tuber, with initially equal sink and pathway properties (v_{max}=5nmol/s, K_m=75mM, l=0.25m), incrementally adding different properties affecting resource partitioning. First, we incorporated differences in source-sink distance, with the leaf sink located at 0.1m and sink roots/tubers at 0.3m from the source, replicating a potato plant architecture. Like before, the sink with smaller pathway length, and thus resistance, experiences higher resource partitioning (Fig. 3.8A, Blue line). Secondly, we incorporated differences in xylem flow, setting leaf sink evaporation at 10% of that of mature leaves, and water potential in the soil at 0MPa. Differences in xylem flow strongly benefits leaves sucrose partitioning (Fig. 3.8A, Orange line). Combining length and xylem flow differences demonstrates that these effects are largely additive (Fig.3. 8A, Green line).
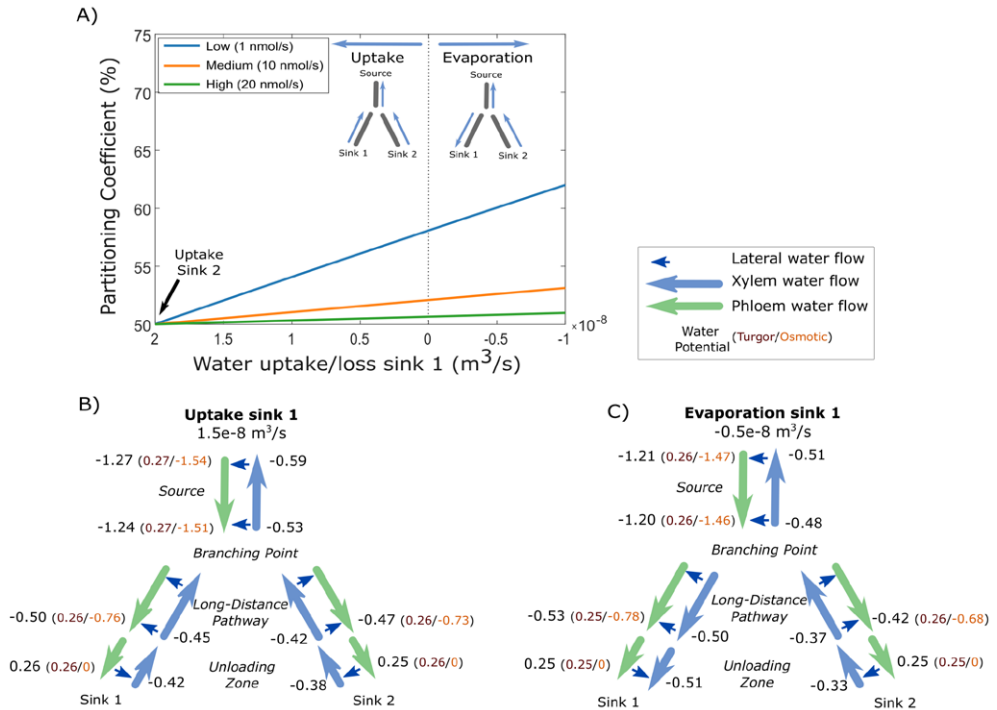
Figure 3.6. The effect of xylem boundaries on carbon partitioning between two sinks. (A) Partitioning coefficient for three loading rates as a function of xylem water boundary conditions in sink 1, for a constant sink 2 water uptake of 2e-8 m³/s. Water potentials of phloem and xylem (in MPa) at various locations in the model for a situation in which sink 1 evaporates at a rate of 0.5e-8 m³/s **(B)** or takes up water at a rate of 1.5e-8 m³/s **(C)**. The scenarios in B and C are taken from the low loading rate conditions of A. For the phloem water potential, the separate contributions of turgor and osmotic potential are given in brackets.

Next, we incorporated SWEET-mediated sucrose efflux along the long-distance pathway, following van den Herik (2021), with radial efflux amounting to up to 23% of total sucrose loading rate. Trivially, sucrose export along the long-distance phloem aggravates the resource partitioning disadvantage due to increased pathway length (Fig. 3.8B, Blue lines). However, also the disadvantage due to different xylem flow conditions (Fig. 3.8B, orange lines) and their combination (Fig. 3.8B, Green lines) are aggravated, indicating that xylem flow differences also impact radial sucrose transport. Note that, for low loading rates (below 15% of max. unloading rate), partitioning towards tubers is close to 0%. For these low loading rates, whilst the phloem localized SWEETS still experience sufficient sucrose, the resulting efflux of sucrose along the pathway causes almost no sucrose to arrive at sinks. The longer pathway length and different xylem flow conditions results in larger sucrose efflux towards tubers, resulting in a near zero

partitioning coefficient despite leaf sucrose yield also being very low (Fig. S3.3). Smaller length differences or lower leaf evaporation rate decreased the regime in which partitioning towards roots/tubers is 0% (Fig. S3.4).

Efflux mitigation and increased sink strength mediated by SP6A work in different saturation regimes

SWEET-mediated sucrose efflux is reduced by 40% upon the introduction of the FT-like protein SP6A in the phloem (Abelenda et al., 2019). However, there is currently no mechanism known that would restrict the loading and transport of SP6A specifically to tuber directed phloem. We hypothesize that instead, the cumulative disadvantage tubers experience from their longer source-sink distance, xylem flow and sucrose export may enable undirected SP6A (i.e. present in all long-distance phloem) to preferentially increase tuber sucrose partitioning. Based on
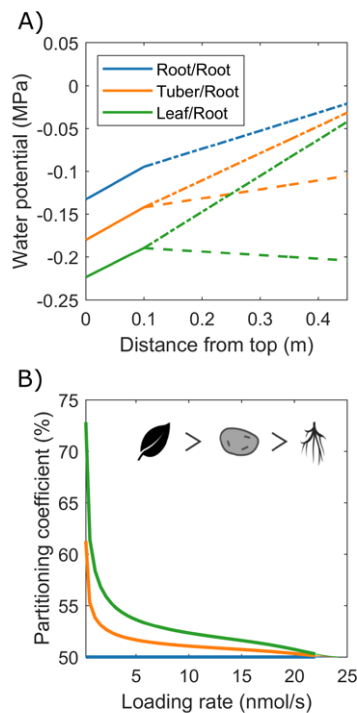
Figure 3.7. Resource allocation differences between roots, tubers, and developing leaves. A) Xylem water potential along the plant for the three specific organ scenarios. Solid lines represent water potential in the part of the plant stem containing source leaves, dashed lines the water potential along the long-distance pathway leading towards sink 1 (Root/Tuber/Leaf) and dash-dotted lines the water potential along the long-distance pathway ending at sink 2 (Root). **B)** Partitioning coefficient as a function of loading rate for the same three organ type cases as shown in A. The symbols show the organ priority.

the experimental data, the undirected SP6A effect on sucrose transport was incorporated into our model by reducing for all long-distance pathways, independent of the sink organ they are directed towards, the v_{max} parameter to 60% of its original value. Indeed, undirected SP6A introduction preferentially enhanced sucrose delivery towards roots/tubers (Fig. 3.8C, red line) mostly through decreasing the regime of loading rates for which no sucrose reaches the roots/tubers due to radial efflux. Still, this SP6A effect does not enable tubers to become the dominant sucrose sinks. Besides its role in sucrose efflux-mitigation, SP6A has been previously identified
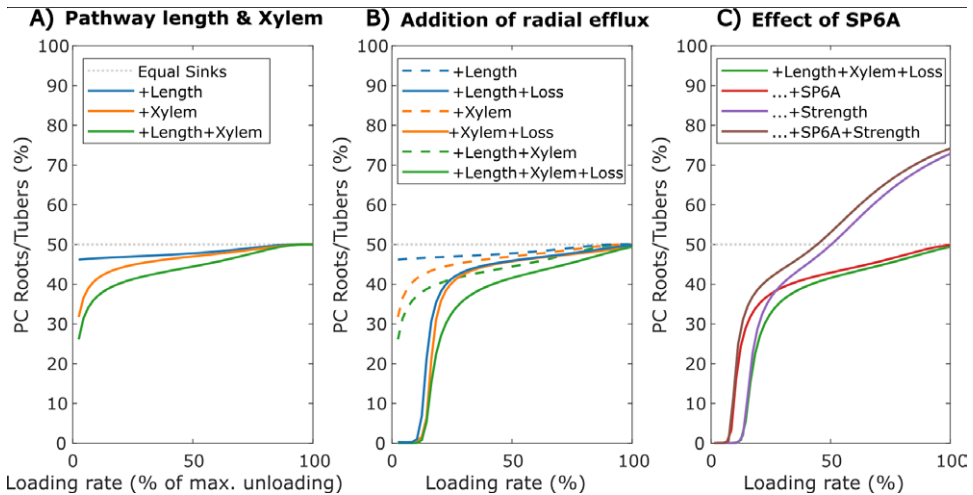
Figure 3.8. Individual and combined effects of pathway properties and SP6A on sucrose partitioning towards roots/tubers. A) Individual and combined effect of pathway length and xylem water flow for further equal sink-leaves and roots/tubers sink and pathway characteristics. B) The effect of radial efflux on resource partitioning towards roots/tubers. C) The dual effect of SP6A, mitigating efflux and increasing roots/tubers sink strength.

as important factor initiating tuberization. During tuberization, the switch in unloading mode together with sink expansion increases sink strength. We therefore investigated the effect of increased sink strength and the interplay with SP6A-mediated efflux-mitigation. Experimental observations suggest sink-source feedback, with sink-strength affecting loading rates, likely through phloem sucrose levels (Chiou & Bush, 1998). We therefore assumed the tuber sink strength increase to be accompanied by an equal sized source strength increase. An increased tuber sink-strength (5 nmol/s to 15 nmol/s) enhanced tuber partitioning particularly at higher loading rates (Fig. 3.8C, Purple line). For very low loading rates, no sucrose arrived at the roots/

tubers, rendering enhanced sink strength irrelevant. Beyond these loading rates, the effect of tuber sink strength increased with loading rate due to enhanced sink saturation (Fig. S3.5). As a result, for high loading rates, tubers can now become the dominant sink organ. When combining SP6A-mediated efflux-mitigation and sink strength increase (Fig. 3.8C, Brown line), we observe mostly additive effects, with efflux-mitigation effects dominating at low and increased sink strength effects dominating at high loading rates. Combined, these results indicate that undirected SP6A sucrose efflux reduction broadens the range of loading rates over which tubers obtain significant amounts of sugars.

Discussion

Yield of harvestable plant organs critically depends on sucrose partitioning between competing sinks. Understanding the mechanisms determining resource partitioning is thus of great agro-economic relevance, and modeling studies play an important role in unraveling the complex underlying processes. In this modeling study we performed a systematic investigation into the individual and combined effects of sink characteristics (unloading strength, sucrose affinity and water uptake or evaporation) and pathway properties (length, resistance, and radial sucrose efflux) on sucrose partitioning, taking potato tuber sucrose delivery as an example case.

We demonstrated that in our biophysically detailed model, the effects of sink-strength and -affinity, as well as pathway resistance/length, are significantly enhanced compared to earlier studies using simplified sucrose transport models (Bancal & Soltani, 2002; Minchin et al., 1993). These differences could be attributed to the underestimation of sucrose concentration and pathway resistance in the simplified models. We further show that these effects are relevant in a much broader loading rate range compared to Bancal & Soltani (2002) due to higher source concentrations. Our findings on the importance of pathway properties are supported by recent findings that source-sink distance differences drive divergence in yield between grapes (Pallas et al., 2010; Zhu et al., 2021). Additionally, we observed that the previously reported phenomenon of weakest sink prioritization – the larger than expected sucrose allocation to the weaker sink for non-saturating sucrose loading – occurs not only for sinks differing in sink-strength, but also for differences in sucrose affinity or pathway length.

Interestingly, we found that in addition to phloem pathway length, the rate and direction of the coupled, parallel xylem flow, also impacted sink partitioning. For equal sink characteristics,

sucrose partitioning to a sink linearly increased with xylem flow and potential. This effect could be explained from the hydraulic coupling between phloem and xylem, and the concomitant changes in both phloem osmotic and turgor pressure. Thus, while previous research focused on the impact of xylem flow, via leaf water potential and photosynthetic activity on plant organ growth (Solari et al., 2006),here we show that even for constant photosynthesis and hence loading rates, the hydraulic coupling between xylem and phloem causes xylem flow to impact sucrose transport and growth.

In the case of potato tubers, we showed that their limited water uptake causes them to be at an advantage in terms of resource partitioning relative to roots that take up considerably more water, yet at a disadvantage to young leaves, that evaporate limited amounts of water. An additional disadvantage arises from the larger distance tubers and roots have compared to young leaves from source leaves. Both disadvantages are increased when including SWEET-mediated radial sucrose export. This exacerbated disadvantage enables undirected SP6A-mediated export-mitigation to preferentially benefit root/tuber resource allocation. This export-mitigating effect of SP6A, that dominates at lower loading rates for which phloem transport resistance and xylem water flow differences are relevant, complements the effect of SP6A on tuber sink-strength that becomes fully effective for high, saturating loading rates. Overall, the undirected SP6A-signal significantly broadens the range of loading rates over which tubers obtain significant amounts of sugars.

A major point of discussion is the *in planta* relevance of the reported results. In essence, this issue revolves around the question whether sinks under most physiological conditions operate at/near saturation, or rather operate under non-saturating conditions. As our, and previous results (Bancal & Soltani, 2002; Minchin et al., 1993) show, under saturating conditions the ratio between sink-strength (v_{max}) dictates resource partitioning. It is only under non-saturating conditions that other factors such as sink-affinity, pathway resistance/length, xylem flow rate and direction and radial sucrose efflux significantly affect resource partitioning, weakest sink prioritization occurs and SP6A efflux mitigation effects weigh in. Classical experiments have demonstrated that upon chemically (Farrar & Minchin, 1991), or cooling induced sink strength reduction (Minchin et al., 1997) sucrose import in unaffected sinks adjusts to the new conditions on a timescale of hours. This slow adaptation has been taken as evidence for sink saturation, reasoning that enhanced uptake requires upregulation of sink uptake capacity (Minchin & Lacointe, 2005). Here we challenge this view. First, only if remaining sinks are unable to import

any additional sucrose would this support prior sink saturation, while if remaining sinks are unable to import all extra sucrose immediately this merely implies that maximum sink uptake capacity is now exceeded. Secondly, upon enhanced sucrose availability, sucrose metabolism requires upregulation. This delayed increase in utilization could lead to sucrose accumulation with negative feedback on sink uptake limiting the initial increase in uptake (Farrar & Minchin, 1991). Similarly, feedback regulation between sink demand and source supply may result in reduced source loading upon sink removal due to sugar accumulation in phloem or leaves, limiting actual extra sucrose availability. Finally, our model generates a one to two hour timescale for partitioning to adapt to instant changes in one sink, without any changes occurring in the second sink (Fig. S3.6). This demonstrates that delayed adaptation of partitioning can at least partly be explained by slow adaptation of the long-distance transport and does not necessarily imply sink upregulation and prior saturation.

3

In further support of the relevance of pathway properties and incomplete sink saturation for resource partitioning, many stress conditions such as water shortage, salt stress and infections will reduce harvestable organ sucrose availability through either reducing photosynthesis efficiency or affecting energy budget allocation. We thus stress that while simple partitioning models, such as relative growth rate approaches, may serve as a first order approximation for predicting harvestable organ yields, they do not take into account all relevant factors. Therefore, in case substantial deviations with experimental observations occur or more detailed predictions are need, more biophysically detailed and biologically realistic models are essential. These are particularly relevant when studying regulatory mechanisms impinging on sucrose transport, such as the SP6A-SWEET interaction studied here. For future work, it would be of great interest to study resource partitioning in a dynamic, growing architecture. Here, we used a static architecture to study the effects of sink and pathway properties, as inclusion of a growing, more complex, architecture would generate complex feedbacks, further complicating interpretation of the results. Similarly, the current model does not include variations in sieve element architecture or vascular bundle numbers along the long-distance phloem or between different organ types. Including such details in the hydraulic architecture of the model is expected to further improve our understanding and capability to predict resource partitioning. Nonetheless, with the insights and modeling from this paper, it should now already be possible to interpret resource partitioning in more complex scenarios, which can give insights in important agro-economic factors such as tuber size distribution.

Conflict of interest

The authors declare that the research was conducted in the absence of any commercial or financial relationships that could be construed as a potential conflict of interest.

Author contributions

BH developed, implemented, and analyzed the model and wrote the manuscript. KT conceived the project, analyzed the model and wrote the manuscript.
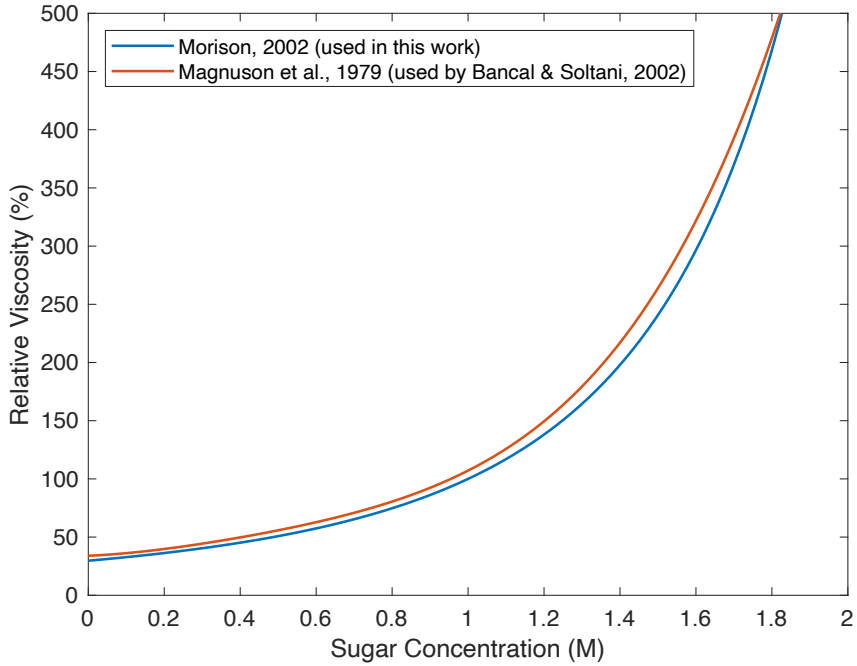
Funding

Acknowledgments

Supplementary figures

Supplemental figure 3.1. Relative viscosity (compared to a viscosity of 3MPa s for Magnuson et al, and the viscosity at 1M for Morison) as used in the VKR (red line) and biophysically detailed (blue line) models.

Supplementary figures
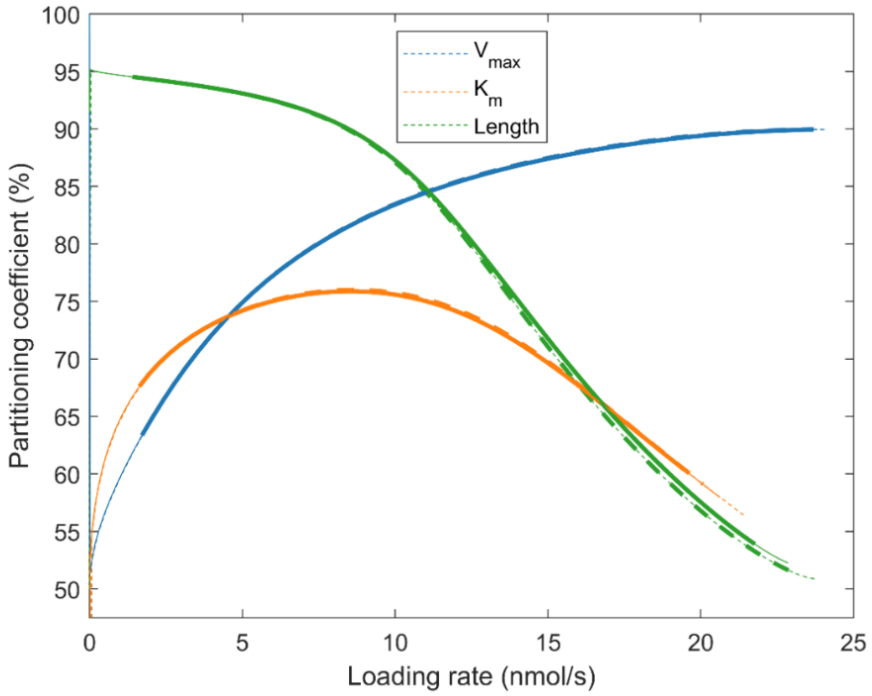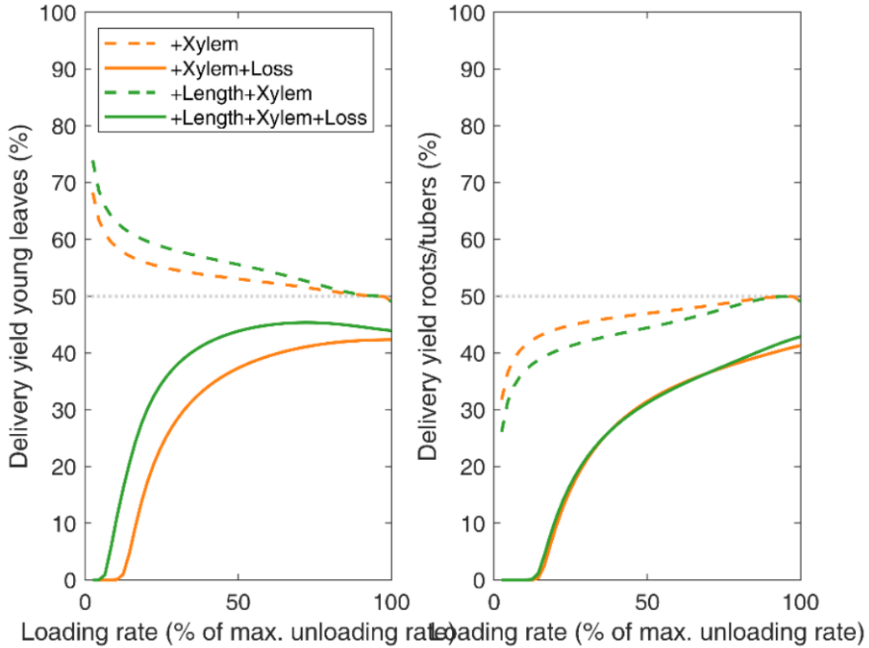

Supplemental figure 3.2. Effect of a non-zero shared pathway resistance. Bold lines depict a simulation of the biophysically detailed model without a shared pathway with standard sink characteristics. Dashed lines depict a simulation in which a shared pathway of 0.25m was included.

Supplementary figures

Supplemental figure 3.3. Delivery yield (v_i/v_o) for young leaves (A) and roots/tubers (B) for the same simulations as shown in Fig. 7B. Delivery yield is defined as sink unloading over total loading rate. For no radial efflux this is equal to the partitioning coefficient, but when including radial loss these two measures differ. Delivery yield specifically shows delivered sucrose to a sink, relative to total sucrose loading, instead of relative to total sucrose unloading at the sink. For the loss scenario, it can clearly be seen that for low loading rates no sucrose reaches the root/tuber sinks and almost non reaches the leaves, making that the partitioning coefficient gives an incomplete representation of the situation.

Supplementary figures

Addition of Loss
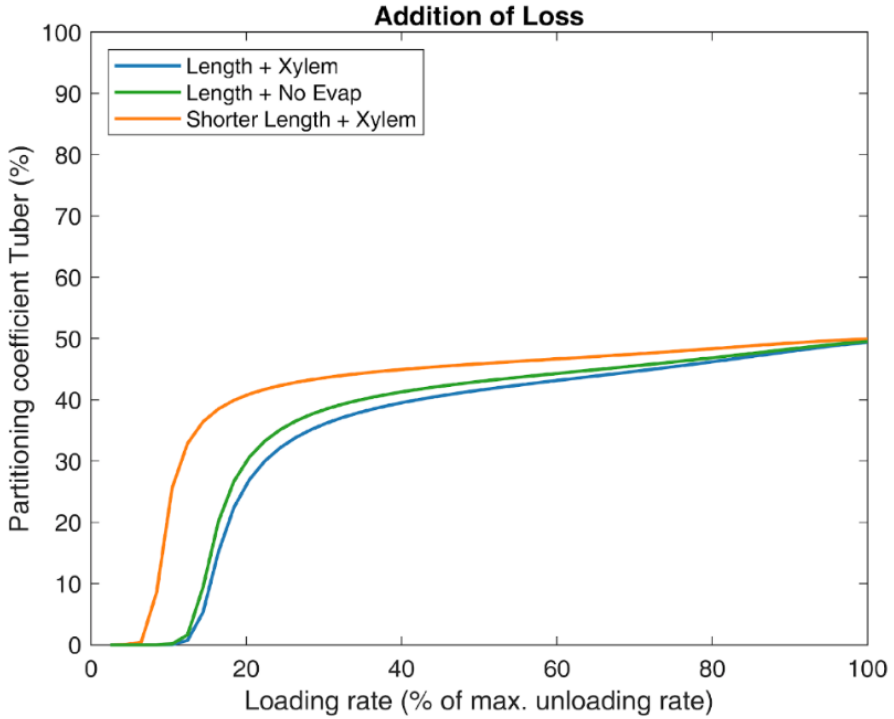
Supplemental figure 3.4. Partitioning towards roots/tubers for smaller pathway length differences (0.1m/0.15m instead of 0.1m/0.3m, orange line) and without evaporation in the leaf sinks (green line). The blue line shows conditions as used in fig. 7B, i.e., with 0.3m distance of roots/tubers and evaporation in the leaf sink.
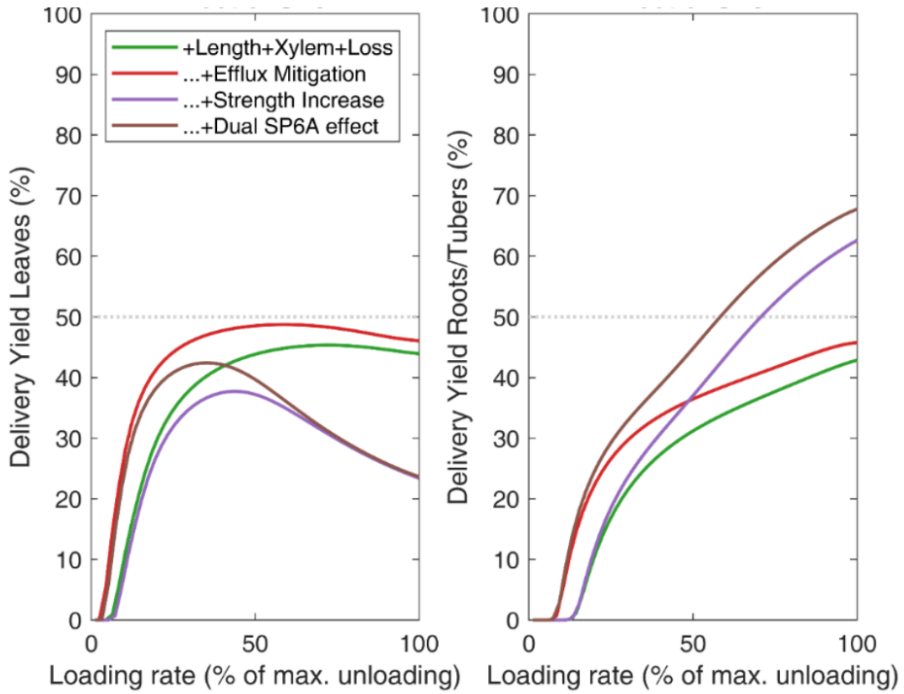
Supplementary figures

Supplemental figure 3.5. Delivery yield (v_i/v_o) for young leaves **(A)** and roots/tubers **(B)** for the same simulations as shown in Fig. 7C. Increased sink-strength of tubers makes that not only the partitioning towards tubers increased, but also total sucrose delivery becomes dominant.

Supplementary figures
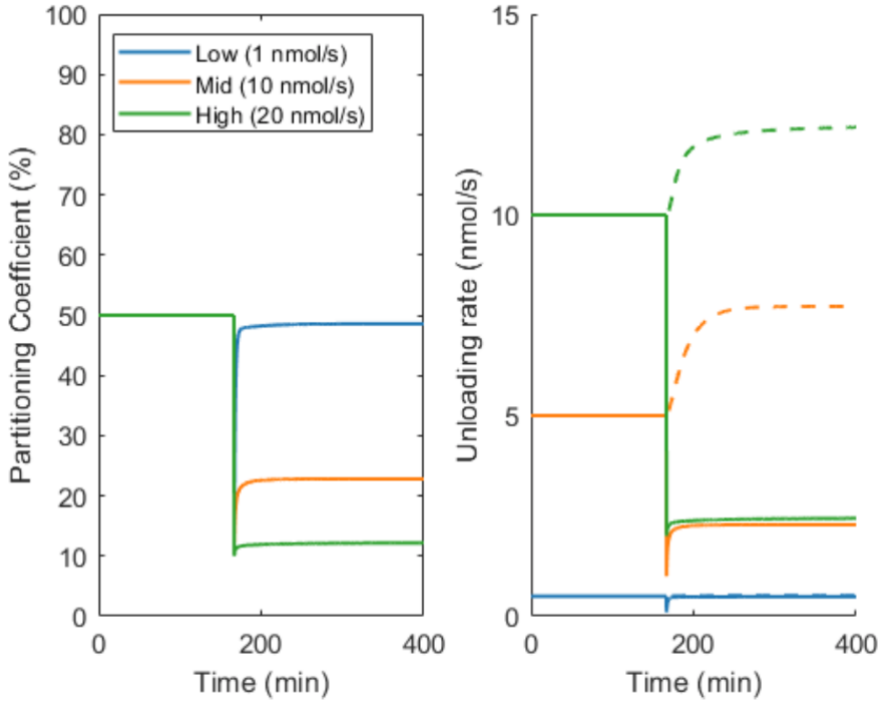
Supplemental figure 3.6. Time dynamics of the adaptation of partitioning to changed sink-conditions. At t=180 min sink unloading rate was changed from equal for both sinks (12.5nmol/s) to 2.5nmol/s for sink 1 (solid lines) whereas sink 2 was kept equal at 12.5nmol/s (dashed line). Adaptation to this sink change took approximately 2 hours for high loading rates, and about 1 hour for low loading rates. For lower loading rates the adaptation time was shorter due to strong influence of the weakest sink prioritization.

Chapter 4

A coordinated switch in sucrose and callose metabolism enables enhanced symplastic unloading in potato tubers

Bas van den Herik, Sara Bergonzi, Yingji Li, Christian W.B. Bachem, Kirsten ten Tusscher

Abstract

StSP6A mediated induction of tuberization is a first step in establishing a new strong sucrose sink. One of the earliest changes upon tuber induction is the switch from apoplastic to symplastic unloading. Whether and how this change in unloading mode contributes to sink-strength has remained unclear thusfar. In addition to changes in unloading mode, developing tubers also change from an energy to storage-based sucrose metabolism, which may also affect tuber sink strength. Here we investigated the coordination between changes in unloading mode and sucrose metabolism and their relative role in tuber sink strength by looking into callose and sucrose metabolism gene expression combined with a model of apoplastic and symplastic unloading. Decreased callose deposition in tubers was confirmed using fluorescence microscopy. Interestingly, this decline is caused by decreased callose synthase activity and not increased degradation. Analysis of existing gene expression data indicates that changes in callose metabolism and sucrose metabolism are strongly correlated, indicating a well-coordinated developmental switch. Our modelling indicates that symplastic unloading is not the most efficient unloading mode per se, as is often assumed. Instead, it is the concurrent metabolic switch that provides the physiological conditions necessary to potentiate symplastic transport and thereby enhance tuber sink strength.

Introduction

In potato, the tuberigen *StSP6A* induces tuber onset (Navarro et al., 2011) which is a major developmental transition, associated with large changes in plant physiology among which is the emergence of a new, and strong, sucrose sink. Besides its role in tuber establishment by switching on the tuber developmental program, *StSP6A* was shown to inhibit sucrose export from the phloem to the apoplast through inhibition of SWEET-transporters (Abelenda et al., 2019) thereby enhancing the efficiency of sucrose delivery to sink tissues (van den Herik et al., 2021). Using a biophysical model of sugar and water transport we recently demonstrated that this dual role of *StSP6A*, tuber induction and inhibition of SWEET-mediated export, preferentially enhances sucrose allocation to the tuber sink (van den Herik & ten Tusscher, 2022). A remaining open question is what processes make tubers strong sinks, and to what extent *StSP6A* is involved in controlling these processes.

While *StSP6A* mediated induction of tuberization is a logical first step in establishing a new strong sink, whether and how the switch from apoplastic to symplastic unloading (Viola et al., 2001) contributes to sink-strength has remained unclear. Although symplastic unloading is generally believed to enhance unloading efficiency and thereby contribute to sink strength (Fernie et al., 2020; Viola et al., 2001), this is largely based on data comparing different species and tissues rather than the comparing the two distinct unloading modes for a single tissue. Additionally, the processes guiding this unloading switch and the potential role of *StSP6A* therein have not yet been elucidated. In addition to inhibition of the apoplastic route through *StSP6A* inhibition of SWEETs, a coordinated promotion of the symplastic route is likely to occur.

Plasmodesmal aperture, a key factor determining the efficiency of symplastic transport, is regulated by callose deposition at the neck of the plasmodesmata, with reduced callose deposition opening plasmodesmata. Callose homeostasis is regulated by two antagonistic gene families, callose synthases (CalS), producing callose and β-1,3-glucanase (1,3-BG) degrading callose (Amsbury et al., 2018; De Storme & Geelen, 2014; Wu et al., 2018). We therefore investigate whether upon tuberization onset changes in callose levels and the expression of callose homeostasis genes occur.

Another transition occurring during tuber formation is the switch from energy to storage metabolism. This switch involves a transition from apoplastic cell-wall invertase (cwInv) to

cytoplasmic sucrose-synthase (SuSy) mediated sucrose cleavage (Viola et al., 2001). While the former delivers glucose and fructose for energy metabolism, the latter serves as an initial step in the formation of starch for storage by directly yielding UDP-Glucose, the precursor for starch synthesis (Nazarian-Firouzabadi & Visser, 2017). Potato tubers have been shown to depend on a switch to SuSy usage during tuber growth to prevent inefficient growth and storage (Bologa et al., 2003). During the early stages of tuber growth, a substantial increase in the hexose/sucrose ratio, and a decrease in total sugars occurs. The decrease in total sugars is indicative of an increased starch synthesis rate (Oparka et al., 1990), whereas a decreased hexose/sucrose ratio is likely due to increased rates of metabolism of hexoses derived from sucrose, coupled with an increased flux of sucrose into the developing tip (Davies, 1984; Ross & Davies, 1992). Altogether there is thus enzymatic and metabolic evidence for a functional enzymatic switch to occur. Still, an open question is whether this enzymatic switch is triggered by the change in sucrose delivery due to the apoplastic to symplastic switch, or rather is part of a more coordinated developmental program changing both transport mode and metabolism. We therefore investigate the extent of concurrence of the changes in callose and sucrose metabolism.

The switch to formation and storage of non-soluble starch and concurrent decrease in soluble sugars may enhance sink strength under symplastic unloading by maintaining a concentration gradient towards the sink. Alternatively, the increased sink-strength following the unloading switch may involve the differences between the transport modes themselves. Passive symplastic transport through plasmodesmata is generally regarded one or a few orders of magnitude more efficient than active apoplastic transport (Patrick & Offler, 1996), yet this is largely based on comparisons across different tissues and species rather than within a single context. Moreover, symplastic transport reduces the energy spent on sucrose delivery by eliminating the energy required to maintain the proton motive force and reduces the requirement for significant investment in vascular tissue (Patrick & Offler, 1996). The relative efficiency of the two modes of transport will thus likely depend on the physiological conditions present in the stolon and tuber, and enhanced sink strength may involve both transport mode and metabolism. To investigate the coupling between transport mode and metabolism, we used a biophysical model to compare apoplastic versus symplastic unloading efficiency as a function of transporter and plasmodesmata densities, local sucrose concentration and concentration gradients. Our model reveals how prior to tuber formation, apoplastic transport results in more efficient sucrose delivery to stolons, debunking the widely held notion symplastic transport

4

is always more effective. It is only upon tuber formation that non-linear interactions between sucrose concentration and gradients and the efficiency of symplastic transport causes this transport mode to be far more efficient. It is thus the coordinated switch to symplastic unloading and starch metabolism that generate a strong tuber sink.

Materials & Methods

In vitro plant growth and microscopy

Solanum Andigena was propagated *in vitro* on MS20 medium (MS, 20g/L saccharose, pH5.8), and cultivated at 24 °C for four weeks. The nodes from the upper three nodal stem sections were selected with each node containing an expanded leaf and a single axillary bud. At least 40 decapitated single-node cuttings were cut and propagated in MS20 medium under dark conditions at 20 °C for 5 to 10 days. Explants with elongated stolons were moved to tuber induction medium (MS, 80g/L saccharose, 1.5mL/L 6-Benzylaminopurin (BAP), pH5.8) and cultivated in similar conditions as stolon elongation.

For microscopy five samples were harvested at three different development stages; non-swelling stolon (stage 1), swelling stolon/small tuber (stage 2 or 3), large tuber (stage 4) as described by Viola et al. (2001). Harvested stolon and tuber samples were cut using a hand microtome. Samples were then stained in a 150mM K2PO4 (PH=9) and 0.01% aniline blue solution for 2 hours in the dark. Callose deposition was imaged with a DAPI filter (4FL) and an excitation wavelength of 370nm.

Sequence retrieval, phylogenetic analysis and functional annotation

Protein sequences of the β-1,3-glucanase, Callose Synthase and Invertase families were identified using the Phytozome database (Goodstein et al., 2012) and a PSI-BLAST (Altschul et al., 1997) search was performed for each family to identify similar sequences missing or wrongly annotated in the Phytozome database. For each family, multiple sequence alignments were made with the auto option in MAFFT v7.310 (Katoh & Standley, 2013) and trimmed with trimAl v1.4.rev15 (Capella-Gutiérrez et al., 2009) using a gap threshold of 10%. Phylogenetic trees were constructed with IQ-TREE v1.5.5 (Nguyen et al., 2015) using ModelFinder (Kalyaanamoorthy et al., 2017) and ultrafast bootstrap approximation (Hoang et al., 2018). The 1,3BG family was functionally annotated for features previously associated with the protein family, similarly to the approach used by Paniagua et al. (2021); Signal peptide (SP), glycosylphosphatidylinositol-

anchors (GPI-anchors), and X8 (CBM43) domains were identified. Preduction of these features was done using SMART (Schultz et al., 2000) and Interpro (Mitchell et al., 2019). Signal peptides (SP) were further predicted using SignalP v5.0 (Almagro Armenteros et al., 2019), and presence of GPI anchor was also predicted using PredGPI (Pierleoni et al., 2008). Sequence signatures were considered present when predicted by two or more databases.

In silico gene expression analysis

Microarray expression data of 24 tissue and organ samples from *S. tuberosum* Group Phureja DM 1-3 516 R44 (DM) was obtained from spudDB (Pham et al., 2020). These samples were a selection of all samples without applied stress and/or treatment free. Similarly, 15 samples from S. *tuberosum* Group Tuberosum RH89-039-16 (RH) (Zhou et al., 2020) were analyzed to confirm the observations in DM. The DM dataset contained two stolon and three tuber samples which were investigated in more detail. Analysis of the expression data was performed in python using the clustermap function from the seaborn package (Waskom, 2021), expression was normalized using Z-score normalization and hierarchical clustering was performed using the 'ward' method implemented in seaborn.

Unloading model

Unloading rates for three different unloading modes are compared for varying sucrose concentration in the phloem (C_{phloem}) and parenchyma ($C_{parenchyma}$). Below we describe the models and parameter derivation, all parameter values are given in Table 4.1. Apoplastic or active unloading (Ia) is described by a Michaelis-Menten term dependent on the phloem sucrose concentration (eq. 1).

$$I_a = v_{max} \frac{C_{phloem}}{C_{phloem} + K_m} \qquad \text{(eq. 1)}$$

For this mode it is assumed that phloem unloading from the sieve-element/companion-cell (se-cc) complex is limiting, i.e. SWEET-transporter kinetics are the bottleneck in this step, we therefore parameterized this step with SWEET-specific parameters. Expected differences between SWEET and SUT-transporters facilitating uptake in the parenchyma are small (van den Herik et al., 2021). SWEET rates were reported as 34.9 ± 4.6 pmol/oocyte/min (Chen et al., 2012), which was rewritten to 0.9e-19 mol/μm^2/s by using reported oocyte dimensions (Wallace & Selman, 1981). Reported SWEET K_m values range from 10-75mM (Chen et al., 2012), here an intermediate value of 50mM was used.

To simulate symplastic transport we used the model for simple plasmodesmata developed by Ross-Elliott et al. (2017). This model described two symplastic unloading modes; diffusive symplastic transport and symplastic bulk flow, both through plasmodesmata. Both models therefore need plasmodesmal area as important input. Individual plasmodesmal area is calculated by subtracting the surface area of the desmotubule from the total area, assuming that both the plasmodesmal and desmotubule surface area is circular. Total plasmodesmal area (A_{PD}) is then calculated by multiplying individual area with the total number of plasmodesmata per μm^2:

$$A_{PD} = N\left(A_{outer} - A_{desmotubule}\right) = N\pi\left(r^2_{outer} - r^2_{dt}\right)$$ (eq. 2)

Diffusive unloading through plasmodesmata (I_D) is described as standard diffusion through a simple collection of pores (eq. 3) with area A_{PD} and pore length l. Diffusion thus relies on the sugar concentration gradient between the phloem and parenchyma (ΔC):

$$I_D = DA_{PD}\frac{\left(C_{phloem} - C_{Parenchyma}\right)}{l}$$ (eq. 3)

Bulk flow through plasmodesmata (I_b) is described by the volumetric water flow through the plasmodesmata (Q) as well as the sugar concentration in the phloem (eq. 4).

$$I_b = C_{phloem}Q = C_{phloem} * A_{PD} * u_{PD}$$ (eq. 4)

The volumetric water flow through plasmodesmata is driven by the pressure differential between the phloem and parenchyma, we here assume that this pressure differential is solely dependent on the osmotic pressure differential, and as such that turgor pressure in the phloem and surrounding parenchyma is equal (eq. 5)

$$\Delta P = \Delta\Pi = RT\Delta C = RT\left(C_{phloem} - C_{Parenchyma}\right)$$ (eq. 5)

With R being the universal gas constant and T the absolute temperature.
Water flow velocity through plasmodesmata is estimated as flow through a straight slit of width w (where w = r_{outer} - r_{dt}) and length l as described in detail by Ross-Elliot et al. (2017), resulting in equation 6.

$$u_{PD} = \frac{w^2 \Delta P}{(12l + 32\pi w)\eta}$$ (eq. 6)

In this model version the viscosity of the solution flowing through the plasmodesmata (η) was solute dependent (eq. 7). Plasmodesmal sugar concentration was estimated as the average between phloem and parenchyma.

$$\eta = \eta_0 exp\left(\frac{4.68*0.956\phi}{1-0.956\phi}\right) \ where \ \ \phi = \frac{V_{suc}\frac{(C_{phloem}-C_{parenchyma})}{2}}{V_{suc}\frac{(C_{phloem}-C_{parenchyma})}{2}+V_{phloem}}$$ (eq. 7)

Thus, bulk transport is linearly dependent on phloem sucrose concentration (Eq. 4), linearly dependent on the phloem parenchyma sucrose concentration difference determining the osmotic pressure differential (Eq. 5), and non-linearly dependent on this same concentration difference via the viscosity of the phloem sap (Eq. 7).

Results

Callose deposition at the phloem decreased during tuberization
To investigate whether callose levels decrease during tuber formation we used fluorescence microscopy, using aniline blue to stain callose. Callose was visualized in stolon and tuber samples, with clear presence of callose in both phloem rings in the stolon (Fig. 4.1A, B). Xylem vessels were also clearly visible due to the fluorescent properties of lignin (Albinsson et al., 1999). Callose abundance was strongly decreased in the vascular region of tuber samples (Fig. 1C,D). Precise quantification of callose in tubers was prohibited by the large amount of starch interfering with the callose signal, preventing a more quantitative comparison between stolon and tuber callose levels. Nonetheless, a decrease in callose levels from the stolon to tuber stage was consistently observed in all samples (n=5 stolons and tubers).

Sequence retrieval and phylogeny of the 1,3-BG, CalS and invertase gene families
To investigate gene expression patterns, a classification of sugar and callose metabolism gene families was needed. While the SuSy (Van Harsselaar et al., 2017; Xu et al., 2019), SWEET (Manck-Götzenberger & Requena, 2016) and SUT (Chen et al., 2022; Chincinska et al., 2008) families were previously classified (Table 4.2), an overview of potato 1,3-BG, CalS and sucrose invertase genes was lacking. We first identified the genes constituting these families and performed a phylogenetic and functional analysis to get an overview of the number of

Table 4.1. *Variables and parameters for the potato sucrose unloading model. Values in brackets represent the reported range of the parameter in potato.*

Parameters	Symbol	Value (range)	Units	Reference
Sucrose concentration phloem	C_{Phloem}	Var.	mol m^{-3}	-
Sucrose concentration parenchyma	$C_{Parenchyma}$	Var.	mol m^{-3}	-
Maximum transport rate	V_{max}	0.93 (0.5-2)	10^{-19}mol µm^{-2} s	Chen et al., 2012
Michaelis-Menten constant	K_M	50 (10-75)	mol m^{-3}	Chen et al., 2012
Plasmodesmata density	N	4 (3-6)	µm^{-1}	Oparka (1985)
Diffusion constant sucrose	D	5e-10	m^2 s^{-1}	-
Cell wall thickness	I	1 (0.3-1.2)	µm	Gibson, (2012) Reeve et al. (1973)
Plasmodesmata outer radius	r_{outer}	10	nm	Ross-Elliot et al., 2017
Desmotubule radius	r_{dt}	8	nm	Ross-Elliot et al., 2017
Cystoplasmic sleeve width	w	2	nm	Ross-Elliot et al., 2017
Gas constant	R	8.31	Pa m^3 K^{-1} mol^{-1}	-
Temperature	T	293	K	-
Partial molal volume sucrose	V_{suc}	0.22	dm^{3}mol^{-1}	-
Dynamic viscosity of water	η_0	1.002	mPa s	-

genes (Table 4.2) present and their expected functional role in tuber development. A total of 62 1,3-BG genes encoding callose degrading enzymes were identified using the phytozome database combined with a psi-BLAST search. Together with a group of 8 Arabidopsis 1,3-BG genes previously identified to be plasmodesmata-associated (Levy et al., 2007; Wu et al., 2018) containing one or more representatives of each of the 3 previously identified clades (α,β,γ) (Doxey et al., 2007) a phylogenetic tree was constructed (Fig. S4.1). Genes were functionally annotated for the presence of a signal peptide (excretion), GPI-anchor (membrane anchorage)

and a X8-domain (carbohydrate binding/plasmodesmata association). Our results indicate that the three previously described clades are all present in potato and differ significantly in the presence/absence of functional domains. Specifically, the α-clade is very diverse with regards to the presence of the domains, while the β-clade is characterized by presence of an excretion signal peptide, GPI-anchor, and X8-domain in most proteins (13 out of 17), and the γ-clade is characterised by a complete absence of GPI-anchor and X8-domain, similar to what is found in Arabidopsis (Doxey et al., 2007) and tomato (Paniagua et al., 2021). Based on this, proteins active in callose degradation at the PD are expected to be mainly localized in the α- or β-clade. Indeed, all 1,3-BG characterised to be PD-related in *Arabidopsis* are located in the α-clade (Levy et al., 2007).

A total of 13 CalS genes encoding callose producing enzymes were identified, 6 sequences were discarded as they lacked the UDP-glucose catalytic site needed for enzymatic activity (Hong et al., 2001). The 7 remaining CalS sequences, together with the 13 CalS genes reported in *Arabidopsis* (Richmond & Somerville, 2000) were used to construct a phylogenetic tree (Fig. S4.2). The tree was annotated with known functions for the *Arabidopsis* genes (Wu et al., 2018), inferring similar roles for potato genes from their *Arabidopsis* orthologs. Based on this analysis two putative PD-associated proteins were identified (Soltu.DM.07G023050 & Soltu. DM.01G001920).

Finally, with regards to invertases involved in sucrose degradation, three main clades exist, acidic cell wall invertase (cwInv), neutral/alkylic soluble invertase (Inv), and vacuolar invertases (vInv). These three classes have largely different physiological roles (Roitsch & González, 2004). A total of 25 invertase genes were identified in potato. Not all genes were functionally annotated, and function was therefore inferred using their phylogeny and partial annotation in potato (Fig. S4.3), based on this analysis 9 cwInv, 11 Inv and 5 vInv are present.

The highly diverse 1,3-BG and CalS families show clear developmental expression clusters
We next investigated the expression patterns of the 1,3-BG and CalS families to investigate changes in callose homeostasis during tuberization. For this we made use of a dataset containing microarray gene expression data across a variety of organs of S. *tuberosum* Group Phureja DM1-3 (DM) (Pham et al, 2020). Distinct developmental expression clusters are present, with flowers and, stamens, petioles, fruit, stolons and tubers all clustering separately (Fig. S4.4). Stolons did show partially similar expression patterns to shoot and root samples, which is
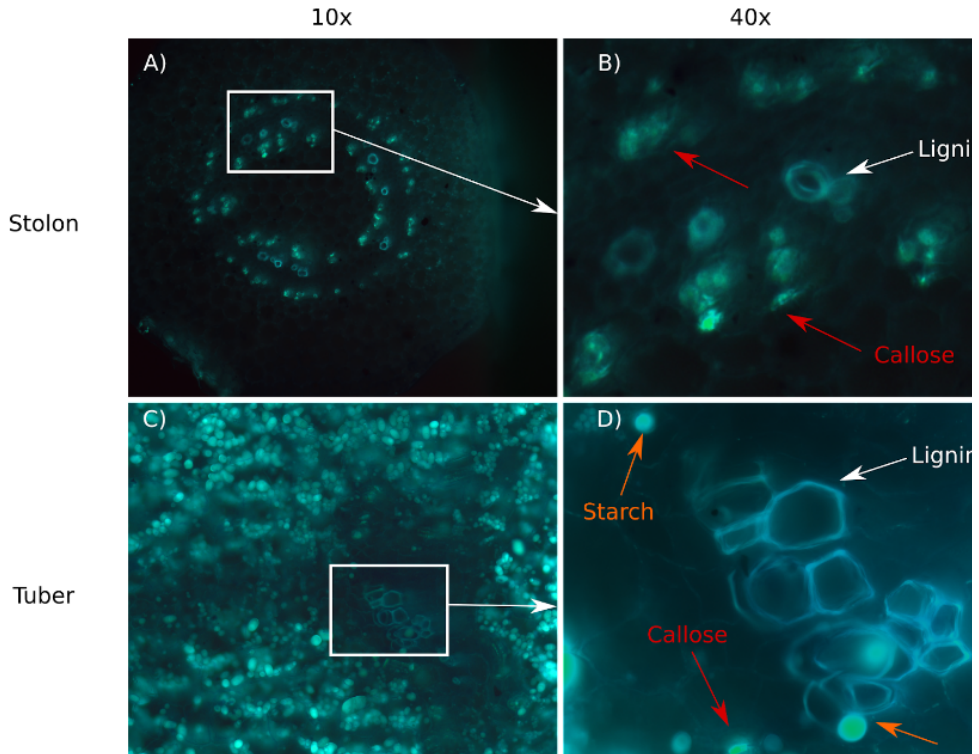
Figure 4.1. Callose presence at stolons and tubers. A) Longitudinal sample of a non-swelling stolon at 10x magnification B) 40x magnification of part of the sample in A. Callose (red arrows) and lignin (white arrows) are clearly visible in the phloem and xylem C) Longitudinal sample of the vasculature of a large tuber (stage) at 10x magnification D) 40x magnification of part of the sample in C. Callose (red arrows), lignin (white arrows) and starch (orange arrows) are visible in the phloem and xylem

expected from the shared stem-like nature of these three organ types. The observed clusters reflect the functional diversity of callose besides its role in regulation of the plasmodesmal aperture, as callose also plays a role in cell wall integrity and mechanics, response to (a)biotic stresses, pollen development and cellular differentiation (Levy et al., 2007; Wu et al., 2018; Amsbury et al., 2018).

Subsequently, three tuber and two stolon tissue samples available in the DM-dataset were investigated in more detail, In these five samples a subset of 52 of the 62 1,3-BG genes and all 7 identified CalS genes were expressed (Fig. 4.2). Stolon samples clustered together, with all CalS genes active in stolon samples and none showing high activity in the tubers. Tuber samples were also strongly correlated, with two showing very strong overlap in 1,3-BG expression and

Table 4.2. Overview of the callose and sucrose gene families

Gene Family	Potato members	Reference
1,3-beta-glucosidase	62	This work
Callose Synthase	7	This work
Invertase	25 (9 cwInv, 11 Inv, 5 vInv)	This work
Sucrose Synthase	11	Van Harsselaar et al. (2017); Xu et al. (2019)
SWEET	35	Manch-Gotzenberger & Requena (2016)
SUT	3	Chincinska et al. 2008; Chen et al. (2022)

the third sample having a separate set of 1,3-BGs expressed. Tuber samples mainly expressed 1,3-BGs from the γ-clade, lacking both a GPI-anchor as well as a X8-domain, with only 2 out of the 21 1,3 BG genes having a GPI-anchor (Fig. 4.2). In contrast, in stolons expression of α-, and β-clade is dominant and 17 out of 31 1,3-BG genes contained a GPI-anchor domain. The majority of 1,3-BGs active in stolons are thus membrane and/or PD-associated, suggesting a role in callose degradation. In contrast in tubers, expressed genes are associated with pathogen resistance and cell-wall remodeling (Doxey et al. 2007), likely due to their secretory nature. To verify these observations, the same analysis was performed on a stolon and tuber expression dataset of *S. tuberosum* Group Tuberosum RH89-039-16 (RH) (Zhou et al., 2020), providing similar results (Fig. S4.5). Combined, this shows that callose synthase is mainly active in stolons, whereas 1,3-BG is active in both stolons and tubers, albeit that functionally different genes are expressed.

A clear developmental pattern is present for callose and sucrose metabolism
Besides changes in callose homeostasis, a rewiring of sucrose metabolism as well as changes in sugar transporters are known to occur during tuberization (Viola et al., 2001; Jing et al., 2023). To investigate if and how these processes are coupled during tuberization the gene expression of callose (1,3-BG & CalS) and sucrose metabolism (SuSy, cwInc, vInv & Inv) as well as sucrose transporters (SWEET & SUT) were investigated alone, as well as in combination (Fig. 4.3, S4.5, S4.6). Clearly distinct stolon and tuber clusters were observed when considering sucrose metabolism in isolation (Fig. S4.6), as well as combined with sucrose transporters and callose metabolism (Fig. 4.3).
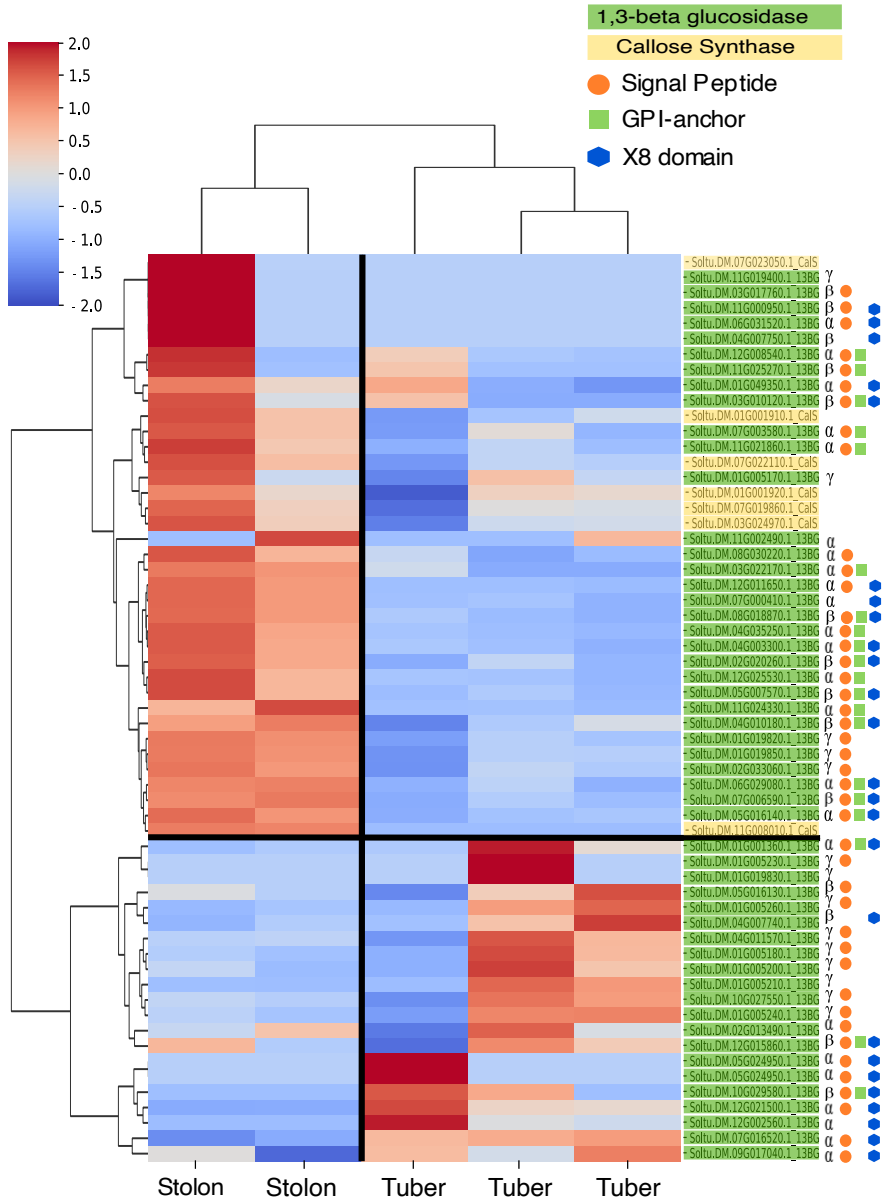
Figure 4.2. 1,3-BG and CalS expression in stolon and tuber samples. Z-score normalized rows with hierarchical clustering shows distinct stolon and tuber clusters. Clade and annotation of signal peptides, GPI-anchors and X8-domains is visualized behind each 1,3-BG gene.

During the developmental switch from stolon to tuber both cytoplasmic and cell wall invertase activity is reported to decrease, whereas SuSy activity increases (Viola et al., 2001). Three out of nine cwInv are expressed in the stolon cluster and show no to very low expression levels in tubers (Fig 4, S6). The other six cwInv were not expressed in either stolons or tubers. Soluble and vacuolar invertases showed more mixed expression patterns, with five active in the stolon cluster, and six active in the tuber cluster. Nine SuSy genes were expressed, with the majority active in tubers (seven out of nine). SWEET and SUT expression patterns were more ambiguous than sucrose and callose metabolism, consistent with earlier observations (Jing et al., 2023), and a more important role for post-translational interactions such as between *StSP6A* and *StSWEET11b*.

Enzymatic changes create favored conditions for passive unloading

Above we demonstrated how the switch from stolon to tuber involves concurrent changes in both sucrose and callose metabolism, both of which may contribute to the formation of a strong tuber sink. Here we investigate the relative importance of sucrose physiology versus unloading mode in determining sink strength. We first describe the physiological changes in terms of phloem and parenchyma sugar concentrations. Combined with estimated sucrose transporter levels and plasmodesmata density, we parameterized a simple apoplastic and symplastic unloading model developed by Ross-Elliot et al. (2017) for the stolon and tuber (Fig. 4.4A) (See methods).

4

Overall sugar levels decrease during the exponential tuber growth phase (Fig. 4.4B, bottom panel, van den Herik et al., 2023), consistent with the observed switch from energy to storage metabolism described above. Individual reducing sugars (glucose, fructose) and sucrose dynamics are more complex (Davies, 1984), with glucose and fructose levels decreasing already during stolon stages and sucrose only decreasing in the exponential tuber growth phase (Fig 4.4C). Here we assumed that the measured sugar concentrations in whole tuber samples are indicative of tuber parenchyma conditions due to the volumetric dominance of the storage parenchyma over the phloem locally delivering the sugar. In absence of data on phloem sucrose levels in the stolon/tuber unloading zone we investigated three different phloem sugar concentration scenarios; 1) Constant concentration over tuber development (Balanced source/sink dynamics: as demand increases supply increases accordingly, thus maintaining phloem concentration) , 2) Coupled phloem/parenchyma concentrations (Local sink dynamics dominate: as demand increases supply cannot keep up and phloem concentration decreases),

3) Leaf-Area Based concentration (Source dynamics dominate: supply and hence phloem concentration is linearly related to leaf area).

Due to the low K_m of SWEET-transporters (50mM) apoplastic transport is close to saturation under most conditions, except for the coupled scenario, where lower concentrations during tuber bulking cause transport to decrease too half the maximum rate during development (Fig 4.4D, grey lines). SUC transporters have an even lower K_m of 10mM, and operate close to saturation for all tested concentrations. As a consequence, apoplastic transport is largely constant across concentrations and scenarios. In contrast, diffusive and bulk flow unloading do show large differences over development and between the scenarios. As diffusion is only dependent on the concentration gradient between the phloem and parenchyma the unloading rate parallels the concentration gradient (Fig 4.4D, insets and green lines). Plasmodesmal bulk flow depends on both the sugar concentration gradient which drives osmotic pressure and hence flow rate, and the concentration of sucrose transported in the phloem. As a consequence, bulk flow increases more strongly with concentration gradient, resulting in a higher unloading potential than diffusion under all conditions, as was also observed in the developing phloem of Arabidopsis (Ross-Elliott et al., 2017).

Our model demonstrates that the switch to storage metabolism that results in a decrease in tuber sugar levels potentiates diffusive and bulk symplastic unloading in both the conservative, constant and data-based, leaf-surface driven scenarios where sugar concentration gradients increase. In both cases, bulk flow significantly exceeds diffusive transport due to the non-linear dependence of bulk flow on concentration levels via osmotic pressure and convective solute flow (Fig. S4.7) In contrast, in the coupled scenario, where concentration gradients remain constant while phloem sucrose levels decrease, diffusive unloading efficiency remains constant while bulk unloading efficiency declines over development. This scenario is however deemed unlikely given the observed leaf growth dynamics, as well as the known negative feedback regulation of sucrose levels on photosynthesis which likely prevents a fully parallel decline of phloem sucrose levels with sink levels.

Importantly, since we estimated transporter expression levels, plasmodesmal densities and apertures, model outcomes depend on precise parameter settings. To test the robustness of our results we performed simulations with 2-fold higher transporter levels, 2-fold lower plasmodesmal densities and these changes combined (Fig. S4.8). Our results show that while
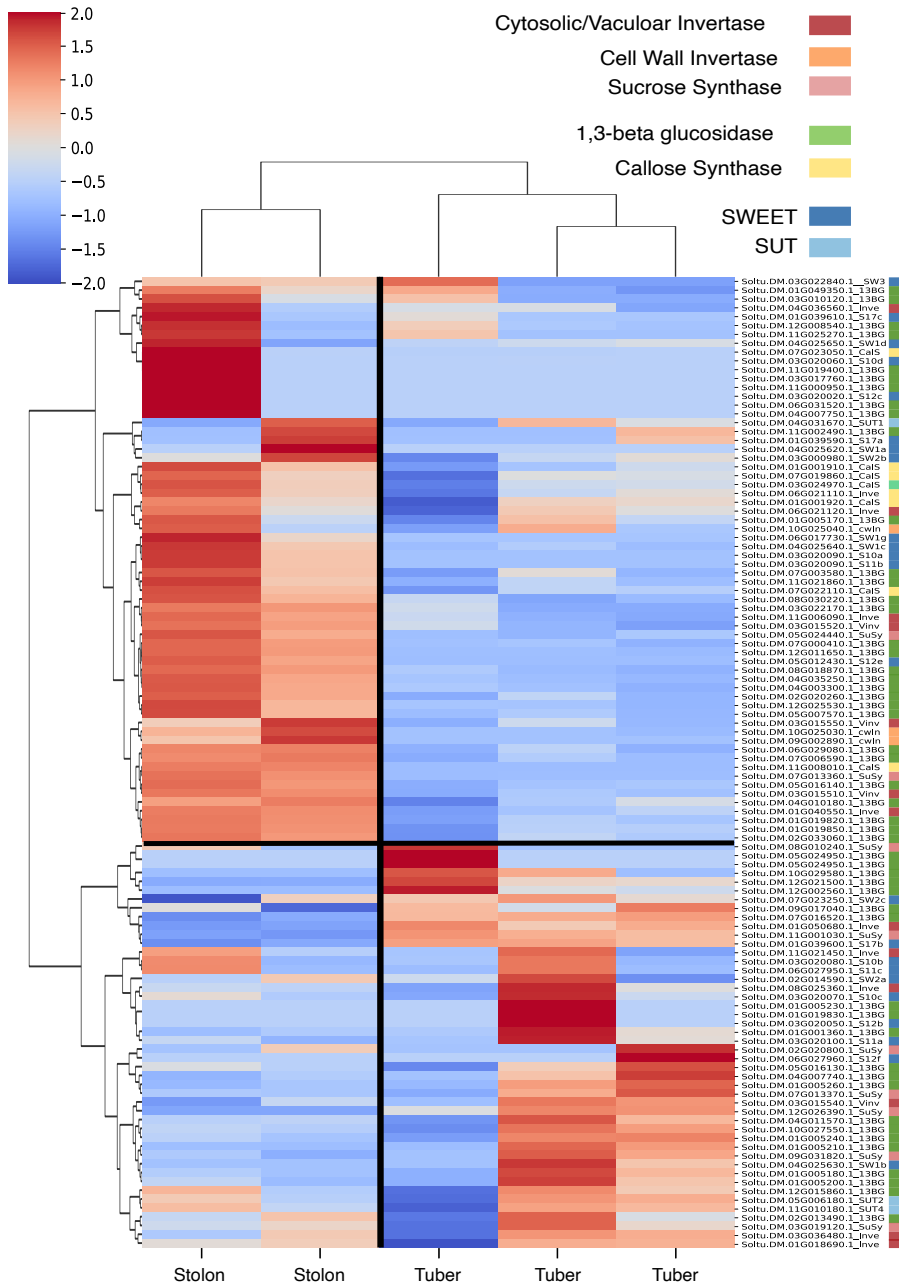
Figure 4.3. Heatmap of expression profiles of sugar metabolism, transport and callose balancing in stolon and tuber samples of DM. Z-score normalized rows with hierarchical clustering show similar stolon and tuber clusters as observed in Fig. 4.2.

the precise rates of transport and the cross-over point from whereon symplastic transport is more efficient shifts, no qualitative changes occur. Put differently, we consistently observe that during early tuber formation apoplastic transport is more efficient, while during later stages symplastic transport dominates. The model thus clearly demonstrates that the physiological conditions created by the enzymatic switch (decreasing parenchyma concentration due to increasing starch synthesis) and general plant dynamics (leaf area increase) unlocks the higher potential of passive unloading.

Discussion

In this study, we explored the significance of the apoplastic to symplastic unloading switch and the transition from energy to storage sugar metabolism on tuber sink-strength increase during and after tuberization. We first investigated whether, in addition to the previously identified *StSP6A* mediated decrease in apoplastic transport upon tuberization, also plasmodesmata further opened. For this we used callose deposition as a proxy for plasmodesmata opening. Using fluorescence microscopy, we showed that callose levels did decrease in tuber samples, indicating an important role for decreased callose deposition in the unloading switch.

With changes in callose deposition confirmed, we continued with investigation of gene expression changes of callose homeostasis genes, i.e. Callose Synthase for synthesis and β-1,3-glucanase for degradation. We observed that while 1,3-BGs from the γ-clade were expressed in tuber samples, expression of α-, and β-clade is dominant in stolons. In *Arabidopsis* the γ-clade proteins have been associated with pathogen resistance and cell-wall remodeling (Doxey et al. 2007). Increased activity of the excreted γ-clade proteins might thus be an indicator of faster cell-growth and has been associated with fast growth in pollen tubes (Wang et al., 2022). The majority of 1,3-BGs active in stolons are membrane and/or PD-associated, suggesting a role in callose degradation. Expression patterns in stolons thus suggest high degradation potential at plasmodesmata, while in tubers this potential is decreased and growth-, and pathogen-associated expression dominates. Phylogenic inference of function for the smaller CalS family revealed clear expression of gametophyte associated proteins in the flower/stamen cluster (Soltu.DM.11G008010) and two putative PD-associated proteins (Soltu.DM.07G023050 & Soltu.DM.01G001920), which were highly expressed in fruit, callus, and stolon samples. No to low expression of CalS in tubers was present. Combined, this analysis suggests that callose homeostasis at plasmodesmata is a constant process of synthesis and degradation in stolons,
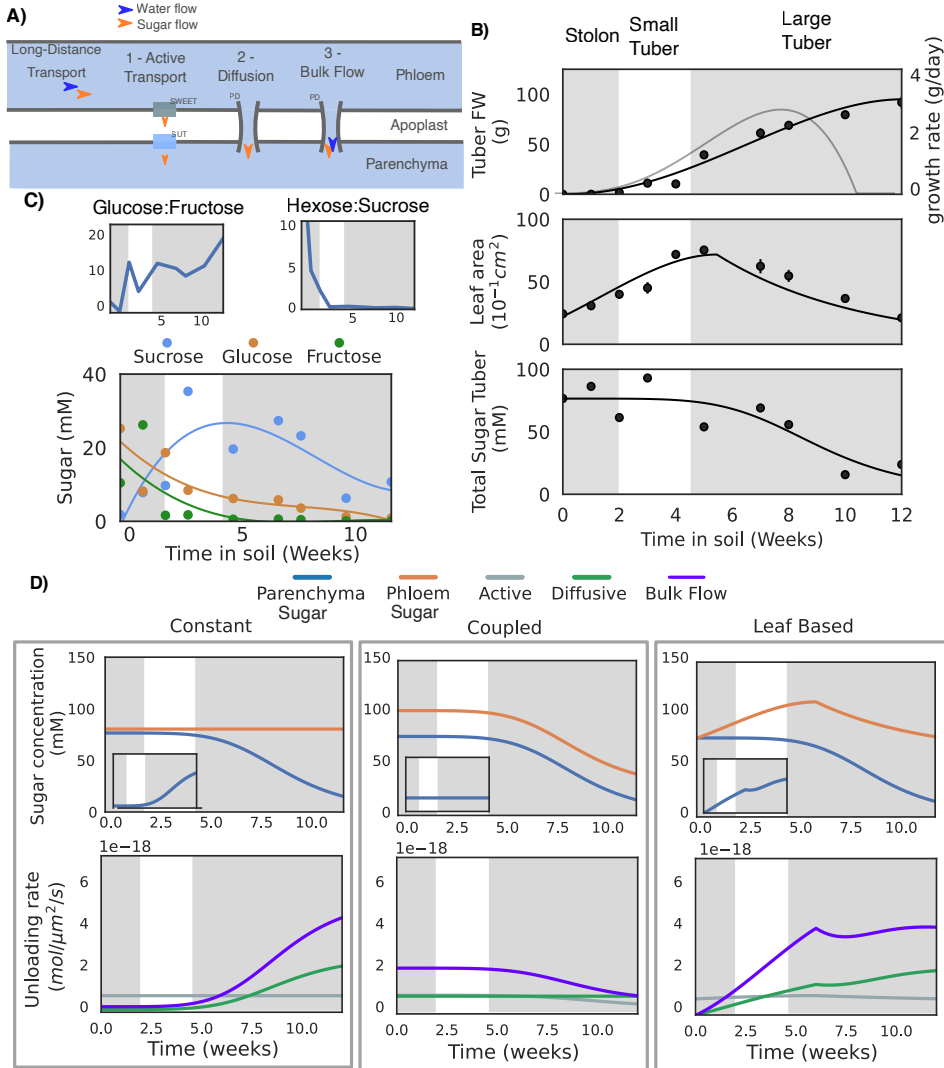
Figure 4.4. Sucrose unloading under different physiological conditions in stolon and tuber. A) Schematic overview of the unloading model. B) Potato tuber fresh weight, leaf area and tuber sugar dynamics over plant development (van den Herik et al. 2023). The first grey box depicts the stolon stage, white small tuber stage and the second grey large tuber stage, as described by Viola et al. (2001) C) Sucrose, fructose and glucose dynamics in stolons and tuber (van den Herik et al., 2023). Glucose:Fructose and Hexose:Sucrose ratios are calculated from the same data. D) Model results for the three phloem concentration scenarios (columns). The top row shows the sucrose levels in the phloem and parenchyma (see B), with the inset showing the gradient between the phloem and sucrose. The bottom row gives the unloading rates for the three unloading modes as obtained from the simulations.

as also observed in *Arabidopsis thaliana* pollen tubes, where callose is transiently present (Abercrombie et al., 2011). While in tubers the transient presence of callose at plasmodesmata is replaced by low callose deposition due to decreased synthesis and relocation of degradation to the apoplastic space. It thus indicates that decreased callose deposition in tubers is caused by decreased synthetic CalS activity and not increased 1,3-BG activity.

We next investigated the concurrence of the changes in callose and sucrose metabolism. Expression of CalS and cwINV are exclusively clustered in stolon samples, whereas SuSy expression dominates in tubers. Low expression of SuSy genes was present in stolons, which can possibly be explained by the need for its product UDP-glucose in both stolons and tubers as it is a shared precursor for both starch and callose metabolism (Barnes & Anderson, 2018). Furthermore, low individual expression levels can be caused by technical or biological noise between samples in this dataset. Overall, this indicates a well-coordinated developmental switch, with a combined transition from growth (cwInv) to storage (SuSy) metabolism, and from callose PD homeostasis to extracellular callose degradation.

Lastly, we set out to understand the implications of this coordinated switch on the unloading potential and thus sink-strength of tubers. To this end, we parameterized a biophysics-based phloem unloading model (Ross-Elliot et al., 2017) for stolons and tubers. Using this model, we demonstrated that it is the combined switching of the unloading mode and the sucrose metabolism that increases tuber sink strength. The metabolic switch ensures maintenance of the concentration gradient necessary for efficient symplastic unloading, while starch metabolism is further activated because of increased cytoplasmic sucrose inflow (Stein & Granot, 2019; Winter & Huber, 2000). Clearly the finding that passive gradient driven transport increases with an enhanced gradient is in itself trivial. Additionally, the exact time point at which symplastic transport exceeds apoplastic transport in efficiency of course depends on the precise parameterization of apoplastic and symplastic transport rates and densities. The key point of our current modeling effort lies in the demonstration that -unless an unrealistic phloem concentration scenario is applied- during initial stolon and tuber development apoplastic transport is more efficient while at later stages symplastic transport is more optimal. This underlines that 1) the *in planta* observed switch in transport mode is physiologically sensible, 2) symplastic transport is not always more optimal. Indeed, in fruit plants sucrose storing fruits and seeds typically depend on a switch to apoplastic unloading to prevent a symplastic back-flow of the soluble sugars down the created concentration gradient (Ma et al., 2019). In the current

model, enzyme levels were kept constant, as e.g. different SWEET subtypes showed different expression dynamics upon tuberization. Additionally, we kept enzyme activity constant, despite the previously demonstrated *StSP6A* mediated decline in *StSWEET11* activity. Thus, in reality, active apoplastic transport would decrease in later stages in all scenarios, further favoring symplastic transport. On a similar note, we kept PD density and area constant, while we showed that callose removal led to an increased openness and thus diameter. Other processes, such as increasing PD-densisty over development or changes in other gating proteins, shown to increase PD conduction (Lucas et al., 2009) were also not considered. These changes would have further favored symplastic over apoplastic unloading. Finally, we here used 'simple' PD architecture, shown to be up to 10x less effective than funnel plasmodesmata (Ross-Elliot et al., 2017). Overall, the model used here is thus a conservative, worst-case, scenario. As such, the model strongly supports that it is the combined switching of sugar metabolism and unloading mode that enables an increased tuber sink-strength.

4

Acknowledgements

Funding

Author contributions

BH performed phylogenetic analysis, gene expression analysis, model construction and analysis of the models. SB designed the *in vitro* growth protocol and performed microscopy. YL grew the plant material, performed microscopy and did the first phylogenetic and gene expression analysis. CB conceived the project and analyzed the data. KT conceived the project, analyzed the data and performed the model construction and analysis. All authors contributed to writing the manuscript and approved the submitted version.

Data availability

No data was generated in this study.

Conflict of Interest

The authors declare there is no conflict of interest

Supplementary figures
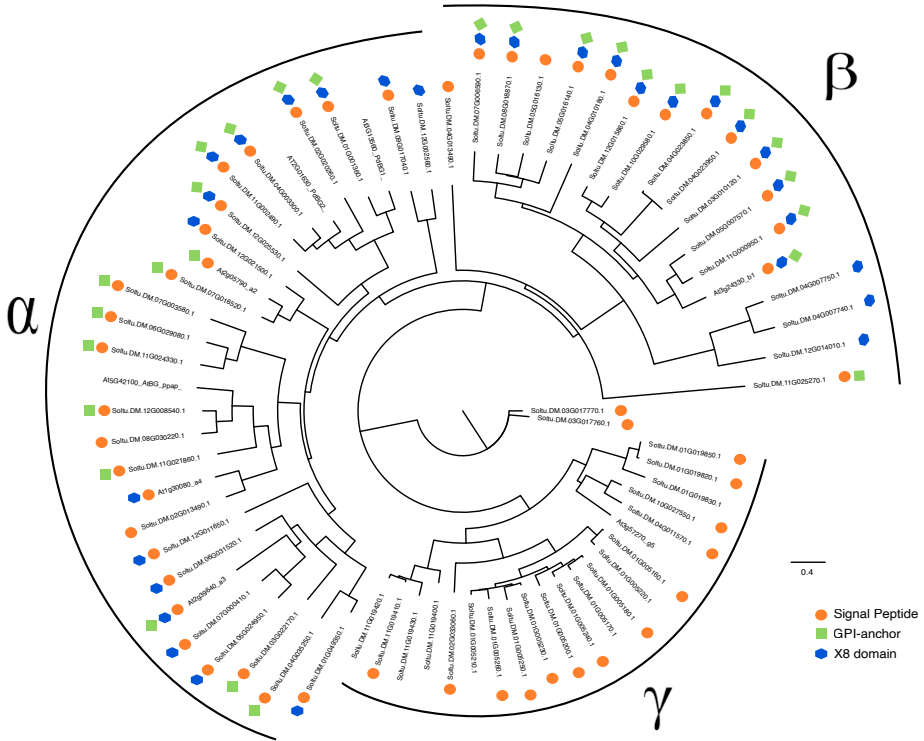
Supplemental figure 4.1. Phylogentic tree of the Beta-1,3-glucosidase family annotated for plasmodesmata related domains. Presence of three functional domains was depicted using symbols next to the gene names. The three clades were highlighted using α, β, and γ as previosuly described by Doxey et al. (2007).

Supplementary figures
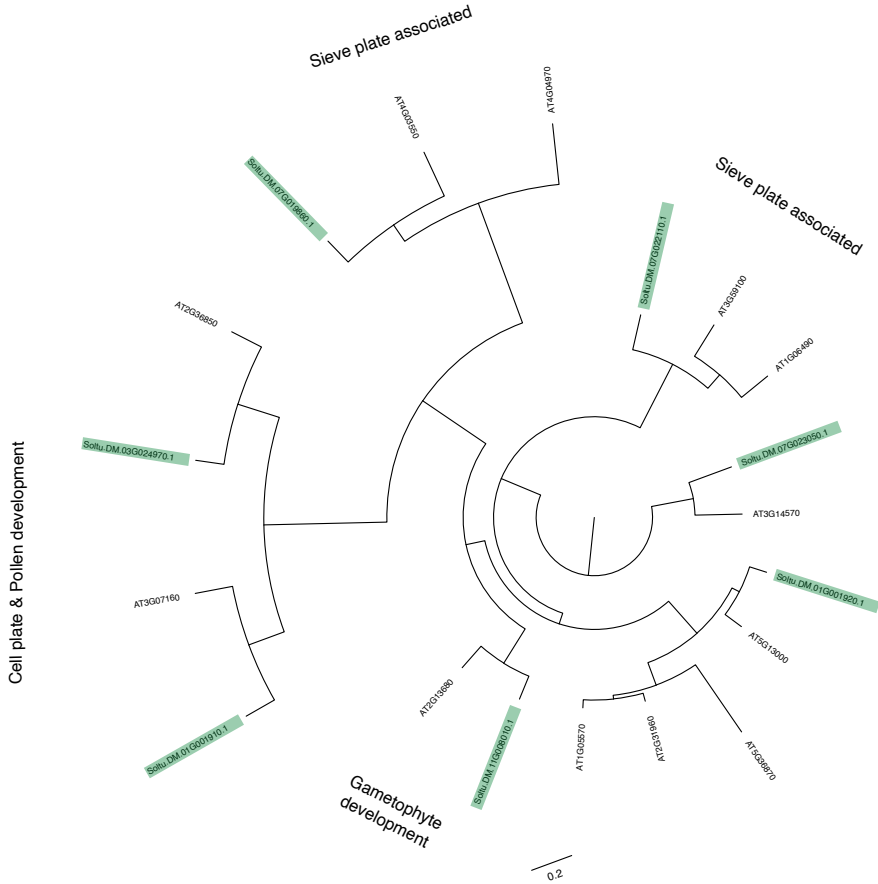
Supplemental figure 4.2. Phylogentic tree of the Callose Synthase family functionally annotated using function derived from the A. thaliana orthologs. Annotation of arabidopsis genes was obtained from Wu et al. (2018). Genes highlighted in green were present in the potato genome, non-highlighted genes were annotated genes from Arabidopsis.

Supplementary figures
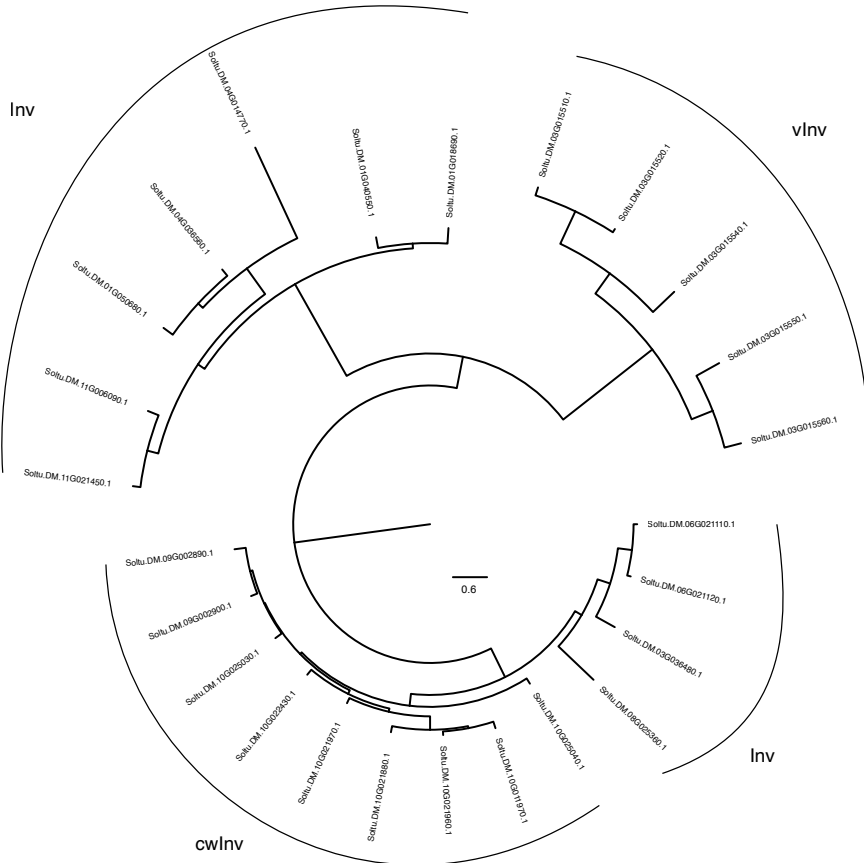
Supplemental figure 4.3. Phylogenetic tree of the invertase gene family. Not all invertase genes found via BLAST search were annotated. Therefore, phylogenetic placement in the tree above was used to functionally annotate the invertase genes that were not annotated as cell wall (cwInv), soluble (Inv) or vacuolar invertase (vInv).

Supplementary figures
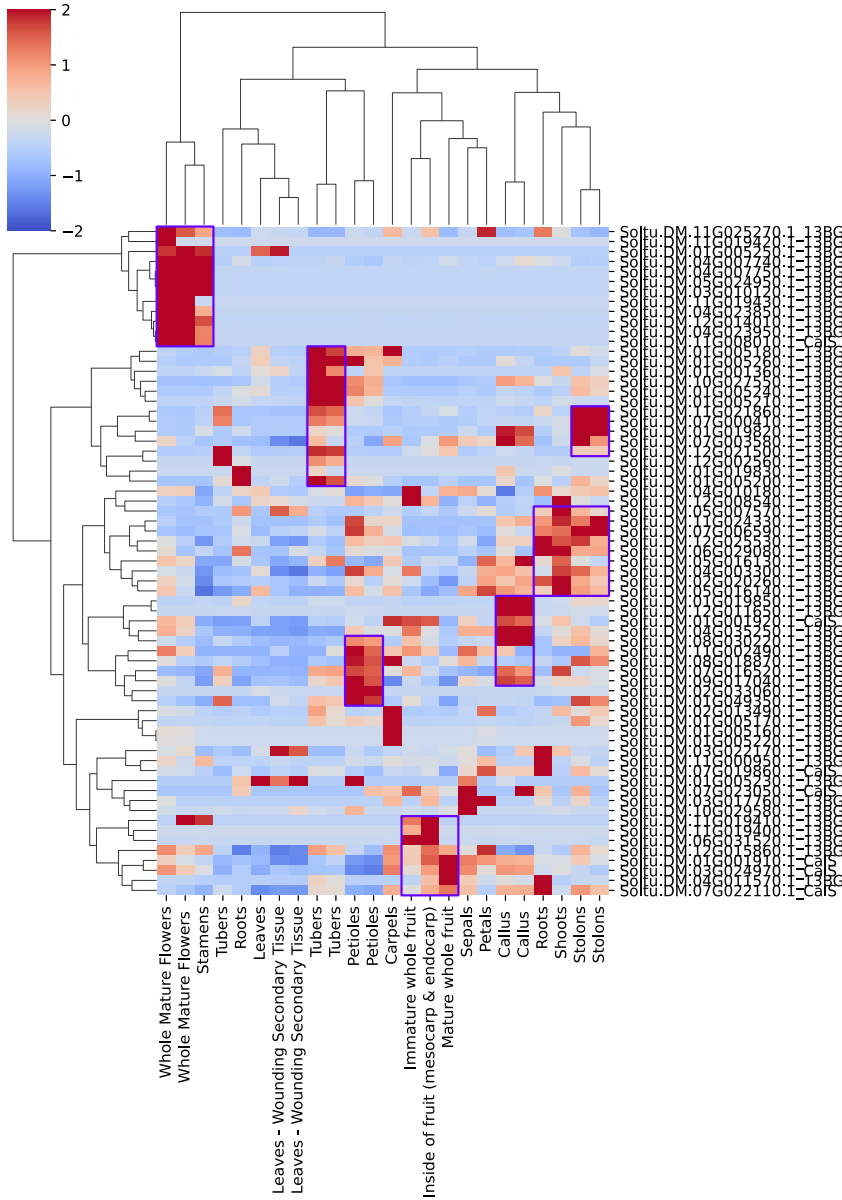
Supplemental figure 4.4. Beta-1,3-glucosidase and Callose Synthase family expression in above- and belowground samples reveal clear developmental patterns. Purple boxes show high expression clusters in specific samples.

Supplementary figures
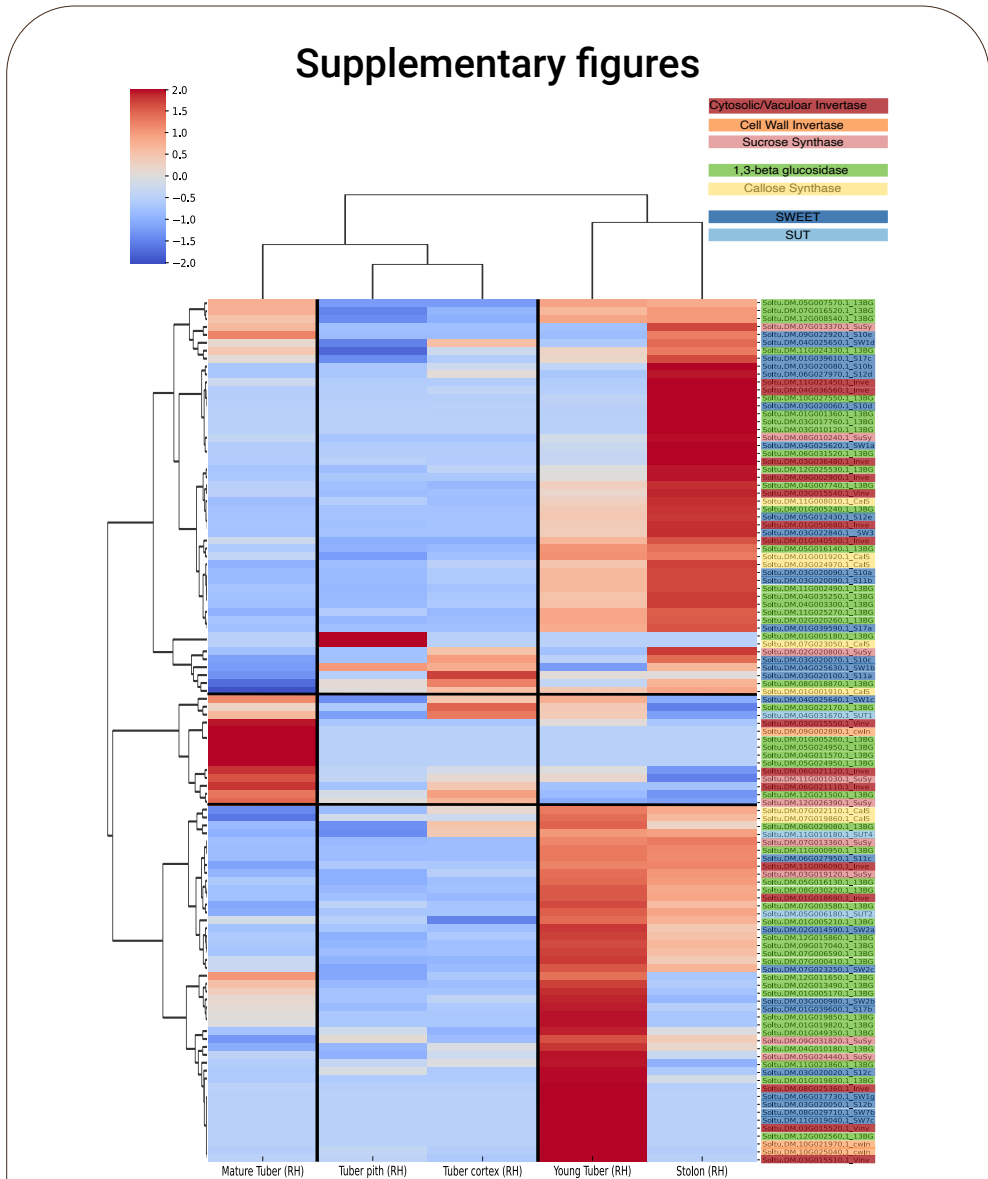
Supplemental figure 4.5. Callose, sucrose and transporter gene families expression in tuber and stolon samples in S. *tuberosum* Group Tuberosum RH89-039-16. Clear developmental cluster are again present for stolons and tubers. In the RH dataset, there is a distinction between young and mature tubers, which do show distinct expression patterns. Patterns are less clear than in DM. Overall, we do again see expression of CalS in stolons and young tubers, and cwInv expression lowest in mature tubers.

Supplementary figures
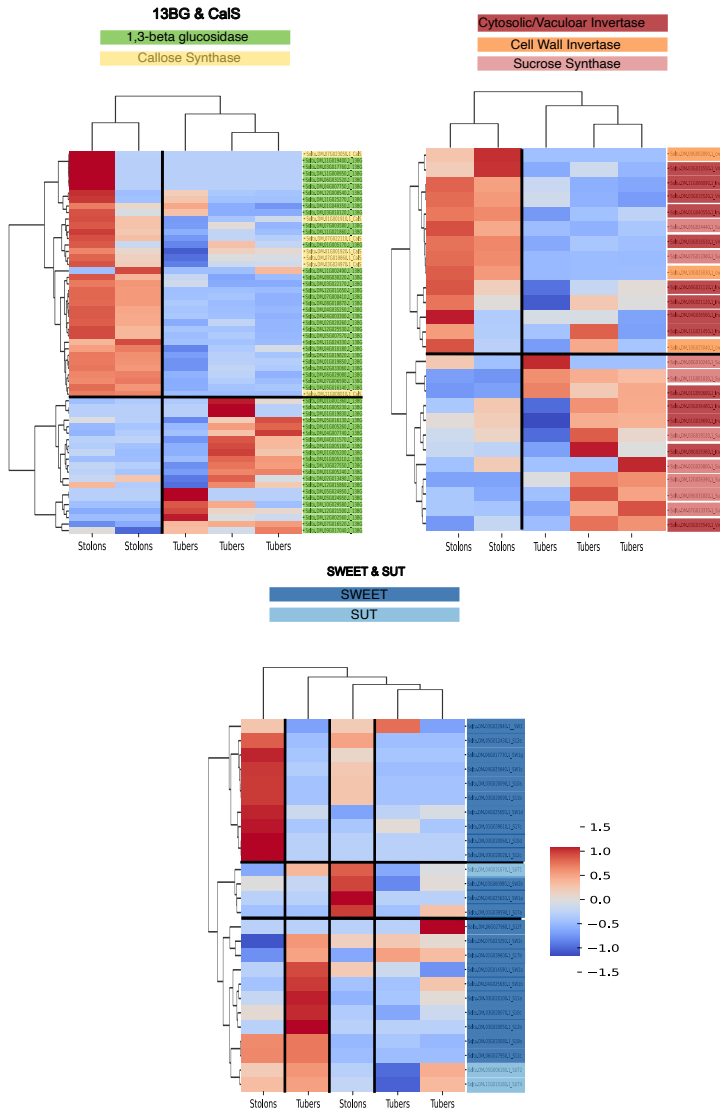
Supplemental figure 4.6. Gene families clustered per functional category in DM samples. These three heatmaps show clear developmental clusters for tubers and stolons in Sucrose and Callose metabolism. On the other hand, SWEET and SUC transporters show more ambiguous expression patterns.

Supplementary figures
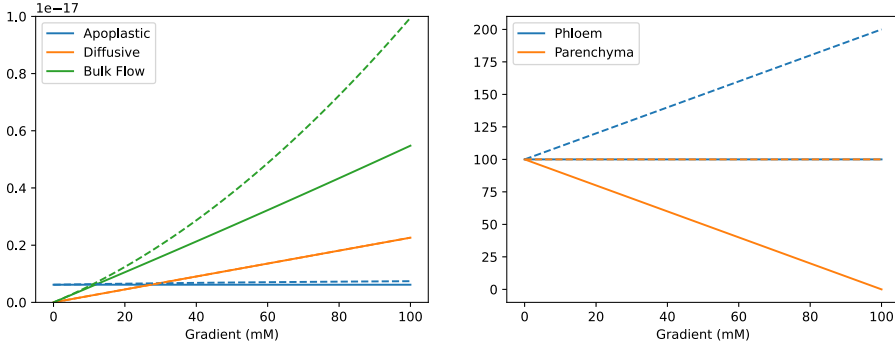
Supplemental figure 4.7. Unloading rates as a function of the concentration gradient.
Dotted lines represent a gradient caused by an increasing phloem concentration and
solid lines a gradient caused by decreasing parenchyma concentration.

4
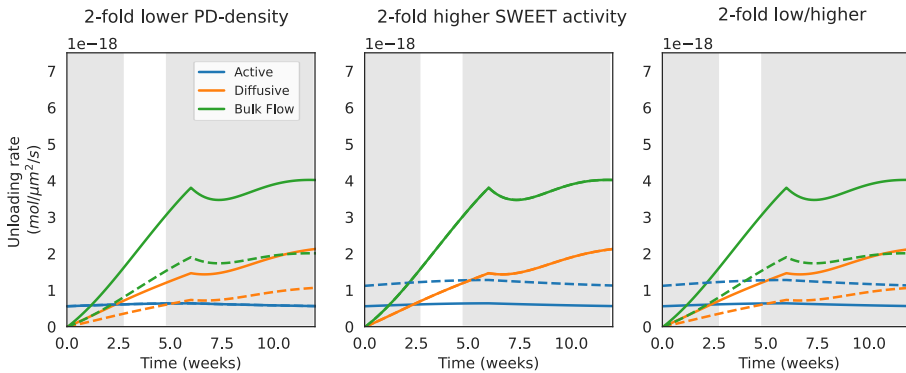
**Supplemental figure 4.8. Robustness of the unloading model to PD-density and
SWEET-activity changes.** Phloem conditions for these simulations were leaf-based
and all parameters were equal to those used in Fig. 4D, except PD-density and SWEET-
activity, as shown in the figure titles. Solid lines are baseline results equal to results
in Fig. 4D, dashed lines represent simulation results with altered parameters. These
plots show that while the exact quantitative results change, qualitative behaviour of
the model does not for realistic parameter regimes.

Chapter 5

Mobile tuberigen impacts tuber onset synchronization and canopy senescence timing in potato

Bas van den Herik, Sara Bergonzi, Christian W.B. Bachem,
Kirsten ten Tusscher

Abstract

Yield of harvestable organs is a complex function of photosynthetic output and timing of competing carbon sinks. In potato (S. tuberosum) the effect of, and interplay between, tuber and flower onset timing and post-tuberization canopy senescence on growth dynamics and tuber fresh weight are poorly understood. To advance our understanding we compared above- and below-tuber traits of wildtype (WT) plants with florigen (SP3Di), tuberigen (SP6Ai) and sucrose export (SWEET11i) knockdown plants and developed simple computational models to aid interpretation of results. Interestingly, we find that SP6Ai results in 2-week delayed tuber onset yet has a 4-to-5-week delayed canopy senescence. Together this results in prolonged tuber growth and increased final tuber fresh weight, at the cost of reduced synchronization in tuber onset and increased variance in tuber sizes. Using a leaf and tuber growth model comparing various leaf senescence mechanisms, we find that resource competition, and not a shared signal, is pivotal to explain the observation that delayed tuberization leads delayed senescence. Our results point to a role for resource competition in the correlated timing of tuber onset and canopy senescence, as well as a leading role for StSP6A in tuber onset synchronization and tuber size uniformity.

Introduction

Photosynthetic output and the subsequent distribution of produced assimilates across different sink organs play a vital role in determining the yield of harvestable plants organs. As such, both the strength and the timing of competition for sucrose between sink organs as well as the dynamics of source organs have a major impact on final crop yield. In potato, the general model is that tuber formation is under control of *StSP6A*, while developmental timing of flowers is under control of *StSP3D*, two FLOWERING LOCUS T (FT)-like proteins of the potato PHOSPHATIDYLETHANOLAMINE BINDING PROTEINS (PEBP) family (Navarro et al., 2011). Upon tuber formation, a new strong sink is formed coinciding with a switch from symplastic to apoplastic unloading (Viola et al., 2001). As a result, sucrose delivery to tubers is substantially increased at the cost of other plant organs (Fernie et al., 2020). *StSP6A* affects tuberization and sucrose delivery through initiation of tuber formation (Navarro et al., 2011) as well as increasing the relative efficiency of resource allocation towards tubers by mitigation of sucrose efflux via the sucrose exporter *StSWEET11* in the long-distance phloem (Abelenda et al., 2019; van den Herik et al., 2021; van den Herik & ten Tusscher, 2022). *StSP3D* initiates flower bud development (Navarro et al., 2011), while *StSP6A* antagonizes this effect by repressing flower bud development (Plantenga, Bergonzi, Abelenda, et al., 2019). Besides these important proteins, flowering and tuberization are also under control of environmental conditions (such as light, temperature, water availability and soil nutrient levels), hormone levels and sucrose availability. For example, flowering is accelerated under high light conditions independent of *StSP3D* (Plantenga, Bergonzi, Bachem, et al., 2019), and increased sucrose export from leaves leads to early flowering as well as increased tuber size (Chincinska et al., 2008). Interestingly, tuberization also occurs in *StSP6A* knockdown plants (Navarro et al., 2011), suggesting that other known tuberization signals such as the *StBEL5* factor, giberellin signalling and sucrose play partly redundant roles (Kondhare et al., 2020). Recently, it was shown that the florigen *StSP3D* also acts as a mobile tuber-inducing protein in the absence of the main tuberigen *StSP6A* (Jing et al., 2023). Thus, while developmental signals control the development of organs for vegetative and sexual reproduction through multiple, partly redundant, pathways, the competition for and dependence on a shared energy resource leads to complex feedback relationships between timing and formation of these different organs.

Interestingly, overall canopy senescence timing (i.e., time point of decline of total leaf area) appears to parallel tuber development, with early tuber forming genotypes also undergoing

earlier senescence, which can be described as post-tuberization senescence. Leaf senescence is a natural developmental transition, which is dependent on organ age, leaf nitrate and sucrose levels. Low nitrate, and both high and low sucrose levels have been described to promote leaf senescence (Rankenberg et al., 2021; Wingler, 2018). Thus, while tuber sink strength is enhanced after tuber formation, subsequent leaf senescence causes overall source-strength to diminish. An open question remains whether causal relations exist between these developmental events and how their precise relative timing impacts tuber yield. In addition to a competition for carbon between distinct organ types, (i.e. tubers, leaves, and flowers), tubers compete with each other for sucrose and this is likely an important factor determining potato tuber size distribution. Again, competition outcome depends on differences in sink strength, architecture and timing. To what extent differences in tuber onset and growth timing merely reflect differences in prior stolon development, and to what extent regulation at the stage of tuberization onset may affect tuber size differences has not been systematically investigated. Open questions to address are thus 1) whether flower/berry and tuber development are largely regulated through *StSP3D* and *StSP6A* or rather also significantly controlled through their competition for sucrose, 2) whether and how differences in tuber developmental timing affect agronomically important parameters such as tuber size distribution and quality, 3) whether post-tuberization canopy senescence is controlled largely in parallel with or is partly a downstream effect of tuber onset.

While previous studies have quantified growth of tubers and sugar/starch levels during development in field level experiments (Plaisted, 1957), during early tuberization (Davies, 1984) or tracked individual tuber volume development (Struik et al., 1988), there are no quantitative, plant level dynamic data sets to answer the questions above. Therefore, we set up an experiment aimed to generate a detailed data set covering the temporal development of individual potato plants, measuring various aspects of shoot and tuber growth, including sugar dynamics. We performed a climate chamber experiment under controlled day-length conditions with an obligate short-day tuber onset genotype, in WT, *StSP6A* RNAi, *StSP3D* RNAi and *StSWEET11*b RNAi lines. The experiment was set up to investigate resource competition between reproductive organs, with the *StSP3D* RNAi lines expected to have delayed flower bud onset, the *StSP6A* RNAi lines to have delayed tuberization, and the *StSWEET11* RNAi lines to have overall hampered sucrose allocation., i.e., decreased tuber yield. To aid the interpretation of experimental results, we combined our experiments with several simple computational models.

5

Materials & Methods

Experimental set-up and measured traits
Plant material and growing conditions
Wild-type (S. *tuberosum* group Andigenum 7540 (referred to as *S. Andigena*) and three transgenic lines were grown in chambers for controlled day-length (16h light/8h dark; LD and 8h light/16 h dark; SD), at a temperature of 20°C day/18°C night), light regime of 300 µM/m2/s and relative humidity of 70%. Transgenic plants with the *StSP3D* RNAi (SP3Di), *StSP6A* RNAi (SP6Ai), *StSWEET11* RNAi (SWEETi) constructs were generated by Agrobacterium mediated transformation of *in vitro* internodes and 2 independent lines per transgenic were used in the experiment. A detailed description of the transformation and primers used can be found in Abelenda et al. (2019). MS-20 tissue culture media with 2% (w/v) sucrose was used for *in vitro* vegetative propagation for three weeks. Tissue culture grown plantlets were planted to small pots (11x11 cm) and transferred to larger 3L pots 50 days after planting (DAP). Plants were initially kept in growth chambers for 4 weeks in LD conditions. After 4 weeks, the photoperiod was changed to SD to induce and synchronize tuber onset.

Sampling of plant material and measurements
Destructive harvests of plants were performed to monitor above- and belowground growth. Starting from before the switch to SD (SD0), the harvest were initially performed weekly and later the frequency was lowered to ensure sampling of plants during senescence (Table 5.1). At each time point, 5 plants per genotype were harvested. Stolon (number), tuber (number, fresh weight, dry weight, size distribution) and shoot (fresh weight, leaf area, stem length, stem diameter) were recorded for all plants (Table 5.2). For tuber dry weight, samples were dried at 70oC for 48 hours. For all timepoints, leaves, tubers and lower stem were harvested for sugar analysis. Soluble sugars were extracted and measured as described by Dinh et al. (2019). At SD8, the 1st fully expanded leaves (~5th leaves from the top of the plant) were harvested for gene expression analysis at ZT3. RNA extraction was performed using the RNeasy Qiagen kit with on column DNase digestion using the RNase free DNase set and according to manufacturer instructions. Script cDNA Synthesis kit was used for cDNA synthesis starting from 1µg of total RNA. Gene expression analysis was carried out in technical triplicates and the housekeeping gene *StEIF3e* was used for normalization. The primer pairs used for expression analyses are given in Table S5.1.

Table 5.1. Harvest timing

Harvest	SD0	SD1	SD2	SD3	SD4	SD5	SD7	SD8	SD10	SD12
Days after planting (DAP)	28	35	42	49	56	63	77	84	98	112

Table 5.2. Measured traits

Aboveground	Belowground
Shoot Fresh Weight (sFW, g)	Tuber Fresh Weight (tFW, g)
Leaf Area (LA, cm^2)	Tuber Dry Weight (tDW, g)
Stem Length (sL, cm)	Tuber Number (tN, -)
Stem Diameter (sD, mm)	Stolon Number (sN, -)

Data analysis and model descriptions

Beta growth function

To describe the growth curves of both leaf area and tuber fresh weight, we used the previously described beta growth function (Yin et al., 2003), which models determinate sigmoidal growth of plant organs. For tuber FW we use:

$$T_{FW} = \begin{cases} T_{FW,max}\left(1 + \dfrac{t_e - t}{t_e - t_m}\right)\left(\dfrac{t}{t_e}\right)^{\frac{t_e}{t_e - t_m}} & \text{for } 0 \leq t < t_e \\ T_{FW,max} & \text{for } t \geq t_e \end{cases}$$

(eq. 1)

where $T_{FW}=0$ at the start of growth (t=0) and $T_{FW}=T_{FW,max}$ at the end of the growth phase (t=te), with maximum growth at t_m.

Growth at specific time-points can be calculated with the equation below, which is the derivative of the equation 2:

$$r_{T_{FW}} = T_{FW,max} \frac{2t_e - t}{t_e(t_e - t)}\left(\frac{t}{t_e}\right)^{\frac{t_e}{t_e - t_m}}$$

(eq. 2)

For the leaf area fit we extended the sigmoidal growth phase with an exponential decay after t_e to represent senescence:

$$LA = \begin{cases} LA_{max}\left(1+\dfrac{t_e-t}{t_e-t_m}\right)\left(\dfrac{t}{t_e}\right)^{\frac{t_e}{t_e-t_m}} & \text{for } 0 \leq t < t_{end} \\ LA_{max}\,e^{-rt} & \text{for } t \geq t_{end} \end{cases} \qquad \text{(eq. 3)}$$

$$r_{LA} = \begin{cases} LA_{max}\dfrac{2t_e-t}{t_e(t_e-t)}\left(\dfrac{t}{t_e}\right)^{\frac{t_e}{t_e-t_m}} & \text{for } 0 \leq t < t_{end} \\ -r\,LA_{max} & \text{for } t \geq t_{end} \end{cases} \qquad \text{(eq. 4)}$$

The tuber FW and leaf area of each transgenic line were fitted individually using curve_fit from the scipy package. The 'trf' method was used as we set t_e boundaries per transgenic line to aid in obtaining a good fit for senescence start for LA fits. The other two parameters ($T_{FW,max}$/LA_{max} and t_m) were not bound.

Simulation of the stochastic onset of tubers

We created a simple model simulating tuber onset as a stochastic process with a tuberization probability. We assume that this probability consists of an SP6A dependent component (high when SP6A is present, zero when SP6A is absent) and an age dependent component (starting low, gradually increasing):

$$P_{age} = P_{age,max}\dfrac{t_{SD}^2}{t_{SD}^2+50^2} \qquad \text{(eq. 5)}$$

For SP6Ai lines the SP6A dependent probability always equals 0, for the other lines we assume that this probability switches to a non-zero value after two weeks in SD conditions, with levels increasing from a baseline to a maximum over the next two weeks to model the time delay between leaf and tuber expression levels as reported by Navarro et al. (2011):

$$P_{SP6A} = min\big(P_{SP6A,max}, max\big(0, P_{SP6A,max}(t_{SD} - 14)\big)\big) \qquad \text{(eq. 6)}$$

A predetermined number of stolons ("potential tubers") is used for each transgenic line, based on the average final number of tubers measured experimentally. We then simulate per day for each not yet tuberized stolon whether it will start tuberization or not. We do this by drawing a random number between 0 and 1, if this number is above the threshold (determined by SP6A presence and plant age) a tuberization event occurs.

ODE model of leaf and tuber growth

We developed a simple leaf area and tuber FW growth model where both LA and TFW are assumed to grow proportional to leaf area, which would result in exponential growth of both leaves and tubers in absence of leaf senescence. TFW was assumed to not decrease during the experiment, therefore we did not include a tuber decay rate in the model (equation 8). On the other hand, LA was observed to decrease due to senescence. To model this, we included a decay rate (d) for LA dynamics (equation 9). We investigated the effects of making this decay rate dependent on Tuber size, and/or Age and /or Leaf Area size (equation 10a). To model the effect of resource competition between leaves and tubers, we included increased senescence for larger tuber size (eq. 10b). This is based on the assumption that a larger tuber would be a stronger carbon sink. Developmental senescence was modeled dependent on the age of the plant (eq. 10c). Finally, we included a senescence inhibiting factor, which decreases the death rate for high leaf area, making sure that senescence due to resource competition is counteracted when carbon supply is abundant (eq. 10d). The equations were fitted to the LA and tuber FW data of WT, SP6Ai and SP3Di lines. Parameters were not constrained and are shared between the different transgenic lines, all differences between the transgenic lines in this model thus result from differences in tuberization timing. Parameter fitting was done using grind.R by R.J de Boer (http://tbb.bio.uu.nl/rdb). Grind.R is an R script that functions as a wrapper for the deSolve and FME R packages (Soetaert et al., 2010).

5

$$\frac{dT}{dt} = \begin{cases} 0 \text{ for } t < t_{tuberization} \\ g_T \, LA \text{ for } t \geq t_{tuberizaiton} \end{cases} \tag{eq. 7}$$

$$\frac{dLA}{dt} = g_{LA} LA - dLA \tag{eq. 8}$$

$$d = d_0 \left(1 + Sen_T + Sen_{age}\right) ReprSen_{LA} \tag{eq. 9a}$$

$$Sen_T = a \frac{T^2}{T^2 + K_T^2} \tag{eq. 9b}$$

$$Sen_{Age} = b \frac{t^2}{t^2 + k_t^2} \tag{eq. 9c}$$

$$ReprSen_{LA} = (1 - c) + c \frac{K_S^2}{K_S^2 + LA^2} \tag{eq. 9d}$$

Results

Under limited flowering SP3Di and WT are phenotypically similar

A priori, it was expected that the knockdown of *StSP3D*, *StSP6A* and *StSWEET11* would all influence resource allocation and shoot versus tuber growth dynamics due to their effects on flowering, tuberization and sucrose transport respectively. In contrast to these expectations, SP3Di behaved very similar to WT plants, whereas SP6Ai and SWEETi plants did show large phenotypic differences in shoot characteristics (Fig. 5.1A). Silencing of *StSP3D*, *StSP6A* and *StSWEET11* was confirmed by qPCR analysis (Fig. S5.1). Limited phenotypic differences between SP3Di and WT could thus not be attributed to the lack of *StSP3D* silencing in SP3Di plants. Intuitively, SP3Di lines are expected to influence growth dynamics via a reduction of resource allocation to flowers (Navarro et al., 2011) enhancing sucrose availability for leaves and/or tubers. However, in our experiments, limited flowering occurred in wild type plants, with no further decrease or delay occurring in SP3Di plants (Fig. 5.1B) , explaining the absence of significant differences between WT and SP3Di. These findings agree with earlier findings on the limited flowering in *S. Andigena* (Plantenga, Bergonzi, Bachem, et al., 2019). Additionally, no differences in tuberisation and canopy dynamics were found between WT and SP3Di, suggesting limited antagonistic effects of florigen on tuberisation. In SP6Ai lines, expected to have enhanced flowering based on the flowering suppressive effects observed for SP6A (Plantenga, Bergonzi, Abelenda, et al., 2019), flowers emerged earlier and developed further.

Delayed canopy senescence concurs with continued apical growth in SP6Ai plants

During the early growth stages under LD, no significant differences in leaf area were observed between the different plant lines (Fig. 5.1C, grey area). In the subsequent exponential growth phase, differences in leaf area between all lines remained small. Differences in shoot characteristics for the initial and exponential growth stages were mainly observed for lower stem diameter (Fig. 5.1E), with diameter significantly lower for SWEETi lines as compared to the other lines. We did not observe an increased stem diameter for SP6Ai plants, opposed to recent observations of decreased stem diameter in *StSP6A* overexpression plants (Lehretz et al., 2021), suggesting a saturating dependence of radial growth on sucrose delivery. At later stages (>60 days after planting (DAP)), stem length and leaf area showed consistent and significant differences between the different plant lines (Fig. 5.1C, F). We fitted the beta growth function, an empirical function for determinate plant growth, to our data to determine growth rates (Fig. 1D, see Methods, Yin et al., 2003) From this we observe that increase in leaf area
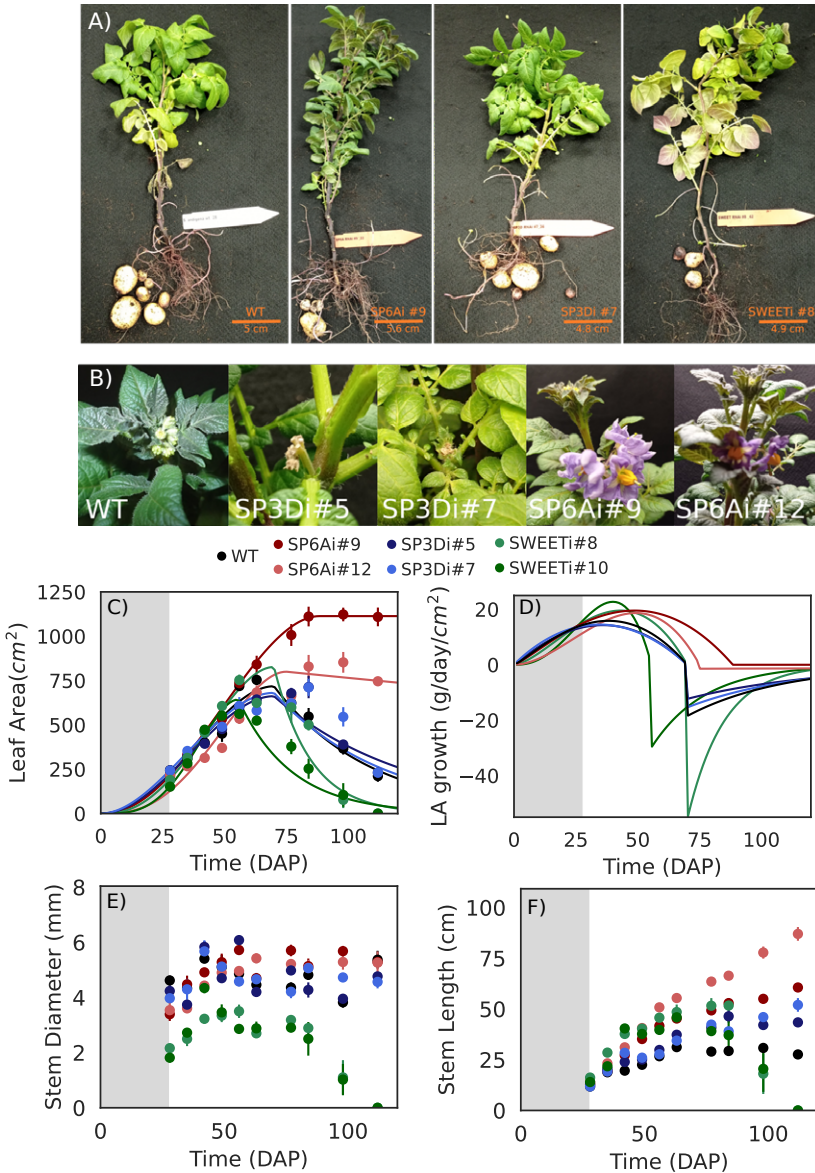
Figure 5.1. Aboveground characteristics and growth dynamics A) Phenotypes of harvested plants at SD7. B) Flower and bud development at SD7. C) Leaf area over time, the gray area represents LD conditions, data was fitted using the beta growth function and an exponential decay function (see Methods). D) Leaf area growth rates over time E) Stem diameter as a function of time F) Stem Length as a function of time

ended around 60 DAP for SWEETi lines, and after approximately 70-80 DAP for WT and SP3Di lines, followed by a decline in overall leaf area reflecting canopy senescence. Leaf area increase is larger and prolonged in SP6Ai lines resulting in a larger final leaf area, with no substantial decline occurring over the timeframe of our experiment (120 days), representing a delay in canopy senescence of 4-6 weeks compared to the control plants. Specifically, apical growth was observed to continue for SP6Ai lines (especially #12, Fig. 5.1F), resulting in an altered shoot morphology, with longer stems and leaf-loss restricted to the lower stem (Fig. 5.1A). As a result, senescence of older leaves was compensated by newly forming leaves, delaying overall leaf area decrease in SP6Ai lines (Fig. 5.1C). These results are consistent with previous experiments demonstrating an early suppression of apical growth in *StSP6A* overexpression lines (Lehretz et al., 2021). Summarizing, *StSP6A* transcriptional levels strongly correlate with overall canopy senescence timing.

Delayed tuberization in SP6Ai plants is mitigated by higher tuber growth rates to reach higher final tuber fresh weight

Next, we compared tuber growth dynamics between the different plant lines (Fig 5.2). Growth dynamics of tuber FW (Fig. 5.2A, B) tuber numbers (Fig. 5.2C), stolon numbers at SD1 (Fig. 5.2D) and overall final tuber FW (Fig. 5.2E) are significantly lower in SWEETi lines compared to other lines. Our tuber growth rate data indicate that this lower final FW results from a lower maximum growth rate and earlier cessation of tuber growth (Fig 5.2B). Importantly, while the fitted beta function appears to suggest SWEETi lines also have a delayed tuberization onset, plotting of individual tuber numbers (Fig. 5.2C) indicates that tuberization onset of SWEETi lines is in fact comparable to WT. This differs from earlier results, where SWEETi lines were observed to have slightly accelerated tuberization (Abelenda et al., 2019). As expected, SWEETi lines showed sugar accumulation in leaves (Fig. S5.2A).

Tuberization dynamics, tuber and stolon numbers and final tuber FW are comparable between WT and SP3Di lines. This is likely to be due to the limited differences in flower development. SP6Ai lines showed an approximately 2-week delayed tuberization onset, consistent with the 2-to-3-week delay observed in previous work (Navarro et al., 2011). Interestingly, in the final harvests (SD8, 10, 12) higher tuber growth rates were reached in SP6Ai lines compared to WT. Additionally, tuber growth continued beyond the time when WT tuber growth halted (Fig. 5.2B), resulting in an overall slightly higher final tuber FW for SP6Ai *#9* (Fig. 5.2E) despite lower tuber and stolon numbers (Fig. 5.2C and 5.2D). In contrast, earlier results showed that SP6Ai plants

had a reduced final tuber FW, similar to that of SWEETi plants (Abelenda et al., 2019). This inconsistency might be due to differences in harvesting time, as we also observe lower FW for SP6Ai for the first 100DAP and only an increase compared to WT at the experiments end. Finally, tuber dry weight and FW show a consistent high correlation for all lines (r=0.99, Fig. S3A), indicating a constant dry matter content across lines. The increased tuber growth for SP6Ai is thus not merely caused by an increased water uptake but also represents an increased dry matter accumulation. Summarizing, under the later harvesting time applied here, the approximately 2-week delay in tuber onset can be (over)compensated by the 4–6-week delay in canopy senescence.

StSP6A knockdown causes gradual tuberization

In addition to differences in leaf/tuber growth dynamics and final tuber FW, we also observed differences in tuber number dynamics (Fig. 5.2C) and number of stolons present before tuberization (SD1, Fig 5.2D). Tubers form nearly simultaneously in SP3Di and WT lines, while for SWEETi lines tuber numbers increase more gradually. Additionally, final tuber number is considerably lower in SWEETi lines, consistent with a lower number of stolons formed at early stages (Fig. 5.2D) resulting in the overall lower yield (Fig. 5.2E). Interestingly, the increase in tuber number for SP6Ai lines was significantly more gradual (dashed lines, Fig. 5.2C) and reached a lower final number of tubers. This is consistent with the increased tuber numbers observed in *StSP6A* overexpression reported by Lehretz et al. 2021. Importantly, in all lines the number of initial non-swelling stolons matches the number of final tubers formed (Fig. 5.2C) indicating that stolon number is not a limitation factor, leading to the more gradual formation of tubers in SP6Ai lines. Instead, the more gradual increase in tuber numbers suggests that *StSP6A* may plays an important role in tuberization synchronization as well as tuber onset.

To investigate this, we created a simple phenomenological model simulating tuber onset as a stochastic process with a tuberization probability. We assumed that this probability consists of the sum of an *StSP6A* dependent component (high when *StSP6A* is present, zero when *StSP6A* is absent) and an age dependent component (starting low, gradually increasing) (see Methods). We start with the predetermined number of stolons as observed in the experiment. It is then determined per day for each stolon whether it will start tuberization or not. This model was used to estimate the *StSP6A* dependent and independent probabilities based on the experimental data. For the SP6Ai line we assumed that the *StSP6A* dependent component of the tuberization probability always equals zero. For the other lines we assume that this component switches to

5
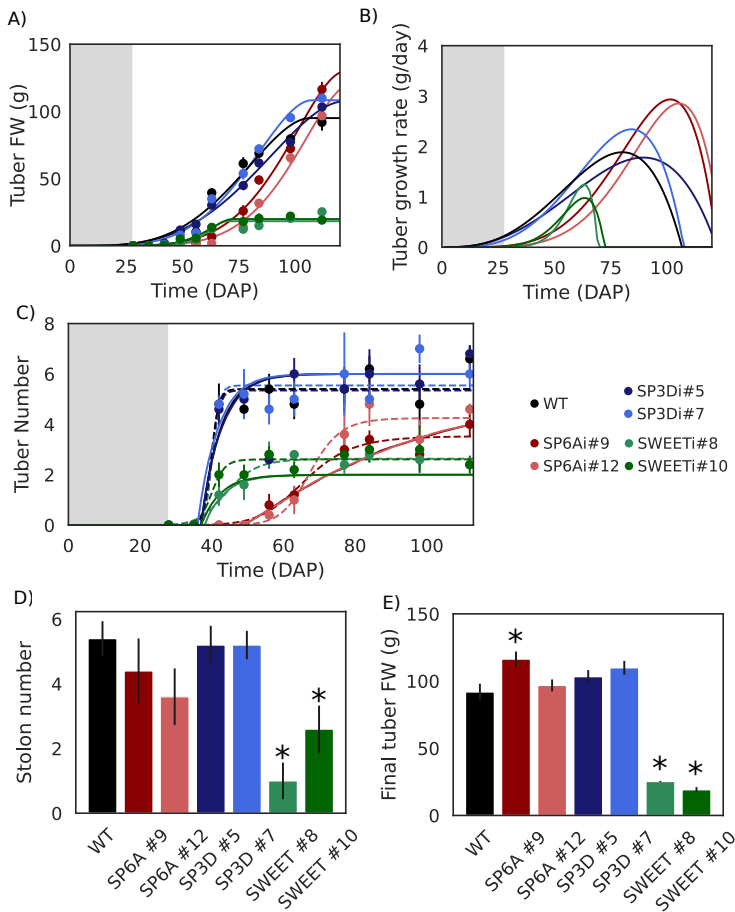
Figure 5.2. Tuber growth characteristics. A) Tuber FW over time, grey area represents LD conditions, data was fitted using the beta growth function **B)** Tuber growth rates over time **C)** Tuber number as a function of time. Dashed lines represent a sigmoidal fit, whereas solid lines represent the stochastic onset model **D)** Stolon number at SD1, just before the first visible signs of tuberization. Stars represent a significant difference with WT (students t-test, p<0.01) **E)** Final harvest tuber FW.

a non-zero value after two weeks in SD conditions, with levels increasing from a baseline to a maximum over the next two weeks (see Methods), to model the time delay between leaf and tuber *StSP6A* mRNA expression levels as reported by Navarro et al. (2011). Fitting this simple model indeed enables us to closely mimic WT and SP6Ai tuberization dynamics (Fig. 5.2C, solid lines) and results in a fitted per-day *StSP6A*-dependent tuberization probability of 15-20% and a *StSP6A*-independent tuberization chance increasing from 1 to 3.5% per day over time. This suggests that *StSP6A* acts as a strong signal for synchronization of tuberization.

Gradual tuberization correlates with increased variance in tuber size distribution

Tuber size distribution is an important agronomic trait, and variability in tuber size has been attributed to heterogeneity in seed tuber storage and growth conditions, stolon length and hierarchy as well as differences in tuberization dynamics (Aliche et al., 2019; Ospina et al., 2021; Struik, 2007). Therefore, we investigated whether the observed differences in tuberization dynamics correlate with differences in tuber size distribution. We see that tuber numbers strongly correlate with overall tuber FW (Fig. S3B). However, the data for SP6Ai lines generally lie below the regression line while data for WT and SP3Di lie above the regression line, indicating fewer tubers for the same FW and hence a larger average tuber size. While we have not measured all individual tuber weights and hence cannot calculate tuber variance directly, we estimated the variability in tuber size distribution from the available data by taking the weight ratio between the largest tuber (g_M) and the average weight of the other tubers (g_{rest}):

$$\frac{g_m}{g_{rest}^-} = \frac{g_m}{\frac{T_{FW}-g_m}{n-1}}$$

(eq. 10)

The higher this ratio, the larger the difference between the largest tuber and the average of the rest is, enabling us to use it as a proxy for variation in tuber size distribution. We clearly see that, at the final harvest for SP6Ai, the largest tuber is significantly larger (Fig. 5.3A), while the average of the other tubers is lower (Fig. 5.3B), resulting in a higher ratio (Fig. 5.3C). This suggests that the delayed and gradual onset of the SP6Ai tubers correlates with an increase in variation in tuber size distribution under pot conditions.

A negative correlation between tuber and leaf growth suggests a role for resource competition

Leaf area, tuber FW and tuber number dynamics described above demonstrated a strong correlation between timing of the onset of canopy senescence (earliest in SWEETi and latest in SP6Ai lines) and the onset and halting of growth of tuber FW (again earliest in SWEETi and latest in SP6Ai lines). To investigate potential mechanisms underlying these correlations, we investigated the interplay between leaf area and tuber and leaf growth dynamics. Tuber FW did not correlate strongly with leaf area (Fig. 5.4A, Pearson's r=0.36, p<0.005), yet tuber growth rate does strongly correlate with leaf area (Fig. 5.4B, r=0.79, p<0.005), consistent with leaf area determining photosynthetic output and thereby growth potential. This correlation furthermore supports our hypothesis that delayed canopy senescence and resulting larger cumulative leaf area causes the enhanced and prolonged tuber growth observed in SP6Ai lines.

5
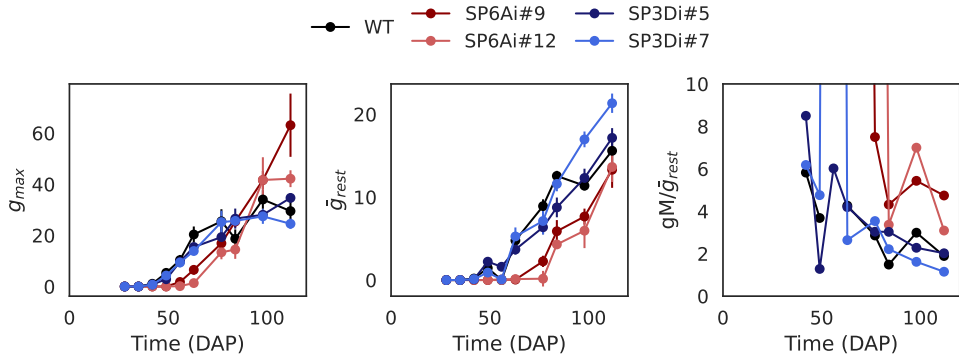
Figure 5.3. A proxy for tuber size distribution variation. A) Largest tuber dynamics **B)** Average size of all tubers except the largest tuber **C)** The ratio of the largest tuber over the average of the other tubers, the larger this ratio is, the larger the variation in tuber size.

Next, we investigated the relation between leaf growth rate and leaf area (Fig. 5.4C), for which we found a weak, non-significant, negative correlation (r=-0.16, p=0.18). Given the clear distinction between an overall leaf area growth and senescence phase, we reinvestigated this relation while separating leaf growth rates occurring pre- or post-tuberization. Pre-tuberization leaf growth rate and leaf area displayed a positive correlation (Fig. 5.4D, r=0.54, p<0.005), while for post-tuberization only a weak correlation was observed (Fig. 5.4E, r=0.32, p=0.015). With SWEETi even displaying a negative correlation. Thus, in absence of tubers, leaf area drives leaf growth as expected, yet post tuberization leaf area only drives tuber growth while simultaneously declining due to senescence. In agreement with the correlated timing of tuberization and canopy senescence onset, we observe a strong negative correlation between tuber and leaf growth rates (Figure 5.4F, r= -0.74, p<0.005). Overall, these correlations suggest a potential role for resource competition in canopy senescence and its timing.

Sucrose concentrations do not clearly affect growth dynamics after tuberization

While our data demonstrate a strongly correlated timing of canopy senescence and tuberization onset, a major question remains whether this is caused by a shared, possibly *StSP6A* dependent regulation or rather arises from tuberization induced resource competition inducing/enhancing senescence, or from a combination. Indeed, senescence has been suggested to be promoted by both elevated as well as lowered sucrose levels, independent of developmental age (Rankenberg et al., 2021; Wingler, 2018). To investigate the hypothesis that resource competition enhances senescence we measured sucrose levels in leaves, stem, and
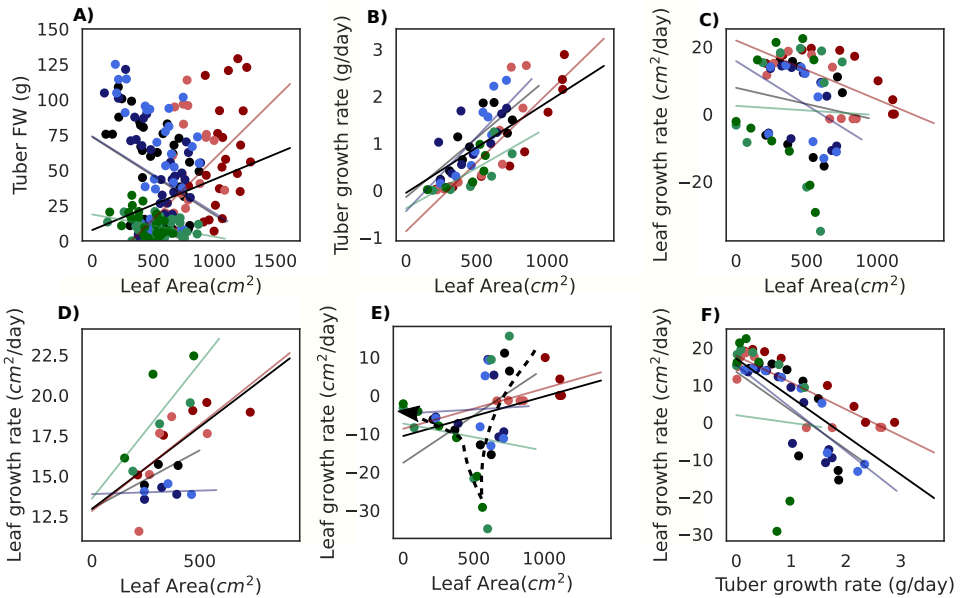
Figure 5.4. Correlations between Leaf Area, tuber FW and tuber and leaf growth rates. A) Leaf area vs. Tuber FW. Black line depicts a regression for all lines combined. Colored lines depict a regression for their transgenic line respectively. B) Leaf area plotted against the tuber growth rate C) Leaf area plotted against the leaf growth rate D) Leaf area plotted against the leaf growth rate pre tuberization (<SD2 for WT, SP3D RNAi and SWEET RNAi lines and <SD4 for SP6A RNAi lines), E) Leaf area plotted against the leaf growth rate post tuberization (<SD2 for WT, SP3D RNAi and SWEET RNAi lines and <SD4 for SP6A RNAi lines). The dashed line represents the post-tuberization senescence trajectory. F) Tuber growth rate plotted against the leaf growth rate

tuber over the course of development in the different transgenic lines (Fig. 5.5A-C). The sucrose data showed elevated levels in the stem for SP6Ai lines, confirming earlier findings on the role of *StSP6A* in reducing *StSWEET* mediated sucrose export (Abelenda et al., 2019). We did not observe a decrease in leaf sugar levels after tuberization onset in any of the lines to support our hypothesis of competition mediated low sucrose levels in leaves enhancing senescence. WT and SP3Di sucrose levels in leaves remained approximately constant, in SP6Ai we observe an increase over time in both leaves and tubers.

To further probe for signals of resource competition by investigating the sugar dependence of growth, we correlated organ sugar levels with organ growth (Fig. 5D-G). We find that tuber growth rate is positively correlated with tuber sucrose levels (r=0.72, p<0.005, Fig. 5.5D) for the

entire duration of the experiment and for all transgenic lines separately. Leaf sucrose levels are negatively (r=-0.55, p<0.005, Fig. 5.5E) correlated with leaf growth rate, yet when again splitting pre- and post-tuberization leaf growth rates, we observe a positive correlation (r=0.63, p<0.005, Fig. 5.5F) pre-tuberization. However, when separating further the data per pair of transgenic lines, we observe that it is mainly the high sucrose concentration in SWEETi lines, and not the variation in leaf growth rate, that drives this positive correlation. Post-tuberization there is again no correlation present (r=-0.01, p=0.94, Fig. 5.5F). Indeed, growth/senescence rates are relatively stable within the transgenic lines for a range of sucrose concentrations. Thus, the sucrose data did neither indicate that tuberization lowers leaf sucrose levels (Fig. 5.5G) nor that sucrose levels strongly determine leaf growth rate (Fig. 5.5E-G).

A simple leaf and tuber growth model suggests a role for resource competition in delayed senescence

While our sugar data do not provide indications for resource competition between tubers and leaves, this may be due to limited spatial resolution of sugar measurements. To further investigate the mechanism underlying the correlated timing of tuberization and canopy senescence onset we therefore developed a simple leaf and tuber growth model (see Methods for details). In the model, we assumed that leaf and tuber growth rate are proportional to leaf area, consistent with our observations (Fig. 5.4B, D), and additionally incorporated leaf senescence. Importantly, our data demonstrate that canopy senescence in SP6Ai lines is further delayed than tuberization onset, suggesting a complicated mechanism, potentially involving sugar status and/or other signaling pathways. Therefore, for canopy senescence we investigated the potential impact of tuber size and plant age promoting, and total leaf area inhibiting canopy senescence.

As a baseline, we performed a simulation with a constant leaf death rate. The best fit (Fig. 5.6, dotted lines) did neither qualitatively nor quantitatively represent the experimental data well. Specifically, no transition from leaf area expansion (leaf growth rate exceeding leaf turnover) to overall shoot senescence (leaf turnover exceeding leaf growth) could be achieved, due to the constant leaf turnover rate. An additional tuber dependent leaf death rate was therefore added, where increasing tuber FW leads to a higher leaf death rate (Fig. 5.6, dashed lines). In the best fit, no substantial overall shoot senescence occurred, instead leaf area became constant. This can be understood from the interplay between tuber size and leaf area, with tuber size negatively impacting leaf area, yet tuber growth positively depending on leaf area. As a result, a balance is reached when leaf growth and turnover are equal, resulting in a constant tuber growth. As different plant lines displayed different tuber growth dynamics, this transition
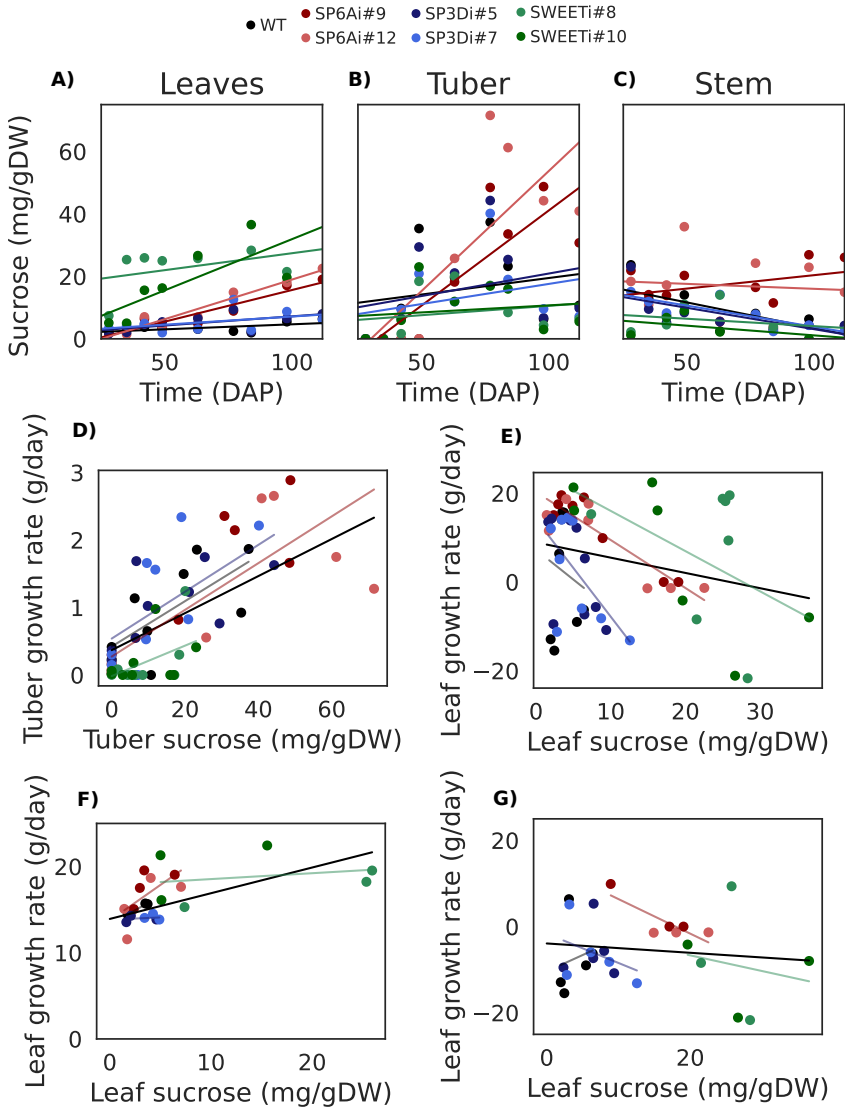
Figure 5.5. Sucrose dynamics and its relation to organ size and growth. A) Sugar concentration dynamics in tubers, a linear regression was done to visualize the general time dynamics of sucrose levels. B) Sugar concentrations dynamics in leaves C) Sugar concentration in whole stem samples D) Tuber sucrose vs. tuber growth rate E) Leaf sucrose vs. Leaf growth rate F) Leaf sucrose vs. Leaf growth rate pre-tuberization G) Leaf sucrose vs. Leaf growth rate post-tuberization

to constant leaf area and linear tuber growth occurred at different time points for the different plant lines. Besides senescence due to resource competition, plant age (i.e. DAP) can be a prominent cause for canopy senescence (Wingler et al., 2018). We therefore included a plant age dependent death rate, adding this to the baseline model with only a constant death rate (Fig. 5.6, large, dashed lines). This led to a best fit where overall shoot senescence started at around 75 DAP for all plant lines. This consistent senescence timing is too late for WT and SP3Di lines, and too soon for SP6Ai lines, and arises from the inability of this model to discriminate between the different plant lines. We next combined age and tuber size dependent models (Fig. 5.6, dash-dotted line), enabling the model to discern plant lines based on differences in tuber size development dynamics. Nevertheless, the best fit was still dominated by plant age resulting in a similar senescence timing for all transgenic lines.

Tuberization onset is delayed by only 2 weeks between SP6Ai and WT/SP3Di, whereas canopy senescence is delayed considerably longer. This may explain why tuberization is insufficient to explain the differences in canopy senescence timing. Differences in leaf area dynamics and maximum achieved canopy sizes affect overall sucrose source strength and may thereby impact the severity of resource competition between tubers and leaves. We therefore hypothesized that differences in tuberization onset may lead by themselves to minor difference, which through affecting source strength, become amplified to larger differences in senescence. We included this hypothesis through the addition of a term that inhibits senescence based on the size of the canopy (source inhibition, Fig. 6, solid lines). We found that only when including a combination of age, tuber and canopy size effects on leaf senescence rate, we could reproduce our experimentally observed leaf area and tuber FW dynamics. While this model cannot proof causality, by varying the threshold level at which tuber size enhances senescence, we can investigate whether tuberization onset and thus induction by a shared signal (low tuber size threshold: $K_T < T$, so rapidly saturating) or rather growth of tubers and thus resource competition (high tuber size threshold $K_T > T$, so gradually increasing) better explains canopy senescence dynamics. The best fit to the experimental data was found to be K_T 147gFW, which is on the higher end of tuber FW (see Figure 5.2A), suggesting that with regards to the tuberization dependent part of senescence control resource competition rather than a shared signal underlies the correlated timing of tuberization and canopy senescence.
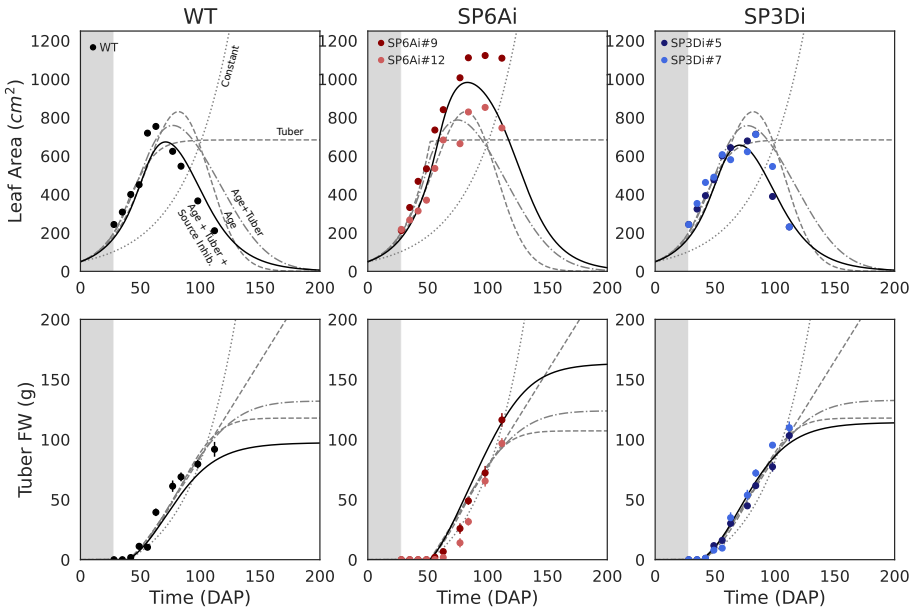
Figure 5.6. Leaf Area and Tuber FW fitted with the simple growth model. Best fit to the leaf area and tuber FW data (dots) using the growth model in solid black lines, for WT, SP6Ai and SP3Di. which likely explains the reduction in tuber growth rate from reduced sucrose allocation, while the observed earlier canopy senescence may be causal for the earlier termination of tuber growth.

Discussion

In this study we performed a temporally resolved climate chamber experiment in combination with simple models to investigate the impact of the presence and timing of different sink organs, the temporal dynamics of source organs, and the interplay between sink and source organs on final tuber FW. *StSP3D* RNAi and *StSP6A* RNAi lines, perturbed in flower and tuber onset respectively, were compared to wild type. Additionally, to perturb overall sucrose allocation we included *StSWEET11*b knockdown lines in our study. We observed flowering and anthesis occurring only in SP6Ai lines as described previously using the same growing conditions (Plantenga, Bergonzi, Bachem, et al., 2019), a likely result of short day and light quality conditions. Plant dynamics of WT and SP3Di were therefore highly similar, prohibiting the investigation of whether there is resource competition between tubers and flowers or berries that affects their development. SWEETi plants displayed higher leaf sucrose levels and reduced stolon and tuber growth, consistent with the failure of source leaves to export sucrose to sink organs.

5

Additionally, leaf senescence was promoted relative to wildtype plants, earlier senescence may itself be a result of elevated leaf sucrose levels and be age independent (Rankenberg et al., 2021; Wingler, 2018). Difficulties in allocating sucrose is also underscored by the formation of aerial tubers (Fig. S5.2B), indicative of blocked phloem transport (Ewing & Wareing, 1978).

Consistent with earlier findings, we observed a 2-week delay in tuberization in SP6Ai lines (Navarro et al., 2011). Recent work showed that *StSP3D* could take over the role of *StSP6A* in tuber onset (Jing et al., 2023), showing the highly redundant nature of the tuberization onset pathway, with a plethora of 'back-up systems'. However, in our SP6Ai lines, *StSP3D* was also strongly repressed (Fig S5.1), suggesting another candidate responsible for tuber onset in our plants. Additionally, tuberization appeared more gradual in these lines, and our experimental data and modeling suggest an important role for *StSP6A* in synchronization of tuberization. Still, the molecular mechanism underlying this synchronization remains to be investigated and could be either through *StSP6A* functioning in switching on tuberization genes, or through *StSP6A* reducing SWEET-mediated sucrose loss with the enhanced sucrose availability dampening inter tuber differences, or a combination of such processes. Our data further suggests that this gradual tuberization correlates with a larger variation in tuber sizes (Fig. 5.3). While differences in tuber onset timing likely play a role in generating this variation in size differences, knockdown of *StSP6A* may have also unmasked other differences. To further substantiate the role of *StSP6A* in tuber onset synchronization and size homogenization, future studies applying rhizotron based imaging of the growth dynamics of individual tubers in WT and *StSP6A* knockdown lines may help decompose the effects of differences in stolon length, width, and hierarchy as well as tuberization timing on final tuber size.

In line with the generally observed 'post-tuberization senescence', we observed a strong correlation between tuberization and canopy senescence dynamics, with SP6Ai lines displaying both the latest tuberization and senescence. The combined early and late time points of final harvesting in our study enabled us to observe that the delay in senescence (4-6 weeks) was substantially more pronounced than the delay in tuberization onset (2 weeks). Furthermore, we observed an increase in final tuber FW in one of the two SP6Ai lines as compared to the WT, whereas in earlier time points SP6Ai tuber FW is below WT, as was observed previously (Navarro et al., 2011; Abelenda et al., 2019). Together this suggests that delayed and more gradual tuberization can be overcompensated by even more delayed canopy senescence, underlining the importance of considering both sink and source dynamics to understand final tuber FW

weight. Interestingly, Struik & Wiersema (1999) already stated that "Fastest overall development is not necessarily associated with the highest yields", which was later shown to be the case even under stress conditions (Aliche et al., 2018). We here now show that this statement also holds true in controlled conditions when only tuber onset timing differs. Nevertheless, given that delayed tuberization correlated with less synchronized tuber development, the minor tuber FW weight increase observed here comes at the cost of enlarged tuber size differences. An agronomically interesting point is thus whether overall tuberization delay and increased total FW can be decoupled from tuberization desynchronization. Additionally, an important question is whether enhanced synchrony can mitigate sucrose competition induced differences in tuber size.

Finally, we sought to investigate whether the correlation in tuberization and canopy senescence timing primarily arises from either a shared inductive signal, a signal downstream of tuberization inducing senescence or rather that there is also a significant role for resource competition between tubers and leaves in canopy senescence timing. We observed clear positive correlations between leaf area and tuber growth rate in all transgenic lines, as well as tuber sucrose levels and tuber growth rate, supporting a prominent role for source size in tuber growth. In contrast, while we observed an inverse relation between leaf and tuber growth rates suggestive of resource competition, neither a decrease in leaf sucrose levels post tuberization nor a clear correlation between leaf sucrose levels and growth rate was found either pre- or post-tuberization. Thus, our sucrose data did not provide clear indications for resource competition between tubers and leaves. This could either imply that competition for sugar does not play a key role in the coordinated timing of tuberization and canopy senescence or rather indicate that the coarse-grained spatial resolution of the applied sucrose measurements, measuring overall sucrose levels irrespective of tissue in only a single leaf per plant, is insufficient to resolve this competition. As an alternative means to investigate potential causal relations between leaf and tuber growth dynamics we developed a simple leaf and tuber growth model, which we fitted to data for WT, SP3Di and SP6Ai lines. Good model fits for canopy dynamics could only be obtained when senescence was not only age dependent but also promoted through gradually increasing tuber size, rather than switching to a higher level beyond a certain tuberization level. Additionally, model fits improved by incorporating that leaf area, and thus source strength, delayed senescence. Combined this model suggests that resource competition rather than a shared signal underlies the correlated timing of tuberization and canopy senescence, and that a complex dependence of senescence on the strength of competing sinks and overall source

5

strength may explain how smaller differences in tuberization timing can become translated into larger differences in canopy senescence timing. Clearly, these model findings neither proof causality, nor that sucrose is the predominant factor next to age controlling leaf senescence. One major trigger for early senescence not considered in this study is the absence of sufficient nitrogen, which leads to degradation of chlorophyll to remobilize nitrogen (Gan & Amasino, 1997; Kim et al., 2009; Qiu et al., 2015). Modeling work done in other crop species, such as wheat, have shown that the carbon/nitrogen (CN)-balance proved to be pivotal in understanding the role of protein turnover and leaf senescence in understanding grain yield (Barillot et al., 2016a, 2016b). An interesting avenue for further investigation could be to use models to investigate to what extent tuberization onset impacts sucrose allocation to roots, thereby impacting their nitrate uptake efficiency and growth, thus indirectly enhancing shoot senescence.

Summarizing, our climate chamber experiments and modeling strongly suggest a role for resource competition in the correlated timing of tuber onset and canopy senescence as well as a leading role for *StSP6A* in tuber onset synchronization and tuber size uniformity. Counter-intuitively they also demonstrate that delayed tuberization may enhance overall tuber yield due to even further delayed canopy senescence, at the cost of a more variable tuber size. Future studies measuring gene expression, sucrose and nitrate dynamics in different leaves and tissues, and measuring not only leaf and tuber but also root growth dynamics are needed to pinpoint the exact role of resource competition in canopy senescence timing. Likewise, more detailed measurements are needed to reveal the molecular mechanisms through which *StSP6A* synchronizes tuberization. Finally, a major open issue is to what extent our results can be generalized from the climate chamber to the field, and how results change when flower and berry formation occurs. Incorporating berry formation through providing suitable environmental conditions and comparing climate and field experiments will be essential to answer these questions.

Acknowledgements

Authorship

BH performed growth experiments and sugar analysis and developed, implemented, analyzed the models and data. SB performed and designed the growth experiments, qPCR and sugar analysis. CB conceived the project. KT conceived the project and analyzed the data and models. All authors contributed to writing the manuscript and approved the submitted version.

Data availability

Generated data is included in the supplementary material.

Conflict of Interest

The authors declare there is no conflict of interest.

5

Supplementary figures
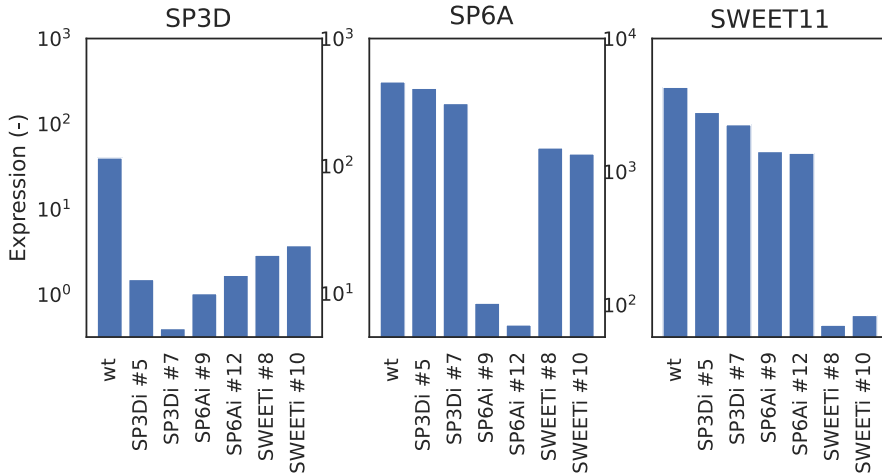
Supplemental figure 5.1. StSP3D, StSP6A and StSWEET11 expression in all transgenic lines at SD8, showing clear silencing at the respective lines.

A)
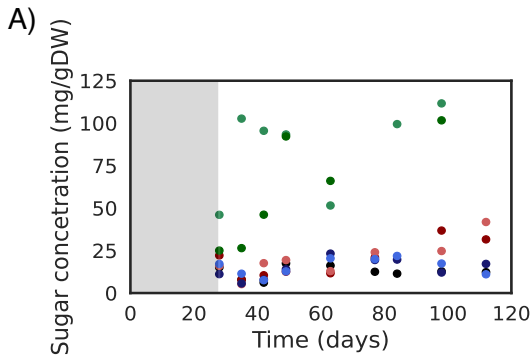
B)

Supplemental figure 5.2. Hampered sucrose export from SWEET11 RNAi plants A) Soluble sugar (Sucrose, Glucose, Fructose) levels in the leaves **B)** Aerial tuber formation in StSWEET11 RNAi #8

Supplementary figures
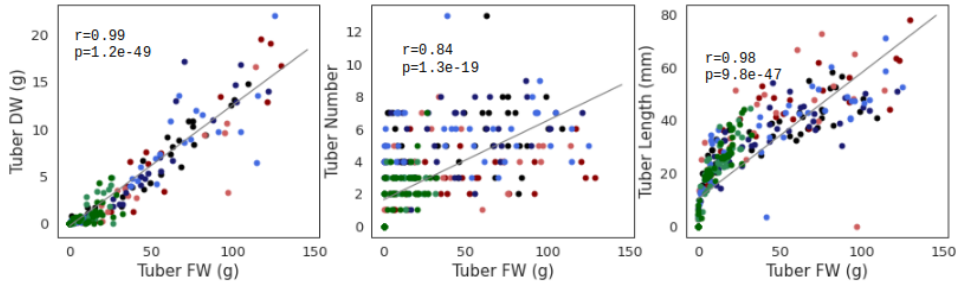
Supplemental figure 5.3. Tuber trait correlations. **A)** Tuber dry weight and fresh weight. **B)** Tuber number and fresh weight. **C)** Tuber Length and fresh weight

Table S5.1. Primers for quantitative expression analysis

Primer name	Target gene	Sequence (5' to 3')
RT_REF_349 for	StEIF3e	GGAGCACAGGAGAAGATGAAGGAG
RT_REF_349 rev	StEIF3e	ATTCTTGGATTGATAGCAGTT
StSP3D-F	StSP3D	GGACCCAGATGCTCCAAGTC
StSP3D-R	StSP3D	CTTGCCAAAACTTGAACCTG
StSP6A-F qPCR	StSP6A	GACGATCTTCGCAACTTTTACA
StSP6A-R qPCR	StSP6A	CCTCAAGTTAGGGTCGCTTG
qStUPA16 For	StSWEET11	GTGATGCATGTGCATGTTTG
qStUPA16 rev	StSWEET11	CAACGGCCAATCTCCTCTAA

5

Chapter 6
General Discussion

Summary

In this thesis, a diverse range of models was employed to explore various aspects of source-sink dynamics in potato. Additionally, where data was lacking we combined our modeling efforts with experiments and bioinformatic analyses. The developed models encompassed different levels of complexity, from a simple ordinary differential equation (ODE) model for plant growth (Chapter 5) to a more complicated model for sucrose unloading in stolons and tubers (Chapter 4), to a highly detailed biophysical transport model (Chapters 2 & 3). The purpose of these models was twofold: 1) to investigate the specific effects of SP6A on source-sink dynamics, and thus sucrose allocation, and 2) to enhance the fundamental understanding of sucrose transport dynamics and allocation among different sinks based on their architectural and physiological characteristics. The interplay between SP6A's role in both tuber initiation and mitigating sucrose efflux was examined across different locations within the plant. The models allowed for an exploration of transport efficiency and sucrose allocation in *the vasculature*, the unloading potential in the *tuber unloading zone*, and the competition and allocation processes at the *whole plant level*.

In **chapter 2** of the thesis, the focus was on substantiating the physiological relevance of SP6A-mediated SWEET11 blockage for long-distance sucrose transport and its ultimate delivery to tuber sinks. A biophysical transport model was developed that incorporated a single-source and a single-sink. The model successfully replicated experimentally measured sap sucrose concentrations and velocities, revealing that high viscosity resulting from high sucrose concentrations in the phloem is the major resistance factor in potatoes. This highlighted the importance of developing species-specific models. Furthermore, the non-linear nature of SP6A-mediated SWEET11 blockage was demonstrated, resulting in an increase in sucrose delivery to the sinks that surpassed the reduction in sucrose efflux caused by SP6A. This non-linear effect arises from the interplay of phloem sucrose concentration gradients, phloem sap viscosity, xylem water flow and pressure gradients, which then recursively feeds back into the sucrose concentration gradients and other variables.

Recognizing that plants have more intricate architectures than a simple single-source and single-sink, in **chapter 3** we extended the model to a single-source and two-sink architecture. With this, we investigated the effects of plant architecture and physiology (pathway length and xylem flow direction) and sink properties (sink strength and affinity) on resource allocation

between the two sinks. The objective was to obtain a more mechanistic understanding of how the interplay between sink characteristics and plant architecture influences resource partitioning. By incorporating biophysically detailed sucrose transport mechanisms, we showed that the effects of sink strength, sink affinity, and pathway resistance (length) were significantly enhanced compared to previous simplified sucrose transport models. The model was applied in a case study involving sink and source leaves, as well as tubers. The investigation highlighted that tubers face significant disadvantages compared to sink leaves due to architectural and physiological properties of the plant, namely the larger distance to source leaves and the xylem counterflow as compared to sink leaves. The cumulative disadvantage experienced by tubers enabled an undirected, plant level reduction of sucrose efflux through SP6A to preferentially benefit tuber resource partitioning. Consequently, the undirected incorporation of SP6A significantly enhanced tuber resource partitioning.

Where chapter 2 and 3 focused on studying the SP6A-SWEET interaction within the vasculature. We shifted attention to the tuber unloading zone in **chapter 4**, where the SP6A-SWEET interaction is expected to impact resource allocation. We employed a combined bioinformatics and modeling approach to improve our understanding of the factors responsible for the switch from apoplastic to symplastic unloading and the accompanying changes in tuber sink strength. We found that the switch was associated with a decline in callose deposition in tubers due to a decrease in callose synthesis as well as a coordinated change in sucrose metabolism towards starch production. Using a biophysical model of sucrose unloading we demonstrated how this coordinated switch to symplastic unloading with a concurrent metabolic switch enhances the sucrose gradient. Combined, this created the physiological conditions necessary to potentiate symplastic transport and enhance tuber sink strength.

In **chapter 5**, a comprehensive dataset of above- and belowground potato growth was generated, focusing on wildtype (WT) and plants with silencing of florigen (SP3D), tuberigen (SP6A), and sucrose export (SWEET11). Silencing of SP6A resulted in a delayed onset of tuber formation by approximately 2 weeks. However, it also led to a significantly delayed senescence of the canopy by 4 to 5 weeks. As a consequence, tuber growth was prolonged, resulting in mildly increased final tuber fresh weight. This delay in tuber onset also correlated with reduced synchronization in tuber formation and increased variance in tuber sizes. These results suggest that resource competition between tubers and leaves, may play a crucial role in determining growth dynamics, and final size of the tubers. Additionally, they indicate a role for SP6A in tuber synchronization

6

and size distribution. To investigate this further a simple ODE growth model was used, which indicated that resource competition, rather than a shared signal like SP6A, is likely the key factor in explaining the observation that delayed tuberization is associated with delayed senescence. Overall, these findings reveal the intricate relationship between tuberization, senescence, and resource allocation in potatoes.

Collectively, chapters 2 to 5 provide valuable insights into the roles of SP6A in sucrose allocation within potato plants and have yielded new insights into sucrose allocation processes. In the coming discussion, we will first evaluate the significance of the multiple roles of SP6A on potato physiology. We will then delve into a more detailed examination of the two primary locations where SP6A influences sucrose allocation, considering their interplay within the broader context of biophysical transport dynamics in the vasculature and unloading strategies in the tuber unloading zone that enhance sink strength in crop species. Additionally, we will discuss recent discoveries regarding redundancy within the SP6A PEBP gene family, including the binding of SP3D and other close relatives to the tuber activation complex (TAC) and SWEET11, and their impact on transport properties. Finally, we will provide an outlook based on the current findings and their implications for future research.

The effect of SP6A on plant physiology in a biophysical background

The multifaceted effect of SP6A on plant physiology
The first role discovered for SP6A in potato was tuber initiation in the stolon tip (Navarro et al., 2011). The arrival of SP6A to the stolon changes the developmental program of these cells, such that they start dividing radially and accumulate starch. This transition has a significant impact on the source-sink balance. Initially, in the vegetative phase, the major sinks are the roots and young leaves of the plant. During tuber initiation tubers become the main sinks for assimilate allocation (Fernie et al,, 2020). However, other factors such as StSP3D (Jing et al., 2023), StTFL1 (Jing et al., 2023) and StBEL5 (Kondhare et al., 2020) have also been shown to be involved in tuber initiation, and tuberization occurs in absence of SP6A, indicating a certain level of redundancy. Importantly, in this thesis we elucidated an important role for SP6A in synchronized tuberization onset, which positively affects tuber size homogeneity. From an evolutionary perspective, timely synchronized tuberization ensures successful vegetative reproduction prior to the end of the growth season. The first role of SP6A can thus be described as being a transcription (co-)factor binding the TAC (Navarro et al., 2011; Abelenda et al., 2014),

affecting the expression of tuber identity genes, and as a result regulating synchronization of strong tuber sinks (Figure 6.1).

The second role discovered for SP6A in potato was the mitigation of sucrose efflux from the phloem by binding to the sucrose transporter SWEET11 (Abelenda et al., 2019). Firstly, this affects sucrose transport dynamics in the vasculature. It leads to a reduction of sucrose efflux from the phloem, reducing resource allocation to stem growth, and as a result the transport efficiency of the phloem to terminal sinks increases (chapter 2). By regulating long-distance phloem transport, SP6A indirectly influences sucrose delivery to sinks, including tubers, independent of its role in tuber development. In this thesis we demonstrated that despite undirected phloem loading of SP6A, it is particularly tuber sinks that profit from the enhanced transport efficiency (chapter 3). This is an example of embodiment in plants. The concept of embodiment describes that plants exhibit complex adaptive behaviors and decisions that are intricately linked to their physical structure, biochemical processes, and interactions with the surrounding environment van (van Schijndel et al., 2022). Secondly, SP6A plays a role in the tuber unloading zone. The blockage of SWEET transporters contributes to the switch from apoplastic to symplastic unloading during tuber development (chapter 4).

For its second role, SP6A acts by directly affecting SWEET11's function. It is unknown whether it is just the peptide, a homo- or heterodimer of the peptide or a more complicated protein complex that binds to SP6A (Abelenda et al., 2019). Nonetheless, in this role it is not a gene regulatory mechanism, but a form of post-translational regulation of SWEETs in which SP6A functions. SWEETs have been previously shown to have enhanced sucrose transport activity after phosphorylation due to drought stress (Chen et al., 2022), indicating that they are prone to different forms of posttranslational regulation. SP6A thus not only has multiple roles at different locations, but it employs different mechanisms to fulfil these roles.

6

SP6A plays a central role in controlling potato growth, development and yield through its effects on tuber initation and synchronisation, efficiency of sucrose delivery towards the tubers and contribution to the switch to symplastic unloading. Given the central hub-like role played by SP6A, possible other downstream effects remain to be discovered. A potential third role for SP6A would be promotion of symplastic unloading in parallel to its inhibition of the apoplastic route (Fig 6.1, grey arrows). This would most likely encompass a role as (co-)transcription factor, similar to tuber initiation to regulate plasmodesmatal aperture via callose metabolism

and potentially a direct impact on the sucrose metabolic switch. A preliminary screening of of whole plant Chip-Seq data did not provide evidence of significant binding sites for the SP6A homolog OsHd3a to callose metabolism genes (Personal communication Salome Prat lab), yet this may be a result of lack of tissue level resolution rather than absence of regulation. Another interesting mechanism of SP6A is the auto-activation of stolon and tuber SP6A expression by leaf-derived SP6A (Navarro et al., 2011). This mechanism is similar to that observed in HY5, which functions similar as SP6A/FT in being light dependent and phloem-mobile (Chen et al., 2016). HY5 promotes both root growth and nitrate uptake, balancing shoot-root growth. Why and how this works is still poorly understood, and this shared mechanism suggests that SP6A might also be important in shoot-root communication. Furthermore, the integration of SP6A with other tuberization factors, such as StBEL5 (Kondhare et al., 2020) is still poorly understood, and additional mechanisms and targets are expected to be uncovered. We believe that further investigation of SP6A and its PEBP gene family is likely to reveal additional functionality.

Growth, development and feedbacks

In chapters 2 and 3, we have demonstrated the impact of transport dynamics on sucrose allocation. The reciprocal interdependence and non-linearity in the long-distance transport pathway, i.e., sucrose concentration differences between sources and sinks drives a pressure gradient, which in turn drives water flow, which affects unloading at terminal and lateral sinks, which in turn again affects sucrose concentration makes that sucrose allocation cannot be accurately predicted by just taking into account the sink and source strengths. Integrating biophysical transport into a source-sink framework adds complexity but enhances our understanding of the intricate dynamics involved. This is evident when comparing our work to earlier modeling studies. For instance, previous research by Minchin et al. (1993) found the importance of implementing a biophysically resolved long-distance pathway. They showed that the weaker sink receives more sugar relative to its strength than the stronger sink, while in absolute numbers, the stronger sink is still dominant. However, a later study by Bancal and Soltani (2002) suggested that within a physiologically relevant range of source concentrations, sink characteristics alone govern resource partitioning, thereby questioning the significance of the transport dynamics. Our findings support the importance of considering detailed biophysical aspects, such as sucrose-dependent viscosity and a spatially explicit transport pathway, to accurately understand the influence of plant architecture on sucrose allocation.
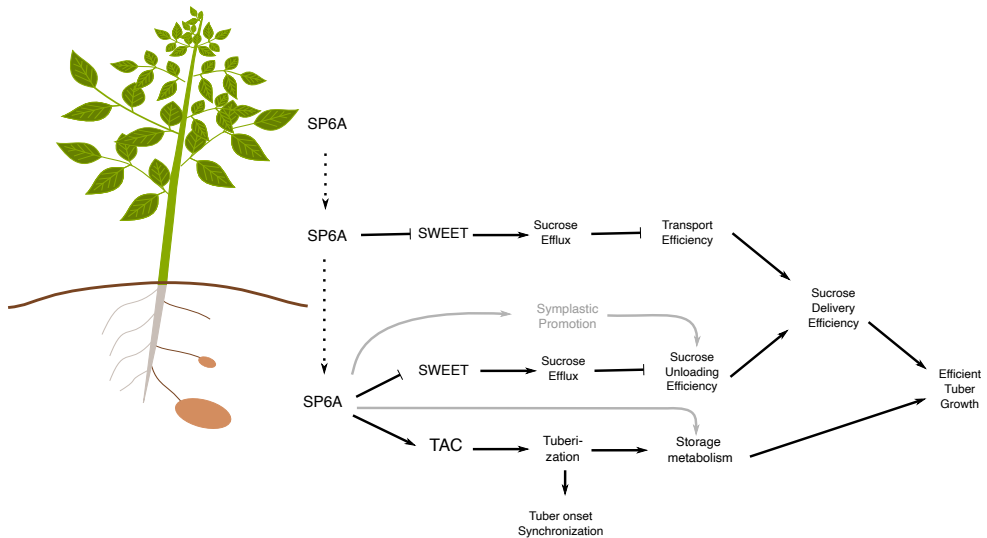
Figure 6.1. SP6As dual role and the effect on tuber growth. The multiple roles of SP6A on efficient tuber growth in different locations of the plant. Light grey lines represent hypothetical roles of SP6A.

We have primarily focused on static sources and sinks, neglecting the complexities associated with plant growth and development and the resulting dynamic transitions in sink numbers and strength and the impact this has on resource competition and plant development. Additionally, we have investigated the multiple roles of SP6A in tuber development largely in isolation, while SP6A's combined influence on tuber initiation and synchronization as well as on long distance transport efficiency and unloading mode potentially give rise to further biophysical feedbacks, particularly given the known role of sugar as an additional tuberization control signal (Hendriks et al., 1991; Chinchinska et al., 2008).

Sources and sinks also assert control over phloem sucrose concentrations via sucrose transport regulations in both loading and unloading zones and metabolic potential in sinks. For example, if sucrose concentrations in the phloem are high due to an imbalance in source and sink, either because of decreased sink-uptake or increased source-activity, SUT-transporters are downregulated on a transcriptional level (Chiou and Bush, 1998). This way, sucrose loading towards the phloem is decreased, and as such the source-sink imbalance in the phloem is reduced. From the biophysical transport viewpoint, this resolved the problem of high viscosity in the transport pathway, as too high sucrose concentrations lead to exponential increases in

sap viscosity, making sucrose transport less optimal. This is especially relevant in crop species, such as potato, which already have high (>1.5M) sucrose concentrations, far higher than the 'optimal' concentration of approximately 1M as estimated by Jensen et al. (2013). Furthermore, accumulation of starch in source leaves due to prolonged high sucrose conditions leads to end-product accumualtion, effectively decreasing photsynthesis rates (Goldschmidt and Huber, 1992). Often, these conditions are caused by high sucrose concentrations in the vasculature. Besides sucrose, phytohormones, such as gibberellins, important for development and cell growth/elongation, also affect sugar allocation via StSUT4 (Chinchinska et al., 2008) and in such a way assert control over the transport pathway.

Finally, in addition to controlling sucrose levels in sources, sinks and phloem, plants control their Carbon/Nitrogen (C/N) and water balance, adjusting physiology, investments in xylem versus phloem and above ground versus below ground tissues (Coruzzi & Bush, 2001). Indeed, the competition for resources between tubers and sinks could partly be indirect, with enhanced carbon allocation to tubers limiting root growth and thereby N uptake, thereby promoting leaf senescence (Wingler et al., 2008 , Chapter 5).

Do we need the biophysical detail?

Despite advocating for plant growth models incorporating biophysically detailed transport and source sink dynamics, many crop and plant growth models ignore the biophysical details of transport and only consider source and sink strength. Given the success many of these models have in fitting experimental observations and generating valuable predictions, an open question is when the biophysical detail is in fact needed. Trivially, in case substantial deviations with experimental observations occur or more detailed predictions are need, more biophysically detailed and biologically realistic models are essential. This was nicely shown in a study on grapes which suggests that carbohydrate allocation to grapes is affected not only by sink-strength and number, but also by its distribution over the plant, which is not adequately described by only considering source and sink strength (Pallas et al., 2010; Zhu et al., 2021). Biophysical detail is further important in the understanding of physiological stress, particularly stresses having major effects on plant hydraulics and photosynthesis. We investigated this using a simple case study, similar to the work we did in chapter 3, on the effects of drought stress on sucrose allocation within plants (Fig. 6.2). We incorporated drought by decreasing both evaporation in the leaves (closed stomata to decrease water loss, estimated to lead to half the normal evaporation rate) and by decreasing soil water potential (from water saturated

soil potential of 0MPa to a relatively dry soil of -1MPa). This showed that drought stress affects sucrose allocation via the xylem-phloem connection (compare green/orange line with purple/yellow line). The disadvantage the tuber/root sink has compared to the leaves because of the plant architecture (see chapter 3) is decreased by transpiration decrease, but not by differences in soil water potential. Interestingly, under dry conditions it is important for plants to invest in water uptake via root growth. The results from the biophysical model again show that the architecture of plants makes that this, at least partially, happens automatically through the biophysical background of sucrose allocation being favored in this direction under drought.

The impact of SP6A on tuber onset resembles the process of flower initiation in Arabidopsis through AtFT. A mathematical model integrating biophysical transport, leaf, and flower initiation showed that source-sink dynamics, along with florigen dynamics, were essential in explaining flowering phenotypes (Satake et al., 2016). Notably, the transport of sucrose from a flower that acts as a sucrose source was pivotal to prevent the flower reversion phenotype, where flowering is aborted after floral commitment. This underscores the control exerted by sinks and/or sources on the spatio-temporal biophysics of the transport pathway. We expect that on a similar note, integrated modeling of the multiple functions of SP6A in a growing and developing potato plant incorporating source-sink feedbacks is likely to provide additional insights into resource allocation and organ yield. In contrast, if full mechanistic understanding is less essential and computational efficiency is of importance, as is the case for most field level studies (de Wit et al., 2020), the level of biophysical detail applied in this thesis may be less essential and desirable.

Unloading zone – Efficient delivery and its relation to unloading mode

The second location at which SP6A affects sucrose delivery to tubers is the tuber unloading zone. The switch from apoplastic to symplastic unloading in tuber increases the unloading potential via a combined switching of sugar metabolism, but during initial stolon and tuber development apoplastic transport is observed to be more efficient (Chapter 4). Symplastic transport is thus not always more optimal, and physiological conditions matter. Shifts between apoplastic and symplastic unloading pathways are common in fruits and other storage organs of crops (Ma et al., 2018). As an example, in tomato fruit, a symplastic pathway is used in the developing fruit stage, concurrent with starch accumulation, followed by apoplastic unloading during the fast development and ripening stage in which sucrose is remobilized from starch (Ruan and Patrick 1995). Some plant organs even switch multiple times during development.

6
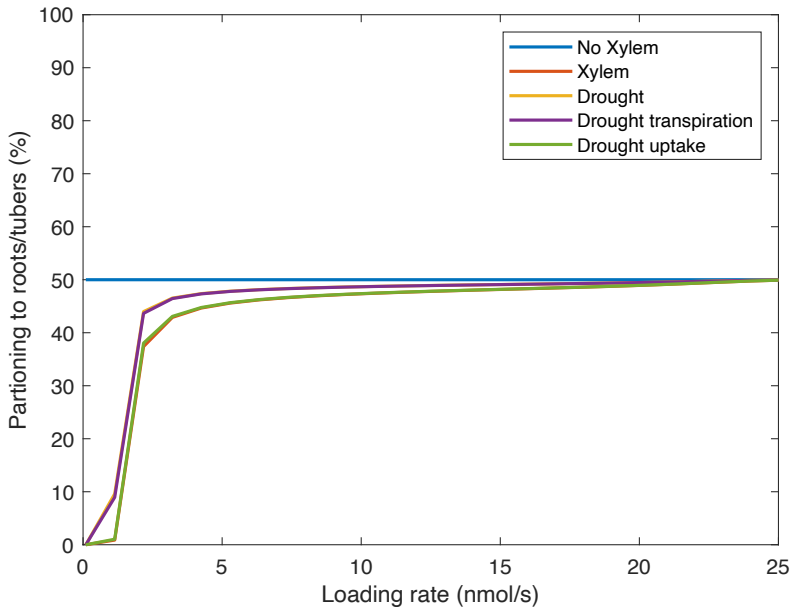
Figure 6.2. The effect of drought on sucrose allocation. Partitioning to the tuber/root sink that takes up water, compared to the growing leaf sink, that evaporates water, similar to Fig 3.6.

Grape and jujube for example, switch from apoplastic to symplastic unloading during early development, but then switches back to apoplastic again at the ripening stage (Zhang et al., 2007; Nie et al., 2010). In sucrose-storing fruits the final switch to apoplastic unloading is required to prevent a symplastic backflow of the soluble sugars down the created concentration gradient (Ma et al., 2018), opposite from what occurs during tuberization (Viola et al., 2001). In contrast, in cotton, phloem unloading switches from symplastic to apoplastic and then to symplastic, coinciding with blockage of plasmodesmata (Ruan et al. 2001). This is believed to be independent of sucrose unloading potential, but instead is coupled to turgor increase by closing plasmodesmata in the intermediate step to drive rapid cotton fiber elongation (Fayant et al., 2010). Overall, these examples show dependency of the most suitable unloading mode on the physiological conditions in the organ. To further generalize the observations above we conducted an analysis of apoplastic and symplastic unloading, specifically examining the relationship between unloading mode, developmental age, and sucrose and starch concentrations. To achieve this we collected data from literature, including 37 samples from 15 different species at various developmental stages, with 7 samples representing symplastic unloading (Fig. 6.3). We observed a consistent pattern where sink organ sugar concentrations

were lower in symplastic unloading compared to apoplastic unloading, while starch levels were higher. This observation aligns with the requirement for a sugar gradient to drive diffusion or bulk flow in symplastic unloading. Apoplastic unloading generally exhibited high sink organ sugar concentrations, with exceptions of low concentrations primarily observed during early development and high concentrations (>500 mM) exclusively found in late development.

Different crops employed different strategies to lower sink organ sucrose and facilitate symplastic unloading. These strategies included sucrose compartmentalization in the vacuole during middle grape development, long-term starch storage in potatoes, and temporary starch storage in the symplastic unloading phase of crops such as tomato, grape, and jujube, which is later converted to sucrose in the ripening phase. An interesting example is sugar cane, which utilizes symplastic unloading and yet maintains high sucrose concentrations in the stem. A sucrose gradient driving symplastic transport is achieved through the isolation of the phloem apoplast and the storage apoplast using specialized fibers. Sucrose is unloaded into the sugarcane storage parenchyma, which, in turn, exports sucrose into the isolated apoplast of the storage parenchyma (Walsh et al., 2004). This data indicates that different species employ either architectural (vacuole, fibers) or metabolic (osmotically inactive starch) means to maintain a symplastic driving gradient.

Redundancy in the PEBP family

In this thesis we have primarily focused on a single PEBP protein, SP6A, out of a total of 15 PEBP proteins identified in potato. SP6A, along with SP3D and SP5G-A/B, belongs to the FT subfamily, closely related to the TFL subfamily, including CEN1, SP/TFL1, and SP9D (Abelenda et al., 2014; Zhang et al., 2022). Based on functional inference from tomato and arabidopsis proteins, it is suggested that the FT-subfamily primarily includes proteins involved in promoting floral development, while members of the TFL-like group are known to inhibit flowering. In addition to their role in flowering, FT-like genes have been reported to participate in other biological processes as a result of substantial functional divergence. The AtFT/StSP3D-homolog StSP6A, that is the focus of this thesis, acquired an entirely new function with tuber initiation in potato (Abelenda et al., 2014; Zhang et al., 2022). Gene motif analysis revealed that most PEBP genes in potatoes, tomatoes, and Arabidopsis share five conserved motifs, among which SP6A. Despite the structural similarities between SP6A and SP3D, they fulfill opposing roles in potatoes (Navarro et al., 2011).

6
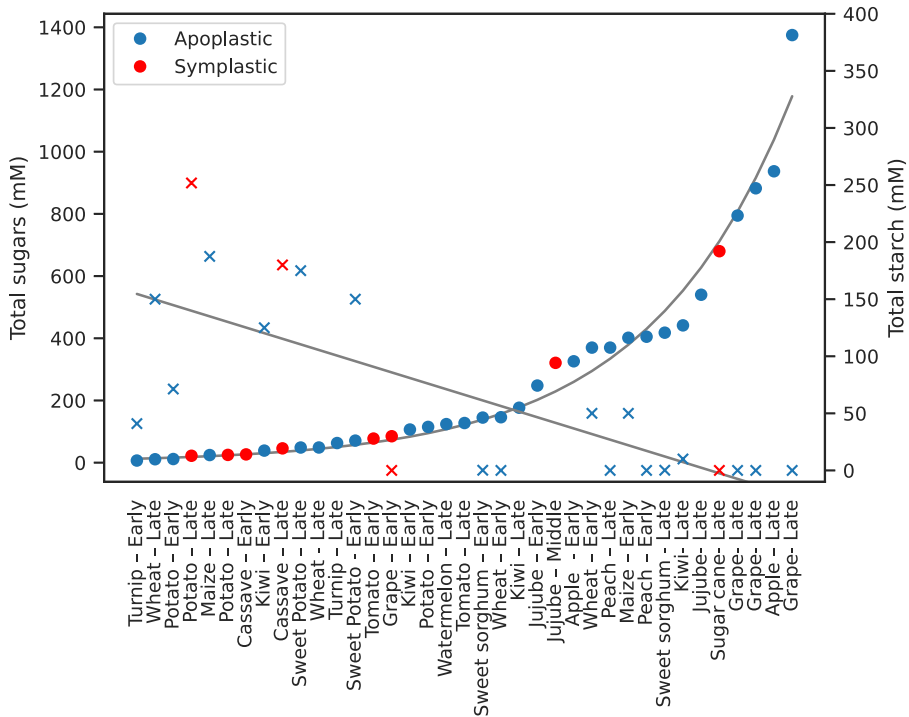
Figure 6.3. Sugar and starch concentrations plotted for different species. Circles represent sugar concentration, and crosses represent starch levels.

Functional redundancy at the transcriptional level

Recent studies have provided further insights into the PEBP gene family, revealing a significant degree of functional redundancy at the transcriptional level, as can be expected from their phylogenetic and structural similarities (Abelenda et al., 2014; Zhang et al., 2022). Jing et al. (2023) demonstrated that the previously described antagonistic roles of these genes are not as strictly divided. They found that overexpression of StSP3D or StFTL1 (StSP5G-like) promotes tuber formation under non inductive long days by binding to the TAC, similar to StSP6A. In this process, StSP3D and StFTL1 reach the stolon tip through phloem transport and locally activate StSP6A expression in the stolon tip. StSP6A can thus be replaced by StSP3D or StFTL1. While a similar process of StSP6A binding to the flower activation complex (FAC) has not been demonstrated, the known repression of flower bud development by StSP6A suggest this is likely to be the case (Plantenga, Bergonzi, Abelenda et al., 2019). Still, in case of tuber formation, the florigen is able to induce tuber formation, thus taking on a similar role as the tuberigen, while in case of flowering the tuberigen appears to antagonize the florigen. In addition to the

closely related StSP3D and StSP5G-like genes, StTFL1 and StCEN also exhibit redundant or antagonistic interactions with the TAC. StTFL1 leads to tuberization under long-day conditions (Guo et al., 2010), while StCEN1 binds to the TAC, inhibiting tuberization. An open question is which differences between the various PEBPs result in redundancy or rather antagonism.

Functional redundancy at the post-translational level

Besides the StSWEET/StSP6A interaction, preliminary research indicates that other PEBP proteins, specifically StSP3D, StTFL1, and StBFT, also interact with StSWEET in yeast-2-hybrid assays (Fig. 6.4a, Master Thesis Lucy McMurtry, 2018). However, while StTFL1 and StBFT bind to StSWEET11 in yeast, they do not inhibit StSWEET11 mediated sucrose transport in protoplast experiments, unlike StSP6A and StSP3D. SP6A was shown to lead to an approximately 40% reduction in sucrose efflux in protoplast experiments, whereas SP3D has an approximately 30% reduction. In contrast, *in planta*, apoplastic sugar concentrations of both StSP3D and StTFL1 RNAi lines show increases in the CE3027 background, suggesting roles for leakage-mitigation for both SP3D and TFL1 (Fig 6.4b). Surprisingly, in the S. andigena background, also used in chapter 5 of this thesis, there was no clear increase in apoplastic sucrose concentration in SP3D and TFL1 knockdown plants. Thus, while there is clear evidence that there is also post-translation interaction of PEBP-proteins besides SP6A with SWEET11, *in planta* their effect on plant physiology is difficult to pin down.

Potential implications of the functional redundancy

The redundancy of PEBP proteins in both the transcriptional regulation of developmental processes and their interaction with SWEET11 transporters has large potential implications for sucrose allocation, and suggests potential competitive binding of targets by SP6A, SP3D, and TFL1. Recently SP3D was shown to bind to the TAC and activate SP6A expression in stolons in absence of shoot-orginated SP6A (either during non-inductive long days, or in SP6A null-mutant *Solanum etuberosum*). This shows that even when there is competitive binding between SP6A and SP3D at the TAC, the result of both PEBPs is functionally similar. Similarly, the post-translational interaction of SP6A and SP3D with SWEET could compete for binding space, but in the end this will only increase blockage effects, as both block sucrose efflux, assuming that both have the same binding affinity and blockage efficiency. More interesting is that the florigen would also benefit tuber sinks that mainly profit from the enhanced transport efficiency due to the mitigation of sucrose-efflux. In the case that SP3D acts physiologically similar to SP6A, tubers will still benefit more due to their larger architectural disadvantage. This could mean

6
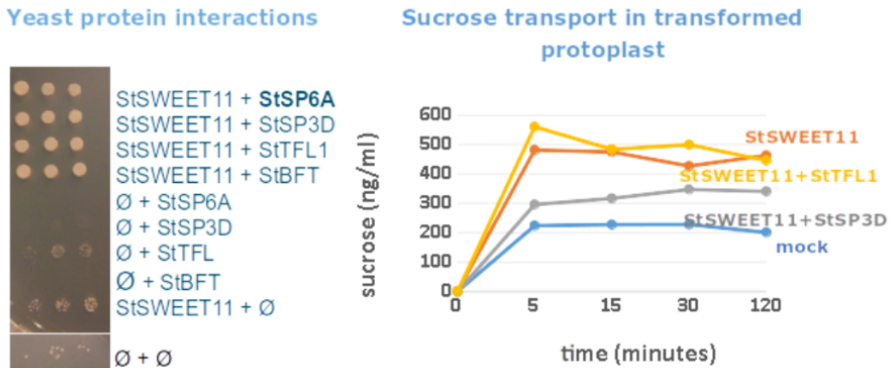
Figure 6.4 Post-translational interaction of PEBPs with SWEET11 (Master Thesis Lucy McMurtry, Preliminary Data). **A)** Yeast2Hybrid results, showing interaction of several PEBP proteins with SWEET11. **B)** Sucrose transport into transformed protoplasts, showing the inhibitory function of SP3D on SWEET transporters.

that a side effect of SP3D, besides activating the FAC, is the ensurance of sucrose allocation towards belowground biomass. However, in this case the temporal dynamics are important as well. Flowering generally occurs before tuberization due to its independence of day-length (Navarro et al., 2011). As such, SP3D expression is expected to be high in the absence of SP6A and tubers. In this growth stage, tubers are no strong sinks yet, and efflux-mitigation due to SP3D might benefit sucrose allocation to flowers instead.

TFL1, also binding SWEET 11, but not inhibiting transport, is a more interesting example of where binding competition might have an effect. If TFL1 is highly expressed, it saturates SWEET11 transporters without prevention sucrose efflux from the phloem. If at the same time SP6A is expressed, SWEET is already bound by non-functional TFL1, prohibiting efflux-mitigation of SWEET by SP6A. Of course, this all depends on relative TFL1 and SP6A levels and binding dynamics, dictated by binding affinity and kinetics. To fully understand the implications, we need to employ models of binding competition of the different PEBPs. In our current models, we have assumed that SP6A presence always decreases sucrose mitigation with 40%. In planta there might be more dynamic behavior directed by protein dosage, binding affinity and kinetics and transport dynamics as discussed above. Integrating these more detailed PEBP-SWEET interactions in our transport models could shed new light on resource competition between sexual and asexual reproduction.

Translation and Final Remarks

We end the discussion with an outlook and final remarks on possibilities to translate our theoretical advancements in understanding transport and source-sink dynamics into more practical applications. In this thesis, most research is performed on potato, but other tuberizing crops, such as the true tuberizing yam (*Discorea alata*) as well as root tuberizing cassava (*Manihot esculenta*) are also agronomically important staple foods. Both these species are also dependent on photoperiod, requiring short days for tuberization (Lowe et al., 1976 ; Susila and Purwestri, 2023). Interestingly, two PEBP proteins (DaFT1 and DaFT2), homologous to SP6A, were found to be associated with tuberization in yam (Hamaoka et al., 2022), indicating a similar mechanism in tuber onset in species other than potato. This suggests that research in other tuber bearing crops could potentially benefit from the insights obtained here for potato.

We have shown here that tuberization synchronization and size variability are dependent on SP6A expression. Combined with the insights from our biophysical model that showed the importance of sink-strength on resource allocation, and the observation that larger/older tubers are stronger sinks, these findings imply that a more synchronized tuber onset reduces tuber size distribution variability. Importantly, research in this thesis has focused on photoperiodic sensitive potato varieties widely used in research. Commercial, agronomic potato varieties lost their photoperiodic dependency on short days to start tuberization (Kloosterman et al., 2013). However, rather than loosing the tuberigen itself, it is expressed in much earlier stages of development. An interesting avenue for future research is to investigate whether in commercial varieties naturally present variation in SP6A expression can be used as a means to reduce tuber size variability. With our research reconfirming the important role of plant architecture and uncovering the relevance of xylem flow direction on sucrose allocation, it underlines the impact of differences in stolon length and vasculature on potato size distribution variability, providing further pointers for breeding.

A logical future translation of our biophysical modeling approach would be the implementation into whole-plant and/or field-scale models. Architecturally resolved whole-plant models, such as functional structural plant models (FSPMs), simulate the feedback between the environment and plant physiology, growth and development (Evers et al., 2018). Currently, these models typically implicitly assume that properties of the transport pathway do not significantly impact sink resource allocation, simply allocating overall available carbon according to relative sink strengths (Lescourret et al., 2011; Da Silva et al., 2014; de Vries et al., 2021). While computationally

6

demanding particularly in combination with growth, these models show promise for the integration of transport dynamics into growing and developing plant models (Seleznyova and Hanan, 2018). As argued above, we expect argued that the integrated modeling of the multiple functions of SP6A is likely to provide additional insights into tuber yield. Additionally, whole plant biophysically detailed models are likely to become particularly relevant for understanding and predicting plant growth and yield under environmental stress conditions such as heat and water stress, which through evaporation and soil water tension affect plant hydraulics and transport dynamics. In addition to using FSP models to simulate multiple plants at the field scale, biophysically realistic transport dynamics could also be incorporated into field-scale models, such as WOFOST (de Wit et al., 2019) to increase their predictive power under environmental stress conditions.

In conclusion, we have investigated the interplay between SP6A's role in both tuber initiation and mitigating sucrose efflux in the context of biophysical transport and unloading in four chapters. Through these modeling approaches, the interactions between SP6A, sucrose transport dynamics, and sink characteristics were investigated and their physiological relevance on sucrose delivery to sinks was shown. We further improved our understanding of the complex feedbacks within and between the vasculature and tuber unloading zone. With this, we have shown that models of sucrose transport and unloading are very useful to understand species-specific processes and to predict organ and whole-plant allocation and growth dynamics.

References

Abelenda, J. A., Bergonzi, S., Oortwijn, M., Sonnewald, S., Du, M., Visser, R. G. F., Sonnewald, U., & Bachem, C. W. B. (2019). Source-Sink Regulation Is Mediated by Interaction of an FT Homolog with a SWEET Protein in Potato. *Current Biology, 29*(7), 1178–1186. https://doi.org/10.1016/j.cub.2019.02.018

Abelenda, J. A., Navarro, C., & Prat, S. (2014). Flowering and tuberization: A tale of two nightshades. *Trends in Plant Science, 19*(2), 115–122. https://doi.org/10.1016/j.tplants.2013.09.010

Abercrombie, J. M., O'Meara, B. C., Moffatt, A. R., & Williams, J. H. (2011). Developmental evolution of flowering plant pollen tube cell walls: Callose synthase (CalS) gene expression patterns. *EvoDevo*, *2*, 14. https://doi.org/10.1186/2041-9139-2-14

Albinsson, B., Li, S., Lundquist, K., & Stomberg, R. (1999). The origin of lignin fluorescence. *Journal of Molecular Structure*, *508*(1), 19–27. https://doi.org/10.1016/S0022-2860(98)00913-2

Aliche, E. B., Oortwijn, M., Theeuwen, T. P. J. M., Bachem, C. W. B., van Eck, H. J., Visser, R. G. F., & van der Linden, C. G. (2019). Genetic mapping of tuber size distribution and marketable tuber yield under drought stress in potatoes. *Euphytica, 215*(11), 186. https://doi.org/10.1007/s10681-019-2508-0

Aliche, E. B., Oortwijn, M., Theeuwen, T. P. J. M., Bachem, C. W. B., Visser, R. G. F., & van der Linden, C. G. (2018). Drought response in field grown potatoes and the interactions between canopy growth and yield. *Agricultural Water Management, 206*, 20–30. https://doi.org/10.1016/j.agwat.2018.04.013

Aliche, E. B., Prusova-Bourke, A., Ruiz-Sanchez, M., Oortwijn, M., Gerkema, E., Van As, H., Visser, R. G. F., & van der Linden, C. G. (2020). Morphological and physiological responses of the potato stem transport tissues to dehydration stress. *Planta, 251*(2), 45. https://doi.org/10.1007/s00425-019-03336-7

Almagro Armenteros, J. J., Salvatore, M., Emanuelsson, O., Winther, O., von Heijne, G., Elofsson, A., & Nielsen, H. (2019). Detecting sequence signals in targeting peptides using deep learning. *Life Science Alliance, 2*(5), e201900429. https://doi.org/10.26508/lsa.201900429

Altschul, S. F., Madden, T. L., Schäffer, A. A., Zhang, J., Zhang, Z., Miller, W., & Lipman, D. J. (1997). Gapped BLAST and PSI-BLAST: A new generation of protein database search programs. *Nucleic Acids Research, 25*(17), 3389–3402. https://doi.org/10.1093/nar/25.17.3389

Amsbury, S., Kirk, P., & Benitez-Alfonso, Y. (2018). Emerging models on the regulation of intercellular transport by plasmodesmata-associated callose. *Journal of Experimental Botany, 69*(1), 105–115. https://doi.org/10.1093/jxb/erx337

Aubry, E., Dinant, S., Vilaine, F., Bellini, C., & Le Hir, R. (2019). Lateral Transport of Organic and Inorganic Solutes. *Plants (Basel, Switzerland), 8*(1). https://doi.org/10.3390/plants8010020

Bancal, P., & Soltani, F. (2002). Source–sink partitioning. Do we need Münch? *Journal of Experimental Botany, 53*(376), 1919–1928. https://doi.org/10.1093/jxb/erf037

Barillot, R., Chambon, C., & Andrieu, B. (2016a). CN-Wheat, a functional-structural model of carbon and nitrogen metabolism in wheat culms after anthesis. I. Model description. *Annals of Botany, 118*(5), 997–1013. https://doi.org/10.1093/aob/mcw143

Barillot, R., Chambon, C., & Andrieu, B. (2016b). CN-Wheat, a functional-structural model of carbon and nitrogen metabolism in wheat culms after anthesis. II. Model evaluation. *Annals of Botany*, 118(5), 1015–1031. https://doi.org/10.1093/aob/mcw144

Barnes, W. J., & Anderson, C. T. (2018). Release, Recycle, Rebuild: Cell-Wall Remodeling, Autodegradation, and Sugar Salvage for New Wall Biosynthesis during Plant Development. *Molecular Plant, 11*(1), 31–46. https://doi.org/10.1016/j.molp.2017.08.011

Bäurle, I., & Dean, C. (2006). The Timing of Developmental Transitions in Plants. *Cell, 125*(4), 655–664. https://doi.org/10.1016/j.cell.2006.05.005

Bethke, P. C., Sabba, R., & Bussan, A. J. (2009). Tuber Water and Pressure Potentials Decrease and Sucrose Contents Increase in Response to Moderate Drought and Heat Stress. *American Journal of Potato Research, 86*(6), 519. https://doi.org/10.1007/s12230-009-9109-8

Bezrutczyk, M., Hartwig, T., Horschman, M., Char, S. N., Yang, J., Yang, B., Frommer, W. B., & Sosso, D. (2018). Impaired phloem loading in zmsweet13a,b,c sucrose transporter triple knock-out mutants in Zea mays. *New Phytologist, 218*(2), 594–603. https://doi.org/10.1111/nph.15021

Bland, W. L., & Tanner, C. B. (1986). Potato tuber water potential components during storage. *American Potato Journal, 63*(11), 649–653. https://doi.org/10.1007/BF02852927

Bologa, K. L., Fernie, A. R., Leisse, A., Loureiro, M. E., & Geigenberger, P. (2003). A bypass of sucrose synthase leads to low internal oxygen and impaired metabolic performance in growing potato tubers. *Plant Physiology, 132*(4), 2058–2072. https://doi.org/10.1104/pp.103.022236

Braun, D. M., Wang, L., & Ruan, Y.-L. (2014). Understanding and manipulating sucrose phloem loading, unloading, metabolism, and signalling to enhance crop yield and food security. *Journal of Experimental Botany, 65*(7), 1713–1735. https://doi.org/10.1093/jxb/ert416

Breia, R., Conde, A., Pimentel, D., Conde, C., Fortes, A. M., Granell, A., & Gerós, H. (2020). VvSWEET7 Is a Mono- and Disaccharide Transporter Up-Regulated in Response to Botrytis cinerea Infection in Grape Berries. Frontiers in *Plant Science, 10*. https://doi.org/10.3389/fpls.2019.01753

Bryan, A. K., Goranov, A., Amon, A., & Manalis, S. R. (2010). Measurement of mass, density, and volume during the cell cycle of yeast. *Proceedings of the National Academy of Sciences, 107*(3), 999–1004. https://doi.org/10.1073/pnas.0901851107

Cabrita, P., Thorpe, M., & Huber, G. (2013). Hydrodynamics of steady state phloem transport with radial leakage of solute. *Frontiers in Plant Science, 4*. https://doi.org/10.3389/fpls.2013.00531

R

Capella-Gutiérrez, S., Silla-Martínez, J. M., & Gabaldón, T. (2009). trimAl: A tool for automated alignment trimming in large-scale phylogenetic analyses. *Bioinformatics, 25*(15), 1972–1973. https://doi.org/10.1093/bioinformatics/btp348

Chang, T.-G., & Zhu, X.-G. (2017). Source–sink interaction: A century old concept under the light of modern molecular systems biology. *Journal of Experimental Botany, 68*(16), 4417–4431. https://doi.org/10.1093/jxb/erx002

Chen, W., Diao, W., Liu, H., Guo, Q., Song, Q., Guo, G., Wan, H., & Chen, Y. (2022). Molecular characterization of SUT Gene Family in Solanaceae with emphasis on expression analysis of pepper genes during development and stresses. *Bioengineered, 13*(6), 14780–14798. https://doi.org/10.1080/21655979.2022.2107701

Chen, X., Yao, Q., Gao, X., Jiang, C., Harberd, N. P., & Fu, X. (2016). Shoot-to-Root Mobile Transcription Factor HY5 Coordinates Plant Carbon and Nitrogen Acquisition. *Current Biology, 26*(5), 640–646. https://doi.org/10.1016/j.cub.2015.12.066

Chen, L. Q. (2014). SWEET sugar transporters for phloem transport and pathogen nutrition. *New Phytologist, 201*(4), 1150–1155. https://doi.org/10.1111/nph.12445

Chen, L.-Q., Qu, X.-Q., Hou, B.-H., Sosso, D., Osorio, S., Fernie, A. R., & Frommer, W. B. (2012). Sucrose Efflux Mediated by SWEET Proteins as a Key Step for Phloem Transport. *Science, 335*(6065), 207–211. https://doi.org/10.1126/science.1213351

Chen, W., Diao, W., Liu, H., Guo, Q., Song, Q., Guo, G., Wan, H., & Chen, Y. (2022). Molecular characterization of SUT Gene Family in Solanaceae with emphasis on expression analysis of pepper genes during development and stresses. *Bioengineered, 13*(6), 14780–14798. https://doi.org/10.1080/21655979.2022.2107701

Chincinska, I. A., Liesche, J., Krügel, U., Michalska, J., Geigenberger, P., Grimm, B., & Kühn, C. (2008). Sucrose Transporter StSUT4 from Potato Affects Flowering, Tuberization, and Shade Avoidance Response. *Plant Physiology, 146*(2), 323–324. https://doi.org/10.1104/pp.107.112334

Chiou, T.-J., & Bush, D. R. (1998). Sucrose is a signal molecule in assimilate partitioning. *Proceedings of the National Academy of Sciences, 95*(8), 4784–4788. https://doi.org/10.1073/pnas.95.8.4784

Cieslak, M., Cheddadi, I., Boudon, F., Baldazzi, V., Génard, M., Godin, C., & Bertin, N. (2016). Integrating Physiology and Architecture in Models of Fruit Expansion. *Frontiers in Plant Science, 7*. https://doi.org/10.3389/fpls.2016.01739

Clerx, L. E., Rockwell, F. E., Savage, J. A., & Holbrook, N. M. (2020). Ontogenetic scaling of phloem sieve tube anatomy and hydraulic resistance with tree height in Quercus rubra. *American Journal of Botany, 107*(6), 852–863. https://doi.org/10.1002/ajb2.1481

Comtet, J., Jensen, K. H., Turgeon, R., Stroock, A. D., & Hosoi, A. E. (2017). Passive phloem loading and long-distance transport in a synthetic tree-on-a-chip. *Nature Plants, 3*(4), Article 4. https://doi.org/10.1038/nplants.2017.32

Corcoran, E., Afshar, M., Curceac, S., Lashkari, A., Raza, M. M., Ahnert, S., Mead, A., & Morris, R. (2023). Current data and modeling bottlenecks for predicting crop yields in the United Kingdom. *Frontiers in Sustainable Food Systems, 7*.

Coruzzi, G., & Bush, D. R. (2001). Nitrogen and Carbon Nutrient and Metabolite Signaling in Plants. *Plant Physiology, 125*(1), 61–64. https://doi.org/10.1104/pp.125.1.61 https://www.frontiersin.org/articles/10.3389/fsufs.2023.1023169

Da Silva, D., Favreau, R., Auzmendi, I., & DeJong, T. M. (2011). Linking water stress effects on carbon partitioning by introducing a xylem circuit into L-PEACH. *Annals of Botany, 108*(6), 1135–1145. https://doi.org/10.1093/aob/mcr072

Da Silva, D., Qin, L., DeBuse, C., & DeJong, T. M. (2014). Measuring and modelling seasonal patterns of carbohydrate storage and mobilization in the trunks and root crowns of peach trees. *Annals of Botany, 114*(4), 643–652. https://doi.org/10.1093/aob/mcu033

Davies, H. V. (1984). Sugar Metabolism in Stolon Tips of Potato during Early Tuberisation. *Zeitschrift Für Pflanzenphysiologie, 113*(5), 377–381. https://doi.org/10.1016/S0044-328X(84)80094-X

De Schepper, V., & Steppe, K. (2010). Development and verification of a water and sugar transport model using measured stem diameter variations. *Journal of Experimental Botany, 61*(8), 2083–2099. https://doi.org/10.1093/jxb/erq018

De Storme, N., & Geelen, D. (2014). Callose homeostasis at plasmodesmata: Molecular regulators and developmental relevance. *Frontiers in Plant Science, 5*, 138. https://doi.org/10.3389/fpls.2014.00138

de Vries, J., Evers, J. B., Kuyper, T. W., Ruijven, J., & Mommer, L. (2021). Mycorrhizal associations change root functionality: A 3D modelling study on competitive interactions between plants for light and nutrients. *New Phytologist, 231*(3), 1171–1182. https://doi.org/10.1111/nph.17435

de Wit, A., Boogaard, H., Fumagalli, D., Janssen, S., Knapen, R., van Kraalingen, D., Supit, I., van der Wijngaart, R., & van Diepen, K. (2019). 25 years of the WOFOST cropping systems model. *Agricultural Systems, 168*, 154–167. https://doi.org/10.1016/j.agsy.2018.06.018

Dinh, Q.-D., Dechesne, A., Furrer, H., Taylor, G., Visser, R. G. F., Harbinson, J., & Trindade, L. M. (2019). High-Altitude Wild Species Solanum arcanum LA385—A Potential Source for Improvement of Plant Growth and Photosynthetic Performance at Suboptimal Temperatures. *Frontiers in Plant Science, 10*. https://www.frontiersin.org/articles/10.3389/fpls.2019.01163

Doxey, A. C., Yaish, M. W. F., Moffatt, B. A., Griffith, M., & McConkey, B. J. (2007). Functional divergence in the Arabidopsis beta-1,3-glucanase gene family inferred by phylogenetic reconstruction of expression states. *Molecular Biology and Evolution, 24*(4), 1045–1055. https://doi.org/10.1093/molbev/msm024

Driever, S. M., Simkin, A. J., Alotaibi, S., Fisk, S. J., Madgwick, P. J., Sparks, C. A., Jones, H. D., Lawson, T., Parry, M. A. J., & Raines, C. A. (2017). Increased SBPase activity improves photosynthesis and grain yield in wheat grown in greenhouse conditions. *Philosophical Transactions of the Royal Society of London. Series B, Biological Sciences, 372*(1730). https://doi.org/10.1098/rstb.2016.0384

R

Duarte-Delgado, D., Ñústez-López, C., Narváez-Cuenca, C., Restrepo-Sánchez, L., Melo, S. E., Sarmiento, F., Kushalappa, A. C., & Mosquera-Vásquez, T. (2016). Natural variation of sucrose, glucose and fructose contents in Colombian genotypes of Solanum tuberosum Group Phureja at harvest. *Journal of the Science of Food and Agriculture, 96*(12), 4288–4294. https://doi.org/10.1002/jsfa.7783

Evers, J. B., Letort, V., Renton, M., & Kang, M. (2018). Computational botany: Advancing plant science through functional–structural plant modelling. *Annals of Botany, 121*(5), 767–772. https://doi.org/10.1093/aob/mcy050

Ewing, E. E., & Wareing, P. F. (1978). Shoot, Stolon, and Tuber Formation on Potato (Solanum tuberosum L.) Cuttings in Response to Photoperiod. *Plant Physiology, 61*(3), 348–353.

FAO. (2021). FAOSTAT [dataset]. https://www.fao.org/faostat/en/#data

Farrar, J. F., & Minchin, P. E. H. (1991). Carbon Partitioning in Split Root Systems of Barley: Relation to Metabolism. *Journal of Experimental Botany, 42*(10), 1261–1269.

Fayant, P., Girlanda, O., Chebli, Y., Aubin, C.-É., Villemure, I., & Geitmann, A. (2010). Finite Element Model of Polar Growth in Pollen Tubes[C][W]. *The Plant Cell, 22*(8), 2579–2593. https://doi.org/10.1105/tpc.110.075754

Fernie, A. R., Bachem, C. W. B., Helariutta, Y., Neuhaus, H. E., Prat, S., Ruan, Y.-L., Stitt, M., Sweetlove, L. J., Tegeder, M., Wahl, V., Sonnewald, S., & Sonnewald, U. (2020). Synchronization of developmental, molecular and metabolic aspects of source–sink interactions. *Nature Plants, 6*(2), Article 2. https://doi.org/10.1038/s41477-020-0590-x

Fisher, D. B., & Cash-Clark, C. E. (2000). Gradients in Water Potential and Turgor Pressure along the Translocation Pathway during Grain Filling in Normally Watered and Water-Stressed Wheat Plants. *Plant Physiology, 123*(1), 139–148. https://doi.org/10.1104/pp.123.1.139

Fisher, D., & Gifford, R. (1987). Accumulation and Conversion of Sugars by Developing Wheat Grains VI. Gradients Along the Transport Pathway from the Peduncle to the Endosperm Cavity during Grain Filling. *Plant Physiology, 82*, 1024–1030. https://doi.org/10.1104/pp.82.4.1024

Fishman, S., & Génard, M. (1998). A biophysical model of fruit growth: Simulation of seasonal and diurnal dynamics of mass. *Plant, Cell & Environment, 21*(8), 739–752. https://doi.org/10.1046/j.1365-3040.1998.00322.x

Furze, M. E., Trumbore, S., & Hartmann, H. (2018). Detours on the phloem sugar highway: Stem carbon storage and remobilization. *Current Opinion in Plant Biology, 43*, 89–95. https://doi.org/10.1016/j.pbi.2018.02.005

Gan, S., & Amasino, R. M. (1997). Making Sense of Senescence (Molecular Genetic Regulation and Manipulation of Leaf Senescence). *Plant Physiology, 113*(2), 313–319.

Gibson, L. J. (2012). The hierarchical structure and mechanics of plant materials. *Journal of the Royal Society Interface, 9*(76), 2749–2766. https://doi.org/10.1098/rsif.2012.0341

Goldschmidt, E. E., & Huber, S. C. (1992). Regulation of Photosynthesis by End-Product Accumulation in Leaves of Plants Storing Starch, Sucrose, and Hexose Sugars. *Plant Physiology, 99*(4), 1443–1448. https://doi.org/10.1104/pp.99.4.1443

Goodstein, D. M., Shu, S., Howson, R., Neupane, R., Hayes, R. D., Fazo, J., Mitros, T., Dirks, W., Hellsten, U., Putnam, N., & Rokhsar, D. S. (2012). Phytozome: A comparative platform for green plant genomics. *Nucleic Acids Research, 40*(Database issue), D1178-1186. https://doi.org/10.1093/nar/gkr944

Gregersen, P. L., Culetic, A., Boschian, L., & Krupinska, K. (2013). Plant senescence and crop productivity. *Plant Molecular Biology, 82*(6), 603–622. https://doi.org/10.1007/s11103-013-0013-8

Guijarro, J. M., & Lagunas, R. (1984). Saccharomyces cerevisiae does not accumulate ethanol against a concentration gradient. *Journal of Bacteriology, 160*(3), 874–878. https://doi.org/10.1128/JB.160.3.874-878.1984

Guo, J.-L., Yu, C.-L., Fan, C.-Y., Lu, Q.-N., Yin, J.-M., Zhang, Y.-F., & Yang, Q. (2010). Cloning and characterization of a potato TFL1 gene involved in tuberization regulation. *Plant Cell, Tissue and Organ Culture (PCTOC), 103*(1), 103–109. https://doi.org/10.1007/s11240-010-9759-8

Hafke, J. B., Amerongen, J.-K. van, Kelling, F., Furch, A. C. U., Gaupels, F., & Bel, A. J. E. van. (2005). Thermodynamic Battle for Photosynthate Acquisition between Sieve Tubes and Adjoining Parenchyma in Transport Phloem. *Plant Physiology, 138*(3), 1527–1537. https://doi.org/10.1104/pp.104.058511

Hall, A. J., Minchin, P. E. H., Clearwater, M. J., & Génard, M. (2013). A biophysical model of kiwifruit (Actinidia deliciosa) berry development. *Journal of Experimental Botany, 64*(18), 5473–5483. https://doi.org/10.1093/jxb/ert317

Hamaoka, N., Nabeshima, M., Moriyama, T., Kozawa, Y., & Ishibashi, Y. (2022). Photoperiodic Regulation of Tuber Enlargement in Water Yam. *Agronomy, 12*(12), Article 12. https://doi.org/10.3390/agronomy12122939

Hammel, H. T. (1968). Measurement of Turgor Pressure and Its Gradient in the Phloem of Oak. *Plant Physiology, 43*(7), 1042–1048. https://doi.org/10.1104/pp.43.7.1042

Hayashi, H., & Chino, M. (1986). Collection of Pure Phloem Sap from Wheat and its Chemical Composition. *Plant and Cell Physiology, 27*(7), 1387–1393. https://doi.org/10.1093/oxfordjournals.pcp.a077237

Hendriks, T., Vreugdenhil, D., & Stiekema, W. J. (1991). Patatin and four serine proteinase inhibitor genes are differentially expressed during potato tuber development. *Plant Molecular Biology, 17*(3), 385–394. https://doi.org/10.1007/BF00040633

Hölttä, T., Mencuccini, M., & Nikinmaa, E. (2009). Linking phloem function to structure: Analysis with a coupled xylem–phloem transport model. *Journal of Theoretical Biology, 259*(2), 325–337. https://doi.org/10.1016/j.jtbi.2009.03.039

Hölttä, T., Vesala, T., Sevanto, S., Perämäki, M., & Nikinmaa, E. (2006). Modeling xylem and phloem water flows in trees according to cohesion theory and Münch hypothesis. *Trees, 20*(1), 67–78. https://doi.org/10.1007/s00468-005-0014-6

Irvine, J., & Grace, J. (1997). Continuous measurements of water tensions in the xylem of trees based on the elastic properties of wood. *Planta, 202*(4), 455–461. https://doi.org/10.1007/s004250050149

R

Jaarsma, R., & de Boer, A. H. (2018). Salinity Tolerance of Two Potato Cultivars (Solanum tuberosum) Correlates With Differences in Vacuolar Transport Activity. *Frontiers in Plant Science, 9*. https://doi.org/10.3389/fpls.2018.00737

Jensen, K. H., Berg-Sørensen, K., Bruus, H., Holbrook, N. M., Liesche, J., Schulz, A., Zwieniecki, M. A., & Bohr, T. (2016). Sap flow and sugar transport in plants. *Reviews of Modern Physics, 88*(3), 035007. https://doi.org/10.1103/RevModPhys.88.035007

Jensen, K. H., Savage, J. A., & Holbrook, N. M. (2013). Optimal concentration for sugar transport in plants. *Journal of The Royal Society Interface, 10*(83), 20130055. https://doi.org/10.1098/rsif.2013.0055

Jing, S., Jiang, P., Sun, X., Yu, L., Wang, E., Qin, J., Zhang, F., Prat, S., & Song, B. (2023). Long-Distance Control of Potato Storage Organ Formation by SELF PRUNING 3D and FLOWERING LOCUS T-like 1. *Plant Communications*, 100547. https://doi.org/10.1016/j.xplc.2023.100547

Jonik, C., Sonnewald, U., Hajirezaei, M.-R., Flügge, U.-I., & Ludewig, F. (2012). Simultaneous boosting of source and sink capacities doubles tuber starch yield of potato plants. *Plant Biotechnology Journal, 10*(9), 1088−1098. https://doi.org/10.1111/j.1467-7652.2012.00736.x

Kalyaanamoorthy, S., Minh, B. Q., Wong, T. K. F., von Haeseler, A., & Jermiin, L. S. (2017). ModelFinder: Fast model selection for accurate phylogenetic estimates. *Nature Methods, 14*(6), Article 6. https://doi.org/10.1038/nmeth.4285

Katoh, K., & Standley, D. M. (2013). MAFFT Multiple Sequence Alignment Software Version 7: Improvements in Performance and Usability. *Molecular Biology and Evolution, 30*(4), 772−780. https://doi.org/10.1093/molbev/mst010

Kehr, J., Hustiak, F., Walz, C., Willmitzer, L., & Fisahn, J. (1998). Transgenic plants changed in carbon allocation pattern display a shift in diurnal growth pattern. *The Plant Journal, 16*(4), 497−503. https://doi.org/10.1046/j.1365-313x.1998.00318.x

Kim, J. H., Woo, H. R., Kim, J., Lim, P. O., Lee, I. C., Choi, S. H., Hwang, D., & Nam, H. G. (2009). Trifurcate Feed-Forward Regulation of Age-Dependent Cell Death Involving miR164 in Arabidopsis. *Science, 323*(5917), 1053−1057. https://doi.org/10.1126/science.1166386

Kloosterman, B., Abelenda, J. A., Gomez, M. del M. C., Oortwijn, M., de Boer, J. M., Kowitwanich, K., Horvath, B. M., van Eck, H. J., Smaczniak, C., Prat, S., Visser, R. G. F., & Bachem, C. W. B. (2013). Naturally occurring allele diversity allows potato cultivation in northern latitudes. *Nature, 495*(7440), Article 7440. https://doi.org/10.1038/nature11912

Kondhare, K. R., Natarajan, B., & Banerjee, A. K. (2020). Molecular signals that govern tuber development in potato. *The International Journal of Developmental Biology, 64*(1-2−3), 133−140. https://doi.org/10.1387/ijdb.190132ab

Konrad, W., Katul, G., Roth-Nebelsick, A., & Jensen, K. H. (2019). Xylem functioning, dysfunction and repair: A physical perspective and implications for phloem transport. *Tree Physiology, 39*(2), 243−261. https://doi.org/10.1093/treephys/tpy097

Krauss, A. (1985). Interaction of nitrogen nutrition, phytohormones, and tuberization. In P.H. Li, ed, Potato Physiology. Academic Press, London, pp 209-231.

Lacointe, A., & Minchin, P. E. H. (2008). Modelling phloem and xylem transport within a complex architecture. *Functional Plant Biology, 35*(10), 772. https://doi.org/10.1071/FP08085

Leggewie, G., Kolbe, A., Lemoine, R., Roessner, U., Lytovchenko, A., Zuther, E., Kehr, J., Frommer, W. B., Riesmeier, J. W., Willmitzer, L., & Fernie, A. R. (2003). Overexpression of the sucrose transporter SoSUT1 in potato results in alterations in leaf carbon partitioning and in tuber metabolism but has little impact on tuber morphology. *Planta, 217*(1), 158–167. https://doi.org/10.1007/s00425-003-0975-x

Lehretz, G. G., Sonnewald, S., & Sonnewald, U. (2021). Assimilate highway to sink organs—Physiological consequences of SP6A overexpression in transgenic potato (Solanum tuberosum L.). *Journal of Plant Physiology, 266*, 153530. https://doi.org/10.1016/j.jplph.2021.153530

Leidreiter, K., Kruse, A., Heineke, D., Robinson, D. G., & Heldt, H.-W. (1995). Subcellular Volumes and Metabolite Concentrations in Potato (Solanum tuberosum cv. Désirée) Leaves. *Botanica Acta, 108*(5), 439–444. https://doi.org/10.1111/j.1438-8677.1995.tb00518.x

Lemoine, R., La Camera, S., Atanassova, R., Dédaldéchamp, F., Allario, T., Pourtau, N., Bonnemain, J.-L., Laloi, M., Coutos-Thévenot, P., Maurousset, L., Faucher, M., Girousse, C., Lemonnier, P., Parrilla, J., & Durand, M. (2013). Source-to-sink transport of sugar and regulation by environmental factors. *Frontiers in Plant Science, 4.* https://doi.org/10.3389/fpls.2013.00272

Lescourret, F., Moitrier, N., Valsesia, P., & Génard, M. (2011). QualiTree, a virtual fruit tree to study the management of fruit quality. I. Model development. *Trees, 25*(3), 519–530. https://doi.org/10.1007/s00468-010-0531-9

Levy, A., Erlanger, M., Rosenthal, M., & Epel, B. L. (2007). A plasmodesmata-associated beta-1,3-glucanase in Arabidopsis. *The Plant Journal: For Cell and Molecular Biology, 49*(4), 669–682. https://doi.org/10.1111/j.1365-313X.2006.02986.x

Liu, H., Si, X., Wang, Z., Cao, L., Gao, L., Zhou, X., Wang, W., Wang, K., Jiao, C., Zhuang, L., Liu, Y., Hou, J., Li, T., Hao, C., Guo, W., Liu, J., & Zhang, X. (2023). TaTPP-7A positively feedback regulates grain filling and wheat grain yield through T6P-SnRK1 signalling pathway and sugar-ABA interaction. *Plant Biotechnology Journal, 21*(6), 1159–1175. https://doi.org/10.1111/pbi.14025

Lowe, S. B., Mahon, J. D., & Hunt, L. A. (1976). The effect of daylength on shoot growth and formation of root tubers in young plants of cassava (Manihot esculenta grantz). *Plant Science Letters, 6*(1), 57–62. https://doi.org/10.1016/0304-4211(76)90179-6

Lucas, W. J., Ham, B.-K., & Kim, J.-Y. (2009). Plasmodesmata—Bridging the gap between neighboring plant cells. *Trends in Cell Biology, 19*(10), 495–503. https://doi.org/10.1016/j.tcb.2009.07.003

Ma, S., Li, Y., Li, X., Sui, X., & Zhang, Z. (2019). Phloem Unloading Strategies and Mechanisms in Crop Fruits. *Journal of Plant Growth Regulation, 38*(2), 494–500. https://doi.org/10.1007/s00344-018-9864-1

R

Mammeri, Y., & Sellier, D. (2017). *A surface model of nonlinear, non-steady-state phloem transport*. https://hal.archives-ouvertes.fr/hal-01372758

Manck-Götzenberger, J., & Requena, N. (2016). Arbuscular mycorrhiza Symbiosis Induces a Major Transcriptional Reprogramming of the Potato SWEET Sugar Transporter Family. *Frontiers in Plant Science, 7.* https://www.frontiersin.org/articles/10.3389/fpls.2016.00487

Minchin, P. E. H., & Lacointe, A. (2005). New understanding on phloem physiology and possible consequences for modelling long-distance carbon transport. *New Phytologist, 166*(3), 771–779. https://doi.org/10.1111/j.1469-8137.2005.01323.x

Minchin, P. E. H., & Lacointe, A. (2017). Consequences of phloem pathway unloading/reloading on equilibrium flows between source and sink: A modelling approach. *Functional Plant Biology, 44*(5), 507. https://doi.org/10.1071/FP16354

Minchin, P. E. H., Thorpe, M. R., & Farrar, J. F. (1993). A Simple Mechanistic Model of Phloem Transport which Explains Sink Priority. *Journal of Experimental Botany, 44*(5), 947–955. https://doi.org/10.1093/jxb/44.5.947

Minchin, P. E. H., Thorpe, M. R., Wünsche, J. N., Palmer, J. W., & Picton, R. F. (1997). Carbon partitioning between apple fruits: Short- and long-term response to availability of photosynthate. *Journal of Experimental Botany, 48*(7), 1401–1406. https://doi.org/10.1093/jxb/48.7.1401

Mitchell, A. L., Attwood, T. K., Babbitt, P. C., Blum, M., Bork, P., Bridge, A., Brown, S. D., Chang, H.-Y., El-Gebali, S., Fraser, M. I., Gough, J., Haft, D. R., Huang, H., Letunic, I., Lopez, R., Luciani, A., Madeira, F., Marchler-Bauer, A., Mi, H., … Finn, R. D. (2019). InterPro in 2019: Improving coverage, classification and access to protein sequence annotations. *Nucleic Acids Research, 47*(D1), D351–D360. https://doi.org/10.1093/nar/gky1100

Moore, C. E., Meacham-Hensold, K., Lemonnier, P., Slattery, R. A., Benjamin, C., Bernacchi, C. J., Lawson, T., & Cavanagh, A. P. (2021). The effect of increasing temperature on crop photosynthesis: From enzymes to ecosystems. *Journal of Experimental Botany, 72*(8), 2822–2844. https://doi.org/10.1093/jxb/erab090

Morison, K. R. (2002). Viscosity equations for sucrose solutions: Old and new 2002. *Proceedings of the 9th APCChE Congress and CHEMECA*.

Mullendore, D. L., Windt, C. W., Van As, H., & Knoblauch, M. (2010). Sieve Tube Geometry in Relation to Phloem Flow. *The Plant Cell, 22*(3), 579–593. https://doi.org/10.1105/tpc.109.070094

Munch, E. (1930). *Die stoffbewegungen in der pflanze*. Jena, G. Fischer.

Navarro, C., Abelenda, J. A., Cruz-Oró, E., Cuéllar, C. A., Tamaki, S., Silva, J., Shimamoto, K., & Prat, S. (2011). Control of flowering and storage organ formation in potato by FLOWERING LOCUS T. *Nature, 478*(7367), 119–122. https://doi.org/10.1038/nature10431

Nazarian-Firouzabadi, F., & Visser, R. G. F. (2017). Potato starch synthases: Functions and relationships. *Biochemistry and Biophysics Reports, 10*, 7–16. https://doi.org/10.1016/j.bbrep.2017.02.004

Nguyen, L.-T., Schmidt, H. A., von Haeseler, A., & Minh, B. Q. (2015). IQ-TREE: A Fast and Effective Stochastic Algorithm for Estimating Maximum-Likelihood Phylogenies. *Molecular Biology and Evolution, 32*(1), 268–274. https://doi.org/10.1093/molbev/msu300

Nie, P., Wang, X., Hu, L., Zhang, H., Zhang, J., Zhang, Z., & Zhang, L. (2010). The Predominance of the Apoplasmic Phloem-unloading Pathway is Interrupted by a Symplasmic Pathway During Chinese Jujube Fruit Development. *Plant and Cell Physiology, 51*(6), 1007–1018. https://doi.org/10.1093/pcp/pcq054

Nieberl, P., Ehrl, C., Pommerrenig, B., Graus, D., Marten, I., Jung, B., Ludewig, F., Koch, W., Harms, K., Flügge, U.-I., Neuhaus, H. E., Hedrich, R., & Sauer, N. (2017). Functional characterisation and cell specificity of BvSUT1, the transporter that loads sucrose into the phloem of sugar beet (Beta vulgaris L.) source leaves. *Plant Biology, 19*(3), 315–326. https://doi.org/10.1111/plb.12546

Nobel, P. S. (2005). *Physicochemical and Environmental Plant Physiology*. Elsevier Science & Technology.

Nölke, G., Houdelet, M., Kreuzaler, F., Peterhänsel, C., & Schillberg, S. (2014). The expression of a recombinant glycolate dehydrogenase polyprotein in potato (Solanum tuberosum) plastids strongly enhances photosynthesis and tuber yield. *Plant Biotechnology Journal, 12*(6), 734–742. https://doi.org/10.1111/pbi.12178

Oparka, K. J., Davies, H. V., Wright, K. M., Viola, R., & Prior, D. A. (1990). Effect of sink isolation on sugar uptake and starch synthesis by potato-tuber storage parenchyma. *Planta, 182*(1), 113–117. https://doi.org/10.1007/BF00239992

Ospina, C. A., Lammerts van Bueren, E. T., Allefs, S., Vos, P. G., van der Linden, G., Maliepaard, C. A., & Struik, P. C. (2021). Association Mapping of Physiological and Morphological Traits Related to Crop Development under Contrasting Nitrogen Inputs in a Diverse Set of Potato Cultivars. *Plants, 10*(8), 1727. https://doi.org/10.3390/plants10081727

Pagliarani, C., Casolo, V., Beiragi, M. A., Cavalletto, S., Siciliano, I., Schubert, A., Gullino, M. L., Zwieniecki, M. A., & Secchi, F. (2019). Priming xylem for stress recovery depends on coordinated activity of sugar metabolic pathways and changes in xylem sap pH. *Plant, Cell & Environment, 42*(6), 1775–1787. https://doi.org/10.1111/pce.13533

Pallas, B., Christophe, A., & Lecoeur, J. (2010). Are the common assimilate pool and trophic relationships appropriate for dealing with the observed plasticity of grapevine development? *Annals of Botany, 105*(2), 233–247. https://doi.org/10.1093/aob/mcp278

Paniagua, C., Perry, L., & Benitez-Alfonso, Y. (2021). *A phylogenetic and transcriptomic study of the β-1,3-glucanase family in tomato identifies candidate targets for fruit improvement* (p. 2021.09.29.462359). bioRxiv. https://doi.org/10.1101/2021.09.29.462359

Patrick, J. W., & Offler, C. E. (1996). Post-sieve element transport of photoassimilates in sink regions. *Journal of Experimental Botany, 47 Spec No*, 1165–1177. https://doi.org/10.1093/jxb/47.Special_Issue.1165

R

Patrick, J. W., Zhang, W., Tyerman, S. D., Offler, C. E., & Walker, N. A. (2001). Role of membrane transport in phloem translocation of assimilates and water. *Functional Plant Biology, 28*(7), 697. https://doi.org/10.1071/PP01023

Perämäki, M., Nikinmaa, E., Sevanto, S., Ilvesniemi, H., Siivola, E., Hari, P., & Vesala, T. (2001). Tree stem diameter variations and transpiration in Scots pine: An analysis using a dynamic sap flow model. *Tree Physiology, 21*(12–13), 889–897. https://doi.org/10.1093/treephys/21.12-13.889

Pescod, K. V., Quick, W. P., & Douglas, A. E. (2007). Aphid responses to plants with genetically manipulated phloem nutrient levels. *Physiological Entomology, 32*(3), 253–258. https://doi.org/10.1111/j.1365-3032.2007.00577.x

Pham, G. M., Hamilton, J. P., Wood, J. C., Burke, J. T., Zhao, H., Vaillancourt, B., Ou, S., Jiang, J., & Buell, C. R. (2020). Construction of a chromosome-scale long-read reference genome assembly for potato. *GigaScience, 9*(9), giaa100. https://doi.org/10.1093/gigascience/giaa100

Pierleoni, A., Martelli, P. L., & Casadio, R. (2008). PredGPI: A GPI-anchor predictor. BMC *Bioinformatics, 9*, 392. https://doi.org/10.1186/1471-2105-9-392

Plaisted, P. H. (1957). Growth of the potato tuber. *Plant Physiology*, 445–453.

Plantenga, F. D. M., Bergonzi, S., Abelenda, J. A., Bachem, C. W. B., Visser, R. G. F., Heuvelink, E., & Marcelis, L. F. M. (2019). The tuberization signal StSP6A represses flower bud development in potato. *Journal of Experimental Botany, 70*(3), 937–948. https://doi.org/10.1093/jxb/ery420

Plantenga, F. D. M., Bergonzi, S., Bachem, C. W. B., Visser, R. G. F., Heuvelink, E., & Marcelis, L. F. M. (2019). High light accelerates potato flowering independently of the FT-like flowering signal StSP3D. *Environmental and Experimental Botany, 160*, 35–44. https://doi.org/10.1016/j.envexpbot.2019.01.004

Pourazari, F., Andersson, M., & Weih, M. (2018). Altered Tuber Yield in Genetically Modified High-Amylose and Oil Potato Lines Is Associated With Changed Whole-Plant Nitrogen Economy. *Frontiers in Plant Science, 9*. https://doi.org/10.3389/fpls.2018.00342

Prusinkiewicz, P. (2004). Modeling plant growth and development. *Current Opinion in Plant Biology, 7*(1), 79–83. https://doi.org/10.1016/j.pbi.2003.11.007

Prusova, A. (2016). *Light on phloem transport (an MRI approach)*. https://doi.org/10.18174/389397

Qiu, K., Li, Z., Yang, Z., Chen, J., Wu, S., Zhu, X., Gao, S., Gao, J., Ren, G., Kuai, B., & Zhou, X. (2015). EIN3 and ORE1 Accelerate Degreening during Ethylene-Mediated Leaf Senescence by Directly Activating Chlorophyll Catabolic Genes in Arabidopsis. P*LOS Genetics, 11*(7), https://doi.org/10.1371/journal.pgen.1005399

Rankenberg, T., Geldhof, B., Veen, H. van, Holsteens, K., Poel, B. V. de, & Sasidharan, R. (2021). Age-Dependent Abiotic Stress Resilience in Plants. *Trends in Plant Science, 26*(7), 692–705. https://doi.org/10.1016/j.tplants.2020.12.016

Reeve, R. M., Timm, H., & Weaver, M. L. (1973). Cell wall thickness during growth of domestic and foreign potato cultivars. *American Potato Journal, 50*(6), 204–211. https://doi.org/10.1007/BF02851771

Richmond, T. A., & Somerville, C. R. (2000). The Cellulose Synthase Superfamily1. *Plant Physiology, 124*(2), 495–498. https://doi.org/10.1104/pp.124.2.495

Riesmeier, J. W., Hirner, B., & Frommer, W. B. (1993). Potato sucrose transporter expression in minor veins indicates a role in phloem loading. *The Plant Cell, 5*, 1591–1598.

Roitsch, T., & González, M.-C. (2004). Function and regulation of plant invertases: Sweet sensations. *Trends in Plant Science, 9*(12), 606–613. https://doi.org/10.1016/j.tplants.2004.10.009

Rosado-Souza, L., Yokoyama, R., Sonnewald, U., & Fernie, A. R. (2023). Understanding source–sink interactions: Progress in model plants and translational research to crops. *Molecular Plant, 16*(1), 96–121. https://doi.org/10.1016/j.molp.2022.11.015

Ross, H. A., & Davies, H. V. (1992). Sucrose Metabolism in Tubers of Potato (Solanum tuberosum L.): Effects of Sink Removal and Sucrose Flux on Sucrose-Degrading Enzymes. *Plant Physiology, 98*(1), 287–293. https://doi.org/10.1104/pp.98.1.287

Ross-Elliott, T. J., Jensen, K. H., Haaning, K. S., Wager, B. M., Knoblauch, J., Howell, A. H., Mullendore, D. L., Monteith, A. G., Paultre, D., Yan, D., Otero, S., Bourdon, M., Sager, R., Lee, J.-Y., Helariutta, Y., Knoblauch, M., & Oparka, K. J. (2017). Phloem unloading in Arabidopsis roots is convective and regulated by the phloem-pole pericycle. *ELife, 6*, e24125. https://doi.org/10.7554/eLife.24125

Ruan, Y. L., Llewellyn, D. J., & Furbank, R. T. (2001). The control of single-celled cotton fiber elongation by developmentally reversible gating of plasmodesmata and coordinated expression of sucrose and K+ transporters and expansin. *The Plant Cell, 13*(1), 47–60. https://doi.org/10.1105/tpc.13.1.47

Ruan, Y.-L., & Patrick, J. W. (1995). The cellular pathway of postphloem sugar transport in developing tomato fruit. *Planta, 196*(3), 434–444.

Sarlikioti, V., de Visser, P. H. B., Buck-Sorlin, G. H., & Marcelis, L. F. M. (2011). How plant architecture affects light absorption and photosynthesis in tomato: Towards an ideotype for plant architecture using a functional-structural plant model. *Annals of Botany, 108*(6), 1065–1073. https://doi.org/10.1093/aob/mcr221

Satake, A., Seki, M., Iima, M., Teramoto, T., & Nishiura, Y. (2016). Florigen distribution determined by a source–sink balance explains the diversity of inflorescence structures in Arabidopsis. *Journal of Theoretical Biology, 395*, 227–237. https://doi.org/10.1016/j.jtbi.2016.01.035

Savage, J. A., Clearwater, M. J., Haines, D. F., Klein, T., Mencuccini, M., Sevanto, S., Turgeon, R., & Zhang, C. (2016). Allocation, stress tolerance and carbon transport in plants: How does phloem physiology affect plant ecology? *Plant, Cell & Environment, 39*(4), 709–725. https://doi.org/10.1111/pce.12602

Schans, J., & Arntzen, F. K. (1991). Photosynthesis, transpiration and plant growth characters of different potato cultivars at various densities of Globodera pallida. *Netherlands Journal of Plant Pathology, 97*(5), 297–310. https://doi.org/10.1007/BF01974225

R

Schnepf, A., Black, C. K., Couvreur, V., Delory, B. M., Doussan, C., Heymans, A., Javaux, M., Khare, D., Koch, A., Koch, T., Kuppe, C. W., Landl, M., Leitner, D., Lobet, G., Meunier, F., Postma, J. A., Schäfer, E. D., Selzner, T., Vanderborght, J., & Vereecken, H. (2023). Collaborative benchmarking of functional-structural root architecture models: Quantitative comparison of simulated root water uptake. *In Silico Plants*, diad005. https://doi.org/10.1093/insilicoplants/diad005

Schultz, J., Copley, R. R., Doerks, T., Ponting, C. P., & Bork, P. (2000). SMART: A web-based tool for the study of genetically mobile domains. *Nucleic Acids Research, 28*(1), 231–234. https://doi.org/10.1093/nar/28.1.231

Schulze, W., Weise, A., Frommer, W. B., & Ward, J. M. (2000). Function of the cytosolic N-terminus of sucrose transporter AtSUT2 in substrate affnity. *FEBS Letters, 6*.

Secchi, F., & Zwieniecki, M. A. (2016). Accumulation of sugars in the xylem apoplast observed under water stress conditions is controlled by xylem pH. *Plant, Cell & Environment, 39*(11), 2350–2360. https://doi.org/10.1111/pce.12767

Seleznyova, A. N., & Hanan, J. (2018). Mechanistic modelling of coupled phloem/xylem transport for L-systems: Combining analytical and computational methods. *Annals of Botany, 121*(5), 991–1003. https://doi.org/10.1093/aob/mcx204

Sevanto, S., Hölttä, T., & Holbrook, N. M. (2011). Effects of the hydraulic coupling between xylem and phloem on diurnal phloem diameter variation. *Plant, Cell & Environment, 34*(4), 690–703. https://doi.org/10.1111/j.1365-3040.2011.02275.x

Shao, C.-H., Qiu, C.-F., Qian, Y.-F., & Liu, G.-R. (2020). Nitrate deficiency decreased photosynthesis and oxidation-reduction processes, but increased cellular transport, lignin biosynthesis and flavonoid metabolism revealed by RNA-Seq in Oryza sativa leaves. *PLoS ONE, 15*(7), e0235975. https://doi.org/10.1371/journal.pone.0235975

Sibout, R., Plantegenet, S., & Hardtke, C. S. (2008). Flowering as a condition for xylem expansion in Arabidopsis hypocotyl and root. *Current Biology: CB, 18*(6), 458–463. https://doi.org/10.1016/j.cub.2008.02.070

Smith, M. R., Rao, I. M., & Merchant, A. (2018). Source-Sink Relationships in Crop Plants and Their Influence on Yield Development and Nutritional Quality. *Frontiers in Plant Science, 9*, 1889. https://doi.org/10.3389/fpls.2018.01889

Solari, L. I., Johnson, S., & DeJong, T. M. (2006). Relationship of water status to vegetative growth and leaf gas exchange of peach (Prunus persica) trees on different rootstocks. *Tree Physiology, 26*(10), 1333–1341. https://doi.org/10.1093/treephys/26.10.1333

Stanfield, R. C., Schulte, P. J., Randolph, K. E., & Hacke, U. G. (2019). Computational models evaluating the impact of sieve plates and radial water exchange on phloem pressure gradients: Sieve Plate and Tube Character Modeling. *Plant, Cell & Environment, 42*(2), 466–479. https://doi.org/10.1111/pce.13414

Stein, O., & Granot, D. (2019). An Overview of Sucrose Synthases in Plants. *Frontiers in Plant Science, 10*, 95. https://doi.org/10.3389/fpls.2019.00095

Stirbet, A., Lazár, D., Guo, Y., & Govindjee, G. (2020). Photosynthesis: Basics, history and modelling. *Annals of Botany, 126*(4), 511–537. https://doi.org/10.1093/aob/mcz171

Struik, P. C. (2007). Above-ground and below-ground plant development. In D. Vreugdenhil (Ed.), *Potato Biology and Biotechnology: Advances and Perspectives* (1st ed., pp. 219–236). Elsevier Oxford. https://www.elsevier.com/books/potato-biology-and-biotechnology/vreugdenhil/978-0-444-51018-1

Struik, P. C., Schnieders, B. J., Kerckhoffs, L. H. J., & Visscher, G. W. J. (1988). A device for measuring the growth of individual potato tubers non-destructively and precisely. *Potato Research, 31*(1), 137–143. https://doi.org/10.1007/BF02360030

Struik, P. C., & Wiersema, S. G. (1999). *Seed potato technology*. Wageningen Academic Publishers. https://doi.org/10.3920/978-90-8686-759-2

Susila, H., & Purwestri, Y. A. (2023). PEBP Signaling Network in Tubers and Tuberous Root Crops. *Plants, 12*(2), Article 2. https://doi.org/10.3390/plants12020264

ten Den, T., van de Wiel, I., de Wit, A., van Evert, F. K., van Ittersum, M. K., & Reidsma, P. (2022). Modelling potential potato yields: Accounting for experimental differences in modern cultivars. *European Journal of Agronomy, 137*, 126510. https://doi.org/10.1016/j.eja.2022.126510

Thompson, M. V., & Holbrook, N. M. (2003). Application of a Single-solute Non-steady-state Phloem Model to the Study of Long-distance Assimilate Transport. *Journal of Theoretical Biology, 220*(4), 419–455. https://doi.org/10.1006/jtbi.2003.3115

Turgeon, R. (2010). The Puzzle of Phloem Pressure. *Plant Physiology, 154*(2), 578–581. https://doi.org/10.1104/pp.110.161679

Van Bel, A. J. E. (2003). The phloem, a miracle of ingenuity. *Plant, Cell & Environment, 26*(1), 125–149. https://doi.org/10.1046/j.1365-3040.2003.00963.x

van den Herik, B., Bergonzi, S., Bachem, C. W. B., & Tusscher, K. ten. (2021). Modelling the physiological relevance of sucrose export repression by an Flowering Time homolog in the long-distance phloem of potato. *Plant, Cell & Environment, 44*(3), 792–806. https://doi.org/10.1111/pce.13977

van den Herik, B., & ten Tusscher, K. (2022). Undirected Sucrose Efflux Mitigation by the FT-Like SP6A Preferentially Enhances Tuber Resource Partitioning. *Frontiers in Plant Science, 13*. https://www.frontiersin.org/articles/10.3389/fpls.2022.817909

Van Harsselaar, J. K., Lorenz, J., Senning, M., Sonnewald, U., & Sonnewald, S. (2017). Genome-wide analysis of starch metabolism genes in potato (Solanum tuberosum L.). *BMC Genomics, 18*(1), 37. https://doi.org/10.1186/s12864-016-3381-z

van Schijndel, L., Snoek, B. L., & Tusscher, K. ten. (2022). Embodiment in distributed information processing: "Solid" plants versus "liquid" ant colonies. *Quantitative Plant Biology, 3*, e27. https://doi.org/10.1017/qpb.2022.22

Viola, R., Roberts, A. G., Haupt, S., Gazzani, S., Hancock, R. D., Marmiroli, N., Machray, G. C., & Oparka, K. J. (2001). Tuberization in Potato Involves a Switch from Apoplastic to Symplastic Phloem Unloading. *The Plant Cell, 13*(2), 385–398. https://doi.org/10.1105/tpc.13.2.385

Vos, J., & van der Putten, P. E. L. (1998). Effect of nitrogen supply on leaf growth, leaf nitrogen economy and photosynthetic capacity in potato. *Field Crops Research, 59*(1), 63–72. https://doi.org/10.1016/S0378-4290(98)00107-5

R

Vreugdenhil, D., Chun, X. X., Jung, S., Lammeren, A. A. M. van, & Ewing, E. E. (1999). Initial anatomical changes associated with tuber formation on single-node potato (Solanum tuberosum L.) cuttings: A re-evaluation. *Annals of Botany, 84*(5), 675–680. https://doi.org/10.1006/anbo.1999.0950

Wallace, R. A., & Selman, K. (1981). Cellular and Dynamic Aspects of Oocyte Growth in Teleosts. *American Zoologist, 21*(2), 325–343.

Walsh, K. B., Sky, R. C., & Brown, S. M. (2005). The anatomy of the pathway of sucrose unloading within the sugarcane stalk. *Functional Plant Biology: FPB, 32*(4), 367–374. https://doi.org/10.1071/FP04102

Wang, B., Andargie, M., & Fang, R. (2022). The function and biosynthesis of callose in high plants. *Heliyon, 8*(4), e09248. https://doi.org/10.1016/j.heliyon.2022.e09248

Wang, D., Liu, H., Wang, H., Zhang, P., & Shi, C. (2020). A novel sucrose transporter gene IbSUT4 involves in plant growth and response to abiotic stress through the ABF-dependent ABA signaling pathway in Sweetpotato. *BMC Plant Biology, 20*(1), 157. https://doi.org/10.1186/s12870-020-02382-8

Waskom, M. L. (2021). seaborn: Statistical data visualization. *Journal of Open Source Software, 6*(60), 3021. https://doi.org/10.21105/joss.03021

White, A. C., Rogers, A., Rees, M., & Osborne, C. P. (2016). How can we make plants grow faster? A source–sink perspective on growth rate. *Journal of Experimental Botany, 67*(1), 31–45. https://doi.org/10.1093/jxb/erv447

Windt, C. W., Vergeldt, F. J., Jager, P. A. D., & As, H. V. (2006). MRI of long-distance water transport: A comparison of the phloem and xylem flow characteristics and dynamics in poplar, castor bean, tomato and tobacco. *Plant, Cell & Environment, 29*(9), 1715–1729. https://doi.org/10.1111/j.1365-3040.2006.01544.x

Wingler, A. (2018). Transitioning to the Next Phase: The Role of Sugar Signaling throughout the Plant Life Cycle. *Plant Physiology, 176*(2), 1075–1084. https://doi.org/10.1104/pp.17.01229

Winter, H., & Huber, S. C. (2000). Regulation of Sucrose Metabolism in Higher Plants: Localization and regulation of Activity of Key Enzymes. *Critical Reviews in Plant Sciences, 19*(1), 31–67. https://doi.org/10.1080/07352680091139178

Wu, S.-W., Kumar, R., Iswanto, A. B. B., & Kim, J.-Y. (2018). Callose balancing at plasmodesmata. *Journal of Experimental Botany, 69*(22), 5325–5339. https://doi.org/10.1093/jxb/ery317

Xu, X., Yang, Y., Liu, C., Sun, Y., Zhang, T., Hou, M., Huang, S., & Yuan, H. (2019). The evolutionary history of the sucrose synthase gene family in higher plants. *BMC Plant Biology, 19*(1), 566. https://doi.org/10.1186/s12870-019-2181-4

Yin, X., Goudriaan, J., Lantinga, E. A., Vos, J., & Spiertz, H. J. (2003). A flexible sigmoid function of determinate growth. *Annals of Botany, 91*(3), 361–371. https://doi.org/10.1093/aob/mcg029

Zeeman, S. C., Kossmann, J., & Smith, A. M. (2010). Starch: Its metabolism, evolution, and biotechnological modification in plants. *Annual Review of Plant Biology, 61*, 209–234. https://doi.org/10.1146/annurev-arplant-042809-112301

Zhang, G., Jin, X., Li, X., Zhang, N., Li, S., Si, H., Rajora, O. P., & Li, X.-Q. (2022). Genome-wide identification of PEBP gene family members in potato, their phylogenetic relationships, and expression patterns under heat stress. *Molecular Biology Reports, 49*(6), 4683–4697. https://doi.org/10.1007/s11033-022-07318-z

Zhang, W.-H., Zhou, Y., Dibley, K. E., Tyerman, S. D., Furbank, R. T., & Patrick, J. W. (2007). Nutrient loading of developing seeds. *Functional Plant Biology, 34*(4), 314–331. https://doi.org/10.1071/FP06271

Zheng, S.-L., Wang, L.-J., Wan, N.-X., Zhong, L., Zhou, S.-M., He, W., & Yuan, J.-C. (2016). Response of Potato Tuber Number and Spatial Distribution to Plant Density in Different Growing Seasons in Southwest China. *Frontiers in Plant Science, 7*. https://doi.org/10.3389/fpls.2016.00365

Zhou, Q., Tang, D., Huang, W., Yang, Z., Zhang, Y., Hamilton, J. P., Visser, R. G. F., Bachem, C. W. B., Robin Buell, C., Zhang, Z., Zhang, C., & Huang, S. (2020). Haplotype-resolved genome analyses of a heterozygous diploid potato. *Nature Genetics, 52*(10), 1018–1023. https://doi.org/10.1038/s41588-020-0699-x

Zhou, X.-R., Schnepf, A., Vanderborght, J., Leitner, D., Lacointe, A., Vereecken, H., & Lobet, G. (2020). CPlantBox, a whole-plant modelling framework for the simulation of water- and carbon-related processes. *In Silico Plants, 2*(1). https://doi.org/10.1093/insilicoplants/diaa001

Zhu, J., Génard, M., Poni, S., Gambetta, G. A., Vivin, P., Vercambre, G., Trought, M. C. T., Ollat, N., Delrot, S., & Dai, Z. (2019). Modelling grape growth in relation to whole-plant carbon and water fluxes. *Journal of Experimental Botany, 70*(9), 2505–2521. https://doi.org/10.1093/jxb/ery367

Zhu, J., Gou, F., Rossouw, G., Begum, F., Henke, M., Johnson, E., Holzapfel, B., Field, S., & Seleznyova, A. (2021). Simulating organ biomass variability and carbohydrate distribution in perennial fruit crops: A comparison between the common assimilate pool and phloem carbohydrate transport models. *In Silico Plants, diab024*. https://doi.org/10.1093/insilicoplants/diab024

R

Samenvatting

Planten zijn essentieel voor het leven op aarde door hun vermogen om fotosynthese uit te voeren. Dit stelt planten in staat de energie van de zon om te zetten en op te slaan als suikers en om zuurstof te produceren. Op deze manier leveren planten twee essentiële ingrediënten voor leven. Niet in alle delen van een plant vindt echter fotosynthese plaats. De verdeling van geproduceerde suikers van de bladeren waar ze gemaakt worden naar verschillende organen waar ze gebruikt worden speelt dus een belangrijke rol bij het bepalen van plantengroei. Deze verdeling over de plant is niet altijd hetzelfde tijdens de levenscyclus, maar is afhankelijk van het levensstadium en de geschiedenis van de plant. Zo lijken bloemen, zaden en knollen prioriteit te krijgen over nieuwe bladeren wanneer een plant zich moet gaan voortplanten aan het einde van zijn groeicyclus. Verder moeten planten zich snel kunnen aanpassen aan veranderingen in hun omgeving (zoals bijvoorbeeld droogte, hitte en pathogenen) omdat ze zich niet kunnen verplaatsen. Dit doen ze bijvoorbeeld door de verhouding van investeringen in wortels en scheut aan te passen. Bij droogte wordt bijvoorbeeld meer geïnvesteerd in het wortelsysteem, en in schaduwrijke omstandigheden zal de scheut meer prioriteit krijgen. Welke processen hiervoor van belang zijn en hoe de plant dit reguleert is een belangrijk onderzoeksthema. Dit thema is van groot belang voor de verbetering van landbouwgewassen, omdat de opbrengst van deze gewassen vaak gelimiteerd wordt door de hoeveelheid suiker die wordt geleverd aan de graankorrels, knollen, vruchten etc. In de context van suikerverdeling wordt gesproken van suiker 'sources' en suiker 'sinks'. In planten worden organen die netto produceerders zijn van grondstoffen een source genoemd, andersom zijn organen die netto consumeerders zijn een sink. Sucrose (tafelsuiker) is de belangrijkste suiker in planten die wordt vervoerd van sources naar sinks. Het evenwicht tussen de productie van suikers in sources en het gebruik in sinks is cruciaal voor de efficiënte groei van planten. Enerzijds, als er te veel sinks zijn ten opzichte van sources, zijn er niet genoeg suikers beschikbaar zijn om de groei en ontwikkeling van sinks te garanderen. Anderzijds, als er te weinig sinks zijn ten opzichte van sources, kan er een teveel aan suikers ontstaan dat zich ophoopt in de bladeren, wat leidt tot verminderde fotosynthese en uiteindelijk verminderde groei.

Een goede plant om source-sink dynamica te onderzoeken is de aardappel. In aardappelplanten zijn de knollen zeer sterke sucrose sinks die gedurende de levenscyclus worden gevormd door radiale groei van stolonen. Stolonen zijn ondergrondse uitlopers die speciaal worden gevormd voor de knolgroei, welke zorgen voor de vegetatieve voortplanting van de aardappelplant. De

knolvorming zorgt voor een grote verandering in suiker verdeling, wat samen met het grote belang van het landbouwgewas aardappel, zeer interessant is om te bestuderen. Een belangrijk moleculair signaal voor de ontwikkelings transitie van stoloon naar knol is het 'knolgen' StSP6A. Wanneer StSP6A aankomt in een stoloon via de vaatbundels (floëem) zet het een genetisch knop om waardoor de aardappelknol begint met groeien. Daarnaast bindt StSP6A aan een sucrose transporteiwit (SWEET11) dat zowel in het floëem van de stam als in de aardappelknol is gelocaliseerd. Normaliter zorgt dit transporteiwit ervoor dat sucrose uit het floëem kan worden gehaald voor gebruik in de omliggende weefsels. Echter, de SP6A-SWEET interactie vermindert de transportcapaciteit van SWEET11 en heeft zo een effect op lange afstand transport van sucrose en sucrose toelevering richting de knol. Dit komt omdat het suikers in het floëem houdt, in plaats van dat ze naar de stam worden 'gelekt' voor stamgroei en onderhoud, waardoor er meer beschikbaar blijft voor knollen.

De titel van dit proefschrift: "Het efficiënt starten en bij voorkeur vullen van een aardappelknol, het gebruik van modellen om de verschillende rollen van SP6A in source-sink dynamica te onderzoeken" hint op het veelvuldige gebruik van simulatiemodellen. Waar gegevens ontbraken, hebben we deze modellen met experimenten en bio-informatica-analyses gecombineerd. De ontwikkelde modellen variëren in complexiteit, van een eenvoudig systeem van differentiaalvergelijkingen voor plantengroei (Hoofdstuk 5), een complexer model voor het laatste stadium van transport van sucrose in stolonen en knollen (Hoofdstuk 4), tot een zeer gedetailleerd biofysisch model voor het transport van water en sucrose in het vaatweefsel van de aardappelplant (Hoofdstukken 2 en 3). Het doel van deze modellen was tweeledig: 1) om het fundamentele begrip te verbeteren van hoe transportdynamica en competitie tussen verschillende sinks afhangt van het bouwplan van de plant en de fysiologie van de invidivuele organen en 2) om de specifieke effecten van StSP6A op de source-sink dynamiek en competitie voor sucrose tussen verschillende organen te onderzoeken. De dubbelrol van StSP6A in zowel knolinitiatie als het verminderen van sucrose-efflux hebben we daarom onderzocht op verschillende locaties binnen de plant.

In Hoofdstuk 2 lag de focus op het aantonen van de fysiologische relevantie van de StSP6A-SWEET11 interactie voor het transport van sucrose over lange afstanden en de uiteindelijke levering aan knollen. Hiervoor hebben we een biofysisch transportmodel ontwikkeld met een enkele source en sink, waarbij de source kan worden geïnterpreteerd als een volgroeid fotosynthetiserend blad en de sink als een aardappelknol. In biofysische modellen wordt

het transport van sucrose en water in het floëem vaatweefsel gemodeleerd op basis van de hypothese van Műnch, deze stelt dat het verschil in osmotische druk tussen source en sink een verschil in waterdruk veroorzaakt, wat water doet stromen van source (hoge suikerconcentratie) naar sinks (lage suikerconcentratie). Het transport van water in het xyleem weefsel wordt gemodeleerd op basis van capillaire werking. Daarnaast wordt water tussen xyleem en floëem getransporteerd door een verschil in waterpotentiaal over een semi-permeabel membraan. In ons model namen we daarnaast ook de export van sucrose uit het floëem door SWEET exporters en de import van sucrose terug het floëem in door SUC transporters op. Dit was nodig om het effect van de StSPP6A-SWEET interactie te kunnen onderzoeken. Na het parametriseren van het model op aardappelspecifieke data voor plant afmetingen, vaatbundel grootte en aantallen en blad fotosynthese snelheid, bootste het succesvol experimenteel gemeten floëem-sucroseconcentraties en transportsnelheden na. Bovendien liet het model zien dat hoge viscositeit als gevolg van hoge sucroseconcentraties in het floëem de belangrijkste weerstandsfactor is in aardappel. In eerdere modellen van bomen en klimplanten bleek vooral de lengte en vorm van de vaatbundels de bepalende factor voor transportweerstand te zijn. Dit gevonden verschil benadrukt het belang van soortspecifieke modellen. Verder toonden we aan dat er sprake is van een supra-lineair effect van de StSP6A-SWEET11 interactie op de hoeveelheid aan de knol geleverde sucrose, wat betekent dat de toename van de levering van sucrose aan de sinks groter is dan de door StSP6A veroorzaakte afname in SWEET sucrose transport. Dit supra-lineaire effect komt voort uit het complexe samenspel van sucroseconcentratiegradiënten in het floëem, viscositeit van floëemsap, xyleemwaterstroom en drukgradiënten, die op hun beurt terugkoppelen naar de sucroseconcentratiegradiënten.

Planten hebben uiteraard complexere architecturen dan een enkele source en sink, daarom hebben we in Hoofdstuk 3 het model uit het vorige hoofdstuk uitgebreid naar twee sinks. Met dit model konden we de effecten van plantarchitectuur en fysiologie (transportafstand en stromingsrichting van xyleem) en de eigenschappen van de sinks (sinkkracht en sucrose-affiniteit) op de competitie voor sucrose tussen twee sinks onderzoeken. Het doel was in eerste instantie om een meer mechanistisch begrip van de wisselwerking tussen sink-kenmerken en plantarchitectuur op sucrose competitie te krijgen. Door de gedetailleerde implementatie van biofysische mechanismen voor sucrose- en watertransport hebben we laten zien dat de effecten van sinkkracht, sinkaffiniteit voor sucrose en transportafstand aanzienlijk werden versterkt in vergelijking met eerdere vereenvoudigde modellen voor sucrosetransport. De belangrijkste factor in dit verschil is de toevoeging van ruimtelijk detail in de simulaties. Doordat door ons

model op meerdere plekken in de stam de suiker- en water-status wordt bepaald, hoeven we niet aan te nemen dat de suiker gradient in de stam lineair is. Dit blijkt van groot belang op suikercompetitie tussen sinks. Daarna hebben we het model gebruikt voor een casestudie met volwassen (source)bladeren, jonge (sink)bladeren, en knollen. Knollen ondervinden aanzienlijke nadelen in vergelijking met sinkbladeren door architecturele en fysiologische eigenschappen van de plant, namelijk de grotere afstand tot sinkbladeren en de tegenstroom in xyleem in vergelijking met sinkbladeren. Het cumulatieve nadeel ervaren door knollen maakt dat een ongerichte sucrose-efflux mitigatie door StSP6A, die we in hoofdstuk 2 hebben onderzocht, knollen het meeste helpt. Als gevolg verbetert de competetitieve positie van knollen door de blokkering van SWEET11 transporters aanzienlijk ten opzichte van een situatie zonder StSP6A. Dit laat zien dat de rol van StSP6A in het efficienter maken van suikertransport in de stam, en dus de dubbelrol naast knolinitiatie, daadwerkelijk zorgt voor voordeel voor knollen in een situatie waar zonder deze tweede rol de knol in het nadeel zou zijn.

In Hoofdstuk 4 hebben we onze aandacht van het vaatstelsel in de stam van de plant naar lokaal suikertransport van de vaatbundels in de knol verplaatst. Deze vorm van transport bepaalt de snelheid waarmee suikers daadwerkelijk worden opgenomen door de sink. Opnieuw speelt de SWEET-transporter hier een grote rol als belangrijke schakel in suikerlevering via de celwand, ook wel apoplastisch transport genoemd. De verwachting was dan ook dat de StSP6A-SWEET-interactie van invloed zou zijn op de efficientie van sucrose aanlevering. Eerder onderzoek heeft laten zien dat een verandering van het sucrose leveringsmechanisme een van de eerste veranderingen is tijdens de overgang van stoloon naar knol. Dit mechanisme verandert van actief transport door middel van SWEET-transporters waarbij suiker van een cel via de celwand naar de volgende cel wordt getransporteerd naar passief transport via directe cel-cel connecties (plasmodesmata). Deze vorm van transport wordt symplastisch transport genoemd. Onderzoekers hebben tot nu toe aangenomen dat deze overgang van apoplastisch naar symplastisch transport er automatisch voor zorgt dat aardappelknollen effectiever sucrose kunnen opnemen, maar direct bewijs hiervoor ontbreekt. Een logische uitleg voor verminderdt apoplastisch transport is dat SWEET-transport wordt verminderd door StSP6A. Echter, de factoren die ervoor zorgen dat in plaats hiervan het symplastisch transport toeneemt waren nog onduidelijk. Uit ons onderzoek bleek dat de overgang van apoplastisch naar symplastisch gedomineerd transport gepaard gaat met een afname van callose in de plasmodesmata van knollen. Callose is een suikerpolymeer die de opening van de plasmodesmata reguleert, i.e. een afname van callose zorgt voor opening van de plasmodesmata. Om de transitie in

suiker transport verder te onderzoeken hebben we vervolgens bio-informatica- en modellen gecombineerd. Gen-expressie analyse laat zien dat de callose afname een gevolg is van een afname van callose aanmaak in plaats van een toename van degradatie. Verder laat onze analyse een duidelijke verandering in sucrosemetabolisme richting zetmeelproductie in de knol zien, welke is gecoördineerd met de verandering in callose en SWEET expressie. Met behulp van een biofysisch model van sucrose transport hebben we tenslotte laten zien dat deze gecoördineerde overgang naar symplastische transport en zetmeelproductie leidt tot passief suiker transport gedreven door een sterke sucrosegradiënt. Dit mechanisme creëert de fysiologische omstandigheden die nodig zijn voor efficient symplastisch transport om zo de sinkkracht van knollen te verbeteren. Het model laat echter ook zien dat het in stolonen efficienter is om apoplastisch transport te gebruiken, waarmee we aantonen dat symplastisch transport zeker niet altijd efficienter is.

In Hoofdstuk 5 hebben we vervolgens een experiment uitgevoerd om blad, bloem en knolgroei te kwantificeren. In dit experiment hebben we data verzameld van wild type (WT) planten en planten met genetische 'knockdown' van het 'bloemgen' (StSP3D), 'knolgen' (StSP6A) en sucrose-exporters (StSWEET11a). Deze data hebben we daarna gecombineerd met simpele modellen om een beter begrip te krijgen van het effect van knolinitiatie op bladgroei, bloemgroei en blad veroudering. Er bleken weinig verschillen op te treden tussen wildtype planten en planten waarin het bloemgen ontbrak. De reden hiervoor is de zeer beperkte mate waarin bloei optreedt in ons in groeikassen uitgevoerde experiment. Doordat bloei ook in wildtype nauwelijks optreedt heeft het bloeigen weinig relevantie en heeft aan- of afwezigheid ervan weinig effect. Planten waar sucrose transport eiwitten ontbraken hadden daarintegen een zeer sterk fenotype. Verminderd transport van suikers tussen source en sink zorgt voor verslecherde groei van het bladerdek en knollen, ook verouderen deze planten sneller. Het interessantste fenotype was echter de StSP6A knockdown. Verminderde StSP6A expressie leidde tot een vertraagde start van knolvorming met ongeveer 2 weken. Het leidde echter ook tot aanzienlijk uitgestelde veroudering van het bladerdak van 4 tot 5 weken. Hierdoor werd in deze planten de levenscyclus verlengd waardoor ook de knolgroei langer door kon gaan, waardoor er ondanks de tragere start geen afname in knolgrootte en kwaliteit optrad. Deze vertraging leidde echter wel tot een verminderde synchronisatie in knolvorming en verhoogde variabiliteit in knolgrootte. Dit suggereert dat concurrentie voor sucrose tussen knollen en bladeren een cruciale rol kan spelen bij het bepalen van groeipatronen en de uiteindelijke grootte van de knollen. Om dit verder te onderzoeken hebben we een eenvoudig groeimodel gebruikt, dat liet zien dat sucrose

competitie, in plaats van een gedeeld signaal zoals StSP6A, waarschijnlijk de belangrijkste factor is om de waarneming te verklaren dat vertraagde knolvorming gepaard gaat met vertraagde veroudering.

Samen bieden hoofdstukken 2 tot 5 waardevolle inzichten in welke factoren sucrose competitie en dus sucrosetoewijzing naar organen bepalen. Verder hebben we de dubbelrol van het knolgen StSP6A bij de toewijzing van sucrose binnen aardappelplanten uitgediept wat heeft gezorgd voor een meer complete kijk op zowel de (gen)regulatoire functie in knolinitiatie als de post-translationele functie van StSP6A in SWEET11 suiker export blokkade. De wisselwerking tussen deze rollen hebben we met de verschillende modellen laten zien. In hoofdstuk 2 en 3 hebben we laten zien dat de complexe feedbacks en dynamiek van het sucrosetransport, samen met sink karakteristieken, fysiologisch relevant zijn voor de levering van sucrose aan sinks. StSP6A zorgt dus voor efficienter transport over de lange afstand. In de toekomst kunnen we deze inzichten verder testen in achitectureel complexere modellen, op deze manier kan bijvoorbeeld de competitie tussen knollen worden onderzocht. Voor deze uitbreiding kunnen functionele-structurele plant (FSP) modellen gebruikt worden, deze FSP modellen kunnen biofysisch detail koppelen aan complexe groeiende plantarchitecturen. In hoofdstuk 4 hebben we het effect van knolitiatie op de aantrekkingskracht van knollen op suiker onderzocht. Hier hebben we gevonden dat een gecoordineerde overgang van suiker en callose metabolisme ervoor zorgt dat de knol suikers sterker aantrekt door het genereren van een sterkere suikerconcentratie gradient. Naast effectief lange afstandstransport zorgt StSP6A ervoor dat knollen een competitief voordeel krijgen ten opzichte van andere organen door sterkere aantrekkingskracht en de complexe feedbacks uit hoofdstukken 2 en 3. In hoofdstuk 5 hebben we vervolgens laten zien dat de suikercompetitie daadwerkelijk een groot effect heeft op de plant groei en knolgrootte. Kortom, in dit proefschrift hebben we laten zien hoe het knolgen StSP6A en de dubbele rol die het speelt ervoor zorgt dat aardappel knollen efficiënt worden gestart en bij voorkeur worden gevuld.

Acknowledgements | Dankwoord

The first steps into the models we used in this thesis went unexpectedly smooth. Relatively quick (in my memory at least) we had a working model of water and sucrose flow in potato. However, when we slightly increased the complexity of the model, things became more unclear, and the first real difficulties arose. Luckily, some late nights, lots of coffee (and cola), and a bit of head-scratching brought us to this point. I would like to use these final pages to thank the people that were there in the easy and more difficult times in the last four years.

Kirsten, from the first time we've met I have felt taken seriously and inspired by you. On the 5th of December 2018 we sat down in your office, and you started talking about the PhD project I was interested in. It was on a topic I was only half familiar with, transport phenomena in plants. Luckily, you were completely convinced that I could also become familiar with plants and here we are, I've learned a lot on (potato) plants, and I am proud to have made this leap into computational plant science. You're always able to make time for a short (or long) discussion on science or something else important, or not important. I am thankful to have you as my promotor. **Christian**, your never-ending knowledge of potato, combined with your kindness and enthusiasm really showed me how amazing potato plants are. You're a great example of a scientist to me, interested in the why and how, up till the tiniest detail. Thanks for showing me this. **Sara**, you showed me how much perseverance and skill is needed for simple experiments I came up with behind my desk. Thanks for these lessons and teaching me how to grow potatoes.

To my paranymps **Gert-Jan** and **Monica** I first want to say thanks for being my best man and woman as I'm getting married to the university (as that's what's happening according to Wikipedia). **Monica**, I was lucky that you joined our office when you came to Utrecht. In the last two years we have become good colleagues and friends. Thanks for all the long talks on plants, genes, and everything else we talk about. It's truly appreciated. **Gert-Jan**, we've known each other for a long time, meeting as young scouts at the age of 8 (or 9?), through high school we really became friends, then university and now I'm the second of us to finish a PhD thesis. Thanks a lot for all the beers, fun and talks. You're a great friend.

Erdem, we started around the same time in the office, and now we're finishing almost at the same time. Great to have done that at the same time and pace as you. **Sam** thanks for being my partner in the board of social affairs. It has been great to build new bonds and friendships via your drive to organize activities. **David**, **Jeroen M**, **Sarah**, **Arpit**, **Dani**, **Bram(s)**, **Leonie**, **Ling-Yi**, **Erika**, **Meine**, and all other TBB pubcrawlers, it was great and let's keep doing these, and other, great social activities. They make working in the group a lot more fun. **Jan Kees**, even though my models were never in need for the power you provide, I am still very happy with the

stability you provide in a way that I never have to worry about the computer I'm working on. **Paulien**, thanks for the amazing course(s), both on computational biology and on how to cook for groups. Of course, I would like to thank everyone else from **TBB**, I have felt welcome from the start. With all the great science that has been happening around me it has been a pleasure to learn from all of you.

I wouldn't be where I am now without **Aljoscha** showing me how much fun science can be. You're an inspiring teacher and scientist. You really made me want to pursue research and I am very grateful for this.

Er was ook een leven naast werk en promotie de afgelopen jaren, daarom wil ik graag ook al mijn familie en vrienden bedanken voor alle ontspanning en steun. **Matthijs**, we zijn steeds betere vrienden geworden de laatste jaren, en daar ben ik je dankbaar voor. **Jos & Esther**, **Bas & Edith**, **Ineke & Wout**, ik heb altijd steun gevoeld van jullie. Die basis heeft gemaakt dat ik ben geworden wie ik ben. **Maarten & Lieneke**, ik heb me vanaf het begin thuis gevoeld bij jullie en daar ben ik heel erg gelukkig mee.

Mama, bedankt voor je kracht en liefde. Ik ben je dankbaar voor alles wat je voor mij gedaan hebt en hoe je alles altijd zo voor elkaar hebt gehad. Zonder jou was ik nog niet eens halverwege gekomen. **Papa**, ik weet zeker dat je trots zou zijn geweest en dat maakt mij ongelooflijk trots. **Sam**, als ik weer eens op mijn plek gezet moet worden, dan doe je dat. Bedankt lieve broer.

Heleen, zoals ik weleens tegen je heb gezegd; alles gaat altijd precies zoals je bedenkt, maar dan anders. Gelukkig gaat er een ding nooit anders, en dat is dat jij er bent.

Curriculum vitae

Bas van den Herik was born in Gorinchem, the Netherlands, on the 4th of June 1994. He grew up in Hardinxveld-Giessendam. Next to attending and graduating from "Stedelijk Gymnasium Camphusianum", he enjoyed being a scout and is still active at his local scouting group.

After high-school, he started his studies in Life Science & Technology, a joint degree between Technical University Delft and Leiden University. After obtaining his Bachelor's degree in 2016, he started his Master's degree Biochemical Engineering at the Technical University Delft and focused on models of (yeast) metabolism. In his Master's Bas found that he really liked to work with computational models to better understand biology. With this newfound enthusiasm, he started his Master thesis at the research group of prof. Aljoscha Wahl to study the metabolism of yeast using ^{13}C tracer experiments combined with computational modeling. After doing an industrial internship at the bioinformatics department of DSM, Bas knew he wanted to continue his career in academia. Knowing that he wanted to use computational models to better understand biology, he started his PhD under the supervision of prof. Kirsten ten Tusscher. Moving from single celled organisms to plants, which proved to be a great choice. Currently, Bas is still in the group of Kirsten as a Postdoctoral Researcher working on functional structural plant models of nutrient foraging dynamics in *Arabidopsis thaliana*.

List of publications

van den Herik, B., Bergonzi, S., Li, Y., Bachem, C. W., & ten Tusscher, K. H. (2023). A coordinated switch in sucrose and callose metabolism enables enhanced symplastic unloading in potato tubers. bioRxiv. https://doi.org/10.1101/2023.11.24.568555

van den Herik, B., Bergonzi, S., Bachem, C. W. B., & Tusscher, K. H. ten. (2023). Mobile tuberigen impacts tuber onset synchronization and canopy senescence timing in potato. bioRxiv. https://doi.org/10.1101/2023.11.08.566204

van den Herik, B., & ten Tusscher, K. (2022). Undirected Sucrose Efflux Mitigation by the FT-Like SP6A Preferentially Enhances Tuber Resource Partitioning. Frontiers in Plant Science, 13. https://doi.org/10.3389/fpls.2022.817909

van den Herik, B., Bergonzi, S., Bachem, C. W. B., & ten Tusscher, K. (2021). Modelling the physiological relevance of sucrose export repression by an Flowering Time homolog in the long-distance phloem of potato. Plant, Cell & Environment, 44(3), 792–806. https://doi.org/10.1111/pce.13977

Zhang, J., **van den Herik, B.**, & Wahl, S. A. (2020). Alpha-ketoglutarate utilization in Saccharomyces cerevisiae: Transport, compartmentation and catabolism. Scientific Reports, 10(1), Article 1. https://doi.org/10.1038/s41598-020-69178-6